Experimental and Modeling Study of Carbon Dioxide Absorption in Aqueous Ionic Liquid Blended with Amines

Sweta Chetananand Balchandani

Experimental and Modeling Study of Carbon Dioxide Absorption in Aqueous Ionic Liquid Blended with Amines

Thesis

Submitted in partial fulfilment of the

Requirements for the degree of

DOCTOR OF PHILOSOPHY

By

Sweta Chetananand Balchandani

(Roll no. 166107018)

Department of Chemical Engineering

Indian Institute of Technology Guwahati

Guwahati 781039, Assam, India

March 2021

Dedicated

to

G Singh DhillonJi

Department of Chemical Engineering

Indian Institute of Technology Guwahati

Guwahati 781039, Assam, India

CERTIFICATE

It is certified that the work contained in this thesis entitled "Experimental and Modeling Study of Carbon Dioxide Absorption in Aqueous Ionic Liquid Blended with Amines" submitted by Ms. Sweta Chetananand Balchandani for the award of the degree of Doctor of Philosophy has been carried out in the Department of Chemical Engineering, Indian Institute of Technology Guwahati under our supervision and this work has not been submitted elsewhere for the award of any other degree or diploma.

This thesis in our opinion, has reached the standard fulfilling the requirements for the award of the degree of Doctor of Philosophy in accordance with the regulations of the institute.

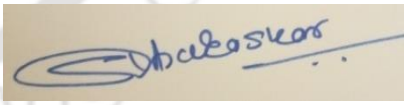

Prof. Bishnupada Mandal
Professor
Department of Chemical Engineering
Indian Institute of Technology Guwahati
Guwahati 781039, India

Dr. Swapnil Dharaskar
Assistant Professor
Department of Chemical Engineering
Pandit Deendayal Petroleum University
Gandhinagar, Gujarat-32007,India

Acknowledgement

I take this opportunity to express my deep sense of respect and sincere gratitude to my thesis supervisors, Prof. Bishnupada Mandal (IITG) and Dr. Swapnil Dharaskar (PDPU) for giving me an opportunity to work under their supervision for my doctoral program at the Indian Institute of Technology Guwahati. I am indebted to Prof. Mandal and Dr. Dharaskar for their valuable guidance and encouragement throughout this research program. I will be always indebt to them for their contribution in my doctoral submission. The experience of working with them was one of the most important learning experience of my life.

I am also thankful to my doctoral committee members, Prof. Tamal Banerjee, Prof. Animes Golder, Department of Chemical Engineering and Prof. Lal Mohan Kundu, Department of Chemistry, for their constructive and contributive suggestions at each and every stage of this research program. I am extremely thankful to Dr. Arvind Kumar (Senior Principal Scientist, CSMCRI-Bhavnagar) and Dr. S. K. Dash (Associate Professor, PDPU) for providing me the lab facilities as and when required.

I must also thank my departmental colleagues at Pandit Deendayal Petroleum University for their constant support and motivation. I would also like to thank the entire PDPU fraternity for providing me the platform for pursuing my doctoral research work and for extending help in every way for the successful completion of thesis work.

I would also like to express my sincere gratitude to Late Prof. S.S. Bandyopadhyay and Dr. Anurag Gupta, Senior Mentors of PDPU, for their valuable suggestions to enhance my doctoral work.

I am also thankful to the technical staffs of our department for their sincere help and support during this work. I would like to thank all the staffs specially Mr. Prashant Patel, Mr. Rajesh Vanaspati of PDPU for their support in various forms

I am also thankful to my Research group colleagues / friends at IIT Guwahati for their support and contribution, Ms. Vinita Das, Ms. Preetisagar Talukdar, Ms. Anusuya Talukdar, Mr. Ankur Pandey, Dr. Rajashree Borgohain, Dr. Pradip Das and Mr. T. Ramesh.

I am also fortunate enough to get excellent colleagues cum friends during my doctoral research tenure, Dr. Leena Santosh, Mr. Darshit Shah, Mr. Manivel M, Dr. Bharti Saini, Dr. Anirban Dey, Dr. Manan Shah, Dr. Pravin Kodgire, Mr. Abhishek Kumar Singh and Dr. Niragi Dave. I would like to thank all of them for their friendly co-operation during my research work.

I express my humble regards and respect to my Parents and family members. Their love, care, sacrifices and encouragement have made it possible for me to come so far. I will always be grateful to god for giving everything in my life.

SWETA

VITAE

Sweta Chetananand Balchandani

Date of birth: December 31, 1988

Email: sweta.balchandani@gmail.com,sweta.balchandani@sot.pdpu.ac.in, sweta0172@yahoo.co.in,sweta.balchandani@iitg.ac.in

Permanent Address: 5, Pushkar Bunglows,
Manjipura Road,
Nadiad-387002, Gujarat

Present Address: C-602, Sarthak Heaven Flats,
PDPU Cross-Road,
Gandhinagar- 382007, Gujarat
Ph: +91-9898133272

Education:

- PhD (Thesis submitted)
  Department of Chemical Engineering
  Indian Institute of Technology Guwahati
  Guwahati, Assam, India
- M.Tech (Cad and Control in Chemical Engineering)
  Department of Chemical Engineering
  Dharamsinh Desai University
  Nadiad, Gujarat, India
  (2009-2011)
- BE (Chemical Engineering)
  Department of Chemical Engineering
  Dharamsinh Desai University
  Nadiad, Gujarat, India
  (2005-2009)

Publications

Journal papers

1. **Sweta Balchandani**, Bishnupada Mandal, Swapnil Dharaskar, "Measurements and modeling of vapor liquid equilibrium of CO_2 in amine activated imidazolium ionic liquid solvents", Fluid Phase Equilibria 521 (2020) 112643.
2. **Sweta Balchandani**, Bishnupada Mandal, Swapnil Dharaskar, Arvind Kumar, S S Bandyopadhyay, "Thermally Induced Characterization and Modeling of Physicochemical, Acoustic, Rheological and Thermodynamic Properties of novel blends of (HEF +AEP) and (HEF +AMP) for CO_2 / H_2S absorption", Environmental Science and Pollution Research, 26 (2019) 32209-32223.
3. **Sweta C Balchandani**, Bishnupada Mandal, Swapnil Dharaskar, "Stimulation of CO_2 solubility in reversible ionic liquids activated by novel 1-(2-aminoethyl piperazine) and bis (3-aminopropyl amine)", Separation and Purification Technology (2020) (https://doi.org/10.1016/j.seppur.2020.118260).
4. **Sweta C Balchandani**, Bishnupada Mandal , Swapnil Dharaskar, "Analysis of 2-Methyl Piperazine as an activator in tertiary amine, physical solvent and ionic liquid systems for CO_2 absorption from flue gas". (to be communicated)
5. **Sweta C Balchandani**, Bishnupada Mandal, Swapnil Dharaskar, "Analysis of physiochemical properties six amine activated solvents for CO_2 absorption for post combustion processes". (to be communicated)

Conference presentations

1. **Sweta Balchandani**, Anirban Dey, Bishnupada Mandal, Swapnil Dharaskar, 'Estimation of Temperature dependent binary interaction parameters of unloaded solvents for CO_2 capture', 12th International Conference on Thermal Engineering: Theory and applications organized by Pandit Deendayal Petroleum University (PDPU), Gandhinagar and Ryerson University, Toronto, Canada, 23rd -26th February 2019 at PDPU, Gandhinagar.
2. **Sweta Balchandani**, Bishnupada Mandal, Swapnil Dharaskar, 'Reaction Kinetics of CO_2 absorption of ionic liquid (HEF) blended amine systems', International Conference on Advances and Challenges for Sustainable Ecosystems, National Institute of Technology, Tiruchirappalli, 6th-8th December 2018.
3. **Sweta Balchandani**, Bishnupada Mandal, S S Bandhyopadhyay, 'Modelling of carbon dioxide solubility in different blends of ionic liquids with amines and diluents using five different statistical correlations and neural networks', International Conference on Oil, Gas and Petroleum , Madridge Conferences, Dubai, UAE, 3rd- 5th April 2017.

Abstract

Experimental and Modeling Study of Carbon Dioxide Absorption in Aqueous Ionic Liquid Blended with Amines

Power plants and chemical process industries face a huge challenge in efficient CO_2 separation from the flue gases over decades. The concern is furthermore important with respect to climate change. Various technologies have been tried for post-combustion CO_2 capture out which chemical absorption using solvents is widely applied and the changes in this technology are well accepted owing to its ease of retrofitting. Development of novel solvents for post-combustion CO_2 capture needs a lot of attention.

The current work examines three potential amine activators, 1-(2-aminotethyl) piperazine (AEP), bis (3-aminopropyl) amine (APA) and 2- methyl piperazine (2-MPZ) for enhancing CO_2 solubility when blended with base solvents. For the current work, selected base solvents are 3-aminopropyl triethoxysilane (TESA), 1-butyl-3-methyl imidazolium acetate ([bmim] [Ac]), *N*-methyldiethanolamine (MDEA), and sulfolane ($TMSO_2$). CO_2 solubility is measured in aqueous systems of [bmim] [Ac], ([bmim] [Ac] + AEP), ([bmim] [Ac] + APA), TESA, (TESA + AEP), (TESA + APA), (MDEA + 2-MPZ), ($TMSO_2$ + 2-MPZ) and ([bmim] [Ac] + 2-MPZ) over a temperature and pressure range of (303.2-323.2) K and (0-400) kPa. ^{13}C NMR and FTIR analysis of unloaded and CO_2 loaded solvents are examined to propose reaction mechanism of the interaction amid CO_2 and solvents. The obtained experimental results are correlated using modified Kent-Eisenberg (KE) model considering the non-ideality in the gas phase. The equilibrium constants of the proposed reactions were estimated using modified KE model through non-linear regressive optimization. The data obtained through modified KE model is further utilized to study the concentration profiles of the associated ionic species at equilibrium conditions and pH of the CO_2 loaded solvents. Further, a new statistical and non-rigorous model is established for correlating the TESA systems. A two layer feed forward artificial neural network (Levenberg-Marquardt back propagation method for training; log sigmoid and linear transfer function for hidden and output layers, respectively) was used to correlated aq. [bmim] [Ac], ([bmim] [Ac] + AEP) and ([bmim] [Ac] + APA) systems. CO_2 cyclic capacity and heat of absorption are also analysed for aq. (MDEA + 2-MPZ) systems. The obtained CO_2 solubility data is also compared with the literature indicating the efficacy of the proposed solvents.

Important thermophysical properties viz. density, viscosity, surface tension, sound velocity and refractive index of the solvents are measured and reported over the temperature range of (298.15-333.15) K. Along with the nine above mentioned solvents, two more non-aqueous solvents based on 2- hydroxyl ethyl ammonium formate (HEF) i.e. (HEF + AEP) and (HEF + 2-amino-2-methyl-1-propanol (AMP)) are also analysed for physiochemical properties. These properties play significant role in understanding the flow behaviour, inter-molecular interactions, designing of the absorber or regenerator column, pumping costs required for solvents, mass transfer and kinetic rates of CO_2 in the solvents. Density and viscosity were modeled using first principle model i.e. Redlich-Kister and Grunberg-Nissan. New models were proposed for correlating sound velocity, refractive index and surface tension. All the properties were correlated as a function of temperature and composition. The results indicated less deviation amid the experimental and modeled data indicating the accuracy of the models. The experimental results were further used to estimate various important derived properties such as excess molar volume, viscosity deviation, diffusivity of N_2O and CO_2 in the solvents, isentropic compressibility, thermal expansion coefficient, enthalpy and entropy of activation of viscous flow through literature established empirical correlations.

LIST OF CONTENTS

LIST OF FIGURES

LIST OF TABLES

Chapter 1

INTRODUCTION, LITERATURE REVIEW AND OBJECTIVES

This chapter discusses the impact of greenhouse gas emissions on the environment. The various carbon capture technologies along with a brief discussion on their effective implementation have been presented. An extensive literature review corresponding to chemical absorption using single and blended ionic liquids and amines is discussed. The importance and objectives of the research work taken are elaborated along with the background of the work.

1.1 Background

The effect of massive emission of greenhouse gases and other substances such as chlorofluoro carbons (CFCs) have resulted in global warming. To cure the same, immense measures have been taken by the government and environmentalists globally. Whereas the emission of CFCs has been reduced significantly over the past two decades due to stringent regulations [1,2], greenhouse gas emissions remain a huge environmental concern. Of the many greenhouse gases emitted in the atmosphere, CO_2 is the largest anthropogenic gas and hence its control in the energy sector has been an ever-expanding issue for decades.

The annual emissions of CO_2 (in Mt) over the different sectors of emissions viz. gas, oil, coal, gas flare, and cement counted for the year 2019 have been reported as 7616, 12355, 14362, 430, and 1564, respectively, the total emissions being approximately 36441 Mt CO_2. The emissions of the year 2018 proved to be approximately 14 % higher than being emitted in a decade less [3]. Out of the five major countries emitting CO_2, India stands at position 3rd with a total emission of 2616 Mt CO_2 in comparison to China (1st), United States of America (2nd), Russian Federation (4th) and Japan (5th) with the emission of 10175, 5285, 1678 and 1107 Mt CO_2, respectively [3].

According to a recent report by Energy Information Administration (EIA) [4], the energy sector being one of the major contributors to CO_2 emissions is highly unstable in both the low or high

oil price cases. The latter is owing to several factors such as resource availability, petroleum supply conditions, fuel switching, development and application of extent of non-traditional resources of energy such as nuclear, wind, hydro, geothermal and solar power, energy consumption, economic activities, etc. This can also be verified with the fact that only 2 % rise was observed in CO_2 emission over one year from 2017 to 2018. The highest CO_2 emissions in terms of per capita are attributed to the oil-producing countries whereas India leads with an average of 1.84 tonnes of CO_2 per person annually in 2017. The difference in per capita in different countries is observed primarily due to the population, level of income, and the choice of energy resources [5]. Owing to the many reasons contributing towards the rise in CO_2 in the atmosphere, it has reached a substantial level of 414.2 ppm as recorded by NOAA's Mauna Loa Atmospheric Baseline Observatory in May 2019. The observed CO_2 is approximately 8.95 % higher than that observed in 2010 [6]. Thus, CO_2 emissions have to be controlled in continuation with the required sustainable economic growth of the globe. This can be successfully achieved with decreased usage or improving the technologies which rely on carbon-based fuels along with the development of new technologies with lower carbon footprints. Hence, carbon capture, storage, and utilization play a very vital role in achieving a sustainable atmospheric level of CO_2.

1.2 Carbon capture, utilization and storage

The energy sector requires advanced processing technologies for effective reduction in CO_2 emission or capture so as to suppress global warming. Carbon capture, utilization and storage (CCUS) refers to the capture of CO_2 from large point sources such as thermal power plants and subsequently utilizing it for various processes such as in enhanced oil recovery, de-methanation in coal fields, beverage production, fertilizer manufacture, etc. The unutilized CO_2 has then to be stored safely in ocean. Since, coal based thermal power plants contribute around 80 % of CO_2 produced worldwide, one of the major focus has always been in efficiently capturing CO_2 from such sources. There are three main approaches to capture CO_2 from coal based thermal power plants: Oxy-combustion, Pre-combustion and Post-combustion [7]. The captured CO_2 is then compressed, liquefied and transported and sequestrated safely. The economic viability of any CCUS system largely depends on the CO_2 capture cost since it accounts for around 75% of the total cost. The electricity cost produced through a coal-based thermal power plant increases twice

when the plant is retrofitted with a CCUS systems [8]. The conceptualization of an economic CCUS system leads to the efficient capture of CO_2 which is hereby identified to be the most crucial and energy intensive step in the entire system.

1.2.1 Carbon dioxide capture processes

The selection of any of the three main approaches of CO_2 capture system is significantly dictated by the extent of retrofitting which can be done over an existing system producing CO_2 and the cost incur for the same.

1.2.1.1 Oxy-fuel combustion

It is the process of burning a fuel using pure oxygen instead of air as the primary oxidant. Fuel consumption is greatly reduced (approximately 75 %) since the heat required for heating nitrogen of air is not required. It also leads to the achievement of higher flame temperatures and the major products being CO_2 and H_2O. This also results in H_2O with high concentration which makes separation further easier. Additionally, the production of nitrogen oxide and dioxide is also greatly reduced, since nitrogen along with oxygen is not allowed to enter the system. The most important advantage for using oxy-fuel combustion is to produce a CO_2 rich flue gas ready for storage and utilization with least impurities included. Although, the methods provide a lot of advantages over the others, it is less preferred due to the high cost of production of oxygen while separating it from air [9]. The process follows a sequence of first separation of oxygen from air thereby combusting the carbon-rich fuel in combustors where energy is generated and is sent for electricity generation (Figure 1.1). As side products of combustion of fuel, CO_2 and H_2O rich stream are generated which is first led to easy removal of H_2O via condensation route and subsequently, CO_2 is sent for sequestration or utilization.

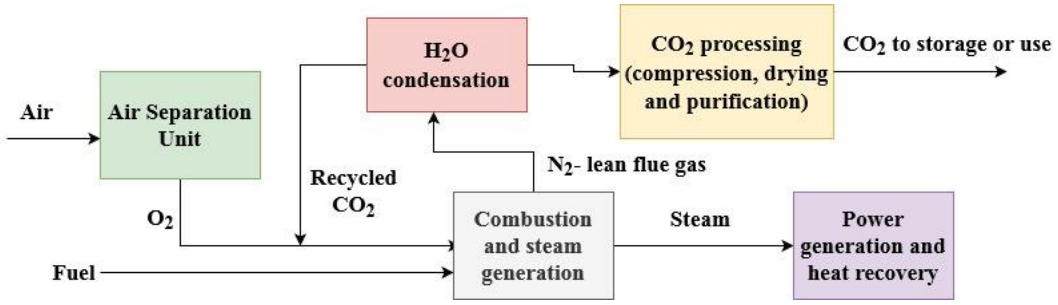

Figure 1.1 Oxy-fuel combustion method for CO_2 removal

1.2.1.2 Pre-combustion

In this process, CO_2 is removed from fossil fuels before combustion is completed. A pre-combustion system involves first converting solid, liquid or gaseous fuel into a mixture of hydrogen and carbon dioxide using gasification processes. In the pre-combustion process, fuel is incompletely combusted in dual presence of steam and air with a requirement of high pressure and temperature. The resulting products form majorly synthesis gas, which is a combination of H_2, CO, CO_2, and CH_4 (relatively small quantities) with varying compositions depending on the type of fuel. The mixture is then led to undergo water-gas shift reaction which results in the conversion of CO and H_2O to H_2 and CO_2 producing a hydrogen and carbon dioxide rich mixture. The composition of CO_2 in the product formed is as high as 15-50 % by volume. The CO_2 so formed is separated from H_2 following which H_2 is subsequently used as a fuel or other applications and CO_2 is sequestrated, stored, or utilized. The process although seems to be very efficient and simple (Figure 1.2) but owing to the high capital cost of gasification processes and the cost incurred to the system while dealing with almost pure hydrogen streams, makes the process less economically viable [10].

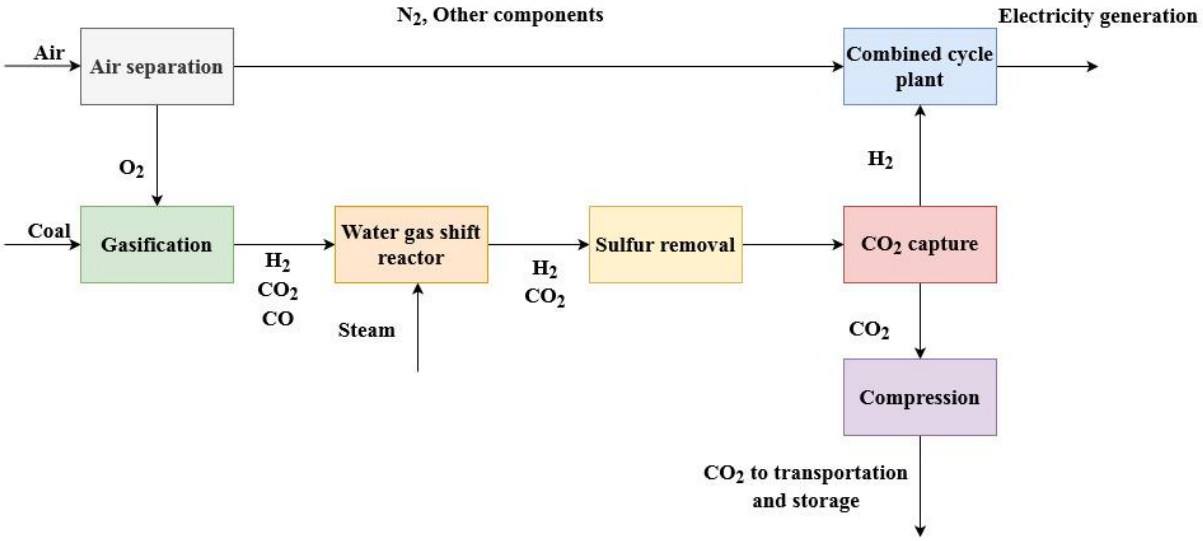

Figure 1.2 Pre-combustion method for CO_2 removal

1.2.1.3 Post-combustion CO_2 capture

Here, the separation of CO_2 from other gases in the flue stack takes place after combustion of the fossil fuel majorly in thermal power plants. As for combustion in spite of oxygen, air is used, hence huge volumes of the hot product gases are required to be dealt with in comparison to oxy-fuel and pre-combustion processes [11]. The detailed block diagram of the process is shown in Figure 1.3.

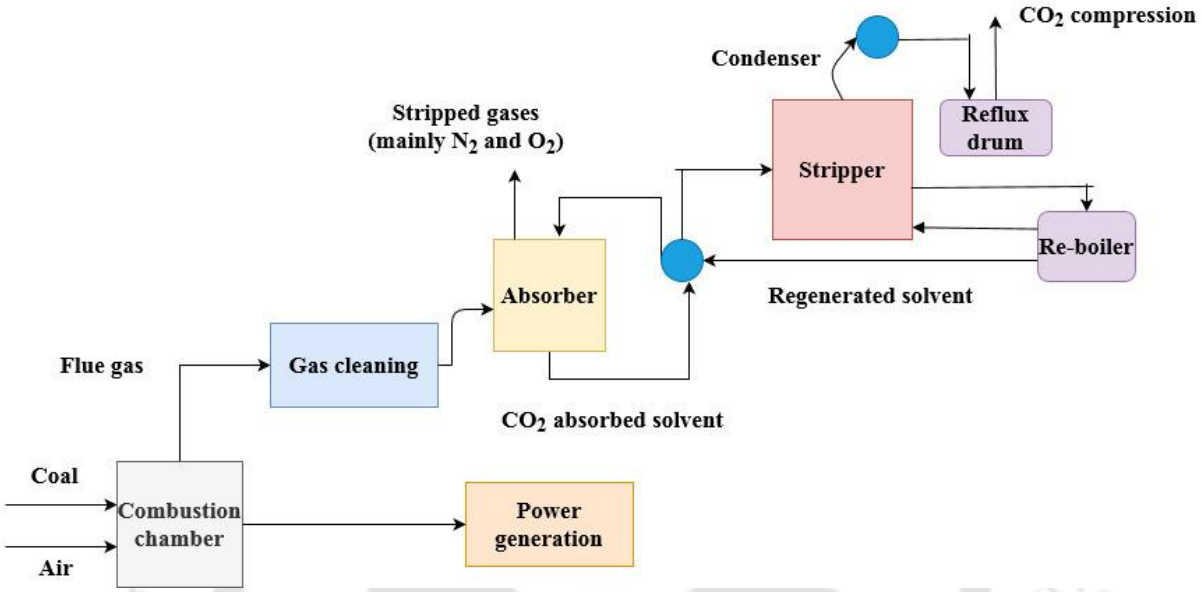

Figure 1.3 Post-combustion method for CO_2 removal

1.3 CO_2 capture technologies: post-combustion

The entire coverage of post-combustion CO_2 capture technologies include a variety of different approaches such as adsorption, physical absorption, chemical absorption, cryogenic separation, membrane separation, micro algae systems, etc. The application of each of the technique highly depends on the suitability of the same in line with the concentration of CO_2 to be separated, the quantities of the flue gas to be dealt with, the impurities or other compounds present in the flue gases, the extent of retrofitting required in the current system of separation, etc. CO_2 separation technologies can be broadly classified as shown in Figure 1.4. Of the many available technologies, chemical absorption using various solvents is widely applied in industries owing to its easy retrofitting nature with the existing system. The brief description and subsequent conditions of applications of each of the technologies are also presented.

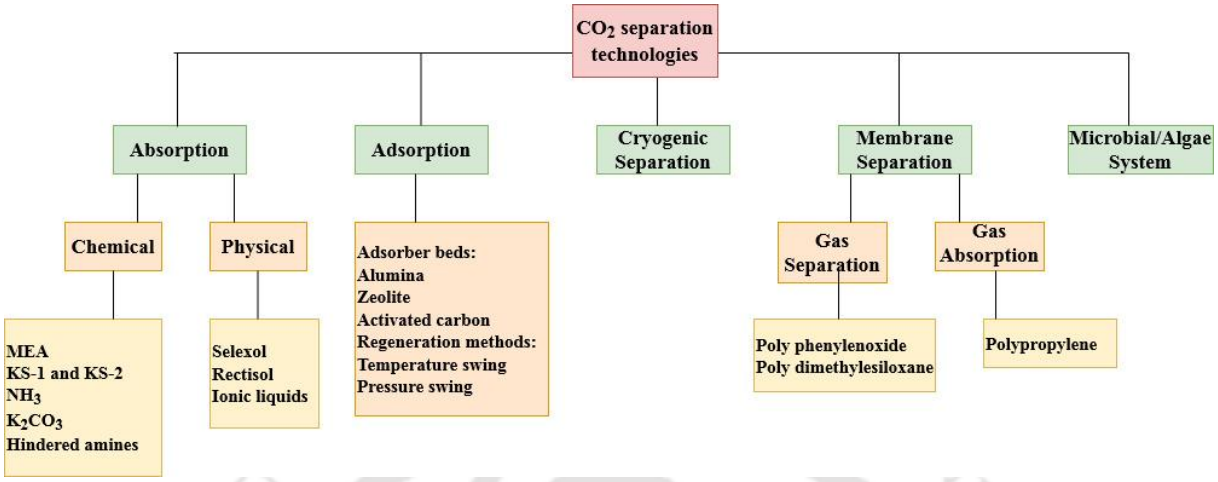

Figure 1.4 Classification of post combustion CO_2 capture technologies (PCC)

1.3.1 Chemical absorption

The absorption and regeneration of CO_2 using a suitable solvent in post-combustion CO_2 capture unit is presented in Figure 1.5. The entity can be observed as a back fit or modernized unit in the existing CO_2 capture unit. Typically, a suitable solvent is used to absorb CO_2 and subsequently, CO_2 is desorbed or regenerated with heat effects followed by its suitable utilization or storage. Usually, one of the most difficult problems of such systems lies in dealing with huge volumes of flue gases. The input and output streams are also integrated with each other usually indirectly in order to utilize the available temperatures of the hot and cold streams. Before the flue gas stream is entered into CO_2 capture/ absorption unit, it is required to pre-clean the flue gas from NO_x and SO_x system if the solvent applied is only efficient for CO_2 capture and the required target is not simultaneous removal of CO_2, NO_x and SO_x. After efficient CO_2 capture, the remaining gases which are not harmful to the environment are released in the atmosphere.

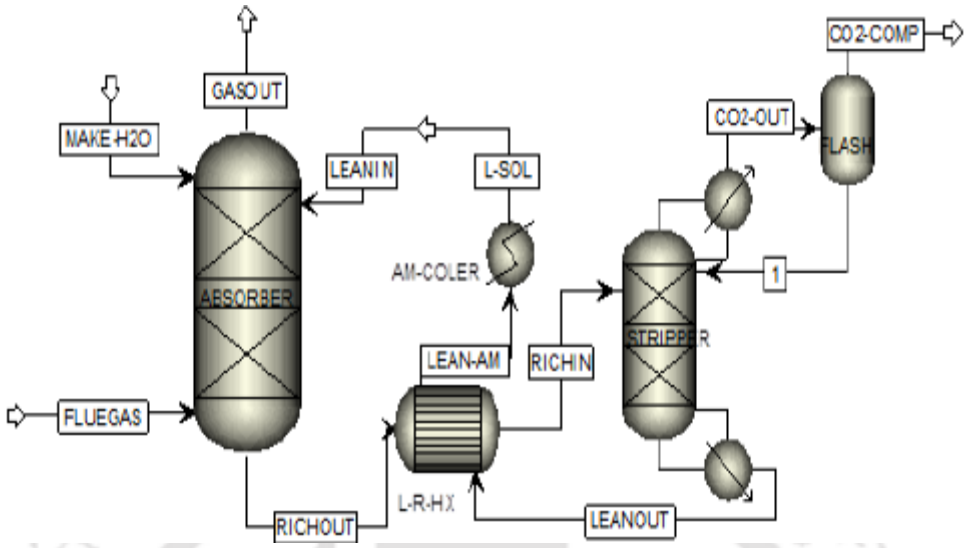

Figure 1.5 CO_2- solvent (amine) absorption technology

1.3.1.1 Chemical absorption using alkaloamines

The most commonly used chemical solvents for the chemical absorption processes are aqueous alkanolamines, aqueous carbonates, etc. Amine-based cyclic regenerative absorption process is one of the potential options for CO_2 capture. Alkanolamines contain both amino and hydroxyl groups, and hence, are suitable as solvents for chemical absorption. The hydroxyl group reduces vapor pressure and increases water solubility, while the amino group provides the required alkalinity in aqueous solution to react with CO_2. Primary amines like monoethanolamine (MEA) and secondary amines like diethanolamine (DEA) have been the most widely employed acid gas treating solvents. However, the drawback of using primary or secondary amines for CO_2 capture is that the reactions of CO_2 with these amines are highly exothermic. As a result, substantial energy input is necessary for the regeneration step to reverse the reaction and strip the CO_2 from the CO_2-rich amines. Besides, these carbamate forming amines have a lower equilibrium capacity for CO_2. In recent years, methyldiethanolamine (MDEA), a tertiary amine, has been used as gas treating solvent because of its low heat of reaction and high equilibrium capacity. However, the MDEA-CO_2 reaction is slow because CO_2 cannot react directly with MDEA. Before reacting with any tertiary or sterically hindered amine, CO_2 must react with water to form

carbonic acid which is a slow reaction. Sterically hindered amines such as AMP and piperazine (a cyclic diamine) belong to a special class of primary/ secondary amines with bulky groups attached to the nitrogen atom of the amine molecule so as to partially shield the amine group from the reacting acid gas [12]. Alternatively, blended amine solvents, which consist of a mixture of a primary/secondary amine with higher reaction rate, and a tertiary/sterically hindered amine with higher equilibrium capacity, can be used to realize the advantage of both. MEA has been blended either with amines that are less corrosive and require less steam to regenerate, or with the additive piperazine (PZ) that is of high reaction rate and higher resistance to thermal degradation and allows the use of lower MEA concentrations.

The post-combustion CO_2 capture studies using amines are focused on the process modeling [13] and economics since the process has already been demonstrated on large scale CO_2 capture from natural gas and syn-gas.

1.3.1.2 Chemical/physical absorption using ionic liquids

Usually, amines are considered for CO_2 absorption owing to the fact that the amine group has a higher affinity to CO_2 in comparison to other groups. However, the regeneration costs of amines are very high and hence solvent recovery for reuse/ recycle becomes expensive and more energy intensive [2]. Due to this, discovery of new solvents which do not compromise on the CO_2 solubility yet which is easy to recover has been a thrust area of research. One such category of solvents explored is ionic liquids.

Ionic liquids (ILs) are organic salts with melting points usually near room temperature, below 100°C. ILs are largely made of ions and short-lived ion pairs. They are liquids at low temperature due to poor packing of respective ions. This poor packing is achieved by making ionic liquids from relatively large, non-coordinating asymmetric ions. At least one of these ions is organic in nature. The choice of the cation has a strong impact on the properties such as stability of the ionic liquid. The chemistry, functionality, and properties such as density and viscosity of the Ionic liquid are in general controlled by the choice of the anion. The cations are usually large, bulky asymmetric organic and the anions are frequently small organic or inorganic structures such as Cl^-, BF_4^-, PF_6^-, NTf_2^-, DCA, etc. ILs are also termed as designer solvents since

a particular cation along with selective anion impacts the various physicochemical or thermal properties such as density, viscosity, conductivity, polarity, etc. ILs find tremendous applications in various applied sciences due to their several advantageous properties naming a few being negligible vapor pressure, non-flammability , tunable polarity high thermal and electrochemical stability and high solvating power and easy recycling. These attributes make them attractive candidate absorbents for CO_2 capture and separation from post-combustion flue gases from coal-fired power plants. Recently, many diverse applications of ILs such as separation processes, extraction processes, homogeneous and heterogeneous catalysts, biological reaction media, treatment of high-level nuclear waste, removing of metal, purification of gases, etc. have been also studied.

The cations are broadly classified as (i) pyridinium (ii) imidazolium (iii) phosphonium and (iv) pyrrolidinium. The other types of ionic liquids are ammonium and sulfonium based ILs. The solubility of CO_2 gas in imidazolium-based ionic liquids is reported to be high in comparison to other ILs [14, 15]. The desorption of CO_2 from ionic liquids requires more thermal energy in case of chemical absorption as compared to physical absorption [16]. Further, the viscosity of ionic liquids is relatively high, about 5-fold higher than that of a conventional aqueous solution of MEA and increases with CO_2 loading, leading to an additional energy penalty in pumping the absorbent [17].

Commonly ionic liquids physically absorb CO_2 selectively over O_2 and N_2 but the physical solubility of CO_2 in the Ionic liquid is too low practically. Hence, to achieve the chemical absorption seen in the amine absorbents but also keep the properties of ILs, an amine group is tethered to the ionic liquid. Studies show that by tethering an amine functional group to the anion such as amino acid on an ionic liquid, one can achieve a one CO_2 to one IL reaction ratio which is twice as much as an aqueous amine or tethering the amine functional group to the cation [14]. But, when amino acid based ionic liquids reacts with CO_2, their viscosity increases significantly making them difficult to use for CO_2 capture.

1.3.2 Physical absorption

In physical absorption, the flue gas is contacted with a solvent which normally does not involve any chemical reaction. Physical absorption is preferred when the CO_2 partial pressure is high (>1.5 MPa) and it is a preferred choice for pre-combustion CO_2 capture which is typically operated near 40 °C [18]. When the CO_2 partial pressure is low, the preferred method is chemical absorption. A brief summary of commonly used physical and chemical solvents for CO_2 removal is presented in Table 1.1. Structural formulas for some important amines for CO_2 capture are presented in Table 1.2. Physical solvents are commercially used to remove CO_2 from natural gas, ammonia synthesis gas and hydrogen. Some commercially used physical solvents include dimethyl ether and polyethylene glycol (Selexol), tetramethylene sulfone (Sulfolane), N-methyl-2-pyrrolidone (NMP) and cold methanol (Rectisol). Due to the low CO_2 partial pressure in flue gas, application of physical absorption for post combustion CO_2 capture is not feasible. In some cases, blends of physical and chemical solvents, known as hybrid solvents, are used to take advantages of high physical solubility and reactivity towards CO_2 offered by physical and chemical solvents, respectively.

Table 1.1 Commercial CO_2 scrubbing solvents used in gas treating industry

Process Type	Solvent	Trade Names
Physical absorption	Chilled methanol	Rectisol
	N-Methyl-2-pyrolidone (NMP)	Purisol
	Dimethylether of polyethylene glycol	Selexol
	Propylene carbonate	Flour solvent
Chemical absorption Organic (amine based)	Monoethanolamine (MEA) (20-35 wt% in water)	SNPA
	Diethanolamine (DEA) (30 wt% in water)	SNPA
	Diglycolamine (DGA) (30 wt% in water)	Econamine
	N-Methyl diethanolamine (MDEA)	Ucarsol HS, SIPM
	Diisopropanolamine	ADIP
	Hindered amine	Flexsorb, KS-1, KS-2
Inorganic	Promoted potassium carbonate	Benfield, Catacarb, Giammarco vetrocoke
Hybrid Solvent	Mixture of MDEA or DIPA, water and tetrahydothiopene dioxide or diethylamine	Sulfinol – M, Sulfinol – D
	Mixture of MEA, DEA, methanol and tetrahydothiopene dioxide or diethylamine	Amisol
	AMP-sulfolane-water	Flexsorb PS
Rate activator	Piperazine	

Table 1.2 Structural formulas for some important amines in CO_2 capture

Class	Name	Structural Formula
Primary amine	Monoethanolamine (MEA)	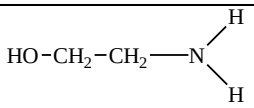
	Diglycolamine (DGA)	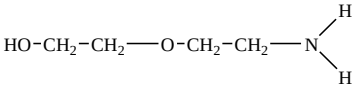
Secondary amine	Diethanolamine (DEA)	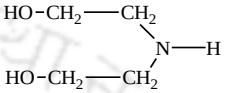
	Diisopropanolamine (DIPA)	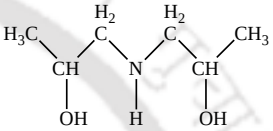
Tertiary amine	Triethanolamine (TEA)	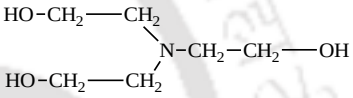
	N-Methyldiethanolamine (MDEA)	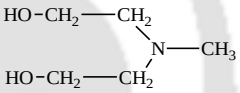
	Dimethylethanolamine (DMEA)	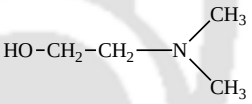
Hindered amine	2-Amino-2-methyl-1-propanol (AMP)	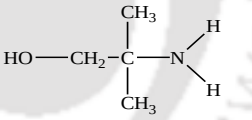
	2-Piperidine ethanol (PE)	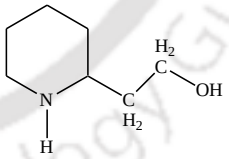

1.3.3 Adsorption using solid sorbents

A number of solid adsorbents, such as activated carbon and zeolites can be used for adsorption of CO_2 from flue gas streams. Examples of commonly used adsorbents are alumina or silica. Recent research is focusing on CO_2 adsorption in amine coated active carbon molecular sieves, metal organic frameworks (MOFs), amine grafted zeolites and supported amine sorbents. Commonly

used reactants along with adsorbents include amines such as polyethylenimine or Na_2CO_3 sorbents to capture CO_2 from flue gas streams. But the implementation of this pathway for CO_2 capture from power plant flue gas is difficult due to the elevated pressure of the adsorption process.

The development of an alternate adsorption based technique for CO_2 capture is mostly driven by the synthesis of novel adsorbent materials which can selectively adsorb reasonable amounts of CO_2 [19]. MOFs are being widely investigated for their potential to efficiently remove CO_2 from process streams. But poor stability towards moisture makes them unrealistic for any practical separation application.

1.3.4 Cryogenic separation

CO_2 can be separated from other gases by cooling and condensation. Cryogenic separation is widely used commercially for streams that already have high CO_2 concentrations (typically > 90%) but it is not used for dilute CO_2 streams [20]. The major disadvantage of this technology is the high energy requirement to provide the needed refrigeration for the process, particularly for dilute gas streams. Another disadvantage is that some components, such as water, have to be removed before the gas stream is cooled, to avoid blockages. Cryogenic separation has the advantage that it enables direct production of liquid CO_2, which is needed for certain transport options, such as transport by ship. Cryogenics would normally be applied to high concentration, high pressure gases, such as in pre-combustion capture processes or oxy-fuel combustion.

1.3.5 Membrane separation

A membrane is a selective barrier between two phases. The molecules or small particles can transport from one phase to the other through the membrane. A CO_2 selective membrane can be utilized in CO_2 separation process for CO_2 capture and to enhance the hydrogen/electricity generation. The selective nature of a membrane can be attributed to one or more of the following mechanisms: (a) Knudson diffusion; (b) surface diffusion; (c) capillary condensation; (d) molecular sieving; (e) solution diffusion; and (f) facilitate transport. Most CO_2 selective membranes are based on either solution diffusion or facilitate transport mechanism since the CO_2 molecule is significantly larger. An amine-based carrier is often used to facilitate the

transportation of CO_2 from the retentate side to the permeate side [21]. As a result, a hydrogen selective membrane can be made of metallic, inorganic (ceramic), porous carbon, polymer, or hybrid materials while most of the CO_2 selective membranes for separating CO_2 from hydrogen are polymeric. The desirable features of a membrane include good permeability, selectivity, reliability, and tolerance to contaminants. For commercial applications in gasification processes, it should also be affordable, thermally stable, and durable. Of all the H_2-selective membranes, metallic membranes, and ceramic membranes are the most extensively studied. The metallic H_2-selective membranes generally have very high selectivity and thermal stability. The potential candidates include palladium, platinum, tantalum, niobium, and vanadium.

Although it is still in the developmental stage, gas separation membranes can be used for removing CO_2 from flue gas streams. There are many different types of gas separation membrane, including porous inorganic membranes, polymeric membranes that are used for separation of the gas mixture. Another type of membrane is being developed, called an absorption membrane. These membranes are impregnated with a liquid that selectively reacts with CO_2. The membrane separation process has certain advantages. It has no moving parts. Its other advantages are its modularity, small footprint, and no regeneration energy requirement. Current membranes are either not selective enough towards CO_2 or not permeable enough, hence, cannot usually achieve high degrees of separation, so multiple stages and/or recycling of one of the streams is necessary. This leads to increased complexity, energy consumption, and costs. More recently, some researchers have focused on developing hybrid processes in which membrane separation is combined with another separation process such as chemical absorption. However, further development is needed before membranes could be used on a large scale for CO_2 capture from in power plant flue gas streams.

Polymer membranes have been used successfully in a number of industrial applications, including the production of high-purity nitrogen, gas dehydration, and recovery of hydrogen from process streams for recycling. However, successful use of a polymer membrane in post-combustion CO_2 capture process requires a membrane that is thermally, chemically, and mechanically stable at high temperatures. Unfortunately, the commercially available polymeric materials currently employed are not stable in such demanding environments to the degree

required. The current commercial membrane has CO_2/N_2 separation factors of around 18-19 and work at relatively low temperatures. The process design study has to explore at this stage the interplay between the operational energy requirement and cost of installation for a set of data. Any increased energy requirement for the capture process will indeed increase the secondary CO_2 emission, which has obviously to be minimized. Thus, the energy efficiency of a capture process is a key issue.

CO_2-facilitated transport membrane can achieve high selectivity and permeability based on the reversible reaction of the target gas with the active carrier incorporated into the membrane. Hence, the use of novel amine carriers for the synthesis of CO_2-selective thin-film membrane is an attractive option for post-combustion CO_2 capture.

1.3.6 Microbial /algae system

Theoretically, to convert CO_2 in fixed carbon, photosynthesis is still one of the powerful tools for the safe and viable sequestration route of CO_2. Along with land plants, recently a variety of microalgae have been studied for the efficient CO_2 capture [22]. Studies reveal that the carbon fixation rates of such microalgae systems is an order of magnitude higher than the land plants. Although, microalgae culturing is expensive since it necessitates the maintenance of proper temperature and available nutrients requirements but such microalgae is also being studied for the production of high-end value products making the entire system of CCUS cost effective. A simple process for carbon dioxide sequestration using photosynthetic microalgae is shown in Figure 1.6. As specified in the figure, a photo bioreactor is used for developing the microalgal culture at the designed temperature of the system. The major benefit of such a system for sequestrating CO_2, purification of CO_2 is not required and any available SO_x or NO_x in the flue gas, in turn, will be consumed as a nutrient by the culture thereby increasing the overall yield and quality of the algal product. This will shorten the CO_2 separation process from the flue gas and hence can make the overall CCUS more cost effective.

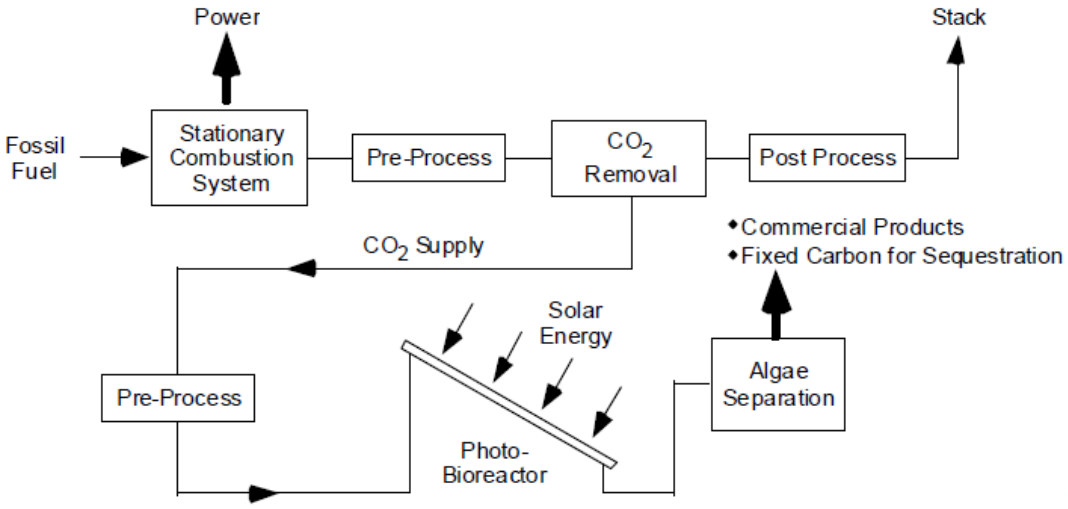

Figure 1.6 A general idea for a microalgae-based CCUS system

1.4 Literature review

The application of ionic liquids for CO_2 capture has been studied extensively along with amine technology over the past decade. Though amines have higher CO_2 loading capacities in comparison to either ionic liquids or physical solvents, the disadvantage of corrosive products, high regeneration energies, etc. still is a question for the application of the same. The usage of any solvent for CO_2 capture industrially depends on many factors such as the available data of CO_2 solubility, physiochemical properties, kinetics of the reactions involved, etc.

1.4.1 CO_2 absorption in a single ionic liquid

The vapor-liquid equilibrium data for single pure ionic liquids studied in the literature is reviewed and presented in Table 1.3 [23-39]. Some of the generalized aspects found while studying the CO_2 solubility in pure ionic liquids is discussed in the present section. Room temperature ionic liquids (RTILs) can be defined as liquid organic salts composed of organic cation and either an inorganic or organic anion and the same are widely studied for the application of CO_2 capture. Many of the ionic liquids are stable above 400 ^oC [34, 40]. Ionic

liquids are also called as tailoring solvents where the choice of the cation and the anion constituting an ionic liquid can be changed according to the desired properties of viscosity, density, conductivity, and polarity. The selection of an appropriate IL for a particular application would require a comprehensive database of the fundamental properties like stability, density, miscibility, viscosity, and polarity of ionic liquids over a wide range of temperature and pressure. Although CO_2 solubility in traditional ILs are relatively low under ambient conditions compared with the amine based absorbents, but they are explored due to their advantages over amines. Ionic liquids offer both physical and chemical absorption depending on the nature of the constitutive ions of the specific ionic liquid utilized and how these interact with the molecules of CO_2. Although the absorption capacity of ionic liquids that absorb chemically is low but the reversibility of the process will be simpler and more economically favored if the ILs absorb physically [41]. If ILs are used as physical absorbents to develop CO_2 capture process, it is economical to operate the absorber at a relatively lower temperature and pressure. Hence, designing ILs with a higher physical absorption capacity of CO_2 is of great interest these days. Usually, the long alkyl side chains are attached to the cations. This long side chain is assumed to expand the free volume and increase CO_2 absorbed in the space. Hence, it can be assured that a high CO_2 absorption capacity is majorly dictated by the length of cation. If the alkyl chain is very long, then the interaction between cation and anion is weak and hence the interaction between cation and CO_2 becomes strong which leads to an increase in CO_2 absorption in other words, the weak interactions between cation and anion is more conducive for CO_2 absorption [14, 42, 43]. The general cations for ionic liquids being Pyridinium, Imidazolium, Phosphonium, Pyrrolidinium, Ammonium, Sulfonium, etc. Of the many, imidazolium based ionic liquids are majorly studied for the absorption of CO_2 due to comparatively high CO_2 solubility because of the presence of imidazole group which attracts the CO_2 molecule and ease of synthesis [44]. However, tar formation and reactivity at the acidic C_2 site are some of the drawbacks of using imidazolium salts. Pyridinium and Pyrrolidinium based ILs which are considered to be more easily biodegradable and cheaper in comparison to imidazolium based are also recently explored for the application of CO_2 capture [41]. In comparison to imidazolium based ionic liquids, Phosphonium based ILs have proven to provide even better CO_2 solubility with the same anion [27]. Phosphonium based ionic liquids are more resistant to reactions with bases and hence

choosing a blend of Phosphonium based IL with other amines, amine activator, or amino acid salt may prove to result in higher CO_2 solubility. Sulfonium based ILs however have not yet been reported in the literature for CO_2 capture. Fluorinated anions have a favorable interaction with CO_2 e.g. ILs with $[BF_4]$ and $[PF_6]$ as anions irrespective of cations offer better CO_2 solubility. This is due to the fact that fluorinated based anions offer higher basicity being a strong base. However, the interaction between CO_2 and $[BF_4]$ anion should be stronger than that for the $[PF_6]$ anion since $[BF_4]$ is a stronger base. But research indicate that [bmim] $[PF_6]$ have higher solubility for CO_2 than [bmim] $[BF_4]$. Hence, solubility cannot be solely explained by anion-CO_2 interactions. A free volume mechanism plays an important role in this. CO_2 favorably is assumed to be organized around the $[PF_6]$ anions [45]. The CO_2 absorption using pure ammonium based ionic liquids has been studied and reported elsewhere [39, 46]. It can be observed from literature findings that CO_2 solubility in 2-hydroxy ethyl ammonium formate (HEF) and 2-hydroxy ethyl ammonium acetate are better compared to other ammonium based ILs [46]. The maximum solubility of CO_2 in HEF was found to be x_{CO2}= 0.3083, where x_{CO2} is the mole fraction of CO_2 in the liquid phase.

Generally, the absorption of CO_2 in ionic liquids is physical for which high pressure is needed and hence the absorption capacity is low because CO_2 will be attached to the ILs with weak vander Waals forces of attraction. CO_2 is absorbed by occupying the free space between the ions [44]. For achieving a high CO_2 solubility in IL, the input CO_2 stream should be preferably at low temperature and very high pressure. However, the flue gas CO_2 partial pressure is usually less than 10 % of feed pressure. The performance of IL in absorbing CO_2 can be improved by incorporating an amine functional group in the structure of the IL to produce a kind of task-specific ILs (TSILs) for CO_2 capture. General amines used for functionalization of ionic liquids are simple amino acids with only carboxylate and amino functional groups, MEA, etc. These functionalized ILs show high CO_2 solubility and reversible interactions with CO_2. From an energy point of view, it would be interesting for functionalized ILs to interact with CO_2 through weak interactions so that the succeeding regeneration of the absorbent can be attained with low energy input. This would allow the ILs to outperform conventional amine based absorbents. Tethering of amine functionality to either cation or anion is usually achieved for functionalization of ILs. Bates et al. [47] functionalized 1-butyl imidazole group with a bromine

based primary amine to form a better ionic liquid having higher CO_2 capacity. The results indicated that newly synthesized IL has 0.5 mol of CO_2 per mol of solvent and thermally stable to go through five absorption and regeneration cycles without loss of solvent efficiency. However, sometimes the associated hydrogen bonds of $–NH_2$ can lead to an increase in the interactions amongst the anion and cation which subsequently results in limiting the interaction with the CO_2. Xue et al. [44] also investigated CO_2 absorption capacity of a dual functionalized imidazolium cation occupied by a taurine anion. The results indicated that the resultant IL exhibited 0.9 mol of CO_2 per mol of IL at ambient pressure and 303.15 K. Following which at higher pressures the CO_2 solubility of the resultant functionalized IL may result quite competitive to conventional amines. Goodrich et al. [48] synthesized six Phosphonium based anion-tethered ILs where functionalization was achieved using amino acid. All the synthesized ILs suggested to exhibit more than 0.5 mol of CO_2 per mol of solvent at 295.15 K. The results also indicated carbamate formation similar to the reaction between amines and CO_2. But the synthesis of these amine functionalized ILs requires several synthetic and purification steps and is not cost competitive as compared to conventional alkaloamines such as MEA [49]. The usual models applied for co-relation of CO_2 solubility in pure ILs are various Equation of State (EoS) models such as Peng-Robinson, Soave Redlich Kong, etc.

Table 1.3 Summary of the literature review for CO_2 solubility measurements in different pure ionic liquids

Sr. No.	Ionic liquid	Temperature (K)	Pressure (kPa)	X_{CO2}	Reference
1	[bmim] [tcm]	288.2-353.2	94 -1993	0.0082-0.3725	[23]
2	[dmim][$MeSO_3$]	332.9-363.7	1650-43100	0.0629-0.369	[24]
3	[emim][$MeSO_3$]	302.3-342.7	400-46150	0.0556-0.4518	[24]
4	[bmim][$MeSO_3$]	302.4-342.9	550-5750	0.0517-0.2482	[24]
5	[dbim][$MeSO_3$]	302.5-343.2	3250-35700	0.2941-0.5219	[24]
6	[hmim][TCB]	283.6-364.0	271-11086	0.1009-0.7016	[25]
7	[P (14)666][TMPP]	298.0-324.0	1021-3402	0.314-0.595	[26]
8	[P4444][TMPP]	314.0-334.0	1253-3695	0.242-0.495	[26]
9	[P8111][TMPP]	299.0-324.0	1068-3258	0.240-0.510	[26]
10	[P(14)666][DCA]	298.0-323.0	792-3229	0.202-0.527	[26]
11	[THTDP][NTf_2]	292.9-363.4	106-72185	0.169-0.879	[27]
12	[THTDP][Cl]	303.3-363.7	164-24570	0.119-0.800	[27]
13	[TDC][DCN]	313.2-333.2	10.1-1900.7	0.00175-0.2720	[28]
14	[emmp][Tf_2N]	313.2-333.2	9.8-1900	0.00182-0.3165	[28]
15	[TDC][Tf_2N]	313.2-333.2	9.7-1899.8	0.0023-0.36	[28]
16	[BMP][TfO]	303.2-373.4	1880-70200	0.2583-0.7058	[29]
17	[emim][TFO]	303.9-344.6	800-37800	0.2613-0.6268	[30]
18	[hmim][TFO]	303.9-344.6	1250-36300	0.3566-0.7171	[30]
19	[omim][TFO]	303.9-344.6	680-34000	0.2166-0.7414	[30]
20	[hmp][Tf_2N]	303.2-373.2	1060-47550	0.2778-0.8105	[31]
21	[omp][Tf_2N]	303.2-373.2	510-35920	0.2409-0.8176	[31]
22	[hemim][BF_4]	303.2-353.2	114-1194	0.004-0.102	[32]
23	[bmim][ac]	283.2-348.2	10-1999	0.063-0.455	[33]
24	[bmmim][PF_6]	283.2-323.2	9-1300	0.00926-0.219	[34]
25	[h3mp][Tf_2N]	283.2-323.2	7-1300	0.00958-0.376	[35]
26	[Bu3MeP][TOS]	323.1	50-1300	0.00611-0.121	[36]
27	[emim][PF_6]	308.1-366.0	1490-97100	0.104-0.619	[37]
28	[omim][BF_4]	307.8-363.3	571-85800	0.1005-0.7523	[38]
29	[HEA]	313.2-328.2	124-1542	0.0034-0.01364	[39]
30	[BHEAA]	313.2-328.2	126-1505	0.0081-0.08530	[39]
31	[BHEAL]	313.2-328.2	121-1598	0.0036-0.0718	[39]
32	HHEMEA	313.2-328.2	134-1516	0.0024-0.0515	[39]
33	HHEMEL	313.2-328.2	158-1562	0.0029-0.0605	[39]

1.4.2 CO_2 absorption in blended ionic liquid solvents

Practically, it's hard to find or synthesize a novel pure IL with all optimal properties for its intended use. Inclusively, functionalization of ILs being very expensive to be achieved on a large scale with the purity required. Hence, in order to combine both the benefits of high CO_2 solubilities of amines and better solvent properties of ILs, one of the strategies is to utilize binary or ternary mixtures of ILs with amines or amine activators. The key purpose for using these hybrid solvents is to merge the eco-friendly features of ILs with the high binding capacity of amines. Therefore, by mixing high priced and high viscous targeted ILs with low priced and less viscous selective amines, a huge amount of workable hybrid solvents could be synthesized. Combining the advantages of alkanolamine with those of ILs might provide a better route to CO_2 capture technologies. A comprehensive literature review of blended ILs is presented in Tables 1.4 and 1.5.

Table 1.4 (a) Summary of the literature review for CO_2 solubility measurements in different blended ionic liquids

Sr. No.	Blend	Temperature (K)	Pressure (kPa)	Concentration of solvents	X_{CO2}	Reference
1	aq. [P (14)666][TMPP]	298.0-323.0	870-3973	90-95 wt % [P(14)666][TMPP]	0.092-0.432	[26]
2	[P (14)666][TMPP] + [BHMIM][Ac]	298.0-323.0	514-2897	50-80 wt % [P(14)666][TMPP] 20-50 wt % [BHMIM]Ac]	0.095-0.487	[26]
3	$[C_2py][EtSO_4]$+$[C_2mim][NTf_2]$	298.2	100-1620	0-100 wt % $[C_2py][EtSO_4]$	0.0020-0.1174	[42]
4	$[emim][Tf_2N]$ + ethanol	313.2-333.2	610-6200	0-100 wt % $[emim][Tf_2N]$ 0-100 wt % ethanol	0.028-0.715	[50]
5	aq. MDEA + [bmim][Ac]	323.2	122-3859	30-40 wt % MDEA 0-10 wt % [bmim][Ac]	0.0447-0.0878	[51]
6	aq. DEA + [bmim][Ac]	323.2	137-3828	30-40 wt % DEA 0-10 wt % [bmim][Ac]	0.042-0.0905	[51]
7	aq. DIPA + [bmim][Ac]	323.2	157-3859	30-40 wt% DIPA 0-10 wt % [bmim][Ac]	0.0384-0.0768	[51]
8	aq. AMP + [bmim][Ac]	323.2	133-3833	30-40 wt% AMP 0-10 wt % [bmim][Ac]	0.0651-0.1128	[51]
9	aq. MDEA + [gua][FAP]	313.2-353.2	69-3040	2-4 M MDEA 0.1-2.0 G [gua][FAP]	0.013-0.064	[52]
10	aq. MDEA + $[bmim][BF_4]$	303.0-333.0	100-700	4 M MDEA 0-2 mol/l $[bmim][BF_4]$	0.035-0.190	[53]
11	aq. MDEA + [bmim][Ac]	303.0-333.0	100-700	4 M MDEA 0-2 mol/l [bmim][Ac]	0.035-0.204	[53]
12	aq. MDEA + [bmim][DCA]	303.0-333.0	100-700	4 M MDEA 0-2 mol/l [bmim][DCA]	0.038-0.185	[53]
13	aq. MEA + $[bmim][BF_4]$	303.1-323.1	49.8-1500.1	29.3 wt % MEA 70.7 wt % $[bmim][BF_4]$	0.079-0.242	[54]
14	aq. MEA + DEA + $[bmim][BF_4]$	303.2-323.1	49.8-1500.1	33 wt % MEA 16.2 wt % DEA 50.8 wt % $[bmim][BF_4]$	0.096-0.170	[54]

Table 1.4 (b) Summary of the literature review for CO_2 solubility measurements in different blended ionic liquids

Sr. No.	Blend	Temperature (K)	Pressure (kPa)	Concentration of solvents	X_{CO2}	Reference
15	aq. MEA + DEA + [bmim][BF_4]	303.2-323.1	49.9-1500	31.8 wt % MEA 12.1 wt % DEA 56.1 wt % [bmim][BF_4]	0.196-0.273	[54]
16	aq. MEA + MDEA + [bmim][BF_4]	303.1-323.1	49.8-1500.1	31.6 wt % MEA 10.4 wt % MDEA 58 wt % [bmim][BF_4]	0.143-0.272	[54]
17	aq. MEA + MDEA + [bmim][BF_4]	303.2-326.5	49.8-1500.2	30.3 wt % MEA 21.8 wt % MDEA 48 wt % [bmim][BF_4]	0.080-0.274	[54]
18	aq. MEA + DEA + MDEA + [bmim][BF_4]	303.2-323.2	49.8-1500	29.8 wt % MEA 11.7 wt % DEA 12.8 wt % MDEA 45.7 wt % [bmim][BF_4]	0.118-0.228	[54]
19	aq. MDEA + [bmim][Ac]	303.2-343.2	168.9-3871.1	0.3-0.5 wt % MDEA 0.5-0.7 wt % [bmim][Ac]	0.057-0.411	[55]

Table 1.5 Summary of the literature review for CO_2 solubility measurements in different blended ionic liquids

Sr. No.	Blend	Temperature (K)	Pressure (kPa)	Concentration of solvents	α_{CO2}	Reference
1	aq. MDEA + [N1111][Gly]	298.2- 318.2	0-300	10-100 wt % [N1111][Gly] 0-40 wt % MDEA	0.1-1.1	[56]
2	aq. MDEA + [bmim][BF_4]	303.0-333.0	40-100	4 M MDEA 0-2 mol/l [bmim][BF_4]	0.19-3.27	[57]
3	aq. MDEA + PZ + [bmim][Otf]	303.2-313.2	185-4978	30 wt % MDEA 30 wt % PZ 0-20 wt % [bmim][Otf]	0.567-2.217	[58]

It can be seen from Tables 1.4 and 1.5, that the imidazolium based ILs have been explored much in the literature for CO_2 capture. This is owing to the reason of high influence of anion (majorly PF_6, BF_4, etc.) on the diffusion of CO_2 around the imidazolium ring. The CO_2 loading in pure [bmim] cation based ILs increases in the following order: [NO_3] < [DCA] < [BF_4] < [PF_6] < [TfO] < [Tf_2N] < [methide] at 298 K [14, 34, 40]. Aqueous primary, secondary, ternary and sterically hindered amines have been studied well by the researchers [51-55] giving a concluding remark that increasing the amine concentrations in the solvent shall result in high CO_2 solubility. Blending two appropriate ILs which yield higher CO_2 solubilities can also be proposed for the desired application. Pinto et al. [41] studied binary mixtures of the ILs [C_2C_1im] [NTf_2] and [C_2C_1im] [$EtSO_4$]. [C_2C_1im][NTf_2], which is having the highest physical absorption is expensive and toxic but [C_2C_1im] [$EtSO_4$] is cheap, less toxic, and non-fluorinated. Other blends proposed by the same author were [C_2C_1im] [NTf_2] + [C_2C_1im] [$EtSO_4$] and [C_2C_1im] [NTf_2] + [C_4C_2im] [$EtSO_4$]. In addition to CO_2 absorption, the authors also provided a well-structured thorough physical and thermal characterization of the studied blends suggesting the blends provided better solvent properties in comparison to single ILs. One of the major drawbacks which can be concluded from their studies is the higher viscosity of the blended solvents which will make the overall pumping cost of the solvents to be high.

Ahmady et al. [53] studied the absorption of CO_2 in 4 mol/L aq. MDEA + 3 ionic liquids ([bmim][BF_4]), ([bmim][Ac]) and ([bmim][DCA]) as a function of temperature, CO_2 partial pressure and concentration of ionic liquid concentration of 303 to 333 K, 100 to 700 kPa and 0 to 2 mol/L, respectively. The CO_2 loading in the studied mixtures decreases with an increase in temperature and ionic liquid concentration and increases with an increase in the CO_2 partial pressure, at a given temperature. CO_2 loading was observed to be 1 mol/kg for aqueous 4 M MDEA + 2 mol/l [bmim] [BF_4] in comparison with 0.056 mol/kg for pure [bmim] [BF_4] at 100 kPa and 323 K. Afzal et al. [26] studied the effects of addition of water and 1-butyl-3-H-imidazolium acetate in various phosphonium based ILs over a wide temperature and pressure range. It can be inferred from their studies that on additions of water or [bhmim][Ac], the overall solvent is less viscous and provides better CO_2 solubility with the highest being recorded for 0.487 mole fraction of CO_2 in 20 wt% [bmim][ac] and 80 wt % [P(14)666][TMPP] at 2.5 MPa. In addition to aqueous, non-aqueous systems of binary absorbents of amines MEA and MDEA

with four synthesized ILs viz. [bmim][BF_4] , [beim][BF_4], [bpim][BF_4] and [bbim][BF_4] were studied over a temperature range of 298-348 K by Xiao et al. [59]. It was concluded from their work that the increase in carbon chain length in cation results in higher thermal stability and higher CO_2 loading. Along with physical absorption, chemical reactions of ILs with CO_2 have been proved to follow the carbamate formation route in the literature [33, 34, 59].

In addition to aqueous or non-aqueous amines, various other kinds of additives have also been studied in the literature. For instance, Zhang et al. [60] studied the effect of addition of different kind of surfactants X-100, TWEEN 80 and PEG 400 with ILs [bmim] [PF_6], [emim] [OTf], [bmim] [OAc], [hmim] [NTf_2] and [bmim] [BF_4]. Aqueous [emim] [OTf] blended with TWEEN 80 was found to provide CO_2 solubility of 0.798 mol/l under atmospheric conditions along with several other advantages such as low cost, better reproducibility, low viscosity and a better regeneration. The major focus of their studies was on the reduction of viscosity and surface tension of the ILs using variety of surfactants. Mirarab et al. [50] also studied the effect of addition of ethanol in [emim] [Tf_2N] at (313.2-333.2) K and pressure range of 0-7 MPa. They stated that while increasing the concentration of ethanol in the solution, although CO_2 solubility decreases but the viscosity also drops down thereby contributing less to the pumping of the solvents in the regeneration and absorption towers. The equilibrium data obtained by them were correlated with Peng-Robinson equation of state and an artificial neural network model.

Another category of solvents that are considered to have better solvents properties similar to ILs such as thermal stability but are low in cost, are physical solvents which also has been studied extensively in literature either by experimentation or through simulation for CO_2 capture [61-63]. If the concentration of CO_2 is high in the flue gas stream, the efficiency of CO_2 capture using physical solvents is high. Physical solvents have been studied either pure, or in blends with amines to enhance their CO_2 solubility. A brief summary of such physical solvents in presented in Table 1.6 [64-73].

Table 1.6 Literature summary of CO_2 solubility in pure and blended physical solvents

Sr. No.	Blend	Temperature (K)	Pressure (kPa)	Concentration of solvents	α_{co2}/ X_{CO2}	Reference
1	aq. $TMSO_2$	328.2-393.2	189-3666	10-20 wt% $TMSO_2$	X_{CO2}=0.0002-0.0143	[64]
2	aq. $TMSO_2$ +MDEA	328.2-393.2	62-3593	20 wt % $TMSO_2$, 30-40 wt% MDEA	X_{CO2}=0.003-0.118	[64]
3	aq. $TMSO_2$ +MDEA	328.2-363.2	42.5-1157.1	10-20 wt % $TMSO_2$, 30-40 wt % MDEA	X_{CO2}=0.014-0.098	[65]
4	aq. $TMSO_2$	303.2-353.2	86-1328	9.99 -46.92 mol % $TMSO_2$	X_{CO2}=0.0008-0.0403	[66]
5	aq. (AMP + $TMSO_2$)	313.2-373.2	2.86-193	8.2 -30.6 wt % AMP 19.4-41.2 wt % $TMSO_2$	α_{co2}=0.035-1.0	[67]
6	$TMSO_2$ + DEA	303.2-373.2	15.5-2296.8	50 wt % $TMSO_2$ 50 wt % DEA	X_{CO2}=0.166-0.282	[68]
7	$TMSO_2$ + MEA	303.2-373.2	1.5-2210.5	15-30 wt % MEA	X_{CO2}=0.059-0.282	[69]
8	NMP	298.2-373.2	184.8-1438.5	100 wt % NMP	X_{CO2}=0.0105-0.2048	[70]
9	$TMSO_2$	298.2-373.2	81.2-2263.4	100 wt % $TMSO_2$	X_{CO2}=0.0056-0.2106	[70]
10	PC	298.2-373.2	54.7-2228.7	100 wt % PC	X_{CO2}=0.0056-0.2343	[70]
11	$TMSO_2$ + MEA	303.2	62.8-1822.4	15 wt % MEA	X_{CO2}=0.108-0.2169	[71]
12	$TMSO_2$+DEA	303.2	128.7-2043.9	15 wt % DEA	X_{CO2}=0.0742-0.2224	[71]
13	aq. $TMSO_2$ + MDEA + PZ	313.0-333.0	2.067-1355.411	42-48 wt % MDEA 2-8 wt % PZ 10 wt % $TMSO_2$	α_{co2}=0.1079-1.21163	[72]
14	$TMSO_2$	303.2-363.2	11.84-2326.1	100 % $TMSO_2$	α_{co2}=0.076-1.472	[73]

Recently, the applications of silated single component reversible ionic liquids such as (3-aminopropyl)-trimethoxysilane (TMSA), (3-aminopropyl)-triethoxysilane (TESA), (3-aminopropyl)-triethylsilane (TEtSA), and (3-aminopropyl)-tripropylsilane (TPSA) towards energy especially CO_2 capture has gained attention either via absorption or adsorption. This is due to the fact that they require less energy for regeneration and provide a stable intermediate route for CO_2 capture [74]. They are proved to be competitive solvents for CO_2 absorption. Pure ionic liquids and physical solvents hence can be considered for CO_2 capture provided that the CO_2 input stream is at high pressures and low temperatures. It would be hence suggested from the literature that blended ILs and physical solvents along with either conventional amines or amine activators should be used for CO_2 capture from power plants. As many of the conventional amines such as MEA, DEA, MDEA, etc. either have a low CO_2 equilibrium capacity or have a lower rate of absorption, it is also suggested that amine activators which tend to solve the problems associated with the traditional amines would be pertinent.

Pertaining to this a brief analysis of the various amine activators proposed by leading researchers in the CO_2 capture field as discussed further.

1-(2-Aminoethyl) piperazine (AEP), a piperazine derivative has been studied as a rate activator for CO_2 absorption [75]. At high CO_2 loading and low absorption temperature, AEP does not precipitate, unlike PZ. Also, aq. (PZ + AEP) system [76] indicate that the formation of nitrosamine is very less when compared to aq. PZ solution. Besides, AEP also has all the three major functional groups of primary, secondary and tertiary amines dictating its high CO_2 solubility in comparison to PZ. It is also having several advantages such as lower vapor pressure, high boiling point and preferably good solubility in water. In comparison to the alkyl or hydroxyl group, if the substitution occurs on the amine group in saturated amine results in rise in CO_2 absorption rate and solubility extensively [77]. Studies on the cyclic capacity and model parameter estimation using e-NRTL model for aq. (PZ + AEP) have been reported in the literature [78]. The cyclic capacity of (5 + 2) mole of (PZ + AEP) system was found to be 0.86 $mol.kg^{-1}$ which is quite higher in comparison to 7 mole of MEA i.e. 0.5 $mol.kg^{-1}$. Furthermore, analysis of the physiochemical properties and kinetic rate parameters for AEP-CO_2 reactions are also reported in the literature [75]. The results suggested a very high reaction second order rate

constant of 5.6354×10^4 $m^3.kmol^{-1}s^{-1}$ at 313.2 K. Recently, the enhancement of CO_2 absorption in aq. MDEA and AMP by addition of AEP have also been reported [79,80].

A potential activator for CO_2 absorption has been reported recently by many researchers [81, 82] blended with various conventional tertiary and sterically hindered amines. The kinetics of APA-CO_2 reaction in aqueous conditions where the second order reaction rate constant is reported to be 3.5775×10^4 $m^3.kmol^{-1}s^{-1}$ at 303.2 K which is relatively very high in comparison to aqueous MEA or PZ. The molecular structural analysis of APA also suggests that it consists of two primary and one secondary amino groups which has a huge contribution for CO_2 equilibrium solubility as well as rate of the reaction.

Another potential activator which is studied recently is polyamines such as TETA, TEPA, DETA, and EDA for their capabilities to enhance the CO_2 absorption rates in aqueous MDEA [83]. The results indicated that TEPA is a better promoter to aq. MDEA in comparison to other polyamines due to the fact that TEPA has the highest secondary and primary amine groups. Alternatively, other piperazine based potential solvents such as 1-MPZ and 2-MPZ have gained importance in the recent times. The highest CO_2 loading capacity for 4 m piperazine + 4 m 2-MPZ was concluded to be 0.84 mol of CO_2 / (kg amine + H_2O) which is reasonably competitive with the traditionally used aqueous amines. Similar studies of PZ/2-MPZ have also been reported in the literature [84-87]. 2-MPZ and PZ have also been investigated as promoters for conventional solvent i.e. potassium carbonate and the results evaluated disclose its capacity to increase the equilibrium CO_2 solubility as well as rate of the reaction [88].

The major application of the literature study indicates that AEP, APA, and 2-MPZ may prove to be a promoter for CO_2 equilibrium solubility for aqueous or non-aqueous solutions of ionic liquid, physical solvents or tertiary amines.

1.5 Importance and objectives of this work

From the preliminary discussion and literature survey it is apparent that for the design of CO_2 capture units, various experimental and simulation studies are a major requirement. Essentially, amine based technology is still being implemented at a larger scale. Amine technology faces several economic and environmental issues as discussed in earlier sections. The major problems

being low CO_2 partial pressure in the flue gas streams and the high volume of the flue gas streams required to be treated for CO_2 removal. This requires the usage of a solvent, which reacts at a fast pace, produces non-corrosive or less-corrosive products of reaction, thermal stability, and economically viable. Alternatively, combination of various amine activators with non-traditional physical solvents, ionic liquids and reversible ionic liquids are proposed here as an option which can solve many challenging issues.

The principal objective of the present work is to analyze the applicability of various energy-efficient solvents for CO_2 capture.

To accomplish this objective, the following work has been commenced for various blends of aqueous and non-aqueous amines, physical solvents, and ionic liquids activated by amine activators such as AEP, APA and 2-MPZ.

- Measurement of equilibrium solubility data of CO_2 in ([bmim] [Ac] +H_2O), ([bmim] [Ac] + H_2O +AEP), ([bmim] [Ac] + H_2O +APA), (TESA + H_2O), (TESA + H_2O + AEP), (TESA + H_2O + APA), (MDEA + H_2O + 2-MPZ) , ($TMSO_2$ + H_2O + 2-MPZ) ,and ([bmim [Ac] + H_2O + 2-MPZ) varying the solvent composition over the temperature range of (303.2 to 323.2) K and CO_2 partial pressure up to 400 kPa.

- Analysis of thermodynamic model based on equilibrium constants of the reactions i.e. modified Kent-Eisenberg model considering gas phase non-ideality. Valuation of necessary reaction equilibrium constants through non-linear data regression analysis of the model by utilizing the experimental data of the present work.

- Implementation of Feed-forward Neural Network model by using Levenberg-Marquardt (LM) back propagation algorithm and correlation of the same in the experimental results of CO_2 solubility.

- Experimental measurement of various thermodynamic properties (density, viscosity, surface tension, refractive index, sound velocity) of the aqueous and non-aqueous blended solvents over a wide range of temperature (298.15-303.15) K and solvent concentration.

- Analysis of various first principal models such as Redlich-Kister and Grunberg-Nissan thermophysical properties (viz. density and viscosity). Also, development and verification of suitable models for sound velocity, refractive index and surface tension.

1.6 Thesis organization

The main focus of the thesis is on the investigation of various non-aqueous and aqueous blended ionic liquids and amine activators for post-combustion carbon capture application with major prominence on the experimental measurements and simulation analysis of CO_2 equilibrium solubility. The thesis work has been divided into seven chapters. A brief overview of each chapter is presented below:

Chapter 1: Theoretical contextual of the work, widespread literature review, objectives and outline of the thesis have been conferred in this chapter.

Chapter 2: This chapter discusses the various well developed reaction mechanisms for amines. Various modeling approaches for CO_2 solubility used in the current work are also presented.

Chapter 3: Measurement and modeling analysis of CO_2 solubility at equilibrium in aq. ([bmim][Ac]) and its potential blends with AEP and APA as a function of temperature, concentration and CO_2 partial pressure has been testified in this chapter. The reaction mechanism and products of reaction are studied through FTIR and ^{13}C NMR analysis. Along with modified KE model, the applicability of Artificial Neural Network model is also accessed. An improved feed forward neural network model with optimized neurons is employed and results are being compared with predicted CO_2 solubility data from KE model.

Chapter 4: This chapter presents the experimental measurement of CO_2 solubility data in aqueous TESA, aq. (TESA + AEP) and aq. (TESA + APA) over a wide range of temperature, concentration and CO_2 partial pressure. The formation of reversible ionic liquids and corresponding reactions of the constituent chemicals is revealed using FTIR and ^{13}C NMR studies. The CO_2 VLE data is co-related using modified Kent-Eisenberg (KE) model considering the gas phase non-ideality. The equilibrium constants corresponding to the various reactions

involved in the system are obtained using non-linear regression analysis. Furthermore, the speciation analysis and *pH* estimation is also carried out.

Chapter 5: This chapter discusses the vapor liquid equilibrium analysis of aq. MDEA, $TMSO_2$ and [bmim] [Ac] activated by a novel 2-MPZ amine activator. The formation of various carbamate species and bicarbonates is confirmed using FTIR and ^{13}C NMR analysis. The CO_2 solubility data has been correlated using modified KE model considering gas phase non-ideality. The CO_2 partial pressure and loading data is utilized for further calculation of heat of absorption and CO_2 cyclic capacity data. The results of the present work is compared with the conventional amines studied in the literature.

Chapter 6: This chapter presents the measurement of various important thermophysical properties such as density, viscosity, surface tension, refractive index, sound velocity for (HEF + AEP), (HEF + AMP), (TESA + H_2O), (TESA + H_2O + AEP), (TESA + H_2O + APA), ([bmim] [Ac] + H_2O), ([bmim] [Ac] + H_2O + AEP), ([bmim] [Ac] + H_2O + APA), (MDEA + H_2O + 2-MPZ), ($TMSO_2$ + H_2O + 2-MPZ) and ([bmim] [Ac] + H_2O + 2-MPZ) systems as a function of temperature and concentration. The properties were correlated using various first principle models such as Redlich-Kister for density and Grunberg-Nissan for viscosity. Further, new models have been proposed and verified for sound velocity, refractive index, and surface tension. The obtained thermophysical data is extended to find various important properties such as excess molar volumes, kinematic viscosity deviations, isentropic compressibility, thermal expansion coefficients, N_2O and CO_2 diffusivity in proposed solvents, ΔG^o, ΔS^o and ΔH^o, over the wide temperature and composition range.

Chapter 7: At last, overall conclusions are deducted from this work, and the path for future work has been conversed in this chapter.

Abbreviation	**Solvent**
[bmim] [tcm]	1-Butyl-3-methylimidazolium tricyanomethanide
[dmim][$MeSO_3$]	1,3-Dibutylimidazolium methanesulfonate
[emim][$MeSO_3$]	1-Ethyl-3-methylimidazolium methanesulfonate
[bmim][$MeSO_3$]	1-Butyl-3-methylimidazolium methanesulfonate
[dbim][$MeSO_3$]	1,3-Dimethylimidazolium methanesulfonate
[hmim][TCB]	1-Hexyl-3-methylimidazolium tetracyanoborate
[P (14)666][TMPP]	Trihexyl tetradecylphosphonium bis (2,4,4-trimethylpentyl) phosphinate
[P4444][TMPP]	Tetrabutylphosphonium bis (2,4,4-trimethylpentyl) phosphinate
[P8111][TMPP]	Trimethyloctylphosphonium bis (2,4,4-trimethylpentyl) phosphinate
[P(14)666][DCA]	Trihexyl tetradecylphosphonium dicyanamide
[THTDP][NTf_2]	Trihexyltetradecylphosphonium bis (trifluoromethylsulfonyl) imide
[THTDP][Cl]	Trihexyltetradecylphosphonium chloride
[TDC][DCN]	1,2,3-Tris(diethylamino) cyclopropenylium dicyanamide
[emmp][Tf_2N]	Ethyldimethylpropylammonium bis (trifluoro methyl sulfonyl) imide
[TDC][Tf_2N]	1,2,3-Tris(diethylamino)cyclopropenylium bis(trisfluoro methane sulfonyl) imide
[BMP][TfO]	1-Butyl-1-methylpyrrolidinium trifluoromethanesulfonate
[emim][TFO]	1-Ethyl-3-methylimidazolium trifluoromethanesulfonate
[hmim][TFO]	1-Hexyl-3-methylimidazolium trifluoromethanesulfonate
[omim][TFO]	1-Octyl-3-methylimidazolium trifluoromethanesulfonate
[hmp][Tf_2N]	1-Hexyl-1-methylpyrrolidinium bis (trifluoromethylsulfonyl) imide
[omp][Tf_2N]	1-Octyl-1-methylpyrrolidinium bis (trifluoromethylsulfonyl) imide
[hemim][BF_4]	1-(2-Hydroxy ethyl)-3-methylimidazolium tetrafluoroborate
[bmim][ac]	1-Butyl-3-methylimidazolium acetate
[bmmim][PF_6]	1-Butyl-2,3-dimethylimidazolium hexafluorophosphate
[h3mp][Tf_2N]	1-Hexyl-3-methylpyridinium bis (trifluoromethylsulfonyl) imide
[P4,4,4,1][TOS]	Triisobutylmethylphosphonium p-toluenesulfonate
[emim][PF_6]	1-Ethyl-3-methylimidazolium hexafluorophosphate
[omim][BF_4]	1-Octyl-3-methylimidazolium tetrafluoroborate
[HEA]	2-Hydroxyethanaminium acetate
[BHEAA]	Bis (2-hydroxyethyl) ammonium acetate
[BHEAL]	Bis (2-hydroxyethyl) ammonium lactate
HHEMEA	2-Hydroxy-N-(2-hydroxyethyl)-N-methylethanaminium acetate

HHEMEL	2-Hydroxy-N-(2-hydroxyethyl)-N-methylethanaminium lactate
iBu_3MeP][TOS]	tri-isobutyl-methyl phosphonium *p*-toluenesulfonate
[bmim][BF_4]	1-Butyl-3-methyl tetrafluoroborate
[N1111][Gly]	Tetramethylammonium glycinate
[bmim][Otf]	1-Butyl-3-methylimidazolium trifluoromethanesulfonate
[BHMIM][Ac]	1-Butyl-3-H-imidazolium acetate
[C_2py][$EtSO_4$]	1-Ethylpyridinium ethylsulfate
[C_2mim][NTf_2]	1-Ethyl-3-methylimidazolium bis (trifluoromethanesulfonyl) imide
[emim][Tf_2N]	1-Ethyl-3-methylimidazolium bis (trifluoromethylsulfonyl) imide
[gua][FAP]	Guanidium tris (pentafluoroethyl) trifluorophosphate
[bmim][DCA]	1-Butyl-3-methyl-imidazolium dicyanamide
MEA	Monoethanolamine
DEA	Diethanolamine
MDEA	*N*-Methyldiethanolamine
AMP	Amino-2-methyl-1-propanol
$TMSO_2$	Sulfolane
PZ	Piperazine
NMP	*N*-methylpyrrolidone
PC	Propylene carbonate
DIPA	Diisopropanolamine

References

[1]M. Lickley, S. Solomon, S. Fletcher. Quantifying contributions of chlorofluorocarbon banks to emissions and impacts on the ozone layer and climate. Nature Communication 11 (2020) 1380. (https://doi.org/10.1038/s41467-020-15162)

[2]E. L. Fleming, P. A. Newman, Q. Liang, J. S. Daniel. The impact of continuing CFC-11 emissions on stratospheric Ozone (2020) (https://doi.org/10.1029/2019JD031849)

[3]The data is reproduced from the Global Carbon Atlas (www.globalcarbonatlas.org) (2020).

[4]International Energy outlook 2020 Highlights, US Energy information administration, https://www.eia.gov/outlooks/ieo/.

[5]IEA (2020), Global CO_2 emissions in 2019, IEA, Paris. https://www.iea.org/articles/global-co2-emissions-in-2019

[6]J. Oliver, J. Peters, Trends in global CO_2 and total greenhouse gas emissions, 2019, PBL Netherlands Environmental assessment agency.

[7]S. Kumar, J. H. Cho, I. Moon. Ionic liquid-amine blends and CO_2 BOLs: prospective solvents for natural gas sweetening and CO_2 capture technology-a review. International Journal of Greenhouse Gas Control 20 (2014) 87–116.

[8]A. A. Olajire. CO_2 capture and separation technologies for end-of-pipe applications-A review. Energy 35 (2010) 2610-2628.

[9]H. Hamadeh, S. Y. Toor, P. L. Douglas, S. M. Sarathy, R. W. Dibble, E. Croiset. Techno-economic analysis of pressurized oxy-fuel combustion of petroleum coke. Energies 13 (2020) 3463.

[10]C. Ekstrom, F. Schwendig, O. Biede, F. Franco, G. Haupt, G. D. Koeijer, C. Papapavlou, P. E. Rokke. Techno-economic evaluations and benchmarking of pre-combustion CO_2 capture and oxy-fuel processes developed in the European ENCAP project. Energy Procedia 1 (2009) 4233-4240.

[11]A. B. Rao, E. S. Rubin. A technical, economic, and environmental assessment of amine-based CO_2 capture technology for power plant greenhouse gas control. Environmental Science and Technology 36 (2002) 4467-4475.

[12]S. K .Dash, A. N. Samanta, S. S. Bandyopadhyay. Solubility of carbon dioxide in aqueous solution of 2-amino-2-methyl-1-propanol and piperazine. Fluid Phase Equilibria 307 (2011b) 166-174.

[13]B. P. Mandal, S. S. Bandyopadhyay. Simultaneous absorption of CO_2 and H_2S into aqueous blends of *N*-methyldiethanolamine and diethanolamine. Environmental Science and Technology 40 (2006) 6076-6084.

[14]L. M. Galan Sanchez (2008), Functionalized Ionic Liquids: Absorption solvents for carbon dioxide and olefin separation. PhD thesis.

[15]L. A. Blanchard, D. Hancu, E. J. Beckman, J. F. Brennecke. Green processing using ionic liquids and CO_2. (1999). Nature 399 (1999) 28-29.

[16]J. Tang, H. Tang, W. Sun, M. Radosz, Y. Shen. Poly (ionic liquids) as new materials for CO_2 absorption. Journal of Polymer Science. Part A: Polymer Chemistry 43 (2005) 5477-5482.

[17]A. S. Bhown, B.C. Freeman. Analysis and status of post-combustion carbon dioxide capture technologies. Environmental Science and Technology 45 (2011) 8624–8632.

[18]K. Damen, R. Gnutek, J. Kaptein, N.R.Nannan, B. Oyarzun, C. Trapp, P. Colonna, E. V.Dijk, J. Gross, A. Bardow . Developments in the pre-combustion CO_2 capture pilot plant at the Buggenum IGCC. Energy Procedia 4 (2011) 1214–1221.

[19]T. C. Drage, O. Kozynchenko, C. Pevida, M. G. Plaza, F. Rubiera, J. J. Pis, C. E. Snape, S. Tennison. Developing activated carbon adsorbents for pre-combustion CO_2 capture. Energy Procedia 1 (2009) 599–605.

[20]A. L. Kohl and R. B. Nielsen (1997). Gas purification, 5th ed., Gulf publishing company: Houston.

[21]J. Zou, W. S. W. Ho. CO_2- selective polymeric membranes containing amines in cross linked poly (vinyl alcohol). Journal of Membrane Science 286 (2006) 310–321.

[22]K. Skjanes, P. Lindblad, J. Muller. BioCO_2-A multidisciplinary, biological approach using solar energy to capture CO_2 while producing H_2 and high values products. Biomolecular Engineering 24 (2007) 405-413.

[23]L. F. Zubeir, G. E. Romanos, W. M. A. Weggemans, B. Iliev, T. J. S. Schubert, M. C. Kroon. Solubility and diffusivity of CO_2 in the ionic liquid 1-butyl-3-methylimidazolium tricyanomethanide within a large pressure range (0.01 MPa to 10 MPa). Journal of Chemical and Engineering Data 60 (2015) 1544-1562.

[24]Y. H. Jung, J. Y. Jung, Y. R. Jin, B. C. lee, I. H. Baek, S. H. Kim. Solubility of carbon dioxide in imidazolium based ionic liquids with a methanesulfonate anion. Journal of Chemical and Engineering Data 57 (2012) 3321-3329.

[25]M. T. M. Martinez, M. Althuluth, M. C. Kroon, C. J. Peters. Solubility of carbon dioxide in the low-viscosity ionic liquid 1-hexyl-3-methylimidazolium tetracyanoborate. Fluid Phase Equilibria 332 (2012) 35-39.

[26]W. Afzal, X. Liu, J. M. Prausnitz. High solubilities of carbon dioxide in tetralkyl phosphonium based ionic liquids and the effect of diluents on viscosity and solubility. Journal of Chemical and Engineering Data 59 (2014) 954-960.

[27]P. J. Carvalho, V. H. Alvarez, I. M. Marrucho, M. Aznar, J. A. P. Coutinho. High carbon dioxide solubilities in trihexyltetradecylphosphonium- based ionic liquids. Journal of Supercritical Fluids 52 (2010) 258-265.

[28]M. Zoubeik, A. Henni. Experimental and thermodynamic study of CO_2 solubility in promising [Tf_2N and DCN] ionic liquids. Fluid Phase Equilibria 376 (2014) 22-30.

[29]H. N. Song, B. C. Lee, J. S. Lim. Measurement of CO_2 solubility in ionic liquid: [BMP] [TfO] and [P14, 6, 6, 6] [Tf_2N] by measuring bubble-point pressure. Journal of Chemical & Engineering Data 55 (2010) 891-896.

[30]E. K. Shin, B. C. Lee. High-pressure phase behavior of carbon dioxide with ionic liquids: 1-alkyl-3-methylimidazolium trifluoromethanesulfonate. Journal of Chemical & Engineering Data 53 (2008) 2728–2734.

[31]J. H. Yim, H. N. Song, B. C. Lee, J. S. Lim. High-pressure phase behavior of binary mixtures containing ionic liquid [HMP][Tf_2N], [OMP][Tf_2N] and carbon dioxide. Fluid Phase Equilibria 308 (2011) 147-152.

[32]M. Shokouhi, M. Adibi, A. H. Jalili, M. H. Jenab, a. Mehdizadeh. Solubility and diffusion of H_2S and CO_2 in the ionic liquid 1-(2-hydroxyethyl)-3-methylimidazolium tetrafluoroborate. Journal of Chemical & Engineering Data 55 (4) (2010) 1663-1668.

[33]M. B. Shiflett, D. J. Kasprzak, C. P. Junk, A. Yokozeki. Phase behavior of carbon dioxide + [bmim] [Ac] mixtures. Journal of Chemical Thermodynamics 40 (2008) 25-31.

[34]C. Cadena, J. L. Anthony, J. K. Shah, T. I. Morrow, J. F. Brennecke, E. J. Maginn. Why is CO_2 so soluble in imidazolium-based ionic liquids? .Journal of the American Chemical Society 126 (2004) 5300–5308.

[35]M. J. Muldoon, S. N. V. K. Aki, J. L. Anderson, J. K. Dixon, J. F. Brennecke. Improving carbon dioxide solubility in ionic liquids. The Journal of Physical Chemistry B 111 (30) (2007) 9001–9009.

[36]J. L. Anthony, J. L. Anderson, E. J. Maginn, J. F. Brennecke. Anion effects on gas solubility in ionic liquids. The Journal of Physical Chemistry B 109 (13) (2005) 6366–6374.

[37]A. Shariati, C. J. Peters, High-pressure phase behavior of systems with ionic liquids: II. The binary system carbon dioxide+1-ethyl-3-methylimidazolium hexafluorophosphate. Journal of Supercritical Fluids 29 (2004) 43–48.

[38]K. I. Gutkowski, A. Shariati, C. J. Peters. High-pressure phase behavior of the binary ionic liquid system 1-octyl-3-methylimidazolium tetrafluorobo- rate + carbon dioxide. Journal of Supercritical Fluids 39 (2006) 187–191.

[39]K. A. Kurnia, F. Harris, C. D. Wilfred, A. Mutalib, T. Murugesan. Thermodynamic properties of CO_2 absorption in hydroxyl ammonium ionic liquids at pressure of (100-1600) kPa. Journal of Chemical Thermodynamics 41 (2009) 1069-1073.

[40]S. N. V. K. Aki, B. R. Mellein, E. M. Saurer, J. F. Brennecke. High- pressure phase behaviour of carbon dioxide with imidazolium based ionic liquids. Journal of Physical Chemistry B 108 (52) (2004) 20355-20365.

[41]A. M. Pinto, H. Rodriguez, A. Arce, A. Soto. Carbon dioxide absorption in the ionic liquid 1-ethylpyridinium ethylsulfate and in its mixtures with another ionic liquid. International Journal of Greenhouse Gas Control 18 (2013) 296-304.

[42]A. M. Pinto, H. Rodriguez, Y. J. Colon, A. A. Jr. A. Arce, A. Soto. Absorption of CO_2 in two binary mixtures of ionic liquids. Journal of Industrial and Engineering Chemistry Research 52(2013) 5975-5984.

[43]Y. Zhao, X. Zhang, S. Zeng, Q. Zhou, H. Dong, X. Tian, S. Zhang. Density, Viscosity, and performances of carbon dioxide capture in 16 absorbents of amine + ionic liquid + H_2O, ionic liquid + H_2O, and amine + H_2O systems. Journal of Chemical and Engineering Data 55 (9) (2010) 3513-3519.

[44]Z. Xue, Z. Zhang, J. Han, Y. Chen, T. Mu. Carbon dioxide capture by a dual amino ionic liquid with amino-functionalized imidazolium cation and taurine anion. International Journal of Greenhouse Gas Control 5 (2011) 628-633.

[45]M. Ramdin, T. W. D. Loos, T. J. H. Vlugt. State-of-the-Art of CO_2 Capture with Ionic Liquids. Industrial and Engineering Chemistry Research 51 (24) (2012) 814-8177.

[46]X. Yuan, S. Zhang, J. Liu, X. Lua. Solubilities of CO_2 in hydroxyl ammonium ionic liquids at elevated pressures. Fluid Phase Equilibria 257 (2007) 195-200.

[47]E. D. Bates, R. D. Mayton, I. Ntai, J. H. Davis. CO_2 Capture by a Task-Specific Ionic Liquid. Journal of the American Chemical Society 124(6) (2002) 926-927.

[48]B. F. Goodrich, J. C. Fuente, B. E. Gurkan, D. J. Zadigian, E. A. Price, Y. Huang, J. F. Brennecke. Experimental measurements of amine-functionalized anion-tethered ionic liquids with carbon dioxide. Industrial and Engineering Chemistry Research 50 (2011) 111-118.

[49]A. Ahmady, M. A. Hashim, M. K. Aroura. Density, viscosity, physical solubility and diffusivity of CO_2 in aqueous MDEA+ [bmim] [BF_4] solutions from 303 to 333 K. Chemical Engineering Journal 172 (2011) 763-770.

[50]M. Mirarab, M. Sharifi, M. A. Ghayyem, F. Mirarab. Prediction of solubility of CO_2 in ethanol- [EMIM] [Tf_2N] ionic liquid mixtures using artificial neural network based on genetic algorithm. Fluid Phase Equilibria 371 (2014) 6-14.

[51]A. Shojaeian, A. Haghtalab. Solubility and density of carbon dioxide in different aqueous alkanolamine solutions blended with 1-butyl-3-methylimidazolium acetate ionic liquid at high pressure. Journal of Molecular Liquids 187 (2013) 218-225.

[52]N. Aziz, R. Yusoff, M. K. Aroua. Absorption of CO_2 in aqueous mixtures of N-methyldiethanolamine and guanidinium tris (pentafluoroethyl) trifluorophosphate ionic liquid at high pressure. Fluid Phase Equilibria 322-323 (2012) 120-125.

[53]A. Ahmady, M. Hashim, M. K. Aroua. Absorption of carbon dioxide in the aqueous mixtures of methyldiethanolamine with three types of imidazolium- based ionic liquids. Fluid Phase Equilibria 309 (2011) 76-82.

[54]K. Osman, D. Ramjugernath, C. Coquelet. CO_2 solubility in hybrid solvents containing 1-butyl-3-methylimidazolium tetrafluoroborate and mixtures of alkanolamine. Journal of Chemical and Engineering Data 60 (2015) 2380-2391.

[55]A. Haghtalab, A. Shojaeian. High Pressure measurement and thermodynamic modelling of the solubility of carbon dioxide in *N*-methyldiethanolamine and 1-butyl-3-methylimidazolium acetate mixture. Journal of Chemical Thermodynamics 81 (2015) 237-244.

[56]Y. Gao, F. Zhang, K. Huang, J. W. Ma, Y. T. Wu, Z. B. Zhang. Absorption of CO_2 in amino acid ionic liquid (AAIL) activated MDEA solutions. International Journal of Greenhouse Gas Control 19 (2013) 379-386.

[57]A. Ahmady, M. A. Hashim, M. K. Aroua. Experimental investigation on the solubility and initial rate of absorption of CO_2 in aqueous mixtures of methyldiethanolamine with the ionic liquid 1-butyl-3-methylimidazolium tetrafluoroborate. Journal of Chemical and Engineering Data 55 (2010) 5733-5738.

[58]S. N. Khan, S. M. Hailegiorgis, Z. Man, S. Garg, A. M. Shariff, S. Farrukh, M. Ayoub, H. Ghaedi. High pressure absorption study of CO_2 in aqueous *N*-methyldiethanolamine (MDEA) and MDEA-piperazine (PZ) -1-butyl-3-methylimidazolium trifluoromethanesulfonate [bmim] [OTf] hybrid solvents. Journal of Molecular Liquids 249 (2018) 1236-1244.

[59]M. Xiao, H. Liu, H. Gao, W. Olson, Z. Liang. CO_2 capture with hybrid absorbents of low viscosity imidazolium-based ionic liquids and amine. Applied Energy 235 (2019) 311-319.

[60]W. Zhang, L. Ye, J. Jiang. CO_2 capture with complex absorbent of ionic liquid, surfactant and water. Journal of Environmental Chemical Engineering 3 (2015) 227-232.

[61]H. K. Karlsson, M. G. Sanku, H. Svensson. Absorption of carbon dioxide in mixtures of N-methyl-2-pyrrolidone and 2-amino-2-methyl-1-propanol. International Journal of Greenhouse Gas Control 95 (2020) 102952.

[62]M. R. Bohloul, A. Vatani, S. M. Peyghambarzadeh. Experimental and theoretical study of CO_2 solubility in *N*-methyl-2-pyrrolidone (NMP). Fluid Phase Equilibria 365 (2014) 106-111.

[63]M. Ramdin, Q. Chen, S. P. Balaji, J. M. V. Luna, A. T. Knoop, D. Dubbeldam, S. Calero, T. W. D. Loos, T. J. H. Vlugt. Solubilities of CO_2, CH_4, C_2H_6 and SO_2 in ionic liquids and selexol from monte carlo simulations. Journal of Computational Science 15 (2016) 74-80.

[64]A. Haghtalab, A. Shirazizadeh. An electrolyte segmental Wilson – non-random Gibbs model and measurement of carbon dioxide solubility into sulfolane +water and *N*-methyldiethanolamine + sulfolane + water systems. Journal of molecular liquids 296 (2019) 111786.

[65]H. A. Shirazizadeh, A. Haghtalab. Simultaneous solubility measurement of (ethyl mercaptan + carbon dioxide) into the aqueous solutions of (*N*- methyldiethanolamine + sulfolane + water). Journal of Chemical Thermodynamics 133 (2019) 111-122.

[66]M. Shokouhi, A. H. Jalili, A. T. Zoghi, J. S. Ahari. Carbon dioxide solubility in aqueous sulfolane solution. Journal of Chemical Thermodynamics 132 (2019) 62-72.

[67]C. W. Wang, A. N. Soriano, Z. Y. Yang, M. H. Li. Solubility of carbon dioxide in the solvent system (2-amino-2-methyl-1-propanol + sulfolane +water). Fluid Phase Equilibria 291 (2010) 195-200.

[68]F. M. Guevara, E. R. Libreros, A. Trejo. Gas solubility of hydrogen and carbon dioxide in mixtures of sulfolane with diethanolamine at different temperatures. Fluid Phase Equilibria 95 (1994) 163-174.

[69]F. M. Guevara, E. R. Libreros, A. Trejo. Gas solubility of carbon dioxide and hydrogen sulfide in mixtures of sulfolane with monoethanolamine. Fluid Phase Equilibria 86 (1993) 225-231.

[70]F. M. Guevara, A. R. Martinez, A. Trejo. Solubilities of carbon dioxide and hydrogen sulfide in propylene carbonate, *N*- methylpyrrolidone and sulfolane. Fluid Phase Equilibria 44 (1988) 105-115.

[71]F. M. Guevara, E. R. Libreros, A. Trejo. Gas solubilities of carbon dioxide and hydrogen sulfide in sulfolane and its mixtures with alkanolamines. Fluid Phase Equilibria 53 (1989) 1-6.

[72]S. K. Dash, S. S. Bandyopadhyay. Studies on the effect of addition of piperazine and sulfolane into aqueous solution of N- methyldiethanolamine for CO_2 capture and VLE modelling using e-NRTL equation. International Journal of Greenhouse Gas Control 44 (2016) 227-237.

[73]A. H. Jalili, M. Shokouhi, F. Samani, M. H. Jenab. Measuring the solubility of CO_2 and H_2S in sulfolane and the density and viscosity of saturated liquid binary mixtures of (sulfolane + CO_2) and (sulfolane + H_2S). Journal of Chemical Thermodynamics 85 (2015) 13-25.

[74]V. Blasucci, R. Hart, V. L. Mestre, D. J. Hahne, M. Burlager, H. Huttenhower, B. J. R. Thio, P. Pollet, C. L. Liotta, C. A. Eckert. Single component ionic liquids for energy applications. Fuel 89 (2010) 1315-1319.

[75]S. Paul, A. K. Ghoshal, B. P. Mandal. Kinetics of absorption of carbon dioxide into aqueous solution of 2-(1-piperazinyl)-ethylamine. Chemical Engineering Science 64 (2009) 313-321.

[76]Y. Du, Y. Wang, G. T. Rochelle. Thermal degradation of novel piperazine –based amine blends for CO_2 capture. International Journal of Greenhouse Gas Control 49 (2016) 239-249.

[77]P. Singh, J. P. M. Niederer, G. F. Versteeg. Structure and activity relationships for amine-based CO_2 absorbents-II. Chemical Engineering Research and Design 7 (2008) 135-144.

[78]Y. Du, L. Li, O. Namjoshi, K. A. Voice, A. N. Fine, G. T. Rochelle. Aqueous piperazine/N-(2-Aminoethyl) piperazine for CO_2 capture. Energy Procedia 37 (2013) 1621-1638.

[79]A. Dey, S. K. Dash, B. P. Mandal. Equilibrium CO_2 solubility and thermophysical properties of aqueous blends of 1-(2-aminoethyl) piperazine and N-methyldiethanolamine. Fluid Phase Equilibria 463 (2018) 91-105.

[80]A. Dey, S. K. Dash, S. C. Balchandani, B. P. Mandal. Investigation on the inclusion of 1-(2-aminoethyl) piperazine as a promoter on the equilibrium CO_2 solubility of aqueous 2-amino-2-methyl-1-propanol. Journal of Molecular Liquids 289 (2019) 111036.

[81]B. Das, B. Deogam, B. P. Mandal. Experimental and theoretical studies on efficient carbon dioxide capture using novel bis (3-aminopropyl) amine (APA)-activated aqueous 2-amino-2-methyl-1-propanol (AMP) solutions. RSC Advances 7 (2017) 21518–21530.

[82]A. Dey, S. K. Dash, B. P. Mandal. Elucidating the performance of (N-(3-aminopropyl)-1, 3-propanediamine) activated (1-dimethylamino-2-propanol) as a novel amine formulation for post combustion carbon dioxide capture. Fuel 277 (2020) 118209.

[83]A. Hafizi, M. H. Mokari, R. Khalifeh, M. Farsi, M. R. Rahimpour. Improving the CO_2 solubility in aqueous mixture of MDEA and different polyamine promoters: The effects of primary and secondary functional groups. Journal of Molecular Liquids 297 (2020) 111803.

[84]Y. Yuan, B. Sherman, G. T. Rochelle. Effects of viscosity on CO_2 absorption in aqueous piperazine / 2-methylpiperazine. Energy Procedia 114 (2017) 2103-2120.

[85]X. Chen, G. T. Rochelle. Modeling of CO_2 absorption kinetics in aqueous 2-methylpiperazine. Industrial and Engineering Chemistry Research 52 (2013) 4239-4248.

[86]X. Chen, G. T. Rochelle. Thermodynamics of CO_2 / 2-methylpiperazine/ water. Industrial and Engineering Chemistry Research 52 (2013) 4229-4238.

[87]B. Sherman, X. Chen, T. Nguyen, Q. Xu, H. Rafique, S. A. Freeman, A. K. Voice, G. T. Rochelle. Carbon capture with 4 m piperazine / 4 m 2-methylpiperazine. Energy Procedia 37 (2013) 436-447.

[88]Y. E. Kim, J. H. Choi, S. C. Nam, Y. I. Yoon. CO_2 absorption capacity using aqueous potassium carbonate with 2-methylpiperazine and piperazine. Journal of Industrial and Engineering Chemistry 18 (2012) 105-110.

Chapter 2

REACTION MECHANISM AND MODELING METHODOLOGIES FOR CO_2-AQUEOUS IONIC LIQUID- AMINE SYSTEMS

This chapter presents an ample analysis of the fundamental reaction chemistry of aqueous ionic liquid-amine solvent solutions with CO_2. The conceptual thermodynamics and kinetic behavior of the CO_2 absorption in an aqueous ionic liquid - amine system presented here. The discussion comprises reaction mechanisms related to numerous ionic liquid species, and amine groups, developing rate expression, and the elucidation of possible reaction products. The later section of the chapter majorly deals with thermodynamics and the comprehensive description on the several modeling approaches implemented in the present work to correlate the vapor-liquid equilibrium data.

2.1 Introduction

Many of the researchers suggest that in an IL-amine mixture, there are two absorption processes taking place simultaneously (1) physical absorption mainly contributed by ILs and (2) chemical absorption majorly contributed by amines [1,2], whereas many other researchers also suggest that ILs react with CO_2 in a similar fashion as amines [3-5]. In the present research work, the proposal is for the usage of ILs-amine water system. And hence, besides the reaction of ILs with CO_2, all the reactions pertaining to amines and CO_2 are still valid for the system. Absorption of CO_2 in ionic liquids and amine solvents implicates the chemical reaction of the CO_2 with the individual ILs and amines. Further, in the present chapter, it is assumed that the ILs and amines react only with CO_2 and not amongst each other. Hence, it can be concluded that for each category of ionic liquid or amines, different reaction schemes are possible. Many of the reaction mechanisms for different reacting species can be confirmed using different analytical techniques to quantify or qualify the newly formed chemical products due to reaction. This chapter includes

the discussion of various regimes of reaction and the contribution of mass transfer coefficients to the overall reaction rates of CO_2 in aqueous ionic liquid-amine systems.

The prediction of optimum operating conditions is based on two major aspects of CO_2 capture, (1) accurate measurement method and (2) apposite mathematical model. Equilibrium thermodynamics in any blended system is a combination of (a) phase or physical (absorption) equilibrium pertaining to gas (or vapor) –liquid phase and (2) the chemical reaction with respect to the reaction between the solvent and CO_2 or various intermediate species reacting with one another. In the present work, a first principle model viz. modified Kent-Eisenberg model considering gas-phase non-ideality has been utilized for all the solvent blends under study as a thermodynamic model for accurate correlation between the experimental and predicted data. Additionally, for few systems, artificial neural network model has also been tested for VLE prediction. A detailed discussion of both the models is demonstrated in this chapter.

2.2 Reaction mechanism of CO_2-aqueous alkanolamine (or Ionic Liquid) system

The reaction of CO_2 with primary, secondary and sterically hindered amines is described by the zwitterion mechanism and the reaction with tertiary amines is described by base-catalyzed hydration of CO_2 [6, 7].

2.2.1 Zwitterion mechanism

It is a two-step mechanism, which was originally proposed by Caplow and later reintroduced by Danckwerts. It suggests that CO_2 forms a bond to the amine functionality in the first step. In the second step an amine-proton is transferred to a second molecule. The intermediate species in the reaction is a zwitterion [8]. Thus, the mechanism consists of the formation of a zwitterion followed by its deprotonation with a base. Zwitterion mechanism is usually followed by most primary and secondary amines [9]. Additionally, many of the researchers have confirmed the formation of zwitterion while the reaction of CO_2 with ILs [2].

$$CO_2 + Am \longleftrightarrow Am^+COO^- \qquad \text{(R 2.1)}$$

This zwitterion undergo deprotonation by a base (or bases) b, thereby resulting in carbamate formation:

$$Am^{+}COO^{-} + b \xrightarrow{k_b} AmCOO^{-} + bH^{+} \qquad \text{(R 2.2)}$$

The base, b, can be an amine, OH^- or H_2O although the contribution of OH^- can be neglected as its concentration is very low compared with those of amine and H_2O.

Applying the steady-state principle to the intermediate zwitterion,

$$r = k_2[CO_2][Am] - k_{-1}[Z] = [Z]\sum k_b[b] \qquad (2.1)$$

The term Σk_b [b] indicates the contribution of the various bases present to the rate of removal of protons. From eq. (2.1) the concentration of zwitterion,

$$[Z] = \frac{k_2[CO_2][Am]}{k_{-1} + \sum k_b[b]} \qquad (2.2)$$

Replacing [Z] in eq. (2.1) using eq. (2.2), the rate of reaction of CO_2 in aqueous solutions can be expressed as:

$$r_{CO2-amine} = k_2 \times \left(\frac{[CO_2][RNH_2]}{1 + \left(\frac{1}{\sum \left(\frac{k_b}{k-1} \right)[b]} \right)} \right) \qquad (2.3)$$

Where,

k_2 = forward reaction rate constant for the formation of zwitterion

k_{-1} = reverse reaction rate constant for the formation of zwitterion

k_b = forward reaction rate constant for the deprotonation reaction

[Am] = concentration of amine

[CO_2] = concentration of carbon dioxide

[b] = concentration of base

For two asymptotic situations eq. 2.3 may be simplified as follows:

(i) The term $\frac{k_{-1}}{k_b[b]} << 1$. This results in simple second-order kinetics indicating that zwitterion deprotonation reaction is fast in comparison with the reversion rate of CO_2 and amine. Then eq is simplified to:

$$r = k_2 \times [CO_2] \times [Am] \tag{2.4}$$

(ii) The term $\frac{k_{-1}}{k_b[b]} >> 1$.This results in a more complex expressions for the kinetics:

$$r = \frac{k_2 \times k_b \times [CO_2] \times [Am] \times [b]}{k_{-1}} \tag{2.5}$$

It can be seen from the above equation that the overall reaction order is three if the contribution of water towards the deprotonation of the zwitterions is neglected. In the transition region between the two asymptotic cases the reaction order changes between two and three. In the limiting case when the contribution of amine to zwitterion deprotonation is much more significant than that of other bases, such as H_2O and OH^-, the overall reaction is of the second order with respect to amine.

A discussion of CO_2 absorption into aqueous amine solutions is not complete without including the reactions of water and its dissociation products with the gases and the amines. The most important reaction in aqueous chemistry is the water dissociation reaction.

$$H_2O \longleftrightarrow H^+ + OH^- \tag{R 2.3}$$

The following reactions may also take place simultaneously in an aqueous amine solution:

$$Am + H_2O \leftrightarrow AmH^+ + OH^- \tag{R 2.4}$$

$$CO_2 + H_2O \leftrightarrow HCO_3^- + H^+ \tag{R 2.5}$$

$$CO_2 + OH^- \leftrightarrow HCO_3^- \quad \text{(R 2.6)}$$

The reaction between CO_2 and water is very slow (k = 0.026 s^{-1} at 298 K) [10] and may usually be neglected. The reaction between CO_2 and OH^- has a large influence on the overall reaction rate even when the concentration of hydroxyl ion is low. The forward reaction rate for reaction (2.6) can be described as [10]:

$$r_{CO2-OH^-} = k\times_{OH^-}[CO_2]\times[OH^-] \quad (2.6)$$

$$\log_{10}(k\times_{OH^-}) = 13.635 - \frac{2895}{T} \quad (2.7)$$

Where, $k\times OH^-$ = Forward reaction rate constant for hydrolysis reaction

The total rate of all CO_2 reactions in an aqueous solution is given by the sum of the reaction rates from the formation of zwitterion and the hydrolysis as follows:

$$r_{overall} = r_{CO_2-Amine} + r_{CO_2-OH^-} \quad (2.8)$$

$$r_{overall} = k_{overall}\times[CO_2] \quad (2.9)$$

2.2.2 Termolecular mechanism

As per this mechanism, the amine (or amino group) present in the aqueous solvent system reacts concurrently with CO_2 and base 'b' [10, 11]. Subsequently, the proton transfer and bond formation amid amine/IL molecule and CO_2 occurs.

$$CO_2 + Am\cdots\cdots b \longleftrightarrow AmCOO^-\cdots\cdots bH^+ \quad \text{(R 2.7)}$$

The intermediate complex formed is very unstable and hence short-lived. It further dissociates in free amine molecules and CO_2 whereas a small quantity of the intermediate complex subsequently reacts with CO_2/-NH_2/H_2O to form ionic products.

2.2.3 Base catalyzed hydration mechanism

The tertiary alkanolamines (denoted here as R_3N) cannot react directly with CO_2. Such amines have a base-catalytic effect on the hydration of CO_2. This can be represented as [11]:

$$CO_2 + R_3N + H_2O \xrightarrow{k2} R_3NH^+ + HCO_3^- \quad \text{(R 2.8)}$$

In aqueous solutions, an amine dissociation reaction may also occur:

$$R_3N + H_2O \longleftrightarrow R_3NH^+ + OH^- \quad \text{(R 2.9)}$$

The total rate of all CO_2 reactions in an aqueous solution is thus represented by the sum of the reaction rates given by equations (2.9) & (2.10)

$$r_{ov} = (k^*[OH^{-}] + k_2[R_3N])[CO_2] \quad (2.10)$$

Further, k_{ov} is given by:

$$k_{ov} = (k^*[OH^-] + k_2[R_3N]) \quad (2.11)$$

2.3 Modeling of CO_2 solubility data

A sensible design of CO_2 capture system requires experimental and conjectural analysis of vapor-liquid equilibrium of the solvents with CO_2. The VLE data for the aqueous or non-aqueous systems of designed solvents are commonly articulated as total CO_2 concentration in the studied solvent as a function of the CO_2 partial pressure at the equilibrium conditions. Nevertheless, apposite models are always desired for the applied range of composition, temperature, and pressure operating conditions in order to predict the data as and when required.

The forward and reversible reactions in any CO_2- solvent system results in the formation of various ionic species. In general, thermodynamic models are preferred to analyze such reactions in the system due to the fact that the results also provide necessary information about the system such as the heat of absorption, CO_2 cyclic capacity, etc.

Modeling of CO_2 absorption processes have been carried out in two different ways in the literature:

(1) CO_2 capture process modeling using different approaches to optimize the entire process [12-15]

(2) VLE or CO_2 solubility modeling.

This is also subdivided to many ways based on the approaches or outcomes expected as follows:

- Modeling of CO_2 solubility has been much studied in the literature using various approaches such as machine learning through neural networks and neuro-fuzzy approach [16], mathematical regression models such as multiple linear and multiple quadratic approaches [17], cubic and group contribution EoS such as Peng Robinson, Redlich-Knowng [18], e-NRTL [19], UNIQUAC [20], etc.

- CO_2 solubility and process improvement have also been studied using molecular simulation methods such as COSMO-RS [21, 22].

- CO_2 solubility in different solvents have been correlated using mixed thermodynamic and empirical correlations such as modified Kent-Eisenberg model [23, 24], Deshmukh-Mather model [25], Li-Shen model [26, 27], Austgen model [28, 29], Hu-Chakma [30, 31] model, etc. These models have several advantages over EoS based models such as critical properties of the solvents and accentric factors are not required. Hence, with minimal input data, empirical models provide efficient prediction.

2.3.1 Modified Kent-Eisenberg model

A less rigorous thermodynamic model based on the equilibrium constants was proposed by Kent and Eisenberg [23, 24] ignoring the non-idealities in the aqueous CO_2-solvent systems. Initially, the first KE model assumed the equilibrium constants to be a function of only temperature. Later on, many modifications were done in the same model which considered equilibrium constants of the reactions to be a function of CO_2 partial pressure, concentration of amines in addition to temperature. The latter was termed as "modified Kent-Eisenberg model". The modified KE model has been found to provide good predictions by various researchers [25-31]. The convergence of the modified KE model over good prediction capabilities depends on providing a good initial guess value of the reaction equilibrium constants.

2.3.1.1 Thermodynamic framework

The reaction between ILs and CO_2 is assumed to follow the deprotonation and carbamate reaction similar to primary amines as per the literature discussed in **Chapter-1**. The equilibrium reactions of CO_2 along with primary, secondary/tertiary amines/ILs systems can be expressed as follows: (where RNH_2 represents primary amine and R_3N represents tertiary amine)

$$RNH^{3+} \overset{K_{11}}{\rightleftharpoons} H^+ + RNH_2 \quad \text{(R 2.10)}$$

$$R_3NH^+ \overset{K_{11}}{\rightleftharpoons} H^+ + R_3N \quad \text{(R 2.11)}$$

$$RNHCOO^- + H_2O \overset{K_2}{\rightleftharpoons} RNH_2 + HCO_3^- \quad \text{(R 2.12)}$$

$$H_2O + CO_2 \overset{K_3}{\rightleftharpoons} H^+ + HCO_3^- \quad \text{(R 2.13)}$$

$$H_2O \overset{K_4}{\rightleftharpoons} H^+ + OH^- \quad \text{(R 2.14)}$$

$$HCO_3^- \overset{K_5}{\rightleftharpoons} H^+ + CO_3^{2-} \quad \text{(R 2.15)}$$

Where, K_{11} = Equilibrium constant of de-protonation of amine/IL

K_2 = Equilibrium constant of carbamate hydrolysis of amine/IL

K_3 = Equilibrium constant of formation of bicarbonate ion

K_4 = Equilibrium constant of dissociation of water

K_5 = Equilibrium constant of dissociation of bicarbonate ion

The physical solubility of CO_2 in the systems under consideration is expressed by Henry's law as below:

$$P_{CO_2} = H_{CO_2}[CO_2] \quad (2.12)$$

Where, P_{CO2}, H_{CO2}, and $[CO_2]$ are the equilibrium CO_2 partial pressure, Henry's law constant, CO_2 concentration in aqueous amine solutions. The overall amine mass and electro neutrality balance expressions for the primary amine can be represented as:

$$M_1 = [RNH_2] + [RNH_3^+] + [RNHCOO^-] \tag{2.13}$$

$$M_1 \times \alpha_{CO_2} = [CO_2] + [HCO_3^-] + [CO_3^{2-}] + [RNHCOO^-] \tag{2.14}$$

$$[RNH_3^+] + [H^+] - [RNHCOO^-] + [HCO_3^-] + 2[CO_3^{2-}] + [OH^-] = 0 \tag{2.15}$$

Where, all the terms in the bracket in equation (2.12) – (2.15) represent the ionic concentrations of all the species existing in the liquid phase.

The general method for the modified KE model is as follows [32]:

- Proposition of the possible (or confirmed) reactions of the CO_2-IL (or amine) system.
- Development of the charge balance, chemical, and physical equilibria of the system.
- Development of the CO_2 loading equation using the above steps.
- Providing appropriate initial guesses of the equilibrium to be estimated according to the proposed reactions.
- Estimation of concentration of all the ionic species expressed in the reaction equilibria by solving the non-linear equation.
- Calculation of the unknown equilibrium constants, K_i associated with chemical reactions by reducing the AAD between the calculated and experimental CO_2 loading data.

The equilibrium constant related to reactions (R 2.13- 2.15) are available in the open literature. Whereas the solvent explicit equilibrium constants characterized in reactions (R 2.10 – R 2.12) are required to be regressed and calculated to apt the experimental solubility data. The original expression of the equilibrium model and Henry's law constant was framed as a function of temperature alone as presented below:

$$\ln(K) = l + \frac{m}{T} + n \times \ln(T) + o \times T \tag{2.16}$$

where, T is temperature and l, m, n and o are the coefficients.

Lately, the dependency of many variables such as CO_2 partial pressure and amine concentration in varying logarithmic and square forms have been considered to take into account the different non-idealities associated with the prediction [25-31]. In the present work, the equilibrium constants associated with deprotonation and carbamate hydrolysis were used as a function of the described variables as given below:

$$K_{11} = g + (h \times M) + (k \times T) + (l \times M \times T) + (n \times T^2) + (p \times P_{CO_2}) + (q \times P_{CO_2}^2) \tag{2.17}$$

$$K_2 = g + (h \times M) + (k \times T) + (l \times M^2) + (n \times M \times T) + (p \times T^2) + (q \times P_{CO2}) + (r \times P_{CO_2}^2) \tag{2.18}$$

Where, g, h, k, l, n, p, q, and r, are parametric coefficients associated with the equilibrium constants and found through optimization.

2.3.2 Artificial neural network model

2.3.2.1 Neural network modeling

Neural network is an artificial intelligence technique capable of modeling any kind of complex data even with respect to highly non-linear systems. The input layer, hidden layer(s), and output layer of a neural network consists of several neurons. All neurons are connected to neurons of the previous as well as the next layers. The output of each neuron is calculated based on its input employing a transfer function. Neural network modeling has been widely used in the area of CO_2 capture processes for various property predictions as well as for process intensification [17,33]. It is capable of taking into account the nonlinearity of any multivariate system with minute modifications such as normalization of i/p and o/p data. It usually does not require complete technical knowledge of the system into consideration. A neuron calculates the output ‘m’ for any system having input ‘p’ as per the following equation:

$$m = f(\sum_{i=1}^{i=n}(w_i q_i + b_i) \tag{2.19}$$

Where, w_i is the weight vector, q_i is the input vector of the neural and b_i is the bias associated with each weight which may be zero for some accurately measured inputs of the system [34].

Feed forward back propagation network type is being applied to model the values of α_{CO2} as a function of T, P_{CO2} and molarity of the individual components of the solvent. Feed forward neural networks are multilayered networks in which the network input is provided in the first layer. Each layer appearing subsequently in the network is in turn connected with the previous layer. The network output is obtained from the final layer. The input-output non-linearity of many systems can be correlated using Feed forward networks. The network with optimized neurons and architecture can model any finite input-output data relationship. In a feed forward neural network, the connections between the nodes do not form a cycle. The flow of information is unidirectional in nature, from the input-hidden-output nodes. The architecture of the same has been represented in Figure 2.1. In order to have efficient ANN modeling and testing various networks, it is indispensable to have a good amount of data set for training, validation, and testing. The experimental data of solubility are divided randomly (individually) into three data sets: 70% data set is selected for training, 15% of data set is selected for validation and the rest 15% of data set is selected for testing ANN model. CO_2 solubility depends on various easily measurable factors such as temperature, CO_2 partial pressure, and molarity of the components in the solvent system. Hence, the same has been taken as the input vector to predict the solubility of CO_2 in terms of loading as output. The following relationship indicates the same:

$$\alpha_{CO2} = f(T, P_{CO2}, M_{amine}, M_{il}) \tag{2.20}$$

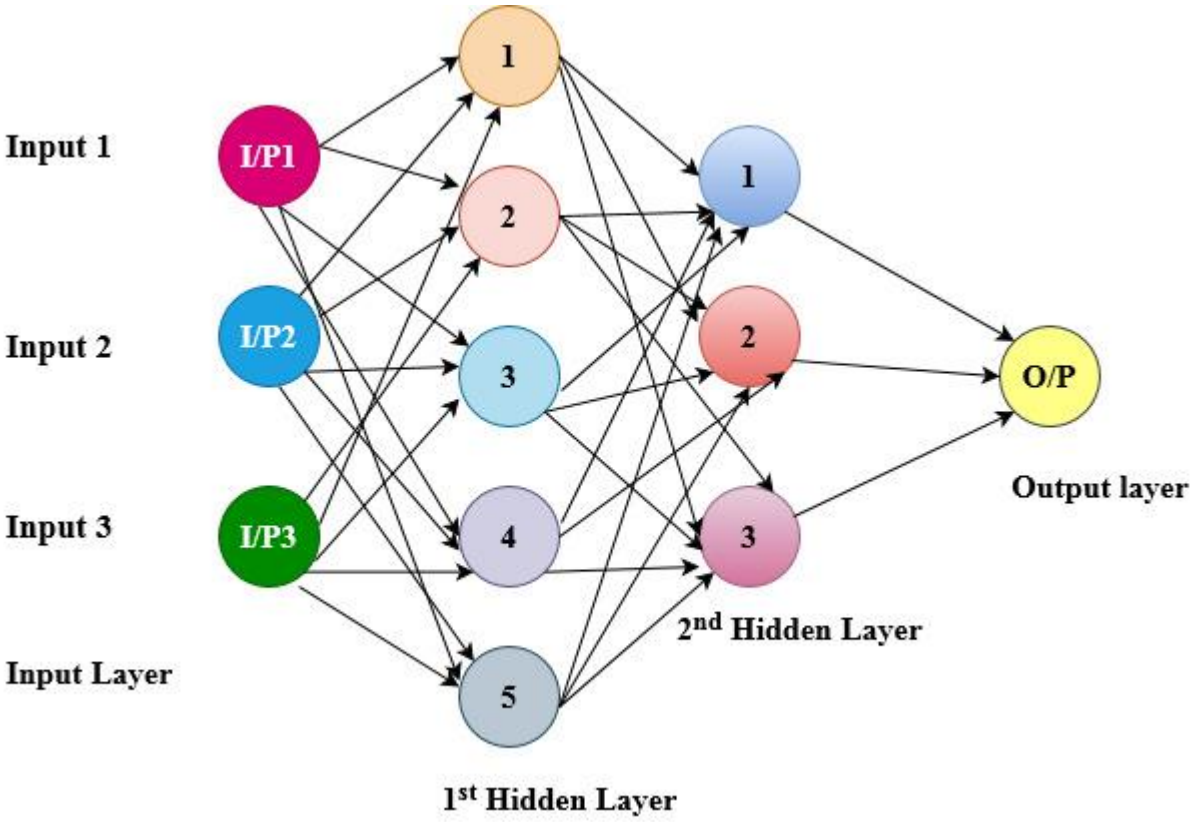

Figure 2.1 Architecture of feed forward neural network with 5 neurons in 1st hidden layer and 3 neurons in 2nd hidden layer

2.3.2.2 Preprocessing of data

If the range of i/p and o/p is very large i.e. in some cases, if i/p values are 10-100 folds more than the o/p, it is more appropriate to normalize the data for better predictions. Hence, before the training of the network, the input data for the CO_2 solubility system (temperature and pressure) are required to be normalized between 0 to 1. However, the input mole/mass fraction data as well as the output data of CO_2 solubility in terms of loading of CO_2 are not required to be normalized, since data are already available in the 0-1 range. The normalization is usually preferred using the following Eq. (2.21):

$$N_i = \frac{(M_i - M_{min})}{(M_{max} - M_{min})} \tag{2.21}$$

Where, N_i is the normalized value of *Mi*, M_{max} and M_{min} are the maximum and minimum values of M_i, respectively [35, 36].

2.3.2.3 Selection of optimal training and learning functions

The choice of training and learning functions play a key role in developing an efficient overall ANN algorithm. The Levenberg-Marquardt back propagation algorithm as a training function and Gradient descent with momentum weight and bias learning were employed as a learning function. The applicability of the same has been well approved in the literature for similar work [35, 36]. The transfer functions employed for hidden and output layers are log sigmoid and linear, respectively. The accuracy of the ANN type and combinations of training and learning functions can be identified using the calculation of many error analysis properties such as *%* Average absolute deviation (AAD) (Eq. 2.22), and *%* Mean Squared Error (MSE) as described in Eq. (2.23):

$$\%AAD = \frac{1}{N} \times \sum_{i=1}^{N} \frac{\left| Y_i^{\exp} - Y_i^{\mathrm{mod}} \right|}{Y_i^{\exp}} \times 100 \tag{2.22}$$

$$\%MSE = \frac{1}{N} \times \sum_{i=1}^{N} \left(Y_i^{\mathrm{mod}} - Y_i^{\exp} \right)^2 \times 100 \tag{2.23}$$

Where, *N*, Y^i_{exp} and Y^i_{mod}, represents the number of data points, experimental value of α_{CO2} and ANN modeled value of α_{CO2}, respectively.

2.4 Conclusions

Different reaction mechanisms pertaining to interaction between amines and CO_2 have been briefly discussed. The correlational analysis of vapor-liquid equilibrium studies of CO_2 with the solvents under study is proposed using modified Kent-Eisenberg model inclusive of gas phase non-ideality and feed-forward artificial neural network model.

References

[1]L. M. G. Sanchez, G. W. Meindersma, A. B. D. Haan. Kinetics of absorption of CO_2 in amino-functionalized ionic liquids. Chemical Engineering Journal 166 (2011) 1104–1115.

[2]L. Bihong, C. sun, N. Liu, W. Li, S. Li. Mass transfer and kinetics of CO_2 absorption into aqueous monoethanolamine/1-hydroethy-3-methyl imidazolium glycinate solution. Chemical Engineering Journal 280 (2015) 695-702.

[3]I. Iliuta, M. Hasib-ur-rahman, F. Larachi. CO_2 absorption in diethanolamine/ionic liquid emulsions-chemical kinetics and mas transfer study. Chemical Engineering Journal 240 (2014) 16–23.

[4]H. Guo, Z. Zhou, G. Jing. Kinetics of carbon dioxide absorption into aqueous [hmim] [gly] solution. International Journal of Greenhouse Gas Control 16 (2013) 197–205.

[5]M. Hasib-ur-rahman, F. Larachi. Kinetic behavior of carbon dioxide absorption in diethanolamine/ionic-liquid emulsions. Separation and Purification Technology 118 (2013) 757–761.

[6]L. S. Tan, A. M. Sharriff, K. K. Lau, M. A. Bustam. Factors affecting CO_2 absorption efficiency in packed column: a review. Journal of Industrial and Engineering Chemistry 18 (2012) 1874 – 1883.

[7]Z. Liang, W. Rongwong, H. Liu, Recent progress and new developments in post-combustion carbon-capture technology with amine based solvents. International Journal of Greenhouse Gas Control 40 (2015) 26-54.

[8]Subham Paul, Absorption of CO_2 by single and blended amine solvents in various gas–liquid contactors, PhD Thesis, Indian Institute of Technology Guwahati, 2008.

[9]J. E. Crooks, J. P. Donnellan. Kinetics and mechanism of the reaction between carbon dioxide and amines in aqueous solution. Journal of the Chemical Society Perkin Transactions 2 (1989) 331- 333.

[10]P. Singh, Ph.D. Dissertation, Amine based solvent for CO_2 absorption - from molecular structure to process, University of Twente, PhD Netherlands, ISBN 978-90-365-3200-6.

[11]T. L. Donaldson, Y. N. Nguyen. Carbon dioxide reaction kinetics and transport in aqueous amine membranes. Industrial and Engineering Chemistry Fundamentals 19 (1980) 260-266.

[12]Q. Zhou, Y. Wu, C. W. Chan, P. Tontiwachwuthikul. Modelling of the carbon dioxide capture process system using machine intelligence approaches, Engineering Applications of Artificial Intelligence 24 (2011) 673-685.

[13]J. C. L.Y. Fong, C. J. Anderson, G. Xiao, P. A. Webley, A. F. A. Hoadley. Multi-objective optimization of a hybrid vacuum swing adsorption and low temperature post combustion CO_2 capture. Journal of Cleaner Production 111 (2016) 193-203.

[14]A. Nalaparaju, M. Khurana, S. Farooq, I. A. Karimi, J. W. Jiang. CO_2 capture in cation exchanged metal organic frameworks: holistic modeling from molecular simulation to process optimization. Chemical Engineering Science 124 (2015) 70-78.

[15]Y. Wu, Q. Zhou, C. W. Chan. A comparison of two data analysis techniques and their applications for modelling the carbon dioxide capture process. Engineering Applications of Artificial Intelligence 23 (2010) 1265-1276.

[16]M. Safamirzaei, H. Modarress. Correlating and predicting low pressure solubility of gases in [bmim] [BF_4] by neural network molecular modelling. Thermochimica Acta 545 (2012) 125-130.

[17]J. S. Torrecilla, J. Palomar, J. Garcia, E. Rojo, F. Rodriguez. Modelling of carbon dioxide solubility in ionic liquids at sub and supercritical conditions by neural networks and mathematical regressions. Chemometrics and Intelligent Laboratory Systems 93 (2008) 149-159.

[18]M. T. Mota Martinez, M. C. Kroon, C. J. Peters. Modeling CO_2 solubility in an ionic liquid: a comparison between a cubic and a group contribution EoS. Journal of Supercritical Fluids 101 (2015) 54-62.

[19]S. K. Dash, A. N. Samanta, S. S. Bandyopadhyay. Vapor liquid equilibria of carbon dioxide in dilute and concentrated aqueous solutions of piperazine at low to high pressure. Fluid phase Equilibria 300 (2011) 145-154.

[20]L. Faramarzi, G. M. Kontogeorgis, K. Thomsen, E. H. Stenby. Extended UNIQUAC model for thermodynamic modeling of CO_2 absorption in aqueous alkanolamine solutions. Fluid Phase Equilibria 282 (2009) 121-132.

[21]X. Wang, J. Chen, J. Mi. Structure –solubility correlation model for carbon dioxide in ionic liquids. Industrial and Engineering Chemistry Research 52 (2013) 954-962.

[22]S. I. Mustapha, P. C. Okonkwo, S. M. Waziri. Improvement of carbon dioxide absorption technology using conductor like screening model for real solvents (COSMO-RS) method. Journal of Environmental Chemistry and Ecotoxicology 5(4) (2013) 96-105.

[23]R. L. Kent, B. Eisenberg. Better data for amine treating. Hydrocarbon process90 (1976) 87–90.

[24]Y. C. Chang, R. B. Leron, M. H. Li. Equilibrium solubility of carbon dioxide in aqueous solutions of (diethylenetriamine+ piperazine). Journal of Chemical Thermodynamics 64 (2013) 106–113.

[25]H. Pahlavanzadeh, S. Nourani, M. Saber. Experimental analysis and modeling of CO_2 solubility in AMP (2-amino-2-methyl-1-propanol) at low CO_2 partial pressure using the models of Deshmukh-Mather and the artificial neural network. Journal of Chemical Thermodynamics 43 (2011) 1775-1783.

[26]Z. Y. Yang, A. N. Soriano, A. R. Caparanga, M. H. Li. Equilibrium solubility of carbon dioxide in (2-amino-2-methyl-1-propanol + piperazine + water). Journal of Chemical Thermodynamics 42 (2010) 659–665.

[27]M. H. Li, K. P. Shen. Calculation of equilibrium solubility of carbon dioxide in aqueous mixtures of monoethanolamine with methyldiethanolamine. Fluid Phase Equilibria 85 (1993)129–140.

[28]D. M. Austgen, G. T. Rochelle, X. Peng, C. C. Chen. Model of vapor-liquid equilibria for aqueous acid gas-alkanolamine systems using the electrolyte-NRTL equation. Industrial and Engineering Chemistry Research 28 (1989) 1060–1073.

[29]D. M. Austgen, G. T. Rochelle, C. C. Chen. Model of vapor-liquid equilibria for aqueous acid gas-alkanolamine systems. 2. Representation of hydrogen sulfide and carbon dioxide solubility in aqueous MDEA and carbon dioxide solubility in aqueous mixtures of MDEA with MEA or DEA. Industrial and Engineering Chemistry Research 30 (1991) 543–555.

[30]W. Hu, A. Chakma. Modelling of equilibrium solubility of CO_2 and H_2S in aqueous amino methyl propanol (AMP) solutions. Chemical Engineering Communications 94 (1990) 53–61.

[31]W. Hu, A. Chakma. Modelling of equilibrium solubility of CO_2 and H_2S in aqueous diglycolamine (DGA) solutions. Canadian Journal of Chemical Engineering 68 (1990) 523–525.

[32]S. J. Hwang, H .K. Kwang, S. Lee. Prediction of VLE for aqueous blended amines using VLE models of single amines, International Journal of Greenhouse Gas Control 49 (2016) 250–258.

[33]M. Mirarab, M. Sharifi, M. A. Ghayyem, F. Mirarab. Prediction of solubility of CO_2 in ethanol-[EMIM] [Tf_2N] ionic liquid mixtures using artificial neural networks based on genetic algorithm. Fluid Phase Equilibria 371 (2014) 6–14.

[34]M. A. Sedghamiz, A. Rasoolzadeh, M. R. Rahimpour. The ability of artificial neural network in prediction of the acid gases solubility in different ionic liquids. Journal of CO_2 Utilization 9 (2015) 39–47.

[35]M. E. Hamzehie, M. Fattahi, H. Najibi, B. V. D. Bruggen, S. Mazinani, Application of artificial neural networks for estimation of solubility of acid gases (H_2S and CO_2) in 32 commonly ionic liquid and amine solutions. Journal of Natural Gas Science and Engineering 24 (2015) 106-114.

[36]M. E. Hamzehie, H. Najibi. Prediction of carbon dioxide loading capacity in amino acid salt solutions as new absorbents using artificial neural network and deshmukh-mather models. Journal of Natural Gas Science and Engineering 27 (2015) 676-685.

Chapter 3

EXPERIMENTAL AND THEORETICAL STUDIES ON EQUILIBRIUM CO_2 SOLUBILITY IN ([BMIM] [AC] + H_2O) AND ([BMIM] [AC] + AEP/APA + H_2O)

The ability of imidazolium-based ionic liquid solvents for the possible application in post-combustion CO_2 capture technology has drawn considerable attention recently owing to its thermal stability and lower regeneration cost. This chapter presents a broad experimental and theoretical analysis on the equilibrium solubility of CO_2 using aqueous 1-butyl-3-methyl-imidazolium acetate and its blends with AEP and APA over an extensive range of temperature and pressure. The experimental vapor-liquid equilibrium data (VLE) were modeled by modified Kent-Eisenberg equilibrium model including the gas phase non-ideality and Feed forward neural network model. Along with this, qualitative ^{13}C NMR and FTIR analysis have been also performed to assess the proposed reaction scheme.

3.1 Introduction

For post-combustion processes, amine technology being the most developed one using traditional solvents (MEA, MDEA, AMP, PZ, etc.) faces several problems such as high regeneration energy, corrosion products, etc. Hence, the need for better solvents is still a thrust area of research. Few emerging technologies have received good appreciation over the past few decades including usage of either pure ILs, blended ILs [1, 2, 3], silyated amines [4], and grafted ILs [5, 6]. The ILs tend to provide ease of regeneration due to low vapor pressures and better thermal stability. But the counter-disadvantages of using pure ILs being the higher cost of processing due to high viscosity of the systems. The regeneration energy costs around 70 % of the total cost of the separation process of CO_2 capture using absorption. Due to the higher thermal stability and lower vapor pressure of the ILs, they are expected to provide the advantage of lower regeneration energy and

less solvent losses. Hence, the amalgamation of ILs and amines is being proposed for post combustion CO_2 capture.

Amongst the many different ionic liquids, cations that are based on imidazole are somewhat well studied in the literature for two major reasons: one being the high CO_2 selectivity due to the presence of imidazole group and the other being cost effective in comparison to another cation based ILs. For the present study, 1-butyl-3-methyl-imidazolium acetate ([bmim] [Ac]) is considered due to its high CO_2 solubility [7]. The detailed structural analysis, physicochemical and critical properties of [bmim] [Ac] have been studied and reported in the literature [7–14]. Studies on the utilization of [bmim] [Ac] with either binary mixture of MDEA, MEA, DEA, DIPA and, AMP [15–17] for CO_2 capture has been also reported. The results obtained in the literature indicated a high CO_2 solubility along with the benefits of extremely low vapor pressure from IL and high CO_2 solubility owing to the presence of amines. However, the reported studies were majorly focusing on pure solvent for CO_2 capture i.e. non-aqueous. Hence, present work is focused on choosing amines that should act as an activator at a lower concentration in comparison to ionic liquid while keeping the total solvent concentration to be optimum.

The blended solvent system which consists of blending two or more solvent as well as blending with appropriate rate activator exhibit very promising result in the acid gas separation technology [17, 18]. Amongst the category of activators, piperazine (PZ) has been explored extensively because of its favorable characteristics such as higher reaction rate, higher equilibrium solubility and lower regeneration temperature compared to a conventionally used solvent such as monoethanolamine (MEA). Researchers have blended PZ with MDEA or AMP based solvents owing to their favorable thermodynamic and kinetic properties. However, the usage of concentrated piperazine is limited since it precipitates at lower temperature and lean CO_2 loading. The usage of derivatives of piperazine such as 1-(2-aminoethyl) piperazine (AEP), 1-methyl piperazine (1-MPZ), 2-methyl piperazine (2-MPZ) [19-23] have been also practiced to overcome the constraints revealed by piperazine. AEP exhibited a higher CO_2-amine reaction rate constant (3.33×10^4 m^3. $kmol^{-1}$ s^{-1} at 303.15 K) compared to PZ and MEA [24]. In addition, AEP can increase CO_2 equilibrium solubility [25]. The efficiency of another amine based activator, bis (3- amino propyl) amine (APA), had been reported elsewhere [26]. The selection of APA was based on the higher pKa values of APA in comparison to PZ. The rate of reaction of CO_2 in aq. (APA + AMP)

have been found to intensify with the increase in APA concentration. The molecular structural analysis of APA also suggests that it consists of two primary and one secondary amino groups which has a huge contribution to CO_2 equilibrium solubility as well as rate of the reaction.

The combination of [bmim] [Ac] with amine activators, AEP and APA, may provide better CO_2 loading compared to conventional aqueous amine solvents with the advantages of lower vapor pressures and easier regeneration of the IL blends. By changing the amine and ionic liquid blend composition will give an effective means for CO_2 capture. A first principle modified Kent-Eisenberg model is used to fit VLE data. The major advantage of the modified KE model is its simplicity and few input variables. However, the subsequent output of the model also demonstrates useful insights such as equilibrium constants associated with the proposed reactions, the concentration profiles of the related species as well as pH of the system.

In this chapter, the measurement of CO_2 equilibrium solubility of the novel aqueous blends of imidazolium based 1-butyl-3-methyl-imidazolium acetate ionic liquid with AEP and APA is carried out in the temperature range of (303.2-323.2) K and (1-390) kPa CO_2 partial pressure. The concentration of [bmim] [Ac] is varied from ca. 2.0 *m* to ca. 2.5 *m* while amine activators is varied in the range ca. (0.5-1.0) *m*.

3.2 Experimental section

3.2.1 Materials

CO_2 gas (> 99 % Pure) was procured from Linde India Ltd. and used without further purification. 1-Butyl-3-methyl-imidazolium acetate ([bmim] [Ac], ≥ 95% Pure), 1-(2-aminoethyl) piperazine (AEP, 99 % Pure), and bis (3-aminopropyl) amine (APA, 98 % Pure) were purchased from Sigma–Aldrich. AEP and APA are used with no auxiliary refinement for the CO_2 solubility study. For solution preparation, [bmim] [Ac] was first analyzed for its initial water content by Karl-fisher method which was found to be 1.7 %. Then the solvent was vacuum dried for 48 h and analyzed again for water content which was now only 0.04 %. The solvent solutions were prepared with double distilled deionized water. Specification details of the chemicals used under the study are given in Table 3.1.

Table 3.1 Specifications of the chemicals

Chemical name	Chemical structure	Molecular weight	Source	Stated mass fraction purity	CAS no.	Purification method
1-butyl-3-methyl-imidazolium acetate ([bmim][Ac])	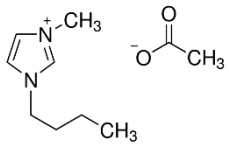	198.26	Sigma Aldrich Co.	≥0.95	284049-75-8	Vacuum drying
1-(2-Aminoethyl) Piperazine (AEP)	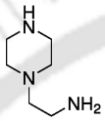	129.21	Sigma Aldrich Co.	0.99	140-31-8	None
Bis(3-aminopropyl)amine (APA)	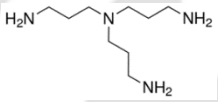	131.22	Sigma Aldrich Co.	0.98	56-18-8	None
Carbon dioxide (CO_2)		44.01	Linde India Ltd.	>0.99	367522-96-1	None

3.2.2 Experimental methodology

3.2.2.1 Vapour liquid equilibrium (VLE) measurement

VLE of the aq. [bmim] [Ac], aq. ([bmim] [Ac] + AEP) and aq. ([bmim] [Ac] + APA) systems was measured in a stainless steel stirred equilibrium cell (600×10^{-6} m^3) connected to a (1200×10^{-6} m^3) SS buffer cell. The schematic of the experimental set-up developed in this work is shown in Figure 3.1. The buffer cell is fitted with a pressure transmitter (0-500 psia, Honeywell STA74L, USA) and has an accuracy of ± 0.065 % of the full scale. The equilibrium cell is fitted with a pressure transmitter (0-100 psia, Rosemount 2051T, Emerson process management, USA) and has an accuracy of ± 0.065 % of the full scale. Temperature sensor (Pt 100, Julabo FRG) with an accuracy of ± 0.1 K are mounted at the respective cell to measure the temperature. A magnetic stirrer (5MLH, Remi Instruments Ltd., India) was used for liquid phase stirring which is placed under the equilibrium cell. The equilibrium and buffer cell assembly is submerged in a

thermostated water bath. The temperature of the water bath is controlled by a water circulating temperature controller (F32HL, Julabo, FRG) with an accuracy of ± 0.1K. The tubing and needle valves used for regulating the gas flow and solvent inlet to the system are of Swagelok make.

For each experimental run, the equilibrium cell and buffer cell were allowed to reach the thermal equilibrium with the external temperature controller to attain the experimental temperature. High vacuum was applied in both cells simultaneously using vacuum pump (IV-50, INDVAC, India). The vacuum pump was then kept disconnected. After the evacuation, the buffer cell was made to fill with pure CO_2 from the external cylinder till it attains a pressure of about 300 psia. The equilibrium cell was then fed with a known amount of aqueous amine solution (50×10^{-6} m^3) from the solvent injection port with the help of an attached burette, and the port was fully closed by operating the needle valve. The amine solution was again degassed to remove any dissolved gases in the liquid by applying an instant vacuum and it was kept under this condition for about 20 minutes so that the liquid inside the cell exists under its own vapor pressure. The vapor pressure corresponding to the experimental temperature inside the equilibrium cell (P^v) and the initial pressure in the buffer cell (P_{b1}) were measured using the pressure transducers mounted on each cell. A certain amount of CO_2 gas from the buffer cell was then transferred to the equilibrium cell by operating needle valve between them. The magnetic stirrer kept under the equilibrium cell was kept on for liquid phase stirring. As CO_2 gas is absorbed by the solution inside the equilibrium cell, the total pressure of the cell decreases. Vapour and liquid phase equilibrium was attained when there was no change of total pressure in the equilibrium cell noted at least for 1 hour. At this condition total pressure in the equilibrium cell, (P^T) and the final pressure in the buffer cell, (P_{b2}) were recorded simultaneously. The equilibrium partial pressure of CO_2 at the experimental temperature was calculated by taking the difference between total pressure and solvent vapor pressure ($P_{CO2}=P^T-P^v$). The liquid phase CO_2 loading (α_{CO2}) was calculated using equations (3.1-3.5) as reported in the literature [25]. This procedure was repeated to obtain liquid phase CO_2 loading at different higher CO_2 partial pressures and at different temperatures.

A similar experimental set-up has also been proved to provide accurate CO_2 solubility data in the literature [27, 28]. These data are also useful in further analyzing the pressure in terms of calculating concentration of various species involved in the reactions, CO_2 cyclic capacity, heat of absorption, etc. However, such calculations cannot be performed while utilizing other

methodologies for CO_2 absorption such as wetted wall column method [29], Rubotherm magnetic suspension balance [30], etc.

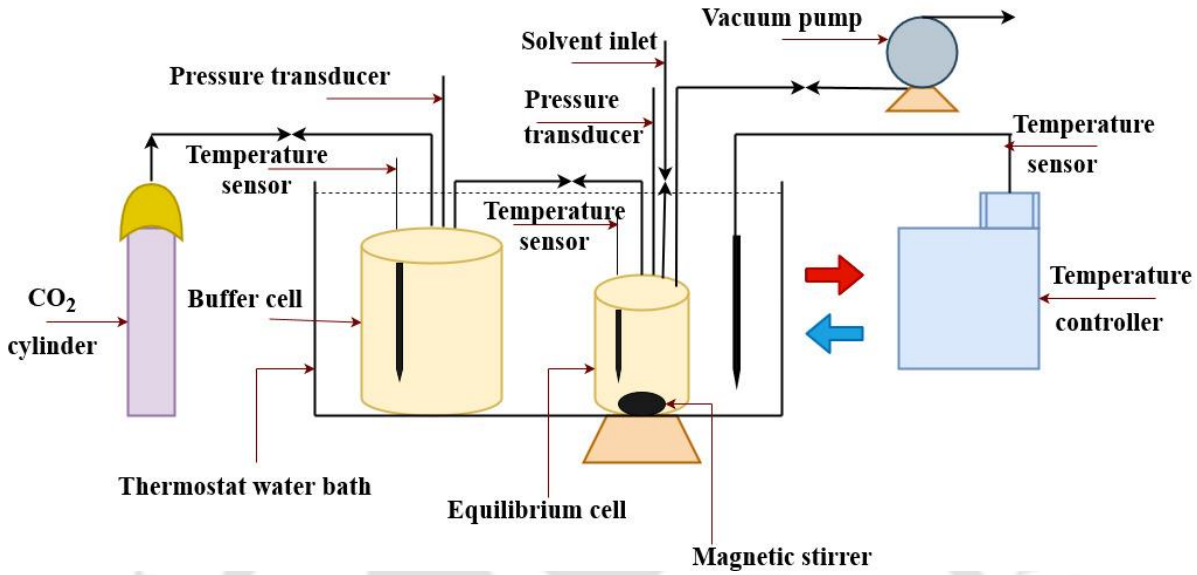

Figure 3.1 Schematic diagram of experimental set-up

The total pressure (P^T) prevailing in equilibrium vessel and solvent vapour pressure (P^v) can be used to evaluate the equilibrium partial pressure of CO_2 (P_{CO2}) at the respective temperature and liquid phase CO_2 loading [31]. The CO_2 loading (α_{CO2}) were further estimated functional of temperature and P_{CO2}.

The total moles of CO_2 for solubility, n_{CO2}, transported from buffer vessel to equilibrium vessel is calculated by using Eq. (3.1)

$$n_{CO2} = \frac{V_b}{R \times T} \times \left(\frac{P_{b1}}{Z_1} - \frac{P_{b2}}{Z_2} \right) \tag{3.1}$$

Where, V_b is volume of the buffer cell, Z_1 and Z_2 are the compressibility factors corresponding to the initial pressure (P_{b1}) and final pressure (P_{b2}) of the buffer cell, respectively. Owing to the gas phase non-ideality at high CO_2 pressures, and compressibility factor (Z) is incorporated while calculation of moles remaining in the gas phase. Here, 'Z_1' and 'Z_2' are calculated using Peng-

Robinson Equation of State (EOS) and the values are used in Eq. (3.1). The residual CO_2 moles in the gas phase (n^g_{CO2}) later the achievement of VLE is estimated by Eq. (3.2).

$$n^g{}_{CO2} = \frac{V^g \; P_{CO2}}{Z_{CO2} RT} \tag{3.2}$$

Where, V^g and Z_{CO2} denote the gas phase volume and the compressibility factor of CO_2 in the equilibrium cell, respectively. Subtraction of liquid volume from equilibrium vessel volume leads to the computation of gas phase volume. The original Peng Robinson Equations of state can be given as follows:

$$P = \frac{R \times T}{v - b} - \frac{a(T)}{v \times (v-b) + b \times (v-b)} \tag{3.3}$$

The above Eq. in form of compressibility factor can be re-written as:

$$z^3 - (1-B) \times Z^2 + (A - 2 \times B - 3 \times B^2) \times Z - (A \times B - B^2 - B^3) = 0 \tag{3.4}$$

Where,

$$A = \frac{a(T) \times P}{R^2 \times T^2} \tag{3.4-a}$$

$$B = \frac{b \times P}{R \times T} \tag{3.4-b}$$

$$a(T) = 0.45724 \times a(T) \times \frac{R^2 \times T_C^2}{P_c} \tag{3.4-c}$$

$$b = 0.07780 \times \frac{R \times T_c}{P_c} \tag{3.4-d}$$

$$a(T) = \left[1 + (0.37646 + 1.4522 \times \omega - 0.26992 \times \omega^2) \left(1 - \sqrt{\frac{T}{T_c}} \right) \right]^2 \tag{3.4-e}$$

Where, P , T , v , and R are pressure, temperature, molar volume and gas constant (8.314 J mol^{-1} K^{-1}). Also, parameters a and b are described in the forms of P_c, critical pressure, T_c, critical temperature and ω, acentric factor of the species.

CO_2 loading at equilibrium (α_{CO2}) consequent to a P_{CO2} can be articulated as moles of CO_2/moles of total ([bmim] [Ac] + AEP/APA) and can be calculated using a vapor and liquid phase mass balance of CO_2. The expression is given by:

$$\alpha_{CO2} = \frac{n_{CO2} - n^{g}{}_{CO2}}{n_{am}} \tag{3.5}$$

Where, n_{am} indicates the total moles of solvent in the liquid phase.

3.2.2.2 Standard uncertainty in the solubility measurement

The estimation of α_{CO2} is associated with standard uncertainty which can be calculated using error propagation theory [31]. A similar concept of uncertainty estimation has been reported and accepted by many researchers [32, 33]. The equation for standard uncertainty calculation is given by:

$$u^2(y) = \sum_{i=1}^{n}\left(\frac{\partial f}{\partial x_i} \times u(x_i)\right)^2 \tag{3.6}$$

Where, $u(y)$ and $u(x_i)$ are the standard uncertainty corresponding to CO_2 loading and standard uncertainties associated with pressure, temperature, reactor volume, and concentration of ingoing solvent, respectively.

3.2.2.3 FTIR-ATR and ^{13}C NMR study

The structural analysis and the confirmation of various reacting species and formation of products is being carried out by performing qualitative ^{13}C NMR (500 MHz NMR spectrophotometer in D_2O, Model: Ascend, Bruker) and FTIR- ATR spectroscopy (Model: Perkin Elmer Inc., Germany) tests. CO_2 unloaded and loaded pure [bmim][Ac] and aqueous ([bmim][Ac] + APA) blend solvents have been tested in the range of 3000 to 500 cm^{-1} and 2000 to 800 cm^{-1}, respectively.

3.3 Proposed chemical reaction

The ^{13}C NMR analysis of the studied solvents is presented in Figures 3.2 and 3.3. The peaks at 18.86 and 18.80 correspond to acetic acid. Also, the presence of a stable carboxylate group has been confirmed through a sharp peak at 36.5. Similar observations were reported in the literature [7, 8] which concludes that the absorption of CO_2 in pure [bmim] [Ac] results in the formation of unstable acetic acid and stable imidazolium carboxylate due to rearrangement of the imidazole group of [bmim] [Ac]. In addition to these major peaks, a very small peak was also observed at 158.22 representing the carbamate formation. Different carbamate groups were confirmed at peaks 164.84, 164.72, 164.29, and 160.43 positions in the low field range of (163-165 ppm) for CO_2 loaded aqueous ([bmim] [Ac] + APA). The formation of carbamate ions while CO_2 reacts in aqueous APA is also confirmed in the literature [34].

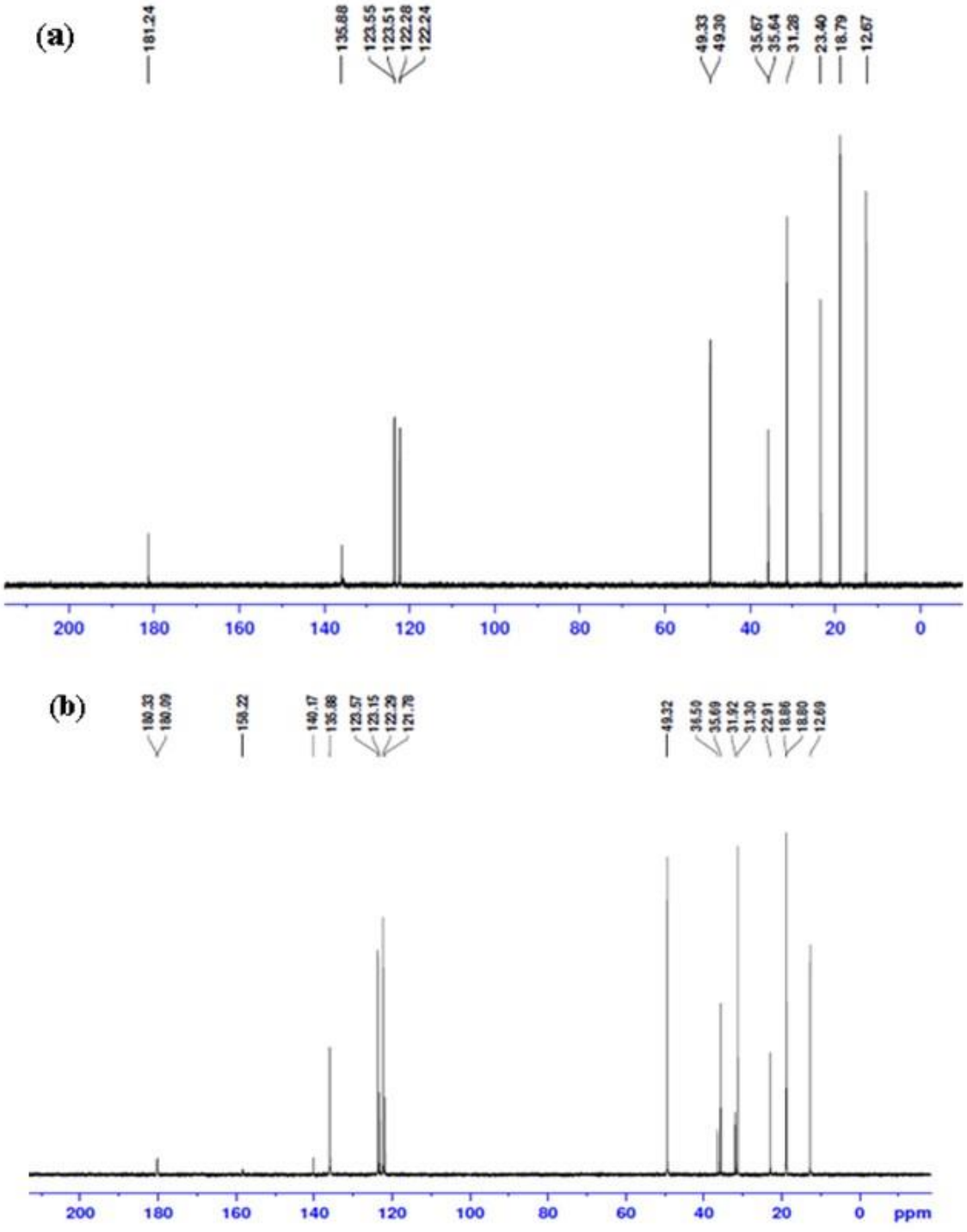

Figure 3.2 ^{13}C NMR spectra of pure [bmim] [Ac] (a) unloaded (b) CO_2 loaded at 303.2 K

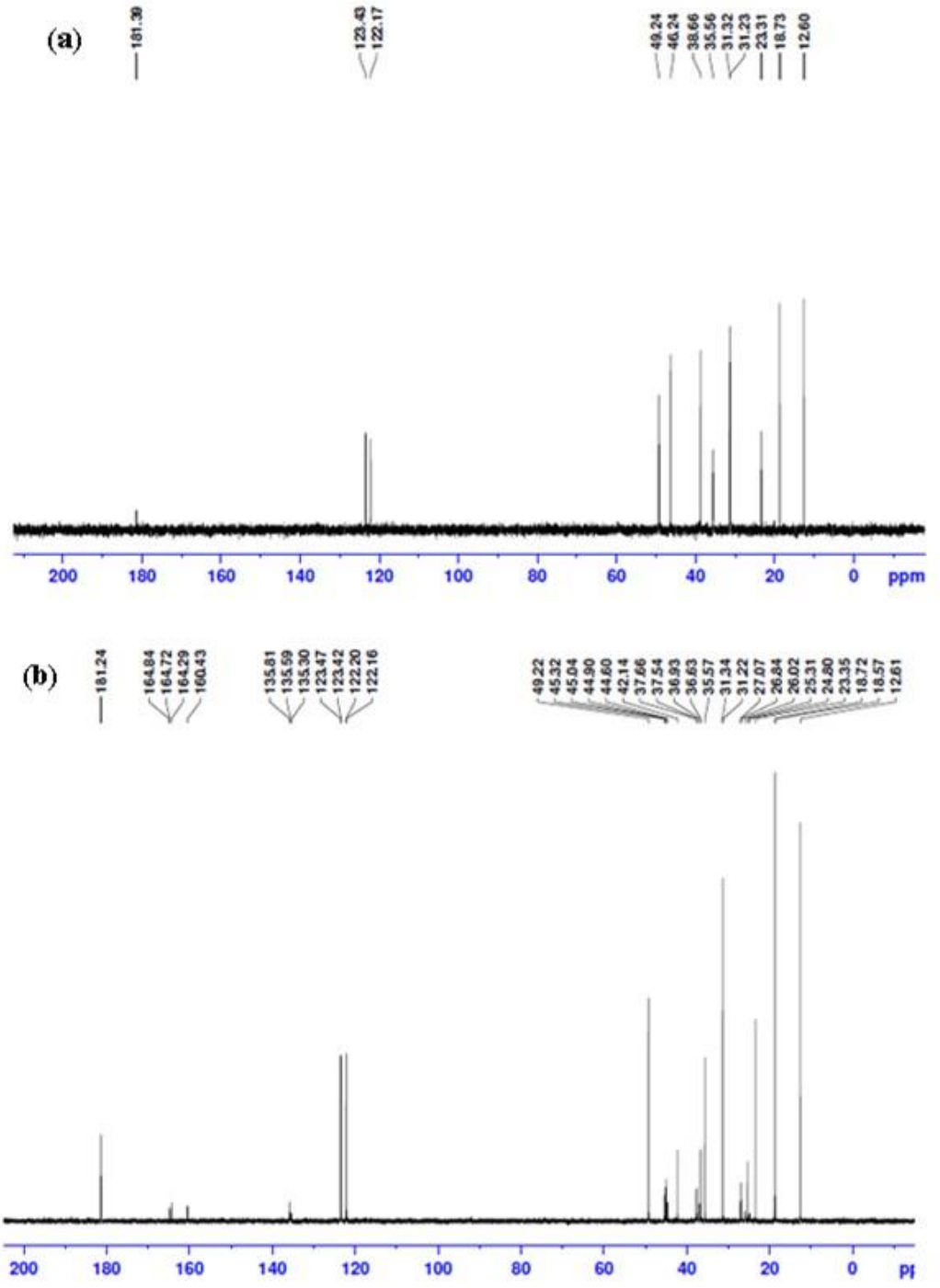

Figure 3.3 ^{13}C NMR spectra of aq. (2.251 *m* [bmim] [Ac] + 0.753 *m* APA) (a) unloaded (b) CO_2 loaded at 303.2 K

Three distinguished FTIR peaks for the loaded solvents corresponding to the oxalate salts $(O_2C\text{-}CO_2)_2^{2-}$, (1665, 1322, 789) cm^{-1} are observed in the present work (Figures 3.4 - 3.5) [7]. Additionally, characteristic peaks at 2958, 2873, 2744, 1600, 1379, 1000 cm^{-1} are also observed confirming stretching asymmetric vibrations in the C-H, stretching symmetric vibrations rocking mode in C-H, stretching symmetric and stretching asymmetric vibrations of C=O, in-plane scissoring (bending) in C-H and in-plane rocking in C-H bonds, respectively.

New bands at 1487 and 1342 cm^{-1} are observed for loaded solvent in comparison with unloaded one, which can be assigned to COO^- symmetric stretching and N-COO^- stretching vibration of the carbamate species, respectively (Figure 3.5). Also, C-OH stretching modes shift is also observed corresponding to the protonation of $APAH^+$ which is confirmed by peak shifts at 1017 cm^{-1}. Likewise, the peaks at 928 and 843 cm^{-1} can be attributed to C-NH_2 twisting for APA. The peak at 1169 cm^{-1} can be consequential due to the asymmetric vibrational stretching of CO-O-C [35, 36]. A reaction scheme for the formation of intermediates while CO_2 reacts with [bmim] [Ac] while forming of acetic acid and stable imidazolium carboxylate is proposed in the present work (Figure 3.6).

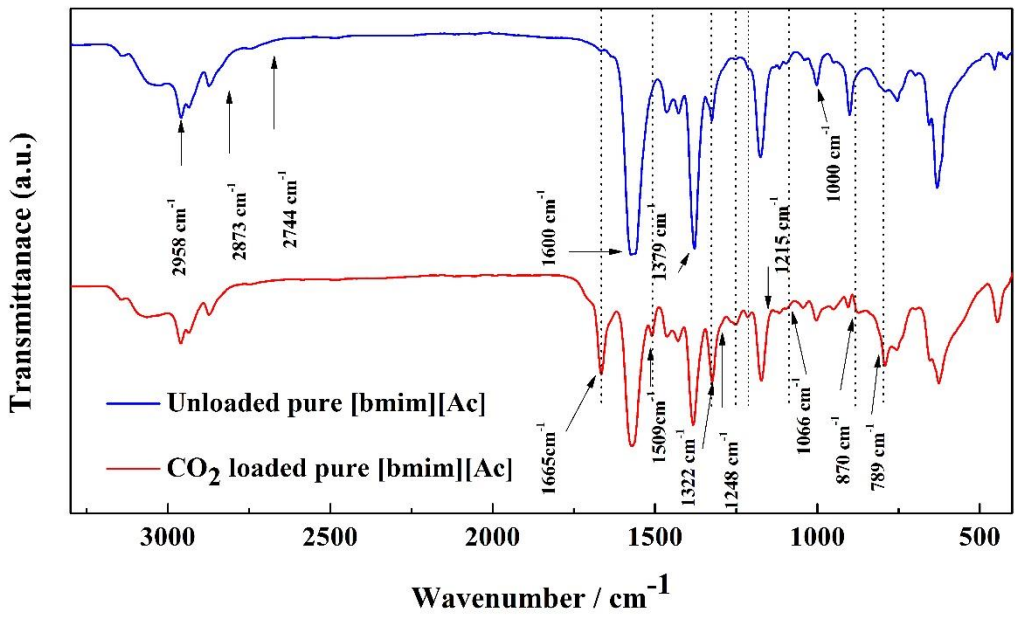

Figure 3.4 FTIR-ATR spectra of pure [bmim] [Ac] unloaded and CO_2 loaded at 303.2 K

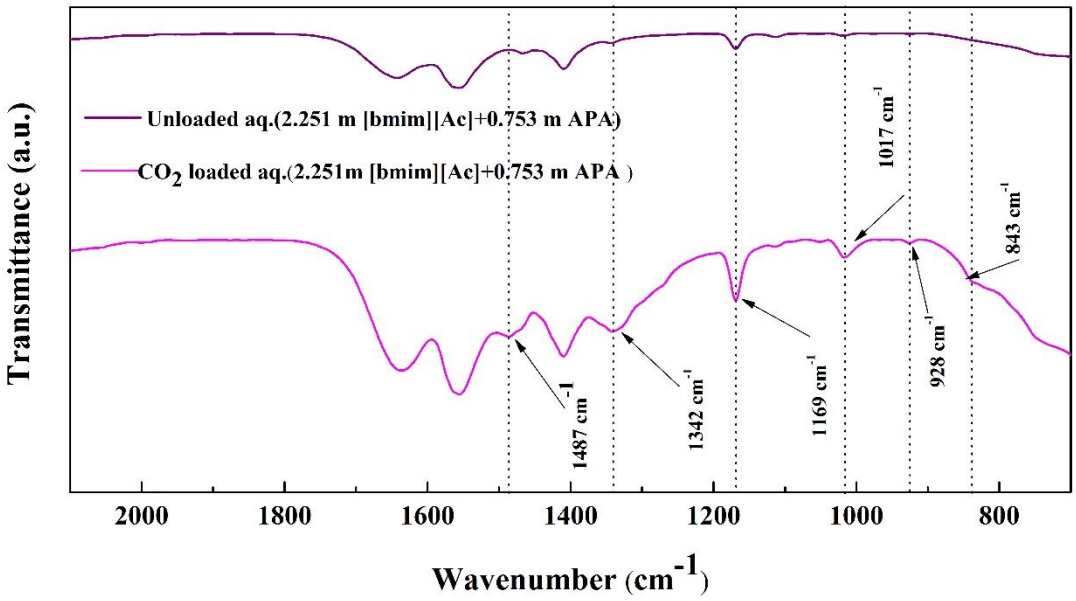

Figure 3.5 FTIR-ATR spectra of aq. (2.251 *m* [bmim] [Ac] + 0.753 *m* APA) unloaded and CO_2 loaded at 303.2 K

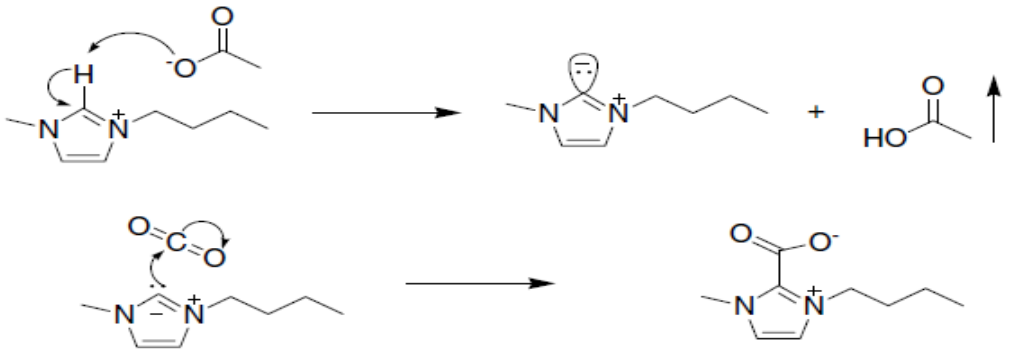

Figure 3.6 Proposed chemical reaction of [bmim][Ac] and CO_2 [7,8]

The equilibrium reactions for ([bmim] [Ac] + H_2O + CO_2), ([bmim] [Ac] + AEP + H_2O + CO_2) and ([bmim] [Ac] + APA + H_2O + CO_2) systems are proposed in this work (Table 3.2).

Table 3.2 Description of reaction and mechanism associated with reactions in the system

Sr. No.	Description of reaction	Reaction mechanism
1	Physical solubility	$CO_2(g) \overset{H_{CO2}}{\leftrightarrow} CO_2(aq)$
2	Dissociation of bicarbonate ion	$HCO^{3-} \overset{K_1}{\leftrightarrow} CO_3^{2-} + H^+$
3	Formation of bicarbonate ion	$CO_2 + H_2O \overset{K_2}{\leftrightarrow} HCO_3^- + H^+$
4	Dissociation of water	$H_2O \overset{K_3}{\leftrightarrow} OH^- + H^+$
5	Deprotonation of [bmim] [Ac] (R_1)	$R_1^+ \overset{K_4}{\leftrightarrow} R_1 + H^+$
6	Carbamate hydrolysis of [bmim] [Ac] (R_1)	$R_1COO^- + H_2O \overset{K_5}{\leftrightarrow} R_1 + HCO_3^-$
7	Deprotonation of AEP	$AEPH^+ \overset{K_6}{\leftrightarrow} AEP + H^+$
8	Carbamate hydrolysis of AEP	$AEPCOO^- + H_2O \overset{K_7}{\leftrightarrow} AEP + HCO_3^-$
9	Deprotonation of APA	$APAH^+ \overset{K_6'}{\leftrightarrow} APA + H^+$
10	Carbamate hydrolysis of APA	$APACOO^- + H_2O \overset{K_7'}{\leftrightarrow} APA + HCO_3^-$

3.4 Modeling of CO_2 solubility

The literature provides the prediction of CO_2 solubility in amine or ionic liquid based solutions using various models based on thermodynamics of the systems such as e-NRTL [31], Peng-Robinson Equation of State (EOS) [37], Deshmukh Mather [38, 39], and RETM model [40]. The EoS based models usually provide a better prediction capability in pure solvents. However, for CO_2 solubility in ILs or blended solvents, these models have proved to yield less accuracy [41]. Comparatively, the modified KE model is quite simple and requires less computation time [42,

43]. Hence, modified KE model has been considered here to correlate the CO_2 solubility data in aqueous blends inclusive of gas-phase non-ideality [44-47].

3.4.1 Modified Kent-Eisenberg model

The VLE data obtained for aq. [bmim] [Ac], aq. ([bmim] [Ac] + AEP) and aq. ([bmim] [Ac] + APA) is modelled using modified KE model. The physical solubility of CO_2 is usually due to the weak van der Walls forces of attraction which here is presented by Henry's law. Reversible reactions in the liquid phase are explained using chemical reaction equilibrium constants through the conceptualization of chemical equilibrium. The liquid phase reaction consists of protonation of both [bmim] [Ac] and APA/AEP amine activators, carbamate formation by APA/AEP and other reactions. The bicarbamate formation of AEP has not been considered [24] since at higher CO_2 loading bicarbonate is the major product of (AEP-CO_2) reaction [48]. The carbamate formation for the reaction between [bmim] [Ac] and CO_2 has been already reported in the literature [7, 8] and also confirmed in the present work by ^{13}C NMR analysis.

In the modified KE model, activity coefficients (γ_i) of all component species in the liquid phase are considered unit. The reactions 1-6 are applicable for CO_2 solubility in the system of aqueous [bmim] whereas reactions 1-10 are valid for CO_2 solubility in ([bmim] + AEP/APA) systems (Table 3.2). The concentration of component species based observable equilibrium constants of reactions are presented as:

$$K_1 = \frac{[CO_3^{2-}][H^+]}{[HCO_3^-]} \tag{3.7}$$

$$K_2 = \frac{[HCO^{3-}][H^+]}{[CO_2]} \tag{3.8}$$

$$K_3 = [H^+][OH^-] \tag{3.9}$$

For simplicity consider, R_1= [bmim] [Ac]

$$K_4 = \frac{[R_1][H^+]}{[R_1^+]} \tag{3.10}$$

$$K_5 = \frac{[R_1][HCO_3^-]}{[R_1COO^-]} \tag{3.11}$$

$$K_6 = \frac{[AEP][H^+]}{[AEPH^+]} \tag{3.12}$$

$$K_7 = \frac{[AEP][HCO_3^-]}{[AEPCOO^-]} \tag{3.13}$$

$$K_6^{'} = \frac{[APA][H^+]}{[APAH^+]} \tag{3.14}$$

$$K_7^{'} = \frac{[APA][HCO_3^-]}{[APACOO^-]} \tag{3.15}$$

Where, the square [ ] brackets indicate the concentration of the chemical species.

Vapor phase equilibrium, which dictates the relationship between CO_2 partial pressure P_{CO2} at equilibrium and physically dissolved CO_2 concentration [CO_2], is expressed here by Henry's law as presented in Eq. (3.16).

$$P_{CO_2} = H_{CO_2} \times [CO_2] \tag{3.16}$$

The general mass and charge balance of various molecular and ionic species present in the liquid phase can be expressed as:

R_1 Balance:

$$[R_1]_t = M_1 = [R_1] + [R_1H^+] + [R_1COO^-] \tag{3.17}$$

CO_2 balance for aqueous [bmim] [Ac] system:

$$\alpha_{CO_2} \times (M_1) = [CO_2] + [HCO^{3-}] + [CO_3^{2-}] + [R_1COO^-] \tag{3.18}$$

Where α_{CO2} is the CO_2 loading and M_1, represents initial R_1 ([bmim] [Ac]) molar concentration.

Charge Balance for aqueous [bmim] [Ac] system:

$$[H^+]+[R_1H^+]=[HCO_3^-]+2\times[CO_3^{2-}]+[OH^-]+[R_1COO^-] \quad (3.19)$$

The system of Eqs. (3.7) - (3.15) and (3.17) - (3.19) can be utilized to develop polynomial equations which are formed in terms of $[H^+]$. The equation hence formed for systems considered associated with the coefficients can be given as follows:

For aqueous [bmim] [Ac] system:

$$A_1\times[H^+]^5+B_1\times[H^+]^4+C_1\times[H^+]^3+D_1\times[H^+]^2+E_1\times[H^+]+F_1=0 \quad (3.20)$$

Where,

$$A_1=K_5 \quad (3.20\text{-a})$$

$$B_1=K_5\times(K_4+M_1) \quad (3.20\text{-b})$$

$$C_1=K_2\times[CO_2]\times(K_4-K_5)-K_5\times K_3 \quad (3.20\text{-c})$$

$$D_1=-K_2\times K_5\times[CO_2](K_4+2\times K_1)-K_3\times K_4\times K_5 \quad (3.20\text{-d})$$

$$E_1=-K_2\times K_4\times[CO_2]\times(K_2\times[CO_2]+2\times K_1\times K_5+K_3) \quad (3.20\text{-e})$$

$$F_1=-2\times K_1\times K_2^2\times K_4\times[CO_2]^2 \quad (3.20\text{-f})$$

Furthermore, the modified form of loading equation for the aqueous [bmim] [Ac] system is derived as:

$$\alpha_{CO_2}=\frac{\varphi_{CO2}\times P_{CO_2}}{(H_{CO_2}\times M_1)}\left[1+\frac{K_2}{[H^+]}+\frac{K_1\times K_2}{[H^+]^2}+\frac{M_1\times K_2\times K_4}{K_4.\times K_5\times[H^+]+K_5\times[H^+]^2+K_2.\times K_4\times\left[\frac{P_{CO_2}}{H_{CO_2}}\right]}\right] \quad (3.21)$$

Where ϕ_{CO2}, is fugacity coefficient contributing to the non-ideality in the gas phase.

Utilizing Virial EOS, fugacity coefficients were estimated. The fugacity coefficient of an acid gas in the gaseous blend is estimated by the fugacity coefficient of the acid gas (total CO_2 pressure in the present case) at its partial pressure.

$$\ln(\phi_{CO2}) = \frac{B_{ii}}{R \times T} \int_0^P dP \tag{3.22}$$

$$\text{or, } \ln(\varphi_{CO2}) = \frac{B_{ii} \times P}{R \times T}$$

Where, *Bii* indicates the interactions between paired molecules and can be considered using Virial EOS.

$$\ln(\phi_{CO2}) = \frac{B_{ii} \times P_C \times P_R}{R \times T_C \times T_R} \tag{3.22-a}$$

Including the accentric factor in the above Eq. (3.22-a), it can be written as:

$$\ln(\varphi_{CO2}) = (U_1 + \omega \times U_2) \times \frac{P_R}{T_R} \tag{3.22-b}$$

Where,

$$U_1 = 0.083 - \frac{0.422}{T_R^{1.6}} \tag{3.22-c}$$

$$U_2 = 0.139 - \frac{0.172}{T_R^{4.2}} \tag{3.22-d}$$

Here, P_R, P_C, T_R, T_C and ω are reduced pressure, critical pressure, reduced temperature, critical temperature and acentric factor which is 0.239 for CO_2, respectively. The values for P_C and T_C were taken as 73.87 bar and 304.2 K, respectively.

α_{CO2} is calculated using Eq. (3.21) which requires the real root of $[H^+]$ obtained from Eq. (3.20). In modified KE model, the equilibrium constants $(K_1 - K_3)$ can be measured functional of temperature as below:

$$\ln K = a_i + \frac{b_i}{T} + c_i \times \ln T \tag{3.23}$$

Where a_i, bi and c_i are coefficients of above equation and are tabulated in Table 3.3. The physical solubility represented by Henry's constant, H_{CO_2} can be given as below [43].

$$\ln H_{CO_2} = 20.2669 - \frac{1.3830 \times 10^4}{T} + \frac{0.0691 \times 10^8}{T^2} - \frac{0.0156 \times 10^{11}}{T^3} + \frac{0.0120 \times 10^{13}}{T^4} \tag{3.24}$$

Where, H_{CO2} is in kPa.m^3.kmol^{-1} and T is in Kelvin. In this work, the equations related to the modified KE model are hence a combination of various linear and non-linear equations which necessarily be solved simultaneously. For the same, an essential requirement stands to be optimization technique along with a specific objective function, which in the present work is taken to be the error deviation. The equilibrium constants K_4, K_5, K_6, K_7, K'_6, and K'_7 which are associated with the deprotonation and carbamate hydrolysis reactions of [bmim] [Ac], AEP, and APA, respectively, and also are obtained as a function of P_{CO2}, T, and solvent concentration using regression analysis in MATLAB (R17). The solution of Eq. (3.20) results in multiple roots of $[H^+]$ but, an only single value of $[H^+]$ that belongs in array of 10^{-12} - 10^{-5} kmol. m^{-3} has been used for α_{CO2} calculations. The essential procedure for used regression analysis is shown in Figure 3.7.

Table 3.3 Parameters corresponding to equilibrium constant used in the KE model

Equation	Reference
$K_1 = \exp\left(220.067 - \frac{12431.7}{T} - (35.482 \times \ln T)\right)$ (kmol.m^{-3})	[3]
$K_2 = \exp\left(235.485 - \frac{12092.1}{T} - (36.782 \times \ln T)\right)$ (kmol.m^{-3})	[3]
$K_3 = \exp\left(140.932 - \frac{13445.9}{T} - (22.477 \times \ln T)\right)$ (kmol.m^{-3})	[3]

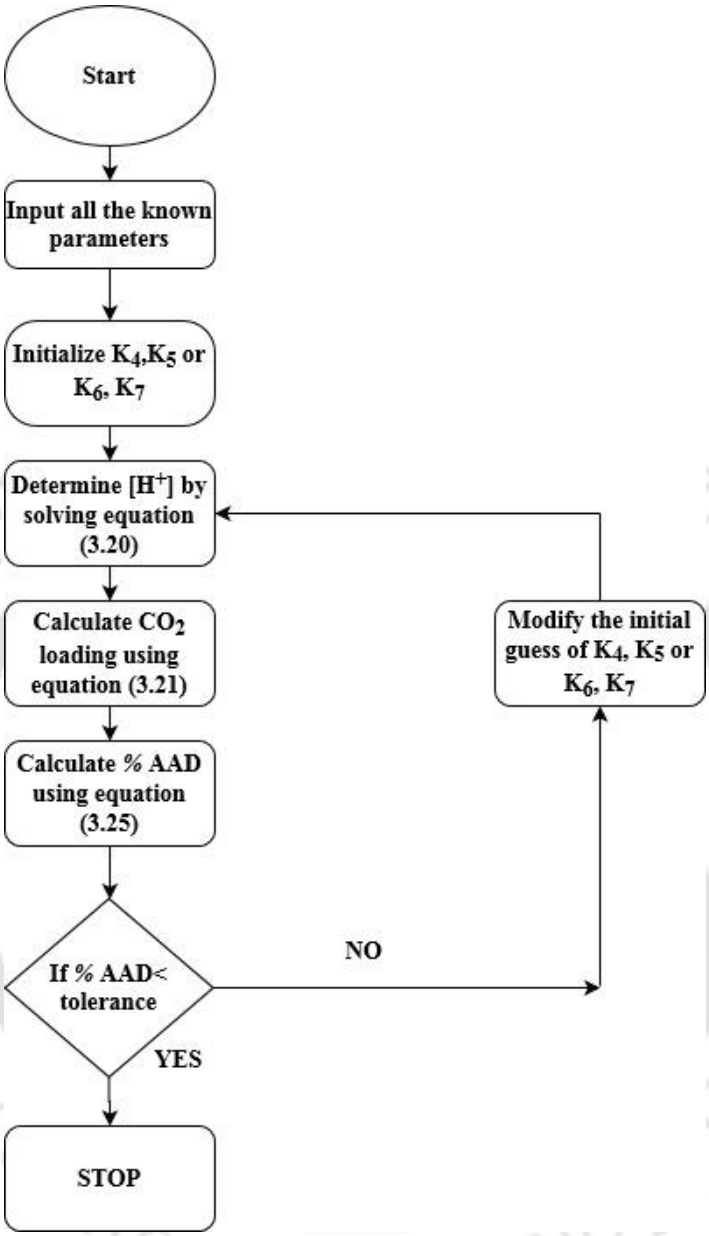

Figure 3.7 Regression algorithm for estimation of equilibrium constants from experimental CO_2 loading data

The precision of modified KE for prediction of the CO_2 loading data sets of all the blends is analyzed using the calculation of *% AAD* as stated below:

$$\text{Average absolute deviation } (\%AAD) = \frac{1}{N} \times \left(\sum_{i=1}^{N} \frac{\left| Y_i^{\exp} - Y_i^{\text{mod}} \right|}{Y_i^{\exp}} \right) \times 100 \qquad (3.25)$$

Where, N, Y^i_{exp} and Y^i_{mod} , represents the number of data points, experimental value of α_{CO2} and modeled value of α_{CO2}, respectively.

3.4.2 Artificial neural network model

The non-linear behavior of the VLE data of the studied solvents is also modeled using a feed forward back propagation neural network model. The details of the used model has already been discussed in Chapter-2. The choice of training and learning algorithms are very critical features for efficient prediction using ANN. Hence, Levenberg-Marquardt back propagation and gradient descent with momentum weight and bias learning functions are used as training and learning algorithms. The competence of these algorithms is also proved in the literature [49-51]. The transfer function applied to the first and layer are log sigmoid and purelin (linear), respectively. The flow chart of the feed forward neural network for aq. ([bmim] [Ac] + AEP) system is shown in Figure 3.8.

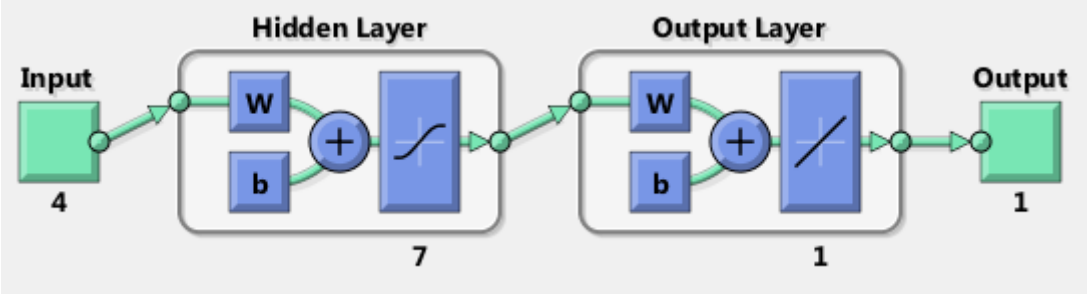

Figure 3.8 Flow of information in ANN for aq. ([bmim][Ac] + AEP) system

3.5 Results and discussion

3.5.1 Equilibrium solubility of CO_2 in aqueous ionic liquid systems

The validation of the experimental set-up and procedure for solubility measurement was done by measuring the equilibrium solubility of CO_2 in aqueous 30 wt % MDEA at 313.2 K using the procedure described in the experimental section and compared with the literature data [52, 53]. The comparison of data is represented in Figure 3.9. It can be concluded from the figure that the measured and literature data are quite comparable indicating the competence of the experimental methodology adopted for the current study. A sample calculation of CO_2 loading and uncertainty pertaining to α_{CO2} is given in APPENDIX I & II, respectively.

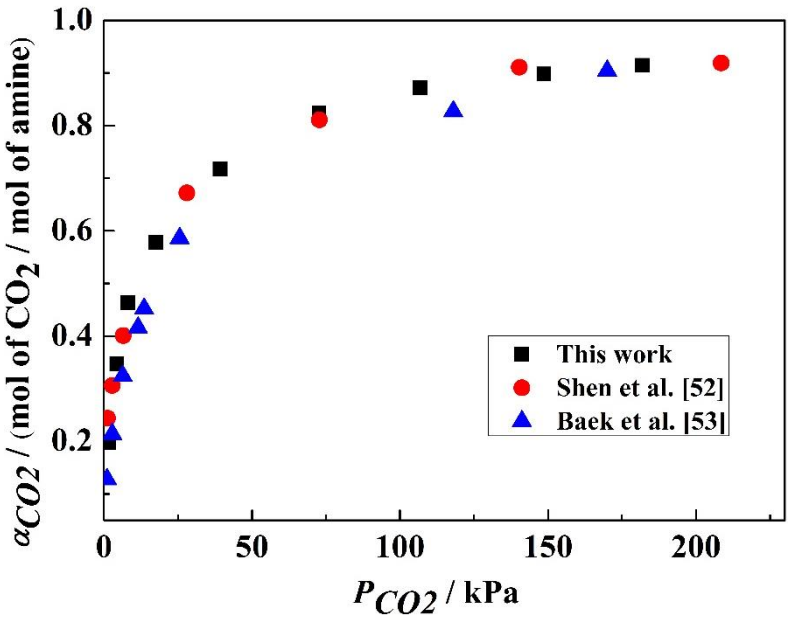

Figure 3.9 Comparison of CO_2 solubility in 30 wt % MDEA with literature at 313.2 K

The equilibrium VLE data is an essential measurement since it provides an understating of the distribution of various species involved in the reaction over different phases. The CO_2 solubility measured in the present work included both: physical and chemical solubility. The same has been presented here in terms of α_{CO2} i.e. mol of CO_2 per mol of solvent as a function of temperature,

solvent concentration, and CO_2 partial pressure. The experimental VLE data inclusive of fugacity coefficients related to each loading of the studied solvents are presented in Tables (3.4-3.12).

Table 3.4 Equilibrium CO_2 solubility data in aqueous 2.500 molal (*m*) [bmim] [Ac] solution

T / K	m_1 / mol.kg^{-1} [bmim][Ac]	P_{CO2} / kPa	α_{CO2}
303.2	2.500	97.9	0.061
	2.500	151.7	0.087
	2.500	189.1	0.106
	2.500	216.2	0.123
	2.500	275.1	0.135
	2.500	367.9	0.203
	2.500	386.5	0.253
313.2	2.500	97.3	0.025
	2.500	128.0	0.059
	2.500	180.8	0.058
	2.500	217.6	0.067
	2.500	254.7	0.071
	2.500	292.0	0.088
	2.500	317.8	0.147
	2.500	334.7	0.275
323.2	2.500	96.3	0.009
	2.500	110.2	0.015
	2.500	128.6	0.021
	2.500	147.4	0.026
	2.500	166.5	0.033
	2.500	190.1	0.041

Table 3.5 Equilibrium CO_2 solubility data in aqueous 2.251 molal (*m*) [bmim] [Ac] solution

T / K	m_1 / mol.kg^{-1} [bmim][Ac]	P_{CO2} / kPa	α_{CO2}
303.2	2.251	101.0	0.030
	2.251	121.9	0.044
	2.251	146.4	0.066
	2.251	195.3	0.079
	2.251	241.2	0.218
313.2	2.251	101.6	0.017
	2.251	129.1	0.029
	2.251	157.8	0.033
	2.251	174.0	0.035
	2.251	194.4	0.045
	2.251	221.5	0.052
	2.251	282.8	0.061
323.2	2.251	84.1	0.011
	2.251	107.4	0.021
	2.251	138.1	0.025
	2.251	171.1	0.034
	2.251	186.6	0.070
	2.251	197.6	0.107
	2.251	217.3	0.178
	2.251	252.7	0.224

Table 3.6 Equilibrium CO_2 solubility data in aqueous 2.006 molal (*m*) [bmim] [Ac] solution

T / K	m_1 / mol.kg^{-1} [bmim][Ac]	P_{CO2} / kPa	α_{CO2}
303.2	2.006	142.7	0.016
	2.006	174.4	0.024
	2.006	210.2	0.046
	2.006	227.9	0.044
	2.006	241.5	0.145
	2.006	269.5	0.153
	2.006	319.9	0.167
313.2	2.006	107.9	0.019
	2.006	125.6	0.025
	2.006	144.7	0.035
	2.006	160.2	0.039
	2.006	184.8	0.046
	2.006	238.6	0.053
323.2	2.006	105.7	0.064
	2.006	138.2	0.124
	2.006	170.0	0.162
	2.006	203.5	0.187
	2.006	235.1	0.212

Table 3.7 Equilibrium CO_2 solubility data in aqueous (2.500 + 0.503) molal (*m*) ([bmim] [Ac] + AEP) solution

T / K	m_1 / mol.kg^{-1} [bmim][Ac]	m_2 / mol.kg^{-1} (AEP)	P_{CO2} / kPa	α_{CO2}
303.2	2.500	0.503	21.9	0.166
	2.500	0.503	87.2	0.223
	2.500	0.503	112.4	0.238
	2.500	0.503	132.6	0.246
	2.500	0.503	160.9	0.253
	2.500	0.503	189.0	0.257
	2.500	0.503	210.0	0.260
	2.500	0.503	229.9	0.268
	2.500	0.503	245.5	0.279
313.2	2.500	0.503	23.4	0.147
	2.500	0.503	75.9	0.215
	2.500	0.503	110.0	0.236
	2.500	0.503	133.6	0.244
	2.500	0.503	151.8	0.252
	2.500	0.503	187.7	0.257
	2.500	0.503	234.5	0.292
	2.500	0.503	249.5	0.339
323.2	2.500	0.503	25.4	0.146
	2.500	0.503	93.2	0.198
	2.500	0.503	124.5	0.211
	2.500	0.503	154.9	0.219
	2.500	0.503	189.9	0.228
	2.500	0.503	227.1	0.232
	2.500	0.503	258.6	0.248
	2.500	0.503	265.6	0.325
	2.500	0.503	316.8	0.459

Table 3.8 Equilibrium CO_2 solubility data in aqueous (2.251 + 0.756) molal (*m*) ([bmim] [Ac] + AEP) solution

T / K	m_1 / mol.kg^{-1} [bmim][Ac]	m_2 / mol.kg^{-1} (AEP)	P_{CO2}/*kPa*	α_{CO2}
303.2	2.251	0.756	1.7	0.242
	2.251	0.756	102.3	0.426
	2.251	0.756	130.6	0.452
	2.251	0.756	167.5	0.477
	2.251	0.756	206.4	0.495
	2.251	0.756	242.8	0.517
313.2	2.251	0.756	11.1	0.184
	2.251	0.756	68.5	0.262
	2.251	0.756	109.1	0.300
	2.251	0.756	144.3	0.320
	2.251	0.756	182.0	0.331
	2.251	0.756	229.5	0.348
	2.251	0.756	290.8	0.362
323.2	2.251	0.756	8.3	0.179
	2.251	0.756	67.8	0.285
	2.251	0.756	106.3	0.315
	2.251	0.756	141.6	0.332
	2.251	0.756	173.1	0.345
	2.251	0.756	218.9	0.359

Table 3.9 Equilibrium CO_2 solubility data in aqueous (2.006 + 1.004) molal (*m*) ([bmim] [Ac] + AEP) solution

T / K	m_1 / mol.kg^{-1} [bmim][Ac]	m_2 / mol.kg^{-1} (AEP)	P_{CO2}/kPa	α_{CO2}
	2.006	1.004	6.0	0.199
	2.006	1.004	51.5	0.329
	2.006	1.004	91.2	0.415
	2.006	1.004	114.5	0.461
303.2	2.006	1.004	148.4	0.494
	2.006	1.004	191.9	0.521
	2.006	1.004	235.0	0.536
	2.006	1.004	288.3	0.566
	2.006	1.004	294.8	0.612
	2.006	1.004	2.6	0.183
	2.006	1.004	50.5	0.291
	2.006	1.004	85.8	0.344
313.2	2.006	1.004	112.3	0.374
	2.006	1.004	143.1	0.392
	2.006	1.004	176.9	0.399
	2.006	1.004	206.4	0.412
	2.006	1.004	3.2	0.168
	2.006	1.004	39.9	0.281
	2.006	1.004	78.7	0.337
	2.006	1.004	102.1	0.369
323.2	2.006	1.004	120.6	0.379
	2.006	1.004	154.0	0.387
	2.006	1.004	188.4	0.396
	2.006	1.004	224.6	0.464
	2.006	1.004	260.1	0.470

Table 3.10 Equilibrium CO_2 solubility data in aqueous (2.500 + 0.504) molal (*m*) ([bmim] [Ac] + APA) solution

T / K	m_1 / mol.kg^{-1} [bmim][Ac]	m_2 / mol.kg^{-1} (APA)	P_{CO2}/kPa	α_{CO2}
303.2	2.500	0.504	25.2	0.168
	2.500	0.504	79.9	0.246
	2.500	0.504	102.0	0.286
	2.500	0.504	119.1	0.305
	2.500	0.504	158.3	0.309
	2.500	0.504	189.4	0.320
	2.500	0.504	267.9	0.333
	2.500	0.504	273.9	0.347
313.2	2.500	0.504	23.7	0.157
	2.500	0.504	62.5	0.257
	2.500	0.504	103.28	0.292
	2.500	0.504	134.9	0.316
	2.500	0.504	180.4	0.328
	2.500	0.504	223.7	0.339
	2.500	0.504	293.2	0.384
	2.500	0.504	315.0	0.433
323.2	2.500	0.504	12.0	0.164
	2.500	0.504	78.0	0.229
	2.500	0.504	123.6	0.248
	2.500	0.504	151.6	0.270
	2.500	0.504	188.0	0.257
	2.500	0.504	216.5	0.263
	2.500	0.504	246.4	0.324
	2.500	0.504	281.8	0.341

Table 3.11 Equilibrium CO_2 solubility data in aqueous (2.251 + 0.753) molal (*m*) ([bmim] [Ac] + APA) solution

T / K	m_1 / mol.kg^{-1} [bmim][Ac]	m_2 / mol.kg^{-1} (APA)	P_{CO2} / kPa	α_{CO2}
303.2	2.251	0.753	4.6	0.210
	2.251	0.753	57.9	0.315
	2.251	0.753	87.7	0.382
	2.251	0.753	119.3	0.437
	2.251	0.753	137.8	0.468
	2.251	0.753	166.8	0.483
	2.251	0.753	224.1	0.497
	2.251	0.753	285.4	0.513
313.2	2.251	0.753	2.0	0.183
	2.251	0.753	43.0	0.310
	2.251	0.753	82.9	0.372
	2.251	0.753	123.4	0.392
	2.251	0.753	134.5	0.423
323.2	2.251	0.753	2.9	0.198
	2.251	0.753	38.9	0.338
	2.251	0.753	106.6	0.396
	2.251	0.753	156.7	0.411
	2.251	0.753	193.7	0.425
	2.251	0.753	242.3	0.437
	2.251	0.753	297.5	0.447

Table 3.12 Equilibrium CO_2 solubility data in aqueous (2.006 +0.996) molal (*m*) ([bmim] [Ac] (1) + APA (2)) solution

T / K	m_1 / mol.kg^{-1} [bmim][Ac]	m_2 / mol.kg^{-1} (APA)	P_{CO2} / kPa	α_{CO2}
303.2	2.006	0.996	1.8	0.199
	2.006	0.996	48.8	0.342
	2.006	0.996	88.1	0.415
	2.006	0.996	97.4	0.479
	2.006	0.996	113.0	0.523
	2.006	0.996	158.1	0.562
	2.006	0.996	184.7	0.587
	2.006	0.996	213.4	0.702
	2.006	0.996	265.7	0.821
313.2	2.006	0.996	0.8	0.227
	2.006	0.996	27.6	0.409
	2.006	0.996	87.1	0.494
	2.006	0.996	118.7	0.539
	2.006	0.996	159.5	0.569
	2.006	0.996	202.0	0.593
	2.006	0.996	238.0	0.609
	2.006	0.996	285.8	0.675
	2.006	0.996	311.1	0.719
323.2	2.006	0.996	2.3	0.181
	2.006	0.996	7.9	0.364
	2.006	0.996	63.4	0.457
	2.006	0.996	107.8	0.510
	2.006	0.996	148.7	0.525
	2.006	0.996	178.4	0.543
	2.006	0.996	215.1	0.557
	2.006	0.996	274.6	0.571

3.5.2 Effect of reaction parameters on vapor liquid equilibrium of studied solvents and CO_2

The usual trend of decrease in solubility of CO_2 while increase in temperature is observed in the absorption studies of aq. [bmim] [Ac], aq. ([bmim] [Ac] + AEP) and aq. ([bmim] [Ac] + APA). This decrease in α_{CO2} is owing to the exothermic nature of the reaction of proposed solvents and CO_2. With rise in activator concentration and keeping the overall concentration of the solvents to be constant, an increase in CO_2 solubility is also observed in the aqueous blends of aq. ([bmim][Ac] + AEP) and aq. ([bmim][Ac] + APA) (Tables 3.4-3.12 and Figures 3.10-3.13). The maximum uncertainty is 0.016 for calculation in α_{CO2}. Also, with increase in P_{CO2}, it is observed that α_{CO2} increases. This is due to the fact that with rise in system pressure, the kinetic energy associated with the gas molecules increases which ultimately leads to enhancement of the rate of diffusion. The number of collisions between gas molecules and liquid surface increases when the CO_2 partial pressure is increased which further results in higher CO_2 loading. However, after this limiting value of P_{CO2} there is no remarkable rise in CO_2 loading.

The CO_2 solubility is observed to be highest at high pressure and low temperatures (Figure 3.14). Further analysis of the data obtained reveals the fact that APA is a better activator for the systems under study rather than AEP. For instance, at invariable pressure of approximately 159 kPa and at 303.2 K, α_{CO2} was found to be improved by around 93.06 % and 76.45% while AEP and APA are increased from ca. 0.5 *m* to ca. 1.0 *m*, respectively. Also, a comparison of CO_2 loading in 2.500 m aq. [bmim][Ac] along with the addition of 0.503 *m* AEP and 0.504 *m* APA yields an increase of CO_2 loading of 92.37 % and 135.90 %, respectively at 303.2 K, which in turn indicates APA being a better activator for CO_2 absorption in aq. [bmim][Ac].

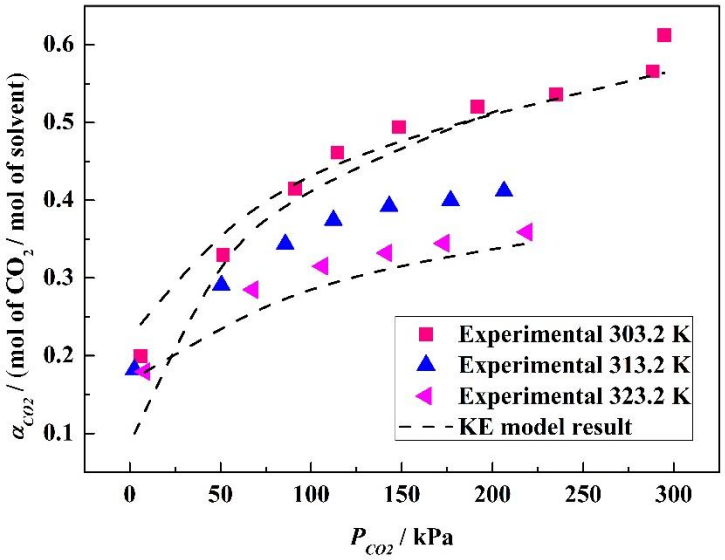

Figure 3.10 Influence of temperature on CO_2 solubility in aq. (2.006 *m* [bmim] [Ac] + 1.004 *m* AEP)

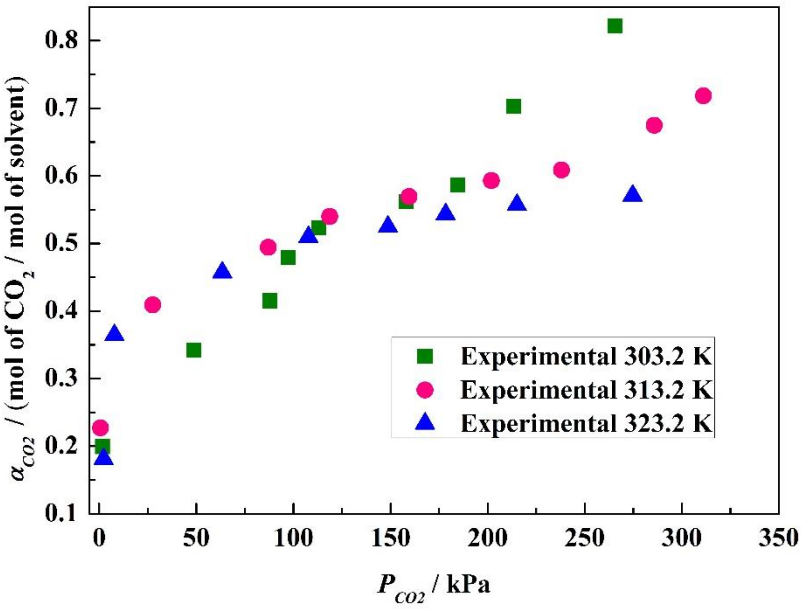

Figure 3.11 Effect of temperature on CO_2 solubility in aq. (2.006 *m* [bmim][Ac] + 0.996 *m* APA)

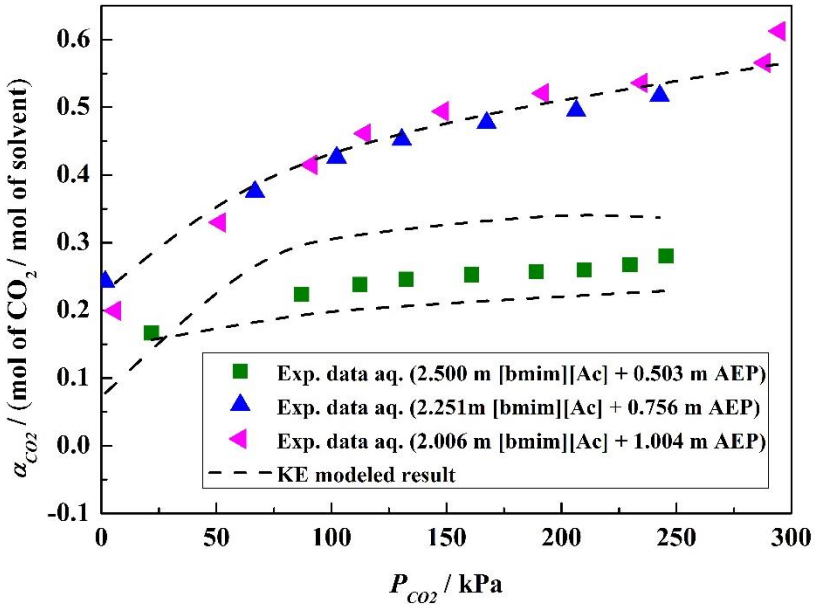

Figure 3.12 Effect of rise in AEP concentration in aq. [bmim][Ac] on CO_2 solubility at 303.2 K

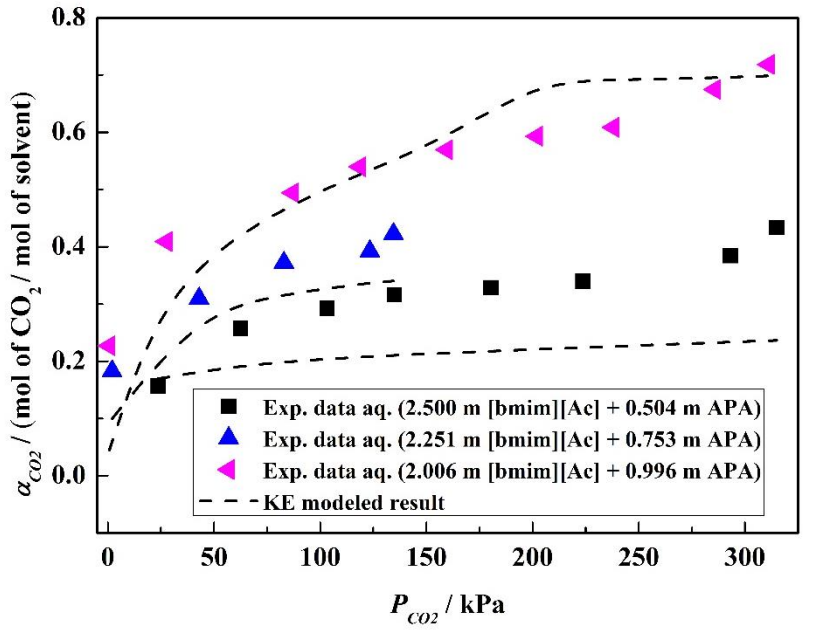

Figure 3.13 Effect of rise in APA concentration in aq. [bmim][Ac] on CO_2 solubility at 313.2 K

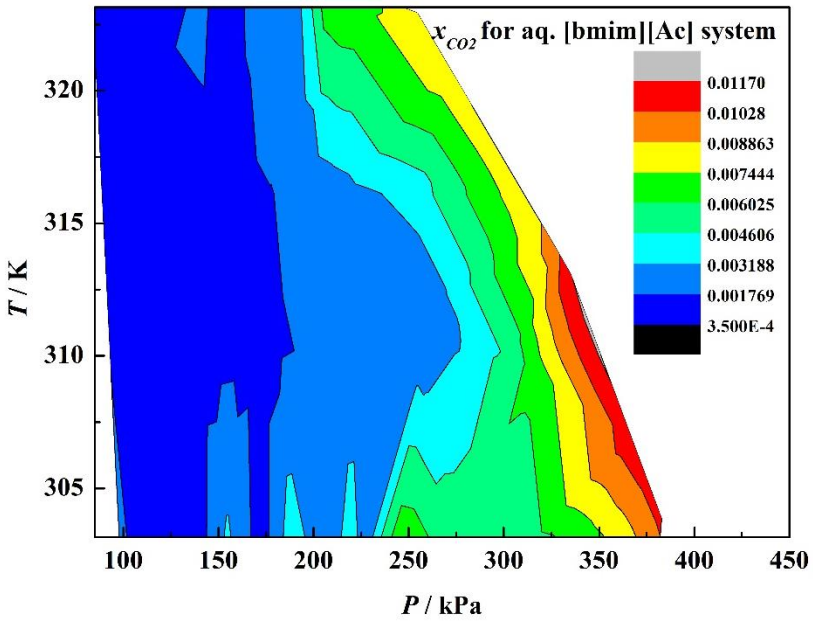

Figure 3.14 Contour plot of CO_2 solubility in aq. [bmim] [Ac] as a function of temperature and pressure

The studies of influence of rise in concentration of APA on CO_2 solubility while the conc. of [bmim] [Ac] is decreased in a total molal solvent of 3 mol/kg at 303.2 K indicates that with rise in APA conc., there is a huge rise in α_{CO2} at the same P_{CO2} (Figure 3.15). A comparison of effect of the addition of both activators AEP and APA in aq. 2.006 m [bmim] [Ac] is shown in Figure 3.16 at 303.2 K. It can be qualified from the figure that there is higher rise in CO_2 solubility with the addition of 0.996 *m* APA in comparison to 1.004 *m* AEP. This concludes that for the studied ionic liquid system, APA serves to be a better amine activator in comparison to AEP for CO_2 solubility.

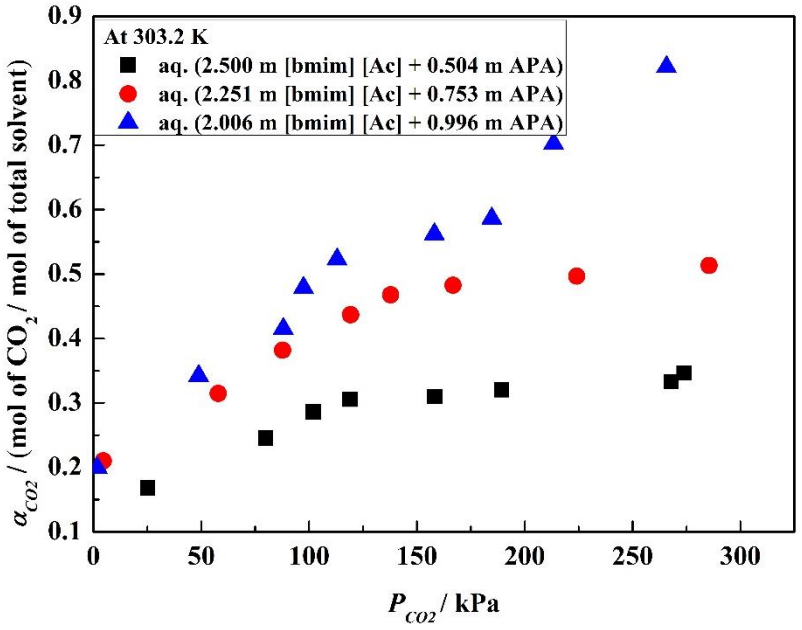

Figure 3.15 CO_2 solubility in aqueous blend of ([bmim] [Ac] + APA) of all compositions at 303.2 K

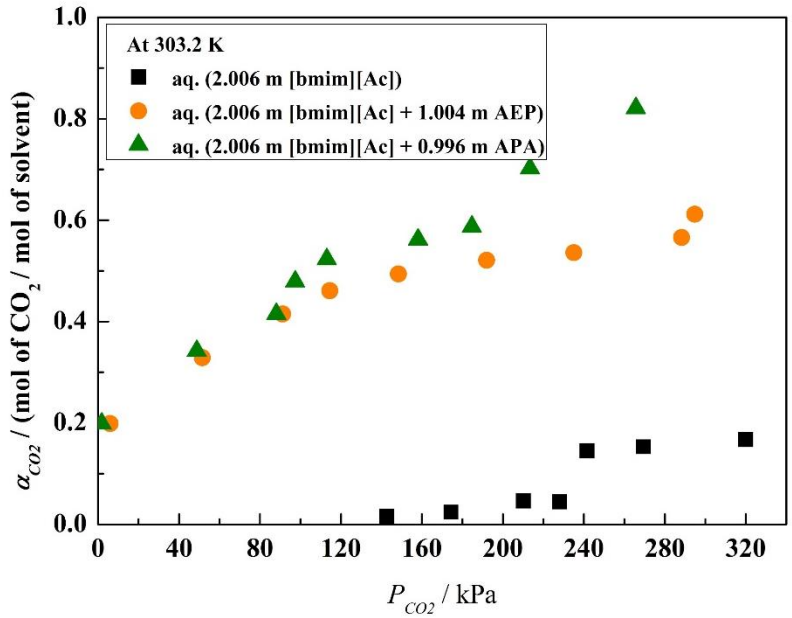

Figure 3.16 Comparison of CO_2 solubility of aq. [bmim] [Ac], aq. ([bmim] [Ac] + AEP) and aq. ([bmim] [Ac] + APA) at 303.2 K as a function of P_{CO2}

3.5.3 Co-relation using modified KE model and artificial neural network

The VLE data has been correlated with modified KE model. The coefficients of equilibrium constants (K_1, K_2, K_3) are taken from the literature [54]. In this work, equilibrium constants K_4, K_5, K_6, K_7, K'_6, and K'_7 which correspond to the deprotonation and carbamate hydrolysis reactions of [bmim] [Ac], AEP, and APA, respectively are estimated. The equilibrium constants are a function of P_{CO2}, T, and solvent concentration are evaluated using regression analysis in MATLAB (R17). The accuracy of the KE towards prediction of the CO_2 loading is analyzed using *% AAD*. The non-ideality of the gas phase was included while estimating the coefficients using the non-linear optimization method with the objective function which further results in better accuracy of prediction of CO_2 solubility in the studied solvents. The evaluated equilibrium constants (K_4, K_5, K_6, K_6', K_7 and K_7') in terms of concentration of solvents, temperature, and P_{CO2} can be expressed as following equations (3.26-3.27):

$$K_4\left(or\ /\ K_6 or\ /\ K_6^{'}\right) = g + \left(h \times M\right) + \left(k \times T\right) + \left(l \times M \times T\right) + \left(n \times T^2\right) + \left(p \times P_{CO_2}\right) + \left(q \times P_{CO_2}^2\right) \quad (3.26)$$

$$K_5\left(or\ /\ K_7 or\ /\ K_7^{'}\right) = g + \left(h \times M\right) + \left(k \times T\right) + \left(l \times M^2\right) + \left(n \times M \times T\right) + \left(p \times T^2\right) + \left(q \times P_{CO2}\right) + \left(r \times P_{CO_2}^2\right) \quad (3.27)$$

Where, g, h, k, l, n, p, q, and r, are parametric coefficients associated with the equilibrium constants and found through optimization.

The calculated values of equilibrium constants are presented in Table 3.13. The equilibrium constants obtained through the KE model were in turn used to predict the CO_2 loading. The calculated % AAD for aqueous [bmim] [Ac], ([bmim] [Ac] + AEP) and ([bmim] [Ac] + APA) systems are 33.57, 14.45, and 20.60, respectively. The comparison of the experimental and model predicted α_{CO2} for aq. ([bmim] [Ac] + AEP) systems (Figure 3.17) exhibit a good agreement between the experimental and modeled values. It is observed that with rise in temperature the CO_2 loading of (2.006 *m* [bmim][Ac] + 0.996 *m* APA) decreases and is found to be least at 323.2 K (Figure 3.18). However, intermediately the values of α_{CO2} have been found to be higher for 313.2 K in comparison to 303.2 K. This change can be attributed to the fact that the viscosity of ionic liquids is lower at higher temperatures. Hence, at a higher temperature of 313.2 K, due to drop in

viscosity and simultaneous rise in diffusivity of CO_2 in the solvent liquid, α_{CO2} increases. But, further increase in temperature reduces the physical absorption ability of [bmim] [Ac] due to reduction of van der Waals forces of attraction which leads to decrease in values of α_{CO2}.

Table 3.13 Estimated equilibrium reaction constants of the systems aq. [bmim] [Ac], aq. ([bmim] [Ac] + AEP) and aq. ([bmim] [Ac] + APA) under study

K_i / kmol.m^{-3}	K_4	K_5	K_6	K_7	$K_{6'}$	$K_{7'}$
g	-4.318×10^{-6}	-1.591×10^{7}	-5.496×10^{-9}	5.120×10	-5.528×10^{-9}	4.567×10
h	-3.719×10^{-4}	-1.263×10^{5}	-1.775×10^{-12}	3.407×10^{-1}	-1.291×10^{-12}	4.669×10^{-1}
k	1.707×10^{-7}	-2.282×10^{3}	-1.661×10^{-11}	-2.586	-1.639×10^{-11}	-2.278
l	1.647×10^{-8}	-3.688×10^{6}	4.058×10^{-13}	1.844	4.483×10^{-13}	1.155
n	6.384×10^{-9}	-1.471×10^{4}	1.327×10^{-13}	1.391	1.179×10^{-13}	8.686×10^{-1}
p	-8.921×10^{-9}	3.714×10^{2}	-5.036×10^{-11}	-1.009×10^{-1}	-4.990×10^{-11}	-1.478×10^{-1}
q	1.369×10^{-13}	-4.276×10^{4}	1.053×10^{-23}	6.372	8.685×10^{-24}	8.118
r	-	-6.654×10^{-1}	-	1.326×10^{-1}	-	1.811×10^{-1}

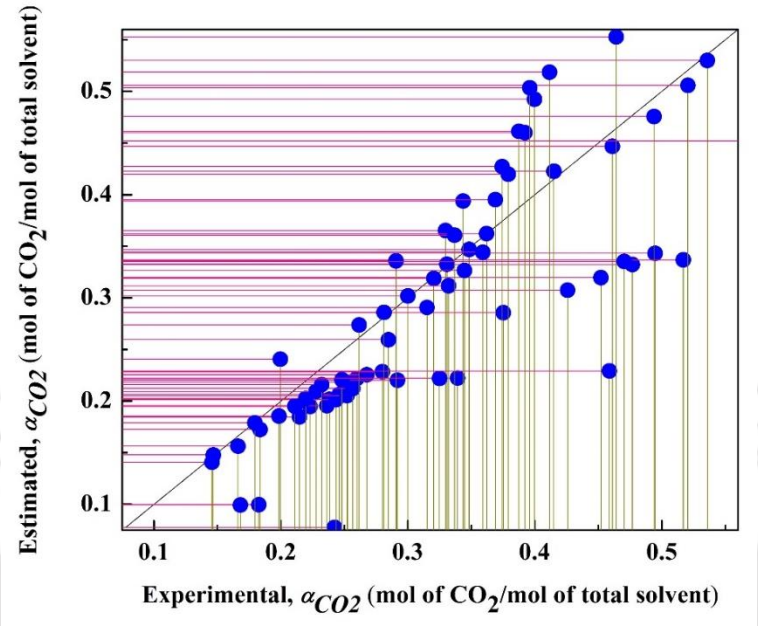

Figure 3.17 Parity plot: comparison between experimental and modified KE model predicted CO_2 loading in aq. ([bmim] [Ac] + AEP) system

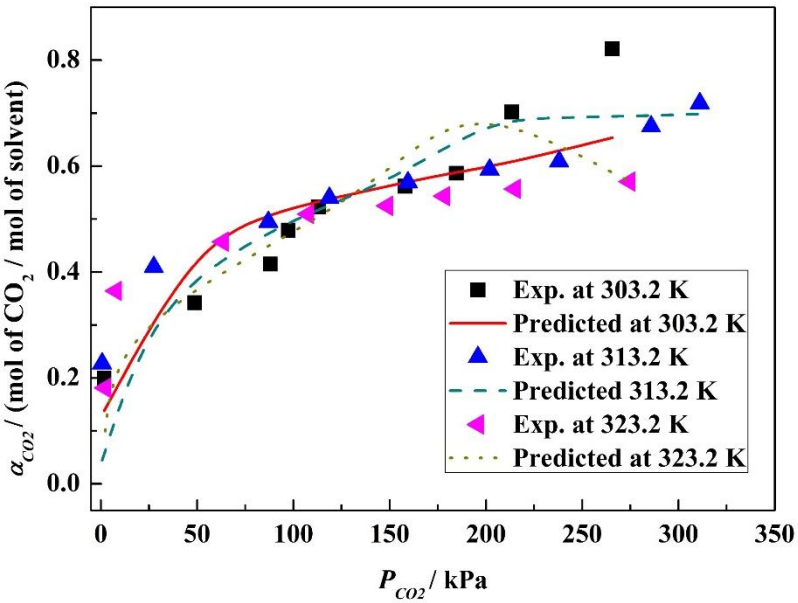

Figure 3.18 Experimental and modified KE model predicted CO_2 loading in aq. (2.006 *m* [bmim] [Ac] + 0.996 *m* APA) system at different temperatures

An important point for successful predictions by ANN is selection of optimum number of neurons. If the number of hidden neurons is very high, then it may lead to over learning of the neural network [32]. On the other hand, if hidden neurons are less in number, the network will be a less learned one. Here, the optimum number of neurons are found from the calculation of MSE in the range of 5 to 20. The optimum number of neurons for aq. [bmim] [Ac], aq. ([bmim] [Ac] + AEP) and aq. ([bmim] [Ac] + APA) are 20, 7, and 16, respectively (Figure 3.19). The % AAD for the predicted and experimental α_{CO2} data is found to be 15.70, 3.31, and 5.05 for aq. [bmim] [Ac], aq. ([bmim] [Ac] + AEP) and aq. ([bmim] [Ac] + APA), respectively. The simultaneous assessment for the capabilities of ANN and modified KE model for aq. ([bmim] [Ac] + APA) systems assures that deviation is very less in case of ANN model in comparison to modified KE model (Figure 3.20).

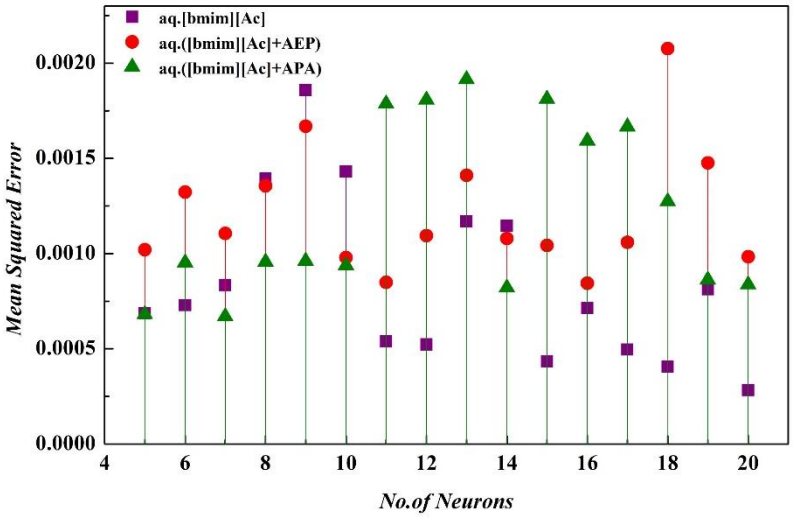

Figure 3.19 Variation of MSE (mean square error) with number of neurons in the hidden layer for ANN model

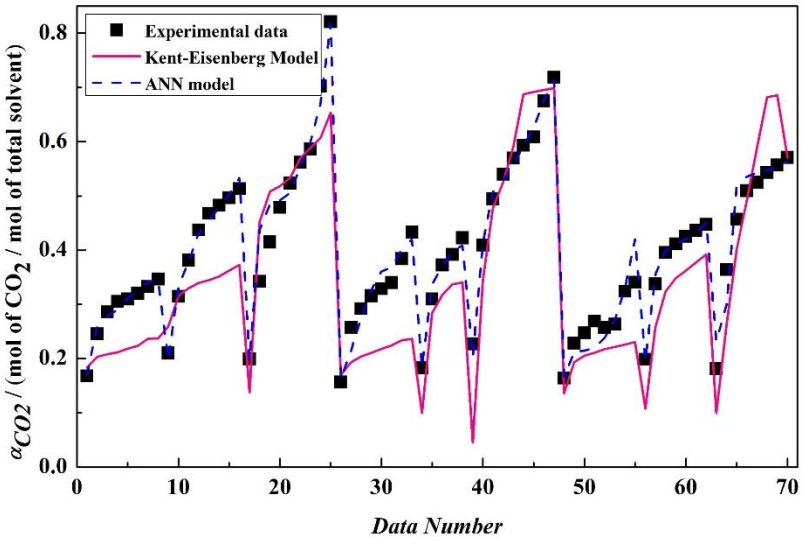

Figure 3.20 Cross plot for comparison of CO_2 solubility with modeled data for aq. ([bmim] [Ac] + APA) system

3.5.4 Liquid phase speciation profile, pH

The equilibrium concentrations of different species available in the liquid phase are further predicted as a function of CO_2 loading using modified KE model. The concentration profiles of diverse species for CO_2 loaded, (2.500 *m* [bmim] [Ac] + 0.503 *m* AEP) at 303.2 K and (2.006 *m* [bmim][Ac] + 0.996 *m* APA) at 323.2 K have been represented in Figures 3.21 and 3.22, respectively. As indicated, there is a sharp decrease in the concentrations of AEP and APA as a function of CO_2 loading indicating it to be a limiting reactant for CO_2 solubility reaction. Also, it is evident from the speciation, HCO_3^- and carbamate, corresponding to IL and amine associated to be the major reaction products.

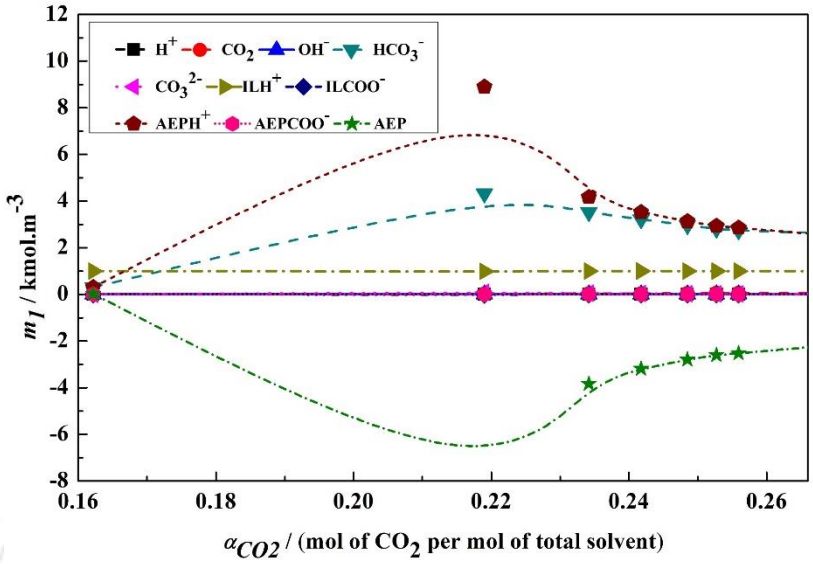

Figure 3.21 Modified KE model predicted various species concentration in the liquid phase of CO_2 loaded in aq. (2.500 *m* [bmim] [Ac] + 0.503 *m* AEP) system at 303.2 K

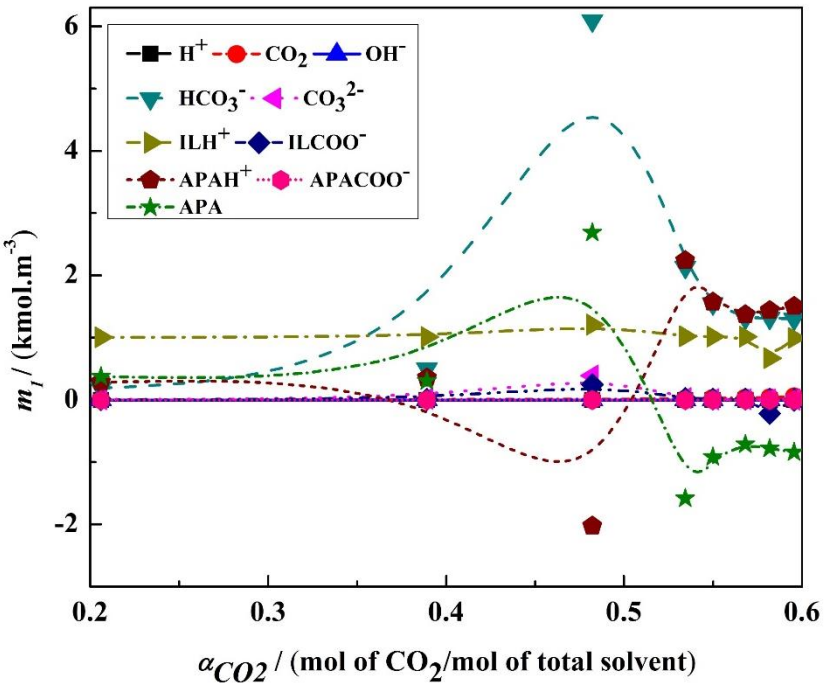

Figure 3.22 Modified KE model predicted various species concentration in the liquid phase of CO_2 loaded in aq. (2.006 *m* [bmim] [Ac] + 0.996 *m* APA) system at 323.2 K

One of the important design parameters for absorption and stripping towers is the pH level of either reactants, products, or intermediates which shall be handled in the system. The reaction products of the CO_2 solubility systems are usually in the pH range of (7-12) [19, 55]. In the current work, modified KE model is further used to assess pH of blended solvent systems as a function α_{CO2}. For aq. (2.251 *m* [bmim] [Ac] + 0.756 *m* AEP) system, the highest pH was observed at a low temperature of 303.2 K (Figure 3.23). With the rise in temperature and loading, pH was observed to decrease consequentially due to the higher H^+ ions in the systems in comparison to OH^- ions at lower temperatures.

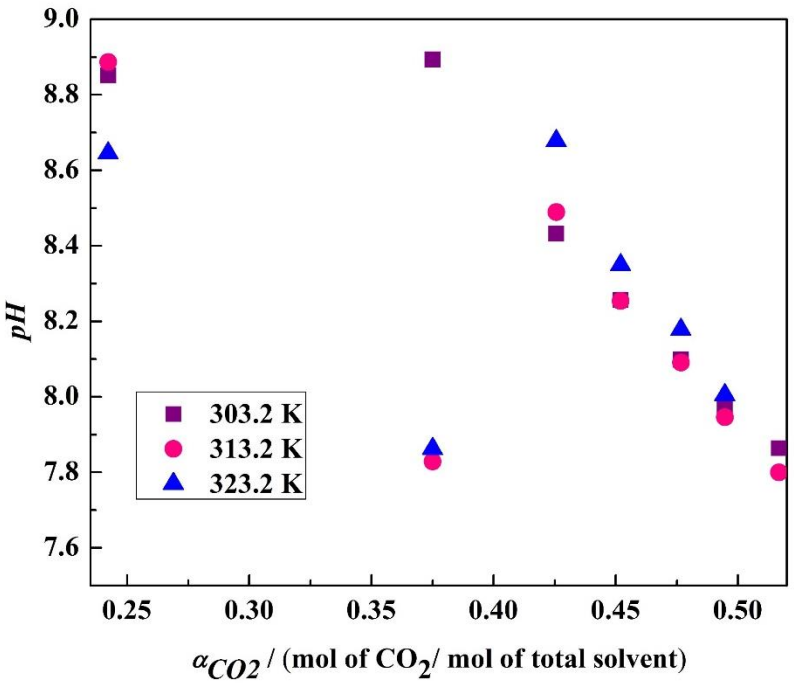

Figure 3.23 Modified KE predicted pH as a function of CO_2 loading in aq. (2.251 *m* [bmim] [Ac] + 0. 756 *m* AEP) solution

3.5.5 Comparison of solvent performance with other conventional amines/blends

A comparison of the studied solvents is done with the available literature. However, due to the lack of literature in the studied range of composition, the nearest available literature was considered. Compared to the literature [15, 56, 57, 58], the current solvent blends are found to yield a very low CO_2 solubility at 303.2 and 323.2 K (Figures 3.24-3.25). But, the composition studied in the literature is highly concentrated with as high as 100 % solvent concentration (amine + [bmim][Ac]) whereas in the present work, the maximum concentration of [bmim][Ac], APA and AEP is kept being very less viz. (26.03, 8.55 and 8.49 %), respectively. Hence, it may be abstracted that specified a higher concentration of either [bmim] [Ac] + AEP/APA may result in higher CO_2 loading.

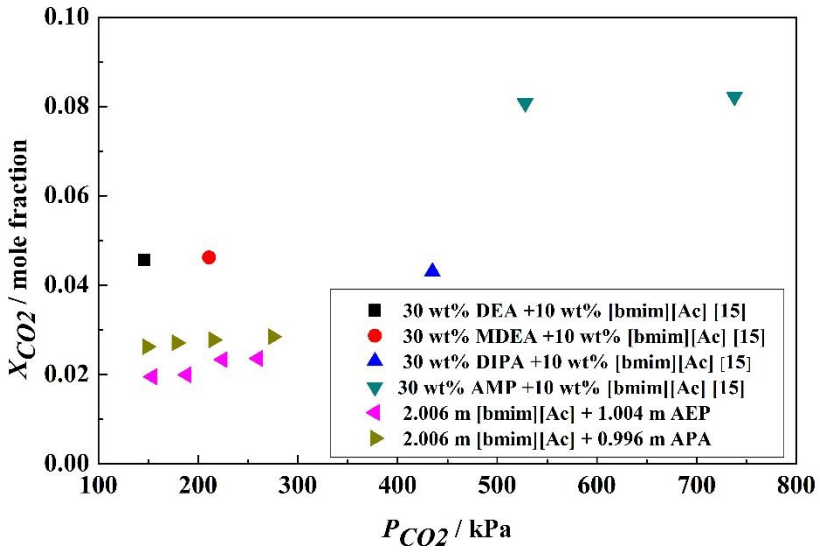

Figure 3.24 Comparison of CO_2 solubility of aq. ([bmim][Ac] + AEP/APA) with the literature at 323.2 K

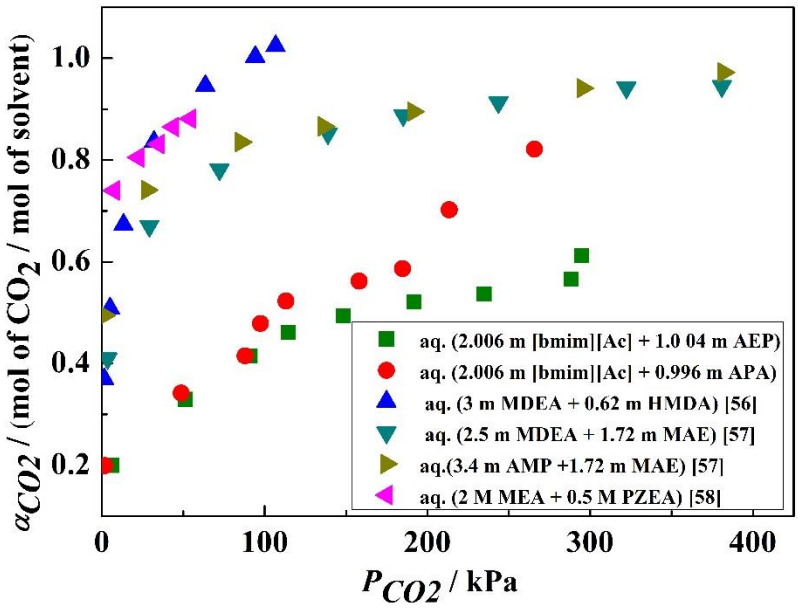

Figure 3.25 Comparison of CO_2 loading as a function of P_{CO2} at 303.2 K with literature

3.6 Conclusions

CO_2 solubility in aqueous [bmim] [Ac] enhanced by various amine activators viz. AEP and APA were studied over a wide range of experimental conditions. Qualitative analysis using FTIR and ^{13}C NMR of the unloaded and loaded solvents indicated the formation of intermediate acetic acid, and imidazolium stable carboxylate. The results evidently specify that CO_2 solubility increases with respect to rise in both P_{CO2} and concentrations of activators in solvent blends. Modified KE inclusive of gas phase non-ideality and ANN model has been developed to correlate the CO_2 solubility data. Quantitative comparison of CO_2 loading in 2.500 m aq. [bmim][Ac] along with the addition of 0.503 m AEP and 0.504 m APA yields an increase of CO_2 loading of 92.37 % and 135.90 %, respectively at 303.2 K, which infer that APA proves to be a better activator in comparison to AEP. The optimized equilibrium constants associated with various reactions as a function of P_{CO2}, solvent concentration, and temperature of absorption has been estimated using

regression analysis. The efficiency of feed forward back propagation neural network was found to be better in comparison to the modified KE model. However, the latter model provides better insights to the process. The speciation and pH data as a function of α_{CO2} have been estimated by means of modified KE model. In addition, an assessment of CO_2 solubility data of aq. [bmim] [Ac] + AEP/APA and various other blends studied in the literature reveals that the considered solvents have good imminent for post combustion CO_2 capture applications.

References

[1] A. Ahmady, M. A. Hashim, M. K. Aroua. Density, viscosity, physical solubility and diffusivity of CO_2 in aqueous MDEA + [bmim] [BF_4] solutions from 303 to 333K. Chemical Engineering Journal 172 (2011) 763-770.

[2] A. M. Pinto, H. Rodriguez, A. Arce, A. Soto. Carbon dioxide absorption in the ionic liquid 1-ethylpyridinium ethyl sulfate and in its mixtures with another ionic liquid. International Journal of Greenhouse Gas Control 18 (2013) 296-304.

[3] W. Afzal, X. Liu, J. M. Prausnitz. High solubilities of carbon dioxide in tetraalkyl phosphonium- based ionic liquids and the effect of diluents on viscosity and solubility. Journal of Chemical and Engineering Data 59 (2014) 954-960.

[4] V. Blasucci, R. Hart, V. L. Mestre, D. J. Hahne, M. Burlager, H. Huttenhower, B. J. R. Thio, P. Pollet, C. L. Liotta, C. A. Eckert. Single component, reversible ionic liquids for energy applications. Fuel 89 (2010) 1315-1319.

[5] W. G. Lee, S. W. Kang. Highly selective poly (ethylene oxide)/ionic liquid electrolyte membranes containing CrO_3 for CO_2/N_2 separation. Chemical Engineering Journal 356 (2019) 312-317.

[6] Z. Dai, R. D. Noble, D. L. Gin, X. Zhang, L. Deng. Combination of ionic liquids with membrane technology: A new for CO_2 separation. Journal of Membrane Science 497 (2016) 1-20.

[7] M. B. Shiflett, D. J. Kasprzak, C. P. Junk, A. Yokozeki. Phase behavior of {carbon dioxide + [bmim] [Ac]} mixtures. Journal of Chemical Thermodynamics 40 (2008) 25-31.

[8] K. G. Bogolitsyn, T.E.Skrebets, T. A. Makhova. Physiochemical properties of 1-butyl-3-methylimidazolium acetate. Russian Journal of General Chemistry 79 (2009) 125-128.

[9] J. O. Valderrama, R. E. Rojas. Critical properties of ionic liquids. Industrial and Engineering Chemistry Research 48 (2009) 6890-6900.

[10] A. Haghtalab, A. Shojaeian. Volumetric and viscometric behavior of the binary systems of *N*-methyldiethanolamine and diethanolamine with 1-butyl-3-methylimidazolium acetate at various temperatures. Journal of Chemical Thermodynamics 68 (2014) 128-137.

[11] J. Safarov, M. Geppert-Rybczynska, I. Kul, E. Hassel. Thermophysical properties of 1-butyl-3-methylimidazolium acetate over a wide range of temperatures and pressures. Fluid phase Equilibria 383 (2014) 144-155.

[12] S. N. Khan, S. M. Hailegiorgis, Z. Man, A. M. Shariff, S. Garg. Thermophysical properties of aqueous 1-butyl-3-methylimidazolium acetate [BMIM] [AC] + monoethanolamine (MEA) hybrid as a solvent for CO_2 capture. Procedia Engineering 148 (2016) 1326-1331.

[13] Y. Hiraga, A. Kato, Y. Sato, R. L. Smith. Densities at pressures up to 200 MPa and atmospheric pressure viscosities of ionic liquids 1-ethyl-3-methylimidazolium methylphosphate, 1-ethyl-3-methylimidazolium diethylphosphate, 1-butyl-3-methylimidazolium acetate, and 1-butyl-3-methylimidazolium Bis-(trifluoromethylsulfonyl) imide. Journal of Chemical and Engineering Data 60 (3) (2015) 876-885.

[14] H. F. D. Almeida, H. Passos, J. A. Lopes-da-Silva, A. M. Fernandes, M. G. Freire, J. A. P. Coutinho. Thermophysical properties of five acetate –based ionic liquids. Journal of Chemical and Engineering Data 57 (11) (2012) 3005-3013.

[15] A. Shojaeian, A. Haghtalab. Solubility and density of carbon dioxide in different aqueous alkaloamines solutions blended with 1-butyl-3-methylimidazolium acetate ionic liquid at high pressure. Journal of Molecular Liquids 187 (2013) 218-225.

[16] A. Haghtalab, A. Shojaeian. High pressure measurement and thermodynamic modelling of the solubility of carbon dioxide in *N*-methyldiethanolamine and 1-butyl-3-methylimidazolium acetate mixture. Journal of Chemical Thermodynamics 81 (2015) 237-244.

[17] A. Ahmady, M. A. Hashim, M. K. Aroua. Absorption of carbon dioxide in the aqueous mixtures of methyldiethanolamine with three types of imidazolium-based ionic liquids. Fluid Phase Equilibria 309 (2011) 76-82.

[18] S. Kumar, J. H. Cho, I. Moon. Ionic liquid-amine blends and CO_2 BOLs: prospective solvents for natural gas sweetening and CO_2 capture technology-A review. International Journal of Greenhouse Gas Control 20 (2014) 87–116.

[19] S. K. Dash, S. S. Bandyopadhyay. Studies on the effect of addition of piperazine and sulfolane into aqueous solution of *N*-methyldiethanolamine for CO_2 capture and VLE modelling using e-NRTL equation. International Journal of Greenhouse Gas Control 44 (2016) 227-237.

[20]H. Li, Y. L. Moullec, J. Lu, J. Chen, J. C. V. Marcos, G. Chen, F. Chopin. CO_2 solubility measurement and thermodynamic modeling for 1-methylpiperazine/water/CO_2. Fluid Phase Equilibria 394 (2015) 118-128.

[21]Y. Yuan, B. Sherman, G. T. Rochelle. Effects of viscosity on CO_2 absorption in aqueous piperazine / 2-methylpiperazine. Energy Procedia 114 (2017) 2103-2120.

[22]Y. Du, Le. Li, O, Namjoshi, K. A. Voice, A. N. Fine, G. T. Rochelle. Aqueous piperazine / *N*-(2-aminoethyl) piperazine for CO_2 capture. Energy Procedia 37 (2013) 1621-1638.

[23]S. Paul, A. K. Ghoshal, B. P. Mandal. Kinetics of absorption of carbon dioxide into aqueous solution of 2-(1-piperazinyl)-ethylamine. Chemical Engineering Science 64 (2009) 313–321.

[24]S. Paul, A. K. Ghoshal, B. P. Mandal. Kinetics of absorption of carbon dioxide into aqueous blends of 2-(1-piperazinyl)-ethylamine and N-methyldiethanolamine Chemical Engineering Science 64 (2009) 1618–1622.

[25] A. Dey, S. K. Dash, B. P. Mandal. Equilibrium CO_2 solubility and thermophysical properties of aqueous blends of 1-(2-aminoethyl) piperazine and *N*-methyldiethanolamine. Fluid Phase Equilibria 463 (2018) 91-105.

[26] B. Das, B. Deogam, B. P. Mandal. Absorption of CO_2 into novel aqueous bis (3-aminopropyl) amine and enhancement of CO_2 absorption into its blends with *N*-methyldiethanolamine. International Journal of Greenhouse Gas Control 60 (2017) 172-185.

[27]A. Najafloo, A. T. Zoghi, F. Feyzi. Measuring solubility of carbon dioxide in aqueous blends of N-methyldiethanolamine and 2-((2-aminoethyl) amino) ethanol at low CO_2 loadings and

modelling by electrolyte SAFT-HR EoS. Journal of Chemical Thermodynamics 82 (2015) 143-155.

[28]T. Sema, A. Naami, R. Idem, P. Tontiwachwuthikul. Correlations for equilibrium solubility of carbon dioxide in aqueous 4-(diethylamino)-2-butanol solution. Industrial and Engineering Chemistry Research 50 (2011) 14008-14015.

[29]A. K. Voice, S. J. Vevelstad, X. Chen, T. Nguyen, G. T. Rochelle. Aqueous 3-(methylamino) propylamine for CO_2 capture. International Journal of Greenhouse Gas Control 15 (2013) 70-77.

[30]A. M. Pinto, H. Rodriguez, A. Ace, A. Soto. Carbon dioxide absorption in the ionic liquid 1-ethylpyridinium ethylsulphate and its mixture with another ionic liquid. International Journal of Greenhouse Gas Control 18 (2013) 296-304

[31]S. K. Dash, A. Samanta, A. N. Samanta, S. S. Bandyopadhyay. Vapour liquid equilibria of carbon dioxide in dilute and concentrated aqueous solutions of piperazine at low to high pressure. Fluid Phase Equilibria 300 (2011) 145-154.

[32]B. K. Mondal, S. S. Bandyopadhyay, A. N. Samanta. Vapor-liquid equilibrium measurement and ENRTL modeling of CO_2 absorption in aqueous hexamethylenediamine. Fluid Phase Equilibria 402 (2015) 102-112.

[33]P. F. D. Santos, L. Andre, M. Ducousso, F. Contamine, P. Cezac. Experimental measurement of CO_2 solubility in aqueous Na_2SO_4 solution at temperatures between 303.15 and 423.15 K and Pressures upto 20 MPa. Journal of Chemical and Engineering Data 65 (2020) 3230-3239.

[34]B. Das, B. Deogam, B. P. Mandal. Experimental and theoretical studies on efficient carbon dioxide capture using novel bis (3-aminopropyl) amine (APA)-activated aqueous 2-amino-2-methyl-1-propanol (AMP) solutions. RSC Advances 7 (2017) 21518–21530.

[35] C. Sun, P. K. Dutta. Infrared spectroscopic study of reaction of carbon dioxide with aqueous monoethanolamine Solutions. Industrial and Engineering Chemistry Research 55 (22) (2016) 6276-6283.

[36] G. Richner, G. Puxty. Assessing the chemical speciation during CO_2 absorption by aqueous amines using in situ FTIR. Industrial and Engineering Chemistry Research 51 (2012) 14317-14324.

[37]L. F. Zubeir, G. E. Romanos, W. M. A. Weggemans, B. Iliev, T. J. S. Schubert, M. C. Kroon. Solubility and diffusivity of CO_2 in the ionic liquid 1-butyl-3-methylimidazolium tricyanomethanide within a large pressure range (0.01 MPa to 10 MPa). Journal of Chemical and Engineering Data 60 (2015) 1544-1562.

[38]A. T. Zoghi, A. Rahimi, F. Feyzi, A. H. Jalili. Measurement and modeling equilibrium solubility of carbon dioxide in aqueous solution of dimethylaminoethanol and 3-methylaminopropylamine. Thermochimica Acta 686 (2020) 178565.

[39]M. E. Hamzehie, H. Najibi. Carbon dioxide loading capacity in aqueous solutions of potassium salt of proline blended with piperazine as new absorbents. Thermochimica Acta 639 (2016) 66-75.

[40]B. Li, Y. Chen, Z. Yang, X. Ji, X. Lu. Thermodynamic study on carbon dioxide absorption in aqueous solutions of choline-based amino acid ionic liquids. Separation and Purification Technology 214 (2019) 128-138.

[41]R. Haghbakhsh, H. Soleymani, S. Raeissi. A simple correlation to predict high pressure solubility of carbon dioxide in 27 commonly used ionic liquids. Journal of Supercritical Fluids 77 (2013) 158-166.

[42]R. L. Kent, B. Eisenberg. Better data for amine treating. Hydrocarbon Processing 55 (1976) 87-90.

[43]Y. H. Hsu, R. B. Leron, M.H. Li. Solubility of carbon dioxide in aqueous mixtures of (reline + monoethanolamine) at T = (313.2 to 353.2) K. Journal of Chemical Thermodynamics 72 (2014) 94–99.

[44]P. Y. Chung, A. N. Soriano, R. B. Leron, M. H. Li. Equilibrium solubility of carbon dioxide in the amine solvent system of (triethanolamine + piperazine + water). Journal of Chemical Thermodynamics 42 (2010) 802-807.

[45]S. Shen, Y. Zhao, Y. Bian, Y. Wang, H. Guo, H. Li. CO_2 absorption using aqueous potassium lysinate solutions: vapor-liquid equilibrium data and modelling. Journal of Chemical Thermodynamics 115 (2017) 209-220.

[46]M. N. Hassankiadeh, A. Jahangiri. Application of aqueous blends of AMP and piperazine to the low CO_2 partial pressure capturing: new experimental and theoretical analysis. Energy 165 (2018) 164-178.

[47]M. J. Khodadadi, S. Riahi, M. Abbasi. Experimental modeling of the solubility of carbon dioxide in aqueous solution of monoethanolamine + 1, 3-diaminopropane. Journal of Molecular Liquids 281 (2019) 415-422.

[48] J. Choi, Y. Kim, S. Nam, S. Yun, Y. Yoon, J. Lee. CO_2 absorption characteristics of a piperazine derivative with primary, secondary, and tertiary amino groups. Korean Journal of Chemical Engineering 33 (2016) 3222-3230.

[49] M. A. Sedghamiz, A. Rasoolzadeh, M. R. Rahimpour. The ability of artificial neural network in prediction of the acid gases solubility in different ionic liquids. Journal of CO_2 Utilization 9 (2015) 39–47.

[50] M. E. Hamzehie, M. Fattahi, H. Najibi, B. V. D. Bruggen, S. Mazinani, Application of artificial neural networks for estimation of solubility of acid gases (H_2S and CO_2) in 32 commonly ionic liquid and amine solutions. Journal of Natural Gas Science and Engineering 24 (2015) 106-114.

[51] M. E. Hamzehie, H. Najibi. Prediction of carbon dioxide loading capacity in amino acid salt solutions as new absorbents using artificial neural network and deshmukh-mather models. Journal of Natural Gas Science and Engineering 27 (2015) 676-685.

[52]K. P. Shen, M. H. Li. Solubility of carbon Dioxide in aqueous mixtures of Monoethanolamine with Methyldiethanolamine. Journal of Chemical and Engineering Data 37 (1992) 96–100.

[53]J. I. Baek, J. H. Yoon. Solubility of Carbon Dioxide in Aqueous Solutions of 2-Amino-2-methyl-1, 3-propanediol. Journal of Chemical and Engineering Data 43 (1998) 635-637.

[54] B. K. Mondal, S. S. Bandyopadhyay, A. N. Samanta. Experimental measurement and kent-eisenberg modelling of CO_2 solubility in aqueous mixture of 2-amino-2-methyl-1-propanol and hexamethylenediamine. Fluid Phase Equilibria. 437 (2017) 118-126.

[55] A. Dey, S. K. Dash, S. C. Balchandani, B. P. Mandal. Investigation on the inclusion of 1-(2-aminoethyl) piperazine as a promoter on the equilibrium CO_2 solubility of aqueous 2-amino-2-methyl-1-propanol. Journal of Molecular Liquids 289 (2019) 111036.

[56] B. K. Mondol, S. S. Bandyopadhyay, A. N. Samanta. Equilibrium solubility measurement and kent-eisenberg modeling of CO_2 absorption in aqueous mixture of *N*-methyldiethanolamine and hexamethylenediamine. Greenhouse Gases Science and Technology 7 (2016) **202-214.**

[57] G. Kumar, M. Kundu. Solubility of CO_2 in aqueous blends of (N-methyl-2-ethanolamine + N-methyl-diethanolamine) and (N-methyl-2-ethanolamine + 2-amino-2-methyl-1-propanol). Journal of Chemical and Engineering Data 57 (2012) 3203-3209.

[58] R. Ramazani, S. Mazinani, A. Hafizi, A. Jahanmiri. Equilibrium solubility of carbon dioxide in aqueous blend of monoethanolamine (MEA) and 2-1-piperazinyl-ethylamine (PZEA) solutions: experimental and optimization study. Process Safety and Environmental Protection 98 (2015) 325-332.

Chapter 4

VAPOUR LIQUID EQUILIBRIUM STUDY OF CO_2 IN AQUEOUS TESA AND ITS PROPOSED BLEND WITH AEP/APA

This chapter demonstrates the experimental vapor liquid equilibrium and simulation studies in a prospective absorbent, aqueous 3-aminopropyl triethoxysilane (TESA) and its blends in various amine activators viz. 1-(2-aminoethyl) piperazine (AEP) and bis (3-aminopropyl) amine (APA) over the wide parametric range of (303.2-323.2) K and (4-350) kPa. The measured data were further correlated with modified Kent-Eisenberg (KE) equilibrium model inclusive of non-ideality in the gas phase. Qualitative studies of the CO_2 loaded, and unloaded solvents were carried out using ^{13}C NMR and FTIR-ATR analysis to comprehend the reaction mechanism and recognize the various significant intermediates and reaction products. The model is also analyzed for prediction of equilibrium solubility as well as pH and speciation profiles of various species involved.

4.1 Introduction

As discussed in **Chapter-3**, ionic liquids have been considered for CO_2 capture either through absorption or adsorption. A few more details of the same have been briefed out here as well. Ionic liquids have dual advantages such as thermal and mechanical stability, extremely low vapor pressures but are also having disadvantages such as high cost and high viscosities leading to higher pumping costs in absorption and regeneration columns. To take into account the advantages of ionic liquids and amines in order to provide better CO_2 capture, many researchers have worked for blending appropriate amines with ionic liquids [1]. In addition to blending of ionic liquids with amines, other types of solvents such as task-specific ILs, reversible ILs, etc. also have been studied by various researchers [2-4].

Applications of ILs in CO_2 capture using adsorption, IL supported membranes, poly IL membranes, composite membranes as well as successful catalytic conversion of CO_2 to useful

products with IL as median have been appreciatively reviewed and reported [5, 6]. The results certainly remark a huge potential of identified solvents for CO_2 capture. Conclusively, the blended solvent system, which consists of blending two or more solvents as well as blending with appropriate rate activators, exhibit very promising result in the acid gas separation technology [7, 8]. *N″, N″*-Pentamethyldiethylenetriamine (PMDETA) indicated absorption capacity of 2.631 mol CO_2/ *l* of the solvent at 303 K and 3:7 molar ratio. Analysis of the systems indicated that major CO_2 absorption takes place due to [TETA] Br and PMDETA was approved to be promoting absorption [9]. Shahrom et al. [10] suggested the application of amino acid based polymerized ionic liquids (AAPILs) over task-specific ionic liquids (TSILs) and polymerized ionic liquids (PILs) due to increased CO_2 capture efficiency of the former owing to the presence of amine tethered at the anion.

CO_2 absorption capacity of silyated amine such as (3-aminopropyl)-trimethoxysilane (TMSA), (3-aminopropyl)-triethoxysilane (TESA), (3-aminopropyl)-triethylsilane (TEtSA), and (3-aminopropyl)-tripropylsilane (TPSA) which are a precursor to corresponding ReVILs has been reported [3]. Although, TPSA has shown better CO_2 absorption capacity but TESA was found to be more thermally stable amine in comparison to others. TESA was found to yield a total CO_2 capacity of 14.76 moles of CO_2 per kg of amine. Apart from absorption, earlier instances related to CO_2 adsorption on functionalized graphite oxide [11] and mesoporous silica SBA-15 [12] using TESA have been also reported in the literature. The studies revealed that the functionalization of substrate using TESA provided high stable CO_2 adsorption uptakes. The studies further stated that the functionalization of TESA on SBAa-15 increased CO_2 absorption capacity up to 48 mg/g [12]. A combination of TESA and (1-ethyl-3-methylimidazolium bis (trifluoromethylsulfonyl) imide) have been investigated for developing efficient silica aerogels for CO_2 adsorption [13]. Hence, TESA has been selected for the present study owing to its preferential thermal stability and affinity towards CO_2. Further, in comparison to the traditional ILs such as imidazolium or phosphonium, reversible ILs are very cost effective and they also provide the characteristics required such as thermal stability of ILs. Additionally, since the amino group present in TESA is surrounded by a single alkyl chain, the CO_2 proton exchange at this junction is less hindered by the alkyl chains, which is expected to provide better CO_2 solubility.

Piperazine (PZ) being one of the primarily used activators for the amine based CO_2 capture technology due to various advantages over other primary, secondary, tertiary, or sterically hindered amines such as higher reaction rate, high equilibrium solubility, and lower regeneration energy [14]. But along with these advantages, one of the major disadvantages is precipitation at a lower temperature and hence formation of slurry in the absorption towers which leads to added mass transfer resistance for CO_2 [2, 14]. Hence, recently another category of amines that act as activators are being proposed and published by our research group i.e. AEP and APA [15-18]. The kinetic studies of both these amines indicated promising solvents towards post-combustion CO_2 capture. The same has been discussed in **Chapter-3**. Hence, it can be concluded from the literature that reversible ionic liquids blended with novel amine activators i.e. (TESA + AEP/APA) may lead to the cost and energy efficient innovative solvents for the application in CO_2 capture process. It is expected that solvent blends of (TESA + AEP/APA) would result in better CO_2 solubility in comparison to blends of ([bmim] [Ac] + AEP/APA) studied in **Chapter-3**.

This work majorly focuses on the exploration of reversible ionic liquids, TESA as cost and energy efficient solvents for the rationale of CO_2 capture process. As discussed earlier, TESA blends with either AEP or APA were chosen as innovative solvents due to superior properties. The concentrations of AEP/APA were varied from ca. 0.5 to ca. 1.0 *m* ($mol.kg^{-1}$). The temperature and pressure were varied between (313.2-323.2) K and (4-350) kPa, respectively. It is envisioned and proved through experimentation and theoretical work using the COSMO-RS method that the amalgamation of TESA with amines AEP and APA shall provide better CO_2 loadings in comparison to conventional solvents [19, 20]. By tuning the amine and reversible ionic liquid blend composition will give an effective route for CO_2 capture. In addition to the modified Kent-Eisenberg model, a non-rigorous statistical model is also proposed for correlating CO_2 solubility data. The competency of both the models has also been analyzed. This study demonstrates our effort in the measurement and modeling of VLE data of CO_2 solubility in novel aqueous blends of silane-based reversible ionic liquids with AEP and APA.

4.2 Experimental section

4.2.1 Materials

3-aminopropyl triethoxysilane (TESA, 99% Pure), 1-(2-Aminoethyl) piperazine (AEP, 99 % Pure), and Bis (3-aminopropyl) amine (APA, 98 % Pure) were purchased from Sigma–Aldrich. CO_2 gas (> 99 % Pure) was procured from Linde India ltd. All the chemicals and CO_2 gas were used for solubility measurements without further purification. The solvent solutions were prepared with double distilled deionized water. Specification details of the chemicals used under the study are given in Table 4.1.

Table 4.1 Specifications of chemicals

Chemical name	Chemical structure	Molecular weight	Source	Stated mass fraction purity	CAS no.	Purification method
3-aminopropyl triethoxysilane (TESA)	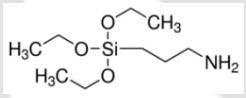	221.37	Sigma Aldrich Co.	0.99	919-30-2	None
1-(2-Aminoethyl) Piperazine (AEP)	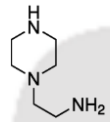	129.21	Sigma Aldrich Co.	0.99	140-31-8	None
Bis(3-aminopropyl) amine (APA)	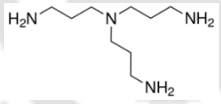	131.22	Sigma Aldrich Co.	0.98	56-18-8	None
Carbon dioxide (CO_2)		44.01	Linde India Ltd.	>0.99	367522-96-1	None

4.2.2 Experimental methodology

4.2.2.1 Vapour Liquid Equilibrium (VLE) Measurement

The experimental set-up described in **Chapter-3** has been used for vapor liquid equilibrium measurements and is also reported elsewhere [17, 19]. Nine solvents with the following compositions are studied in the present work at 303.2, 313.2 and 323.2 K: (1) aq. 2.432 *m* TESA, (2) aq. 1.506 *m* TESA, (3) aq. 0.797 *m* TESA, (4) aq. (2.528 *m* TESA + 0.498 *m* AEP), (5) aq. (2.259 *m* TESA + 0.756 *m* AEP), (6) aq.(2.044 *m* TESA + 1.004 *m* AEP), (7) aq. (2.528 *m* TESA

+ 0.499 *m* APA), (8) aq. (2.259 *m* TESA + 0.753 *m* APA) and (9) aq. (2.044 *m* TESA + 0.991 *m* APA). Here, '*m*' represents mol/kg (molal unit). The experimental data related to CO_2 solubility in studied solvent systems are represented in Tables 4.2 – 4.10.

Table 4.2 Equilibrium CO_2 solubility data in aqueous 2.432 molal (*m*) TESA solution

T / K	m_1 / mol.kg^{-1} TESA	P_{CO2}/ kPa	α_{CO2}
303.2	2.432	81.4	0.205
	2.432	89.1	0.396
	2.432	156.9	0.491
	2.432	201.0	0.524
	2.432	203.7	0.709
	2.432	230.0	0.805
	2.432	237.4	0.894
313.2	2.432	9.9	0.315
	2.432	94.5	0.453
	2.432	141.0	0.486
	2.432	190.0	0.510
	2.432	221.7	0.590
	2.432	248.6	0.660
	2.432	283.0	0.674
323.2	2.432	12.1	0.258
	2.432	62.7	0.453
	2.432	125.3	0.506
	2.432	154.7	0.525
	2.432	189.5	0.551
	2.432	231.2	0.570

Table 4.3 Equilibrium CO_2 solubility data in aqueous 1.506 molal (m) TESA solution

T / K	m_1 / mol.kg^{-1} TESA	P_{CO2}/ kPa	α_{CO2}
303.2	1.506	22.3	0.513
	1.506	108.8	0.725
	1.506	180.7	0.799
	1.506	228.7	0.846
	1.506	248.8	0.895
	1.506	260.9	1.011
313.2	1.506	19.0	0.458
	1.506	114.2	0.585
	1.506	149.5	0.626
	1.506	195.2	0.658
	1.506	230.6	0.678
	1.506	244.7	0.784
	1.506	278.6	0.803
323.2	1.506	17.2	0.399
	1.506	98.5	0.620
	1.506	161.5	0.717
	1.506	191.7	0.771
	1.506	259.2	0.827

Table 4.4 Equilibrium CO_2 solubility data in aqueous 0.8 molal (*m*) TESA solution

T / K	m_1 / mol.kg^{-1} TESA	P_{CO2}/ kPa	α_{CO2}
303.2	0.797	47.9	0.631
	0.797	150.8	0.813
	0.797	178.2	0.929
	0.797	254.0	0.999
	0.797	302.5	1.257
	0.797	320.1	1.521
	0.797	348.1	1.703
313.2	0.797	35.1	0.520
	0.797	128.6	0.665
	0.797	180.4	0.697
	0.797	249.0	0.718
	0.797	324.8	0.739
323.2	0.797	47.3	0.596
	0.797	128.7	0.727
	0.797	161.3	0.778
	0.797	203.2	0.818
	0.797	243.0	0.877
	0.797	285.4	0.913

Table 4.5 Equilibrium CO_2 solubility data in aqueous (2.528 + 0.498) molal (m) (TESA + AEP) solution

T / K	m_1 / mol.kg^{-1} TESA	m_1 / mol.kg^{-1} (AEP)	P_{CO2}/kPa	α_{CO2}
303.2	2.528	0.498	67.2	0.444
	2.528	0.498	109.3	0.533
	2.528	0.498	139.6	0.581
	2.528	0.498	185.0	0.618
	2.528	0.498	219.5	0.647
	2.528	0.498	257.5	0.693
	2.528	0.498	305.4	0.719
313.2	2.528	0.498	9.2	0.306
	2.528	0.498	41.2	0.498
	2.528	0.498	123.9	0.609
	2.528	0.498	168.1	0.644
	2.528	0.498	211.3	0.703
	2.528	0.498	227.6	0.762
	2.528	0.498	255.9	0.772
323.2	2.528	0.498	12.6	0.332
	2.528	0.498	20.6	0.464
	2.528	0.498	130.0	0.611
	2.528	0.498	181.0	0.643
	2.528	0.498	213.9	0.660
	2.528	0.498	257.7	0.674

Table 4.6 Equilibrium CO_2 solubility data in aqueous (2.259 + 0.756) molal (m) (TESA + AEP) solution

T / K	m_1 / mol.kg^{-1} TESA	m_1 / mol.kg^{-1} (AEP)	P_{CO2}/kPa	α_{CO2}
303.2	2.259	0.756	4.6	0.319
	2.259	0.756	69.3	0.536
	2.259	0.756	130.2	0.620
	2.259	0.756	179.6	0.661
	2.259	0.756	206.3	0.699
	2.259	0.756	265.5	0.725
	2.259	0.756	315.6	0.779
	2.259	0.756	333.4	0.827
	2.259	0.756	348.7	0.874
313.2	2.259	0.756	9.8	0.267
	2.259	0.756	32.3	0.507
	2.259	0.756	92.9	0.613
	2.259	0.756	118.3	0.729
	2.259	0.756	180.4	0.761
	2.259	0.756	232.2	0.778
	2.259	0.756	301.3	0.796
323.2	2.259	0.756	11.5	0.241
	2.259	0.756	24.0	0.471
	2.259	0.756	98.0	0.576
	2.259	0.756	132.0	0.613
	2.259	0.756	158.6	0.635
	2.259	0.756	202.0	0.669

Table 4.7 Equilibrium CO_2 solubility data in aqueous (2.044 + 1.004) molal (m) (TESA + AEP) solution

T / K	m_1 / mol.kg^{-1} TESA	m_1 / mol.kg^{-1} (AEP)	P_{CO2}/kPa	α_{CO2}
303.2	2.044	1.004	7.0	0.298
	2.044	1.004	22.8	0.546
	2.044	1.004	98.9	0.666
	2.044	1.004	153.8	0.724
	2.044	1.004	195.3	0.778
	2.044	1.004	254.1	0.811
	2.044	1.004	297.4	0.828
313.2	2.044	1.004	9.4	0.235
	2.044	1.004	20.6	0.477
	2.044	1.004	91.6	0.596
	2.044	1.004	156.7	0.637
	2.044	1.004	198.5	0.652
	2.044	1.004	244.2	0.667
323.2	2.044	1.004	9.9	0.235
	2.044	1.004	17.2	0.447
	2.044	1.004	73.0	0.574
	2.044	1.004	140.0	0.624
	2.044	1.004	178.3	0.650
	2.044	1.004	179.3	0.682
	2.044	1.004	187.6	0.769
	2.044	1.004	216.8	0.741

Table 4.8 Equilibrium CO_2 solubility data in aqueous (2.528 + 0.499) molal (*m*) (TESA + APA) solution

T / K	m_1 / mol.kg^{-1} TESA	m_1 / mol.kg^{-1} (APA)	P_{CO2}/kPa	α_{CO2}
	2.528	0.499	5.5	0.366
	2.528	0.499	38.9	0.578
	2.528	0.499	98.3	0.676
303.2	2.528	0.499	128.9	0.725
	2.528	0.499	153.0	0.748
	2.528	0.499	184.0	0.771
	2.528	0.499	238.7	0.789
	2.528	0.499	9.3	0.225
	2.528	0.499	21.7	0.448
	2.528	0.499	84.1	0.562
313.2	2.528	0.499	117.4	0.604
	2.528	0.499	146.9	0.627
	2.528	0.499	190.9	0.644
	2.528	0.499	218.8	0.662
	2.528	0.499	11.7	0.198
	2.528	0.499	15.2	0.402
	2.528	0.499	52.2	0.534
323.2	2.528	0.499	114.6	0.582
	2.528	0.499	149.3	0.597
	2.528	0.499	174.6	0.614
	2.528	0.499	225.5	0.614

Table 4.9 Equilibrium CO_2 solubility data in aqueous (2.259 + 0.753) molal (m) (TESA + APA) solution

T / K	m_1 / mol.kg^{-1} TESA	m_1 / mol.kg^{-1} (APA)	P_{CO2}/kPa	α_{CO2}
303.2	2.259	0.753	4.3	0.247
	2.259	0.753	8.2	0.542
	2.259	0.753	73.8	0.693
	2.259	0.753	136.6	0.747
	2.259	0.753	186.2	0.770
	2.259	0.753	239.0	0.789
	2.259	0.753	280.6	0.803
313.2	2.259	0.753	9.0	0.199
	2.259	0.753	12.1	0.452
	2.259	0.753	16.6	0.514
	2.259	0.753	77.0	0.623
	2.259	0.753	120.6	0.658
	2.259	0.753	145.3	0.676
	2.259	0.753	169.5	0.690
	2.259	0.753	207.6	0.704
323.2	2.259	0.753	11.5	0.212
	2.259	0.753	15.0	0.426
	2.259	0.753	32.1	0.605
	2.259	0.753	132.2	0.704
	2.259	0.753	175.9	0.713
	2.259	0.753	184.0	0.744
	2.259	0.753	201.7	0.794
	2.259	0.753	208.5	0.873

Table 4.10 Equilibrium CO_2 solubility data in aqueous (2.044 + 0.991) molal (*m*) (TESA + APA) solution

T / K	m_1 / mol.kg^{-1} TESA	m_1 / mol.kg^{-1} (APA)	P_{CO2}/kPa	α_{CO2}
303.2	2.044	0.991	7.5	0.265
	2.044	0.991	9.8	0.531
	2.044	0.991	38.7	0.737
	2.044	0.991	111.9	0.815
	2.044	0.991	147.6	0.841
	2.044	0.991	175.7	0.857
	2.044	0.991	222.9	0.878
313.2	2.044	0.991	7.5	0.273
	2.044	0.991	10.1	0.552
	2.044	0.991	20.9	0.826
	2.044	0.991	82.4	0.977
	2.044	0.991	123.1	1.025
	2.044	0.991	148.8	1.072
	2.044	0.991	172.2	1.109
	2.044	0.991	197.5	1.146
323.2	2.044	0.991	10.3	0.210
	2.044	0.991	14.1	0.433
	2.044	0.991	27.4	0.612
	2.044	0.991	88.8	0.702
	2.044	0.991	120.8	0.730
	2.044	0.991	133.1	0.756
	2.044	0.991	173.8	0.814

4.2.2.2 FTIR-ATR and ^{13}C NMR study

The ^{13}C NMR spectra of unloaded and CO_2 loaded solvents at 313.2 K for 2.432 *m* TESA and (2.259 *m* TESA + 0.756 *m* AEP) blend systems is carried out. The solvents are further also studied through FTIR- ATR spectroscopy within the wavenumber range of 3000 to 400 cm^{-1}. The instrumental details of FTIR and ^{13}C NMR has already been reported in **Chapter-3**.

4.3 Proposed chemical reaction

In order to analyze various reaction products and propose a suitable set of reactions, qualitative FTIR and ^{13}C NMR studies of the blends under investigation were found to be useful. Furthermore, such analysis also gives an understanding of the various bond formations/breakage and intermediates generated during the course of reaction.

The formation of ionic liquid whilst reaction is verified by ^{13}C NMR spectra analysis of aq. TESA and aq. (TESA + AEP) system before and after CO_2 absorption and is presented in Figures 4.1-4.2. Consequent to the carbonyl carbon, three sharp peaks were observed at various positions in the low field range (163-165 ppm) which in turn represent the different carbamate groups. Sharp peaks at 164.38 and 164.15 in both cases, respectively indicate the presence of simple primary carbamate and primary carbamate associated with the dicarbamate. Similar observations were found for the case of aqueous AEP and aqueous (AEP + PZ) [21]. The formation of carbamate ions while CO_2 reacts in aqueous APA is also confirmed in the literature [22].

The field range on the higher side being (61-10) ppm is observed in both the cases of loaded solutions. The highest peak range from (58-34) ppm for loaded aq. AEP systems has been however reported in the literature [21]. Hence, a range of different product formations i.e. reversible ionic liquids are formed over the region from the higher field range of (24-10) ppm. The ^{13}C NMR spectrum of loaded TESA is compared with the literature [23]. According to the literature work, the following peaks were found in the ^{13}C NMR spectra of TESA ionic liquid: 162.5, 57.7, 44.1, 41.5, 23.7, 21.3, 17.9, 7.6 and 7.4. The ^{13}C NMR spectra of CO_2 loaded aq. TESA and aq. (TESA + AEP) systems have shown similar peaks with a small deviation (Figures. 4.1(b) and 4.2(b)). The conceivable reasons for this shift are either (i) due to the presence of water in the present case or (ii) due to the temperature divergence at which absorption of CO_2 is carried out. The comparison of ^{13}C NMR spectra between the literature and present work confirmed the formation of reversible TESA based ionic liquid.

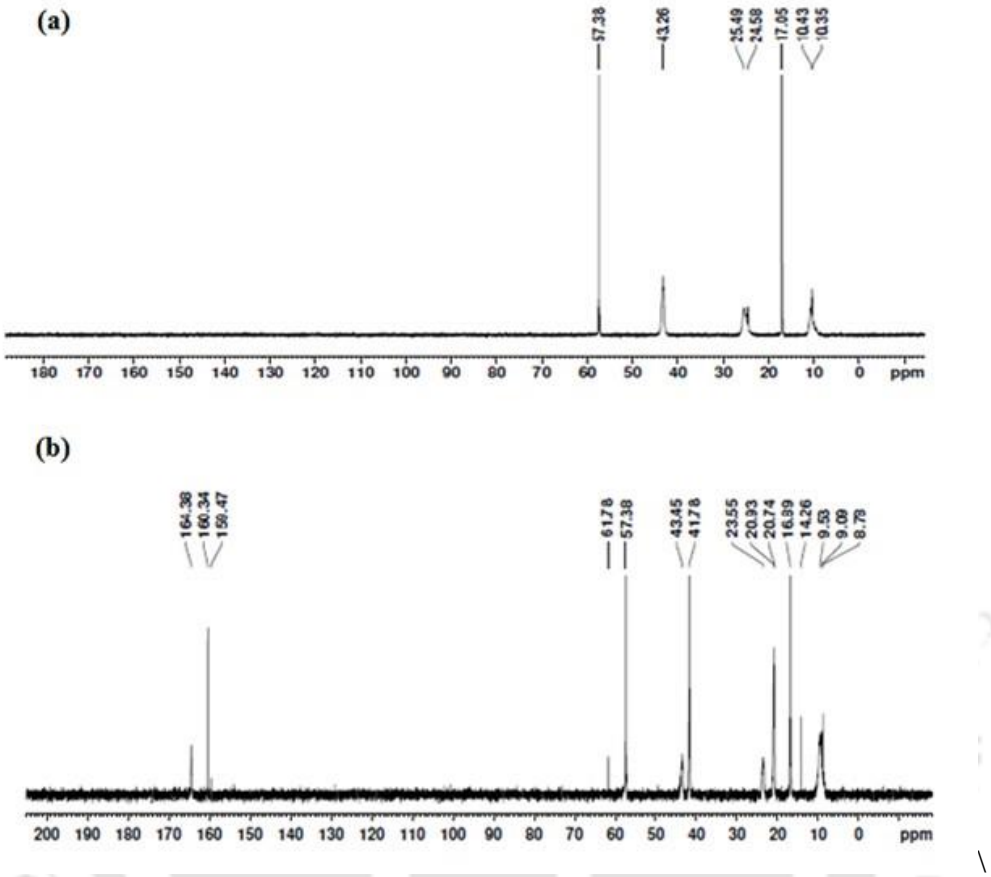

Figure 4.1 ^{13}C NMR spectra of 2.432 *m* aq. TESA solution (a) unloaded (b) CO_2 loaded at 313.2 K

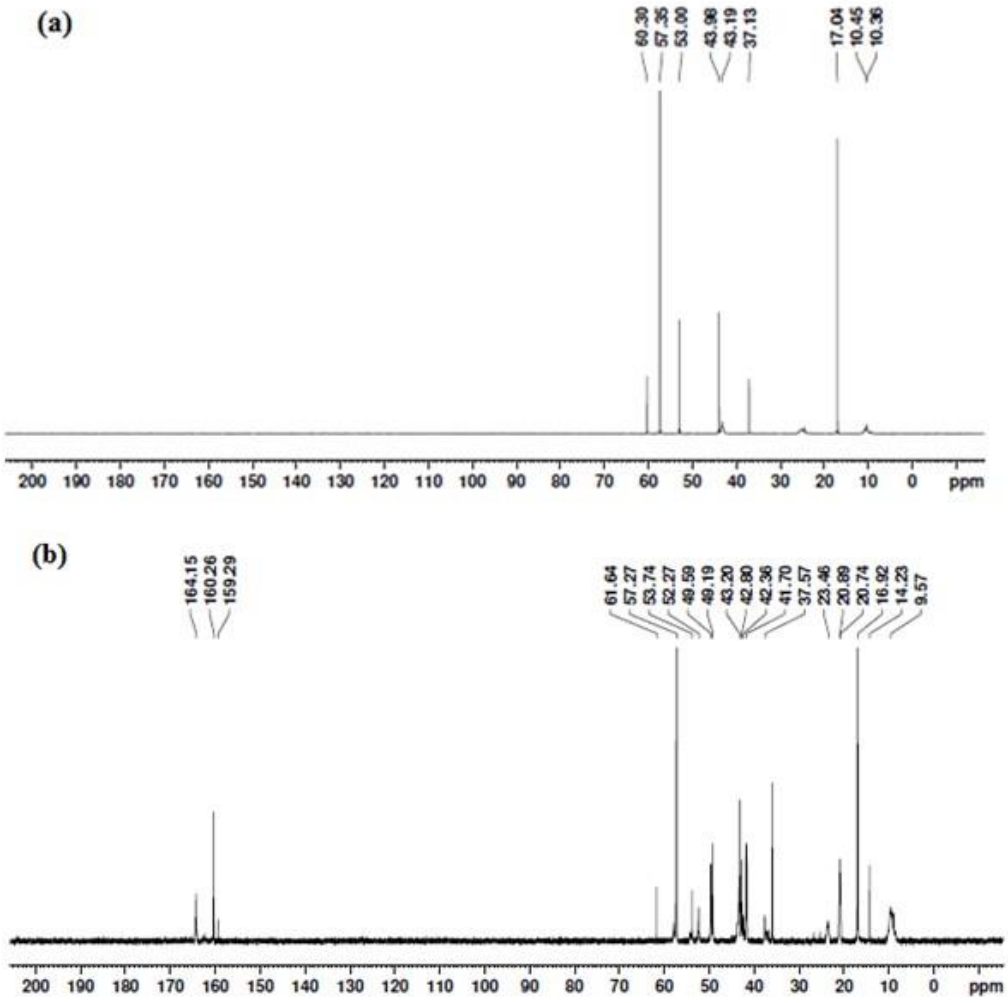

Figure 4.2 ^{13}C NMR spectra of (2.259 + 0.756) *m* aq. (TESA+AEP) solution (a) unloaded (b) CO_2 loaded at 313.2 K

FTIR-ATR has been carried out to analyze the variations in different associated bonds in the reactants which results in the formation of proposed products. The FTIR analysis of CO_2 loaded and unloaded aq. (2.259 *m* TESA + 0.756 *m* AEP) solution is carried out in the present work (Figure 4.3).

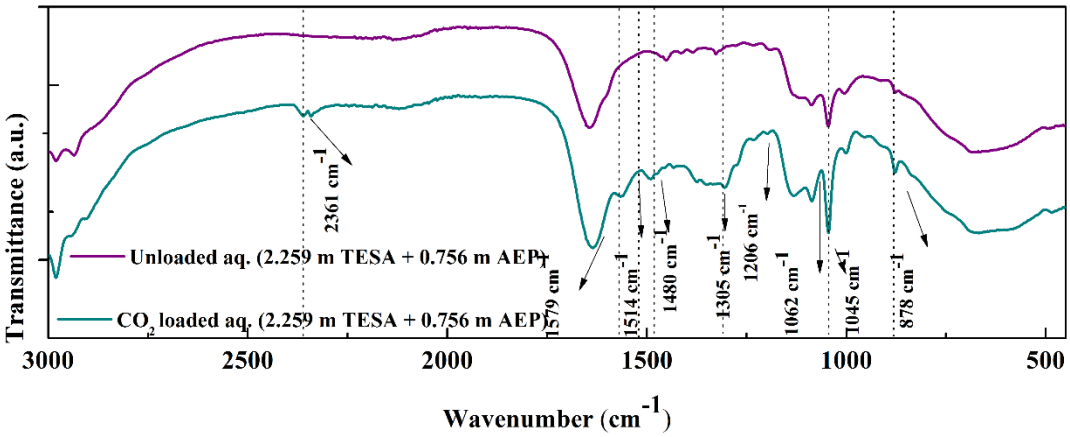

Figure 4.3 FTIR-ATR spectra of aq. (2.259 *m* TESA + 0.756 *m* AEP) unloaded and CO_2 loaded at 303.2 K

A new peak at 2361 cm^{-1} was observed which concludes the asymmetric stretching due to dissolved CO_2. Also, the bands at 1579, 1514, and 1480 cm^{-1} are observed for loaded solvent in comparison with unloaded one, which can be assigned to COO^- asymmetric and symmetric stretching, respectively. However, the peaks at 1305 and 1206 cm^{-1} are anticipated to $NCOO^-$ stretching vibrations of carbamate species and C (O)-O stretching vibrations. Due to the protonation of TESA and AEP, the peaks of C-N and C-O observed a shift from 1075 to 1062 cm^{-1} and 1043 to 1045 cm^{-1}, respectively. Similarly, the peaks at 878 cm^{-1} can be attributed to C-NH_2 twisting for AEP [24, 25]. Through the results of ^{13}C NMR and FTIR, it can be concluded that TESA gets reacted to CO_2 forming anion and cation. Additionally, the comparison of the results of various peaks of the two analysis indicated the reversible nature of the ionic liquid associated with TESA. Hence, the reaction scheme for CO_2 solubility in pure TESA by the formation of anionic carbamate and cation is represented in Figure 4.4.

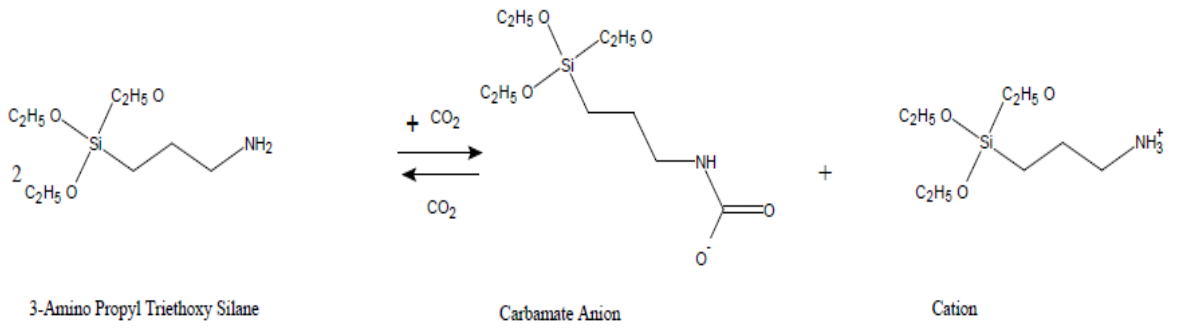

Figure 4.4 Reaction scheme of CO_2 in TESA

The equilibrium reactions for (TESA + H_2O + CO_2), (TESA + AEP + H_2O + CO_2) and (TESA + APA + H_2O + CO_2) expressed using reactions R_1 to R_{10} are proposed for the blends under study:

Physical Solubility

$$CO_2(g) \overset{H_{CO2}}{\longleftrightarrow} CO_2(aq) \quad \text{(R-1)}$$

Dissociation of bicarbonate ion

$$HCO^{3-} \overset{K_1}{\longleftrightarrow} CO_3^{2-} + H^+ \quad \text{(R-2)}$$

Formation of bicarbonate ion

$$CO_2 + H_2O \overset{K_2}{\longleftrightarrow} HCO_3^- + H^+ \quad \text{(R-3)}$$

Dissociation of water

$$H_2O \overset{K_3}{\longleftrightarrow} OH^- + H^+ \quad \text{(R-4)}$$

Deprotonation of TESA

$$TESAH^+ \overset{K_4}{\longleftrightarrow} TESA + H^+ \quad \text{(R-5)}$$

Carbamate hydrolysis of TESA

$$TESACOO^- + H_2O \xleftrightarrow{K_5} TESA + HCO_3^- \quad \text{(R-6)}$$

Deprotonation of AEP

$$AEPH^+ \xleftrightarrow{K_6} AEP + H^+ \quad \text{(R-7)}$$

Carbamate hydrolysis of AEP

$$AEPCOO^- + H_2O \xleftrightarrow{K_7} AEP + HCO_3^- \quad \text{(R-8)}$$

Deprotonation of APA

$$APAH^+ \xleftrightarrow{K'_6} APA + H^+ \quad \text{(R-9)}$$

Carbamate hydrolysis of APA

$$APACOO^- + H_2O \xleftrightarrow{K'_7} APA + HCO_3^- \quad \text{(R-10)}$$

Where, each term has their usual meaning with K_1, K_2, K_3, K_4, K_5, K_6, K_7, K_6', and K_7' being the equilibrium constants associated with respective reactions (R2-R10).

4.4 Modeling of CO_2 solubility

The VLE data in the present study has been correlated using modified Kent-Eisenberg. Furthermore, based on the dependence of CO_2 solubility with respect to temperature, pressure, concentration of TESA and AEP/APA, a new non-rigorous and non-linear statistical model has also been proposed. Similar models reported in the literature have proven to provide an improved precise estimate of CO_2 solubility [26, 27].

4.4.1 Modified Kent-Eisenberg model

The physical solubility of CO_2 is usually due to the weak van der Walls forces of attraction which here is presented by Henry's law. Reversible reactions in the liquid phase are explained using chemical reaction equilibrium constants through the conceptualization of chemical equilibrium. The liquid phase reaction consists of protonation of both TESA and APA/AEP amine activators, carbamate formation by APA/AEP, and other reactions. The bicarbamate formation of AEP has

not been considered here [28] since at higher CO_2 loading bicarbonate is the major product of (AEP-CO_2) reaction [29]. The carbamate formation for reaction between TESA and CO_2 has been already reported in the literature [30, 31] and is also confirmed through ^{13}C NMR and FTIR studies in the present work. A detailed explanation regarding the model has already been presented in **Chapter-3**. The detailed mathematical formulation and Matlab code of modified KE model for aq. (TESA + AEP) is presented in APPENDIX III and IV, respectively.

4.4.2 Non-rigorous statistical model (N_1)

Statistical regressive models have been of interest in the past owing to the ease of calculations of the interaction parameters i.e. the coefficients associated with the model [26, 32, 33]. In addition, these models have also proved to provide better prediction capabilities over a wide range of reaction conditions. Unlike the first principle or deterministic models, these models require fewer input data. Considering this, here a non-rigorous statistical non-linear model is proposed as equation (4.1).

$$\alpha_{CO2} = d_0 + \left(d_1 \times (\log(P_{CO2}))\right) + \left(d_2 \times \left(\frac{1}{T}\right)\right) + (d_3 \times (M)) + \left(d_4 \times \left(\frac{\log(P_{CO2}) \times M}{T}\right)\right) + \left(d_5 \times \left(\frac{\log(P_{CO2}) \times M}{T}\right)^2\right) \quad (4.1)$$

Where, α_{CO2}, P_{CO2}, T, and M are equilibrium CO_2 loading in mol of CO_2 per mol of solvent, CO_2 partial pressure (kPa), temperature (K), and total molarity of the solvent in kmol.m^{-3}, respectively. d_0, d_1, d_2, d_3, d_4 and d_5 are the coefficients. The required non-linear regression is carried out in MATLAB (R17).

4.5 Results and discussion

The standardization of the conceived methodology for the work under consideration is been earlier reported and published elsewhere [17, 19]. The maximum estimated uncertainty of CO_2 loading is calculated to be 0.038.

4.5.1 Effect of reaction parameters on the equilibrium CO_2 solubility

The CO_2 loading is observed to increase with P_{CO2} and solvent concentration at a constant temperature for all the blends under study. This is owing to the reason that with rise in P_{CO2}, the kinetic energy between CO_2 gas molecules and liquid surface increases. Further, α_{CO2} is found to

decrease with an increase in temperature at constant pressure and solvent concentration. However, in the present case, the dependency of CO_2 loading with temperature is not uniform. The highest loading in case of (2.528 *m* TESA + 0.498 *m* AEP) was observed at 313.2 K whereas for TESA (0.797 *m*) it was observed at 303.2 K but it was also competitive with that at 323.2 K. For aqueous (2.259 *m* TESA + 0.753 *m* APA) system, the highest CO_2 loading was observed at 323.2 K [34-36]. It was observed that the optimum temperature for the simultaneous absorption of CO_2 and formation of ionic liquids is at 313.2 K for aq. (TESA + AEP) system. The reason may be attributed to the possible pronounced solvent-solute interactions at the corresponding temperature. However, on further increasing the temperature at 323.2 K, the solvent-solute interaction decreases due to the reversible nature of the ionic liquids formed. One of the leading conclusion is that the aqueous TESA system yields the highest CO_2 loading at 303.2 K but by addition of activators AEP and APA to the aqueous TESA system, the highest CO_2 loading was found at higher temperatures [34-36]. The same has been presented in Figures 4.5-4.7. Figure 4.7 represents the comparison of α_{CO2} loading as a function of P_{CO2} at various temperatures for (2.528 *m* TESA + 0.499 *m* APA). It can be seen from this figure that with rise in temperature the CO_2 loading decreases and found to be least at 323.2 K.

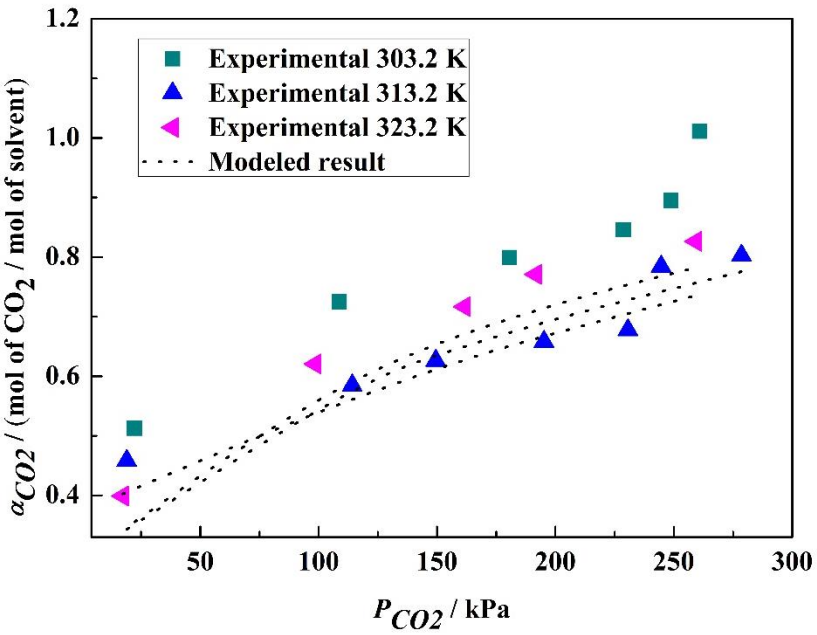

Figure 4.5 Influence of temperature on the CO_2 solubility in aqueous 1.506 *m* TESA

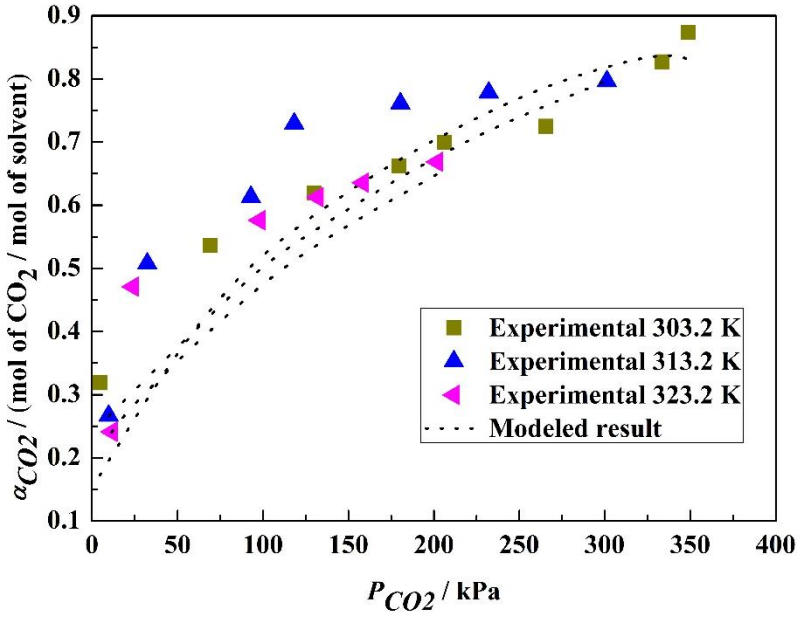

Figure 4.6 Influence of temperature on CO_2 solubility in aqueous blend of (2.259 *m* TESA + 0.756 *m* AEP)

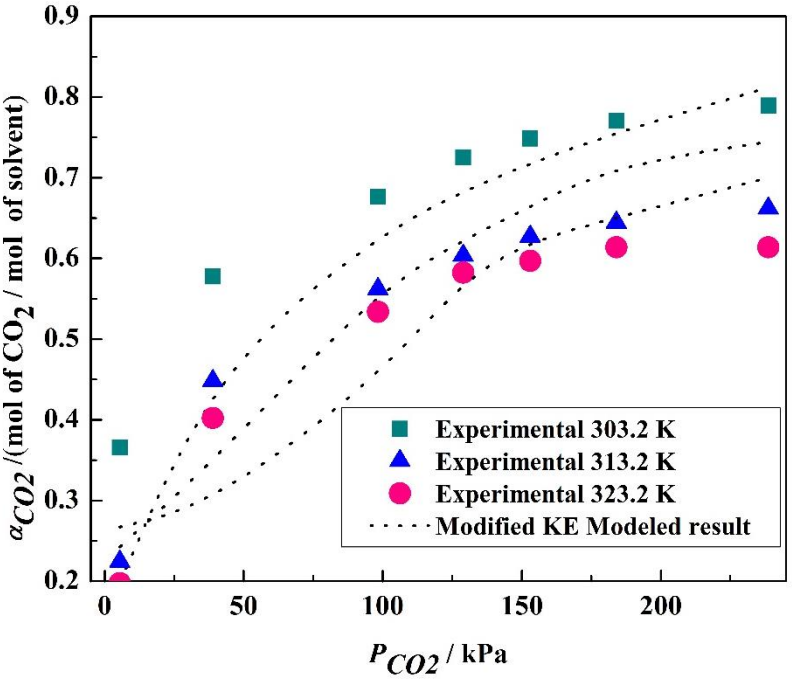

Figure 4.7 Influence of temperature on CO_2 solubility in aqueous blend of (2.528 *m* TESA + 0.499 *m* APA)

CO_2 loading α_{CO2} is observed to increase whilst the rise in AEP/APA concentration in respective solvent systems (Figures 4.8-4.9, Tables 4.5-4.10). For instance, at a pressure of approximately 180 kPa and at 303.2 K, α_{CO2} was found to increase substantially by around 20 % and 11% for corresponding increment in the activator concentration from 0.499 *m* to 0.991 *m* for AEP and APA, respectively. Also, comparative evaluation of CO_2 loading in 2.432 m aq. TESA along with the addition of 0.498 *m* AEP and 0.499 *m* APA also showed an increase of CO_2 loading of 16.96 % and 49.71 %, respectively at 303.2 K. This further indicates that APA is a better activator for CO_2 absorption in aq. TESA when compared to AEP (Tables 4.2-4.10). The obtained analysis is owing to the more no. of amino groups attached to APA molecule in comparison to AEP. Hence, the probability of CO_2 molecule is more to react with APA molecule than AEP.

The VLE data has been correlated using modified KE model where the coefficients of the equilibrium constants, K_4, K_5, K_6, K_6', K_7 and K_7'have been regressively evaluated including gas phase non-ideality. The equilibrium constants (K_4, K_5, K_6, K_6', K_7 and K_7') discussed in terms of concentration of solvents, temperature, and P_{CO2} can be presented as:

$$K_4(or/K_6 or/K_6^{'}) = g + (h\times m) + (k\times T) + (l\times m\times T) + (n\times T^2) + (p\times P_{CO_2}) + (q\times P_{CO_2}^2) \quad (4.2)$$

$$K_5(or/K_7 or/K_7^{'}) = g + (h\times m) + (k\times T) + (l\times m^2) + (n\times m\times T) + (p\times T^2) + (q\times P_{CO_2}) + (r\times P_{CO_2}^2) \quad (4.3)$$

The equilibrium constants (K_4, K_5, K_6, K_7, $K_6^{'}$, $K_7^{'}$) presented in equations (4.2-4.3) have been obtained through KE model presented in Table 4.11. The estimated equilibrium constants were in turn used to predict the CO_2 loading. The calculated % AAD for aqueous TESA, (TESA + AEP) and (TESA + APA) systems are 12.94, 13.21, and 16.21, respectively.

Table 4.11 Coefficients of the equilibrium constants estimated in the present work

K_i/ kmol.m^{-3}	K_4	K_5	K_6	K_7	$K_{6'}$	$K_{7'}$
g	-1.016×10^{-10}	2.216×10	-2.494×10^{-9}	2.948×10	8.963×10^{-9}	1.475×10
h	1.156×10^{-8}	-4.035×10^{-3}	2.278×10^{-12}	-4.626×10^{-1}	2.264×10^{-16}	-1.373×10
k	-2.110×10^{-11}	-7.911×10^{-3}	-2.566×10^{-12}	-1.126	-5.547×10^{-11}	1.404×10
l	1.906×10^{-12}	1.534×10^{-3}	2.224×10^{-13}	-3.637×10^{-1}	4.076×10^{-12}	1.659×10
n	1.230×10^{-13}	8.261×10^{-3}	1.019×10^{-13}	1.122	1.222×10^{-14}	2.813×10^{-1}
p	-7.094×10^{-12}	-2.199×10^{-4}	-5.604×10^{-11}	-2.843×10^{-2}	-6.469×10^{-11}	-1.409×10^{3}
q	-3.639×10^{-18}	7.028×10^{-2}	-5.885×10^{-24}	2.201	-5.248×10^{-18}	1.155×10^{2}

r	-	-2.161×10^{-4}	-	-2.408×10^{-2}	-	-3.480×10

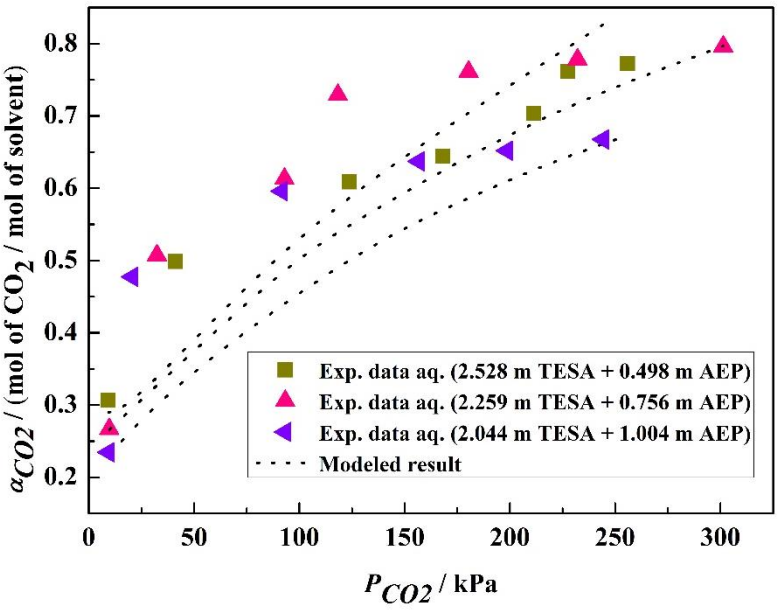

Figure 4.8 Influence of solvent concentration on the α_{CO2} in aqueous (TESA + AEP) solvent blend at 313.2 K

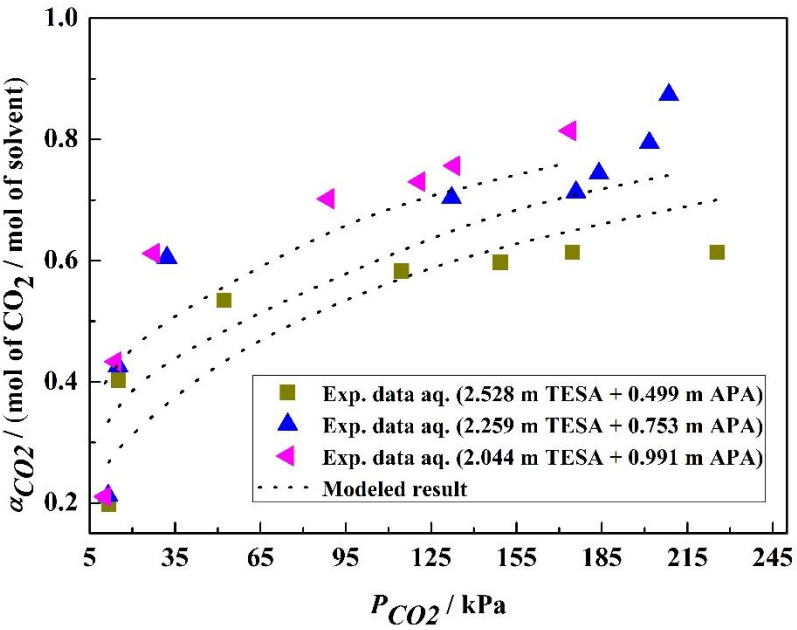

Figure 4.9 Influence of solvent concentration on the α_{CO2} in aqueous (TESA + APA) solvent blend at 323.2 K

4.5.2 Co-relation using model (N_1)

The experimental CO_2 loading data is further co-related using model N_1 with respect to P_{CO2}, T, and molarity of the solvents associated as described in Eq. 4.1. The % AAD for aq. TESA, aq. (TESA + AEP) and aq. (TESA + APA) are estimated to be 16.4, 8.6, and 14.5, respectively. The coefficients of non-linear regression are presented in Table 4.12. Both the models i.e. modified KE and N_1 are found to be quite competitive in predicting CO_2 solubility. The major advantage of modified KE over N_1 model is that the data obtained through former can be further analyzed for the prediction of liquid phase speciation and *pH* of the systems. The experimental and modeled values are for aq. TESA and aq. (TESA + AEP) systems are observed to be in fine concurrence with each other using both the models (Figure 4.10(a-b)).

Table 4.12 Coefficients of the proposed model N_1 estimated in the present work

Predicted Coefficients	aq. TESA	aq.(TESA+AEP)	aq.(TESA+APA)
d_0	-4.232	-1.205	-8.204
d_1	0.402	0.149	0.224
d_2	1.107×10^3	2.686×10	1.725×10^2
d_3	0.630	0.643	3.843
d_4	-8.963×10	-1.240×10	2.288×10
d_5	8.136×10^2	1.866×10^2	-7.848×10^2
100 AAD	16.37	8.55	14.49
SD	0.32	0.21	0.27

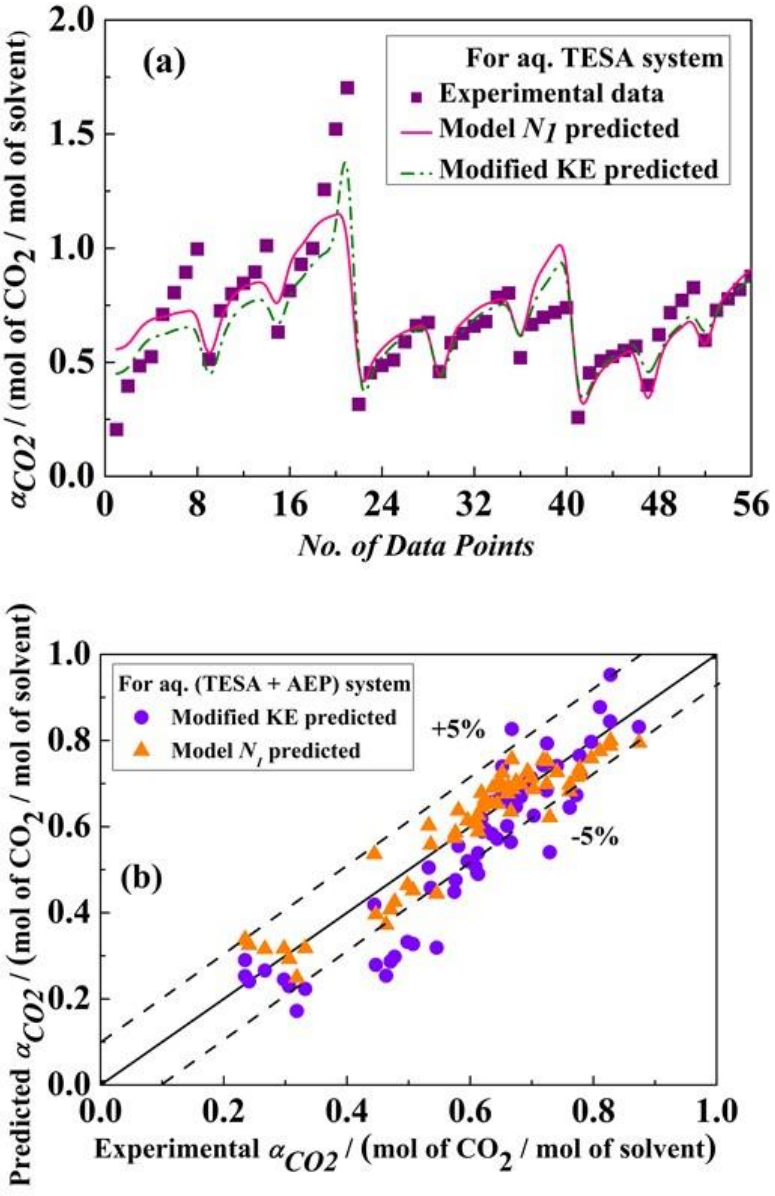

Figure 4.10 Comparison of experimental and modeled CO_2 loading values (a) aq. TESA system: cross plot (b) aq. (TESA + AEP): parity plot

4.5.3 Liquid phase speciation profile, pH, solvent capacity

The equilibrium concentrations of different constituent species available in the liquid phase are further predicted functional to CO_2 loading using modified KE model applied to all the systems. The concentration profile of diverse species for CO_2 loaded aqueous 1.506 *m* TESA and (2.528 *m* TESA + 0.499 *m* APA) at 303.2 K has been represented in Figures 4.11 and 4.12, respectively.

It can be clearly perceived from the speciation plot that the concentration of the reactive species TESA and APA have a decreasing concentration attributive to the reason for their conversion to intermediate species or final products such as bicarbonates, protonated species or carbamates associated with TESA/APA. Also, compared to TESA, APA observe a more steep decrease in the concentration as a function of CO_2 loading indicating APA to be a limiting reactant for CO_2 solubility reaction. Subsequently, it is evident from the speciation plots that TESA depart slowly but surely with α_{CO2} and thereby key reaction products are protonated TESA & bicarbonate ion. The dissociation and formation of $[HCO^{3-}]$ to CO_3^{2-} species (R_2-R_3) leads to an intermediate profile of both the species with a very low concentrations as a function of CO_2 loading.

One of the important design parameters for absorption and stripping towers is the pH level which shall be handled in the system. The reaction products are usually in the pH range of (7-12) [14]. In the current work, modified KE model is further used to assess pH of blended solvent systems functional of CO_2 loading. As indicated in Figure 4.13, for aq. (2.528 m TESA + 0.499 m APA) system, the highest pH was observed at a low temperature of 303.2 K. With rise in temperature and loading, pH was observed to decrease consequentially due to the higher H^+ ions in the systems in comparison to OH^- ions at lower temperatures.

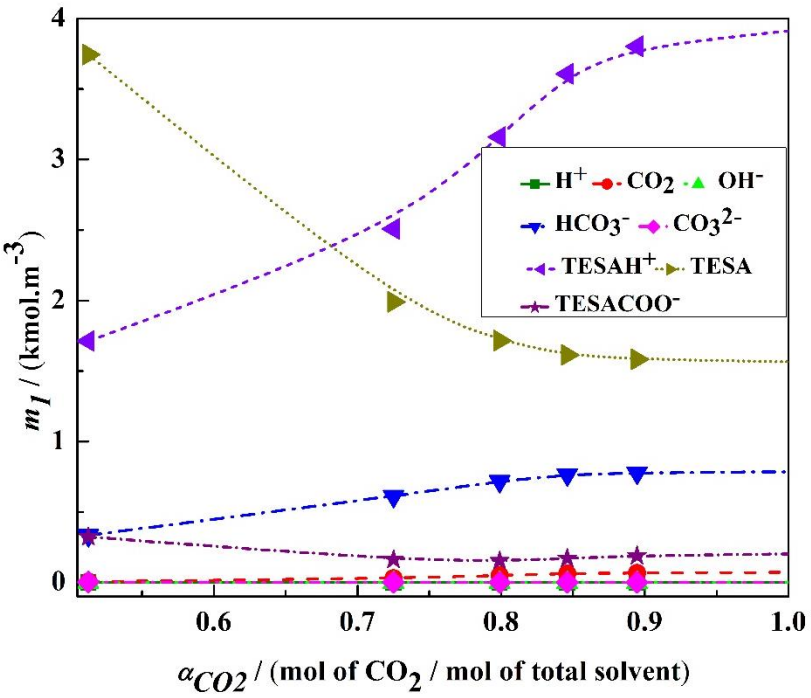

Figure 4.11 Model predicted equilibrium liquid phase concentration of various species in CO_2 loaded aq. (TESA) (1.506 m) solution at temperature T= 303.2 K

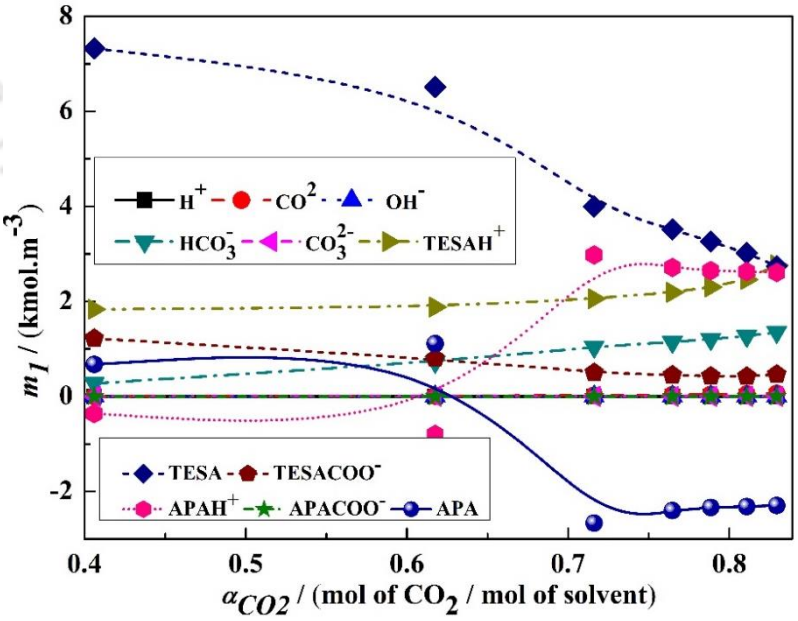

Figure 4.12 Model predicted equilibrium liquid phase concentration of various species in CO_2 loaded aq. (2.528 m TESA + 0.499 m APA) solution at temperature T= 303.2 K

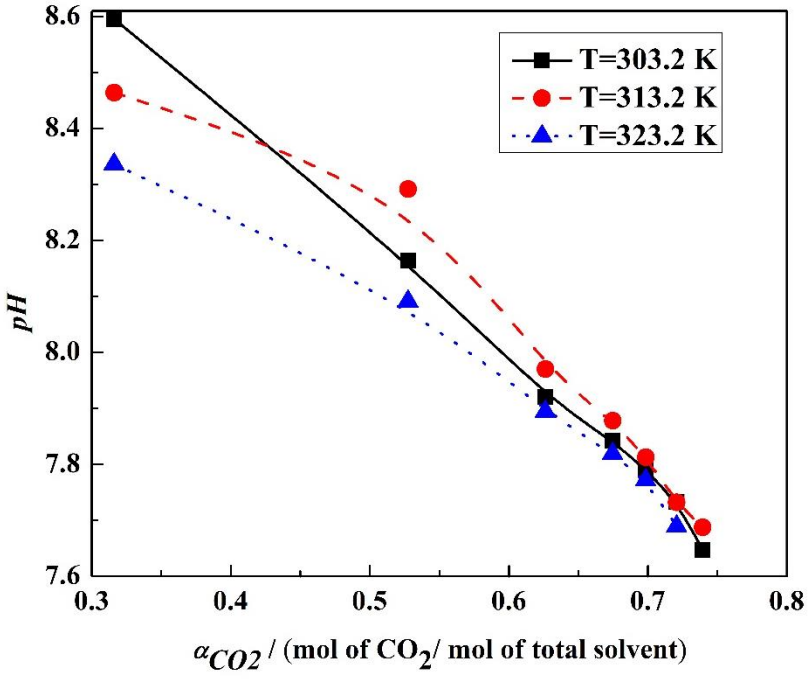

Figure 4.13 Modified KE predicted pH as a function of CO_2 loading in aq. (2.528 m TESA + 0. 499 m APA) solution

4.5.4 Comparison of solubility with other conventional single and blended amines

The competence of the studied solvents with literature is been represented in Figures 4.14-4.17. Due to the limitations of the available literature over the concentration range studied, the nearest available literature is being considered. Single aqueous amines are being compared with the performance of 2.432 *m* aq. TESA≈35 wt. *%* in Figure 4.14. At elevated P_{CO2}, the performance of aq. TESA is better than 30 wt *%* aq. MEA [37], 30 wt *%* aq. DEA [38], Methyl 4-morpholine (2.5 M) [39] , Pyridine (2.5) M [39], 25 wt *%* aq. sodium glycinate solution [40]. The higher values of α_{CO2} can be the results of development of unstable carbamates formed during the reaction between CO_2 and TESA in presence of water. Further, these carbamates may go through a hydrolysis reaction to structure free amine molecules and bicarbonate ions which results in amplification of α_{CO2} subsequently. In addition to this, the formation of reversible ionic liquid in TESA also leads to rise in CO_2 loading in comparison with MEA. The data of CO_2 solubility in literature solvents

is done at a higher concentration range of solvents. So, in general, it can be concluded that while increasing the concentration of TESA and AEP/APA shall significantly improve the CO_2 solubility while forming reversible ILs. For instance, as indicated in Figures 4.15-4.16 while using aqueous blends of AMP [41, 43], MDEA [15, 43], MEA [42, 43], and their blends with aq. K_2CO_3 [43] at higher solvent concentration, keeping AEP/APA concentration nearly same, increasing the concentration of TESA might have resulted in high CO_2 equilibrium loading. Additionally, when comparing the aq. ([bmim] [Ac] + AEP/APA)) [17] results pertaining to CO_2 solubility with aq. (TESA + AEP/APA) systems over the same concentration range, CO_2 solubility was found to be highest for aq. (TESA + APA) system (Figure 4.17).

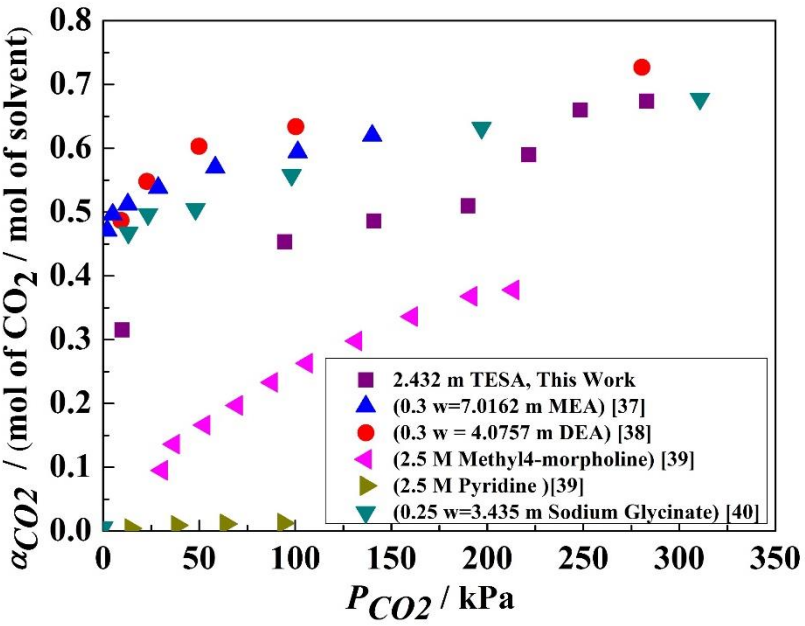

Figure 4.14 Comparison of CO_2 solubility in aq. 2.432 *m* TESA with literature at 313.2 K

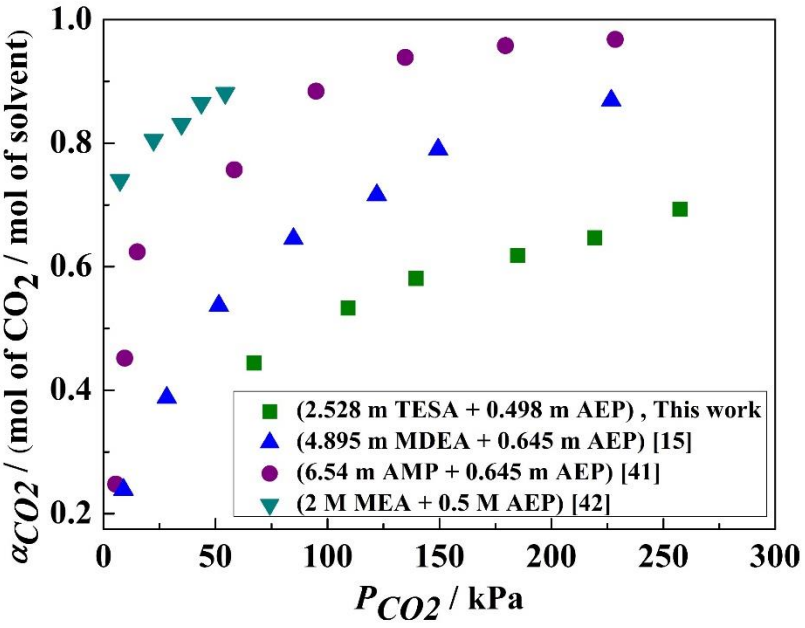

Figure 4.15 Comparison of CO_2 solubility in aq. (2.528 *m* TESA + 0.498 *m* AEP) with literature at 303. 2 K

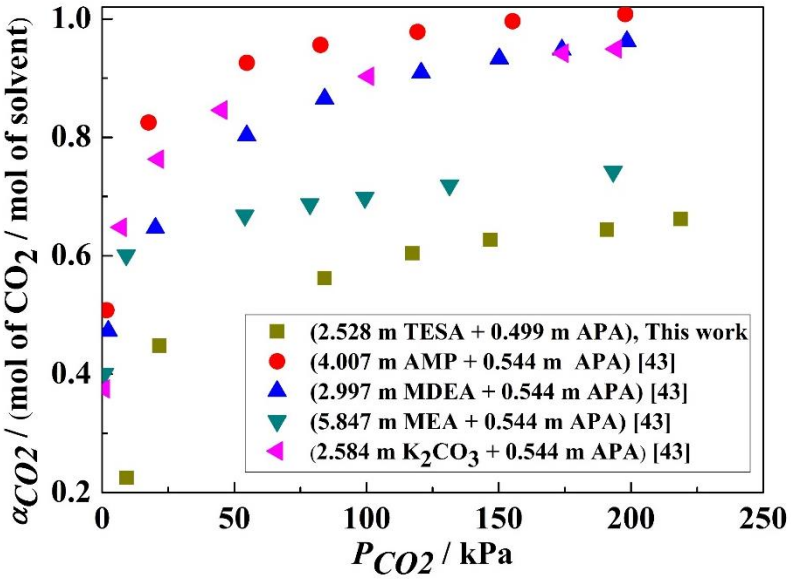

Figure 4.16 Comparison of CO_2 solubility in aq. (2.528 *m* TESA + 0.499 *m* APA) with literature at 313.2 K

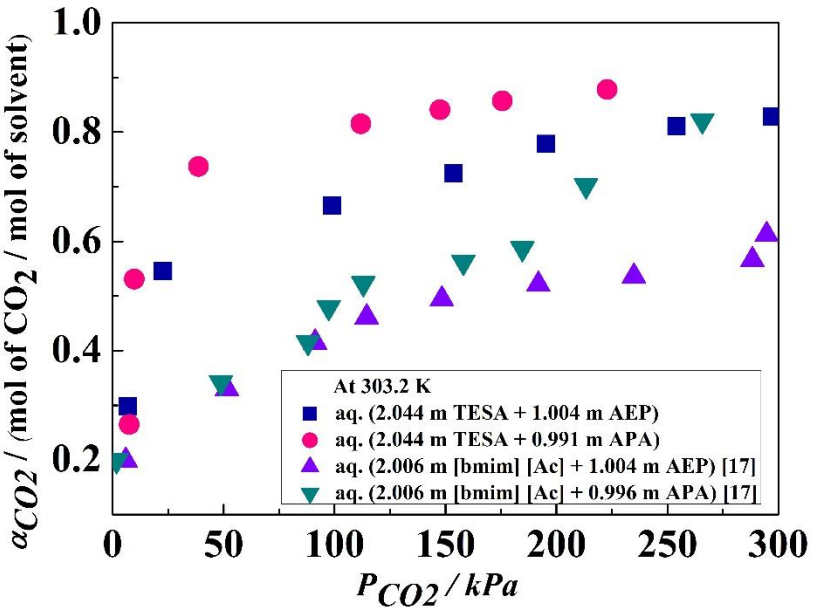

Figure 4.17 Comparison of CO_2 solubility in aq. (TESA + AEP/APA) ca. (2 + 1) *m* with aq. ([bmim][Ac] + AEP/APA) ca. (2 + 1) *m* at 303.2 K

4.6 Conclusions

CO_2 solubility in aqueous based reversible ILs enhanced by various amine activators viz. AEP and APA were studied over a wide range of experimental conditions. The formation of ILs during reaction is confirmed by ^{13}C NMR of the loaded solvents. FTIR analysis of loaded and unloaded solvents emphasizes on formation of various bonds while TESA/AEP/APA reacts with CO_2. Additionally, the analysis confirms the formation of various carbamate, bicarbonate, and protonated ions formation during the reaction of CO_2 with TESA and AEP/APA. The experimental results clearly indicate that CO_2 solubility increases with respect to rise in both partial pressure of CO_2 and concentrations of activators in solvent blends. Further quantifying the results signifies that inclusion of ≈0.5 m AEP/APA to 2.432 *m* aq. TESA intensified the CO_2 solubility by 17 and 50 %, respectively at 303.2 K. This indicates that APA is a better activator compared to AEP. Modified KE model inclusive of gas phase non-ideality has been developed to correlate the CO_2

VLE data. The equilibrium constants associated with various reactions functional of P_{CO2}, solvent concentration, and temperature of absorption has been estimated using nonlinear-regression analysis. The efficient prediction capability of modified KE model can be inferred through the calculated % AAD which are 12.94, 13.21, and 16.21 %, for aq. TESA, aq. (TESA + AEP) and aq. (TESA + APA) respectively. The speciation and pH data functional of CO_2 loading has been estimated by means of modified KE model. A non-linear statistical model is proposed for correlating α_{CO2} with various reaction parameters and was found to have good competency. A comparison of the performance of activated TESA with activated [bmim] [Ac] yielded that the former is having better CO_2 absorption capacity. Hence, an assessment of CO_2 solubility data with literature suggests that the considered solvents have very good potential for post-combustion CO_2 capture.

References

[1]A. Ahmady, M. A. Hashim, M. K. Aroua. Absorption of carbon dioxide in the aqueous mixture of methyldiethanolamine with three types of imidazolium-based ionic liquids. Fluid Phase Equilibria 309 (2011) 76-82.

[2]S. Kumar, J. H. Cho, I. Moon. Ionic liquid-amine blends and CO_2BOLs: prospective solvents for natural gas sweetening and CO_2 capture technology- a review. International Journal of Greenhouse Gas Control 20 (2014) 87–116.

[3]V. Blasucci, R. Hart, V. L. Mestre, D. J. Hahne, M. Burlager, H. Huttenhower, B. J. R. Thio, P. Pollet, C. L. Liotta, C. A. Eckert. Single component, reversible ionic liquids for energy applications. Fuel 89 (2010) 1315-1319.

[4]M. G. Miquel, M. Talreja, A. L. Ethier, K. Flack, J. R. Switzer, E. J. Biddinger, P. Pollet, J. Palomar, F. Rodriguez, C. A. Eckert, C. L. Liotta. COSMO-RS studies: structure-property relationships for CO_2 capture by reversible ionic liquids. Industrial and Engineering chemistry research 51 (2012) 16066-16073.

[5]Z. Z. Yang, Y. N. Zhao, L. N. He. CO_2 chemistry: task specific ionic liquids for CO_2 capture/activation and subsequent conversion. RSC Advances 1 (2011) 545-567.

[6]S. Lian, C. Song, Q. Liu, E. Duan, H. Ren, Y. Kitamura. Recent advances in ionic liquids-based hybrid processes for CO_2 capture and utilization. Journal of Environmental Sciences 99 (2021) 281-295.

[7]M. Afkhamipour, M. Mofarahi, A. Rezaei, R. Mahmoodi, C.H. Lee. Experimental and theoretical investigation of equilibrium absorption performance of CO_2 using a mixed 1-dimethylamino-2-propanol (1DMA2P) and monoethanolamine (MEA) solution. Fuel 256 (2019) 115877.

[8]A. Schaffer, K. Brechtel, G. Scheffknecht, Comparative study on differently concentrated aqueous solutions of MEA and TETA for CO_2 capture from flue gases. Fuel 101 (2012) 148-153.

[9]H. Zhou, X. Xu, X. Chen, G. Yu. Novel ionic liquids phase change solvents for CO_2 capture. International Journal of Greenhouse Gas Control 98 (2020) 103068.

[10]M. S. R. Shahrom, C. D. Wilfred, A. K. Z. Taha. CO_2 capture by task specific ionic liquids (TSILs) and polymerized ionic liquids (PILs and AAPILs). Journal of Molecular Liquids 219 (2016) 306-312.

[11]C. H. Huang, W. Klinthong, C. S. Tan. SBA-15 grafted with 3-aminopropyl triethoxysilane in supercritical propane for CO_2 capture. Journal of Supercritical Fluids 77 (2013) 117– 126.

[12]W. Klinthong, C. H. Huang, C. S. Tan. CO_2 capture by mesoporous SBA-15 grafted with 3-aminopropyl triethoxysilane in supercritical propane. Energy Procedia 37 (2013) 175 – 179.

[13]M. Garip, N. Gizli. Ionic liquid containing amine-based silica aerogels for CO_2 capture by fixed bed adsorption. Journal of Molecular Liquids 310 (2020) 113227.

[14] S. K. Dash, S. S. Bandyopadhyay. Studies on the effect of addition of piperazine and sulfolane into aqueous solution of *N*-methyldiethanolamine for CO_2 capture and VLE modelling using e-NRTL equation. International Journal of Greenhouse Gas Control 44 (2016) 227-237.

[15] A. Dey, S. K. Dash, B. P. Mandal. Equilibrium CO_2 solubility and thermophysical properties of aqueous blends of 1-(2-aminoethyl) piperazine and *N*-methyldiethanolamine. Fluid Phase Equilibria 463 (2018) 91-105.

[16] B. Das, B. Deogam, B. P. Mandal. Absorption of CO_2 into novel aqueous bis (3-aminopropyl) amine and enhancement of CO_2 absorption into its blends with *N*-methyldiethanolamine. International Journal of Greenhouse Gas Control 60 (2017) 172-185.

[17] S. Balchandani, B.P. Mandal, S. Dharaskar. Measurements and modeling of vapor liquid equilibrium of CO_2 in amine activated imidazolium ionic liquid solvents. Fluid Phase Equilibria 521 (2020) 112643.

[18] A. Dey, S. K. Dash, S. C. Balchandani, B. P. Mandal. Investigation on the inclusion of 1-(2-aminoethyl) piperazine as a promoter on the equilibrium CO_2 solubility of aqueous 2-amino-2-methyl-1-propanol. Journal of Molecular Liquids 289 (2019) 111036.

[19]S. C. Balchandani, B. P. Mandal, S. Dharaskar. Stimulation of CO_2 solubility in reversible ionic liquids activated by novel 1-(2-aminoethyl piperazine) and bis (3-aminopropryl amine). Separation and Purification Technology (https://doi.org/10.1016/j.seppur.2020.118260).

[20]S. Balchandani, R. Singh. Thermodynamic analysis using COSMO-RS studies of reversible ionic liquid 3-aminopropyl triethoxysilane blended with amine activators for CO_2 absorption. Journal of Molecular Liquids (2020) 114713. (https://doi.org/10.1016/j.molliq.2020.114713)

[21]Y. Du, G. T. Rochelle. Thermodynamic modeling of aqueous piperazine / *N*-(2-aminoethyl) piperazine for CO_2 capture. Energy Procedia 63 (2014) 997-1017.

[22]B. Das, B. Deogam, B. P. Mandal. Experimental and theoretical studies on efficient carbon dioxide capture using novel bis (3-aminopropyl) amine (APA)-activated aqueous 2-amino-2-methyl-1-propanol (AMP) solutions. RSC Advances 7 (2017) 21518–21530.

[23]C. A. Eckert, C. L. Liotta, Reversible ionic liquids as double-action solvents for efficient CO_2 capture (technical report), Georgia Tech Research Corporation, Atlanta, 2011.

[24]C. Sun, P. K. Dutta. Infrared spectroscopic study of reaction of carbon dioxide with aqueous monoethanolamine solutions. Industrial and Engineering Chemistry Research 55 (22) (2016) 6276-6283.

[25]G. Richner, G. Puxty. Assessing the chemical speciation during CO_2 absorption by aqueous amines using in situ FTIR. Industrial and Engineering Chemistry Research 51 (2012) 14317-14324.

[26]R. Haghbakhsh, H. Soleymani, S. Raeissi. A simple correlation to predict high pressure solubility of carbon dioxide in 27 commonly used ionic liquids. Journal of Supercritical Fluids 77 (2013) 158-166.

[27]S. Kumar, R. Padhan, M. K. Mondal. Equilibrium solubility measurement and modeling of CO_2 absorption in aqueous blend of 2-(diethyl amino) ethanol and ethylenediamine. Journal of Chemical and Engineering Data 65 (2020) 523-531.

[28]S. Paul, A. K. Ghoshal, B. P. Mandal. Kinetics of absorption of carbon dioxide into aqueous blends of 2-(1-piperazinyl)-ethylamine and N-methyldiethanolamine Chemical Engineering Science 64 (2009) 1618–1622.

[29]J. Choi, Y. Kim, S. Nam, S. Yun, Y. Yoon, J. Lee. CO_2 absorption characteristics of a piperazine derivative with primary, secondary, and tertiary amino groups. Korean Journal of Chemical Engineering 33 (2016) 3222-3230.

[30]S. M. Hong, S. H. Kim, K. B. Lee. Adsorption of carbon dioxide on 3-aminopropyl-triethoxysilane modified graphite oxide. *Energy and Fuels* 27 (6) (2013) 3358–3363.

[31]D. V. Quang, T. A. Hatton, M. R. M. A. Zahra. Thermally stable amine-grafted adsorbent prepared by impregnating 3-aminopropyltriethoxysilane on mesoporous silica for CO_2 capture. Industrial and Engineering Chemistry Research 55 (2016) 7842−7852.

[32]J. S. Torrecilla, J. Palomar, J. Garcia, E. Rojo, F. Rodriguez. Modelling of carbon dioxide solubility in ionic liquids at sub and supercritical conditions by neural networks and mathematical regression. Chemometrics and Intelligent Laboratory Systems 93 (2008) 149-159.

[33]F. Xu, H. Gao, H. Dong, Z. Wang, X. Zhang, B. Ren, S. Zhang. Solubility of CO_2 in aqueous mixtures of monoethanolamine and dicyanamide-based ionic liquids. Fluid Phase Equilibria 365 (2014) 80-87.

[34]G. Jing, L. Zhou, Z. Zhou. Characterization and kinetics of carbon dioxide absorption into aqueous tetramethylammonium glycinate solution. Chemical Engineering Journal 181– 182 (2012) 85–92.

[35]Z. Feng, F. C. Gang, W. Y. Ting, W. Y. Tao, L. A. Min, Z. Z. Bing. Absorption of CO_2 in the aqueous solutions of functionalized ionic liquids and MDEA. Chemical Engineering Journal 160 (2010) 691–697.

[36]A. F. Portugal, P. W. J. Derks, G. F. Versteeg, F. D. Magalhães, A. Mendes. Characterization of potassium glycinate for carbon dioxide absorption purposes. Chemical Engineering Science 62 (2007) 6534–6547.

[37]K. P. Shen, M. H. Li. Solubility of carbon Dioxide in aqueous mixtures of Monoethanolamine with Methyldiethanolamine. Journal of Chemical and Engineering Data 37 (1992) 96–100.

[38]D. J. Seo, W. H. Hong. Solubilities of carbon dioxide in aqueous mixtures of diethanolamine and 2-amino-2-methyl-1-propanol. Journal of Chemical and Engineering Data 41 (1996) 258-260.

[39]A. Nouacer, F. B. Belaribi, I. Mokbel, J. Jose. Solubility of carbon dioxide gas in some 2.5 M tertiary amine aqueous solutions. Journal of Molecular Liquids 190 (2014) 68-73.

[40]B. K. Mondal, S. S. Bandyopadhyay, A. N. Samanta. VLE of CO_2 in aqueous sodium glycinate solution-new data and modeling using kent-eisenberg model. International Journal of Greenhouse Gas Control 36 (2015) 153-160.

[41]A. Dey, S. K. Dash, S. C. Balchandani, B. P. Mandal. Investigation on the inclusion of 1-(2-aminoethyl) piperazine as a promoter on the equilibrium CO_2 solubility of aqueous 2-amino-2-methyl-1-propanol. Journal of Molecular Liquids 289 (2019) 111036.

[42]R. Ramazani, S. Mazinani, A. Hafizi, A. Jahanmiri. Equilibrium solubility of carbon dioxide in aqueous blend of monoethanolamine (MEA) and 2-1-piperazinyl-ethylamine (PZEA) solutions: experimental and optimization study. Process Safety and Environmental Protection 98 (2015) 325-332.

[43]B. K. Mondal, S. S. Bandyopadhyay, A. N. Samanta. Equilibrium solubility and enthalpy of CO_2 absorption in aqueous bis (3-aminopropyl) amine and its mixture with MEA, MDEA, AMP and K_2CO_3. Chemical Engineering Science 170 (2017) 58-67.

Chapter 5

ANALYSIS OF 2-METHYL PIPERAZINE AS AN ACTIVATOR FOR CO_2 ABSORPTION IN MDEA, $TMSO_2$ AND [BMIM] [AC]

This chapter proposes the ability of 2-methyl piperazine as an enhancer for CO_2 solubility in aqueous tertiary amine (MDEA), physical solvent ($TMSO_2$), and ionic liquid ([bmim] [Ac]). A comprehensive experimental and modeling analysis on the equilibrium solubility of CO_2 over a broad range of temperature and pressure is carried out. The CO_2 solubility data were co-related using modified Kent-Eisenberg equilibrium model including the gas phase non-ideality. Along with this, qualitative ^{13}C NMR and FTIR analysis have been also performed to assess the chemistry of 2-methyl piperazine. Furthermore, CO_2 cyclic capacity and heat of absorption have been also evaluated from the obtained experimental VLE data.

5.1 Introduction

The importance of amine activators has been discussed in the previous chapters. The increase in CO_2 solubility in various solvents by addition of amine activators such as APA, HMDEA, TETA, etc. has been reported in the literature [1-3]. In the present chapter, one of the PZ-derived activator, 2-methyl piperazine (2-MPZ) is explored for CO_2 absorption. The structural analysis of 2-MPZ indicates that it consists of two primary amino group which are less shielded by the alkyl group and hence it may result in an increase in CO_2 solubility. Brief literature of 2-MPZ and the possible base solvents i.e. MDEA, $TMSO_2$, and [bmim] [Ac] has been discussed subsequently.

The performance of CO_2 loading in potassium carbonate while increasing the amine additives such as 2-MPZ, potassium sarcosinate, and potassium lysinate have been considered in the literature. It was observed that the inclusion of 2-MPZ and potassium lysinate has an affirmative influence on the CO_2 solubility [4]. Nevertheless, the temperature (313.15 K) and pressure range (0 to 50 kPa) were quite narrow in comparison to the horizon of CO_2 absorption applications. The highest CO_2 loading found at 50 kPa with a molar fraction of 0.4 of 2-MPZ in K_2CO_3 was evaluated to be 0.89.

The simulation analysis of CO_2 absorption in aqueous activator blends of PZ/2-MPZ for varying concentrations have also been reported over a wide range of temperature and pressure using Aspen Plus^{TM}. The blends were investigated for CO_2 solubility where the meticulous analysis of the speciation, kinetic parameters, and heat of absorption were evaluated using e-NRTL model [5]. The highest CO_2 loading capacity for 4 *m* PZ + 4 *m* 2-MPZ was concluded to be 0.84 mol of CO_2 / (kg amine + H_2O), which is reasonably competitive with the traditionally used aqueous amines. Similar studies of PZ/2-MPZ have also been reported in the literature [6-9]. The blends have been considered for a major disadvantage of precipitation at lower temperatures of piperazine and higher absorption rates and cyclic capacity offered by 2-MPZ. The selection of optimum concentration ratio of PZ/-2MPZ is also a huge concern since the increase in the concentration of 2-MPZ increases the viscosity of the overall system thereby decreases the CO_2 solubility due to lower diffusion. 2-MPZ and PZ have also been investigated as a promoter for K_2CO_3 over a wide range of temperature and CO_2 partial pressures and concluded that (15 wt % K_2CO_3 + 10 wt % 2-MPZ + 10 wt % PZ) at 313.15 K has shown the highest CO_2 loading and absorption rates [10].

Pure physical solvents such as sulfolane ($TMSO_2$), *N*-methylpyrrolidone (NMP), propylene carbonate (PC), etc. and their aqueous solvents have also been studied over years owing to the advantage of extremely low vapor pressure leading to low energy requirement in the regeneration step for acid gas separation systems [11-13]**.** But due to the low equilibrium CO_2 solubility, and requirement of high pressures of the input streams for effective absorption, the blended solutions of physical solvents with amines have been studied and reported in the literature [14]. The thermodynamic analysis of simultaneous removal of mercaptans and CO_2 using aq. ($TMSO_2$ + DIPA) and aq. ($TMSO_2$ + MDEA) using PC-SAFT and e-NTRL models have also been reported [15]. The results indicated that the solvents studied are found to be better than aqueous sulfolane solutions. The effect of increase in PZ concentration to the blends of aq. (MDEA + $TMSO_2$) with composition (42 wt % MDEA + 8 wt % PZ + 10 wt % Sulfolane) has been indicated a highest CO_2 solubility of α_{CO2}=1.212 mol of CO_2 / mol of (MDEA + PZ) at 303.15 K and 1236.604 kPa [16], which is quite competitive of the traditionally used primary and secondary amines with PZ.

Recently, the simultaneous removal of CO_2 and ethyl mercaptans is also reported [17] using aq. (MDEA + $TMSO_2$) solutions. The experimental results inferred that with increment in MDEA concentration from 30 to 40 % at a constant total concentration of the solvent and temperature of

328.15 K, there was a rise in CO_2 solubility of about 28.30 %. Biphasic solvent mixtures of H_2O, diethylenetriamine (DETA) and $TMSO_2$ have also been proved to be competitive to similar compositions of MDEA, $TMSO_2$, and H_2O with similar experimental conditions with respect to CO_2 solubility and kinetics of the systems [18, 19]. Although, a general conclusion states that most of the carbamate, dicarbamate, tricarbamate, etc. are formed due to the amine phase rather than $TMSO_2$ phase.

In addition, another category of solvents that have been extensively studied over the past few decades is ionic liquids owing to the better solvent properties they offer in comparison to amines. On the other hand, ILs also tend to exhibit lower CO_2 absorption. Hence, blends of amines or amine activators with ILs may prove to increase the efficiency of CO_2 absorption/desorption process [20, 21]. Imidazolium based ILs are well established in the literature [22-26] proving them to be more cost-competitive and higher CO_2 absorption in comparison to phosphonium or pyridinium based ILs. 1-Butyl-3-methyl imidazolium acetate activated by amine activators 1-(2-aminoethyl) piperazine (AEP) and bis (3-aminopropyl) amine (APA) is also one of the promising solvents for CO_2 capture which was earlier reported by our group [27] and the same has been discussed in **Chapter-4**.

Conclusively, aqueous blends of MDEA, $TMSO_2$, [bmim][Ac] i.e. tertiary amine, physical solvent, and ionic liquid with 2-MPZ (amine activator) have been envisioned and studied in order to realize the effect of 2-MPZ on CO_2 equilibrium solubility along with variation in temperature and partial pressure of CO_2 (P_{CO2}). The concentration of the chemicals involved has been chosen rationally in order to get the desired optimum results. Subsequently, the vapor liquid equilibrium data has also been correlated using the Kent-Eisenberg model for CO_2 solubility in aq. (MDEA + 2-MPZ), aq. ($TMSO_2$ + 2-MPZ) and aq. ([bmim] [Ac] + 2-MPZ). The temperature, pressure, and concentration range (activator 2-MPZ) of study are (303.2-323.2) K, (0-380) kPa and ≈ (0.5-1.5) $mol.kg^{-1}$. The efficiency of the selected solvents was also theoretically analyzed by our research group through COSMO-RS studies and is reported elsewhere [28].

5.2 Experimental section

5.2.1 Materials

CO_2 gas (> 99 % pure) was procured from Linde India Ltd. and used without further purification. 1-Butyl-3-methyl-imidazolium acetate ([bmim] [Ac], ≥95% pure), sulfolane ($TMSO_2$, 99 % pure), 2-methyl piperazine (2-MPZ, 95 %) and *N*-methyldiethanolamine (MDEA, ≥99 % pure) were purchased from Sigma–Aldrich. $TMSO_2$, 2-MPZ, and MDEA were used with no auxiliary refinement for the CO_2 solubility study. For solution preparation, the [bmim] [Ac] was first analyzed for its initial water content by Karl-fisher method which was found to be 1.7%. Then the solvent was vacuum dried for 48 h and analyzed again for water content which was now only 0.04%. The solvent systems were prepared using double distilled deionized water. Specification details of the chemicals used under the study are given in Table 5.1.

Table 5.1 Specifications of the chemicals used in the present work

Chemical name	Chemical formula	Molecular weight	Source	Stated mass fraction purity	CAS no.	Purification method
1-butyl-3-methyl-imidazolium acetate ([bmim][Ac])	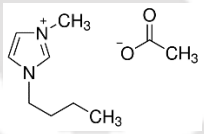	198.26	Sigma Aldrich Co.	≥0.95	284049-75-8	Vacuum drying for 48 hrs
N-Methyldiethanolamine (MDEA)	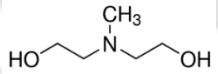	119.16	Sigma Aldrich Co.	≥0.99	105-59-9	None
2-Methyl Piperazine (2-MPZ)	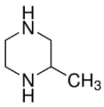	100.16	Sigma Aldrich Co.	0.95	109-07-9	None
Sulfolane ($TMSO_2$)	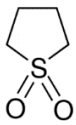	120.17	Sigma Aldrich Co.	0.99	126-33-0	None
Carbon dioxide (CO_2)	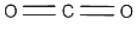	44.01	Linde India Ltd.	>0.99	-	None

5.2.2 Experimental methodology

5.2.2.1 Vapour liquid equilibrium (VLE) measurement

The experimental set-up described in **Chapter-3** has been used for vapor-liquid equilibrium measurements. The details of the experimental setup and the procedure have been reported in our previous chapter and also reported elsewhere [27, 29].

5.2.2.2 FTIR-ATR and ^{13}C NMR study

The particulars of the instruments used for FTIR and ^{13}C NMR analysis has been discussed in **Chapter-3** in detail.

5.3 Proposed chemical reaction

The structural analysis of various bond formations or intermediate formations has been studied through FTIR and ^{13}C NMR examination of unloaded and CO_2 loaded solvents. The ^{13}C NMR analysis of the studied aq. (MDEA + 2-MPZ) solvent is presented in Figure 5.1. Majority of the new peaks formed due to CO_2 loading were observed in the upfield of ^{13}C NMR spectra. The peaks at (16.76- 43.13) associated with the several CH_2 groups of intermediate reactive species are corresponding to MDEA. Whereas, on the other hand, peaks at (47.60-57.61) correspond to various mono and secondary carbamates formed in the system due to the presence of 2-MPZ [30, 31]. Figure 5.2 represents the FTIR-ATR analysis of aq. (MDEA + 2-MPZ) system under unloaded and CO_2 loading conditions at 313.2 K. The characteristic peaks have been identified and apportioned as presented in Table 5.2 conclusive of which protonation of MDEA and different carbamate species formations have been inveterate.

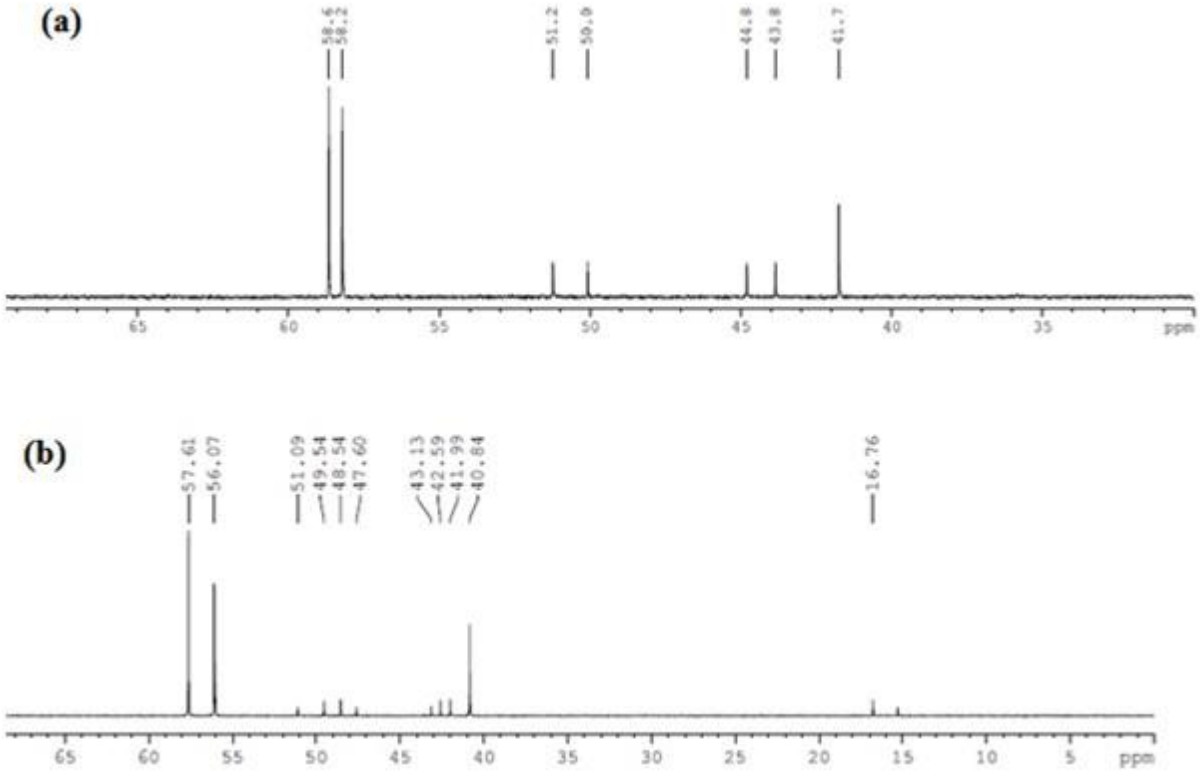

Figure 5.1 ^{13}C NMR spectra of aq. (3.017 *m* MDEA + 1.008 *m* 2-MPZ) solution (a) unloaded (b) CO_2 loaded at 313.2 K

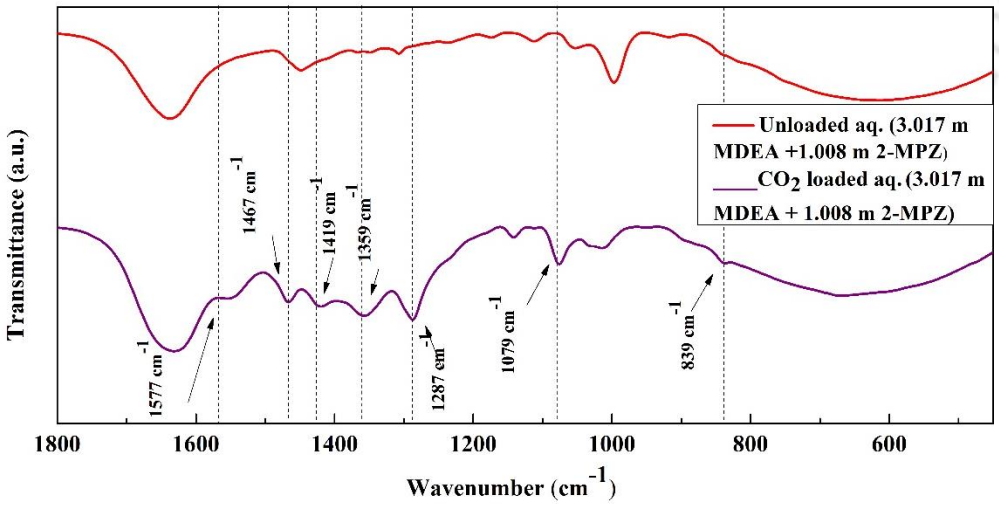

Figure 5.2 FTIR-ATR spectra of aq. (3.017 *m* MDEA + 1.008 *m* 2-MPZ) unloaded and CO_2 loaded at 313.2 K

Table 5.2 FTIR-ATR peaks and ascriptions of aq. (3.017 *m* MDEA + 1.008 *m* 2-MPZ) at 313.2 K

Sr. no.	Wave number (cm^{-1})	Attribution
1	839	C-NH_2 Twisting for 2-MPZ
2	1079	Protonation of MDEA to form $MDEAH^+$
3	1287	N-C stretching vibration of 2-MPZ carbamate
4	1359	HCO_3^-
5	1419	Asymmetric and symmetric vibrations of COO^- of 2-MPZ monocarbamate
6	1467 and 1577	Asymmetric and symmetric stretching of COO^-

For the work considered in this chapter, the liquid phase reaction consists of protonation of both MDEA and 2-MPZ amine activator, carbamate formation by 2-MPZ and [bmim] [Ac] and several other reactions of formation of bicarbonate or carbonate species. The bicarbamate formation of 2-MPZ has not been reflected for the present study since at higher $\alpha_{CO2,}$ bicarbonate is the key product of (2-MPZ-CO_2) reaction [8]. The carbamate formation for reaction between [bmim] [Ac] and CO_2 has been already reported in the literature [22, 27, 32]. Since, sulfolane is a physical solvent, it is assumed to exhibit negligible chemical interactions and only shall have weak van der Walls forces of attraction with CO_2 and other species in the system.

The equilibrium reactions for (MDEA + H_2O + CO_2 + 2-MPZ), ($TMSO_2$ + H_2O + CO_2 + 2-MPZ), and ([bmim] [Ac] + H_2O + CO_2 + 2-MPZ) systems proposed in this work and the equilibrium constants associated to each reaction are given in Table 5.3.

Table 5.3 Reaction, reaction mechanism and equilibrium constants associated with reactions in the system

Sr. no.	Description of reaction	Reaction mechanism	Equilibrium constant associated
1	Physical solubility	$CO_2(g) \overset{H_{CO2}}{\leftrightarrow} CO_2(aq)$	-
2	Dissociation of bicarbonate ion	$HCO^{3-} \overset{K_1}{\leftrightarrow} CO_3^{2-} + H^+$	$K_1 = \frac{[CO_3^{2-}][H^+]}{[HCO_3^-]}$
3	Formation of bicarbonate ion	$CO_2 + H_2O \overset{K_2}{\leftrightarrow} HCO_3^- + H^+$	$K_2 = \frac{[HCO_3^-][H^+]}{[CO_2]}$
4	Dissociation of water	$H_2O \overset{K_3}{\leftrightarrow} OH^- + H^+$	$K_3 = [H^+][OH^-]$
5	Deprotonation of 2-MPZ	$2-MPZH^+ \overset{K_4}{\leftrightarrow} 2-MPZ + H^+$	$K_4 = \frac{[2-MPZ][H^+]}{[2-MPZH^+]}$
6	Carbamate hydrolysis of 2-MPZ	$2-MPZCOO^- + H_2O \overset{K_5}{\leftrightarrow} 2-MPZ + HCO_3^-$	$K_5 = \frac{[2-MPZ][HCO_3^-]}{[2-MPZCOO^-]}$
7	Deprotonation of [bmim] [Ac] (R_1)	$R_1^+ \overset{K_6}{\leftrightarrow} R_1 + H^+$	$K_6 = \frac{[R_1][H^+]}{[R_1^+]}$
8	Carbamate hydrolysis of [bmim] [Ac] (R_1)	$R_1COO^- + H_2O \overset{K_7}{\leftrightarrow} R_1 + HCO_3^-$	$K_7 = \frac{[R_1][HCO_3^-]}{[R_1COO^-]}$
9	Deprotonation of MDEA	$MDEAH^+ \overset{K_8}{\leftrightarrow} MDEA + H^+$	$K_8 = \frac{[MDEA][H^+]}{[MDEAH^+]}$

5.4 Results and discussion

The experimental CO_2 partial pressure with respect to each loading are presented in Tables (5.4-5.12). The details of standardization of the adopted method for VLE measurement has been discussed in **Chapter 3** and **4**.

Table 5.4 Equilibrium CO_2 solubility data in aqueous (3.509 + 0.509) molal (*m*) (MDEA + 2-MPZ) solution

T / K	m_1 / mol.kg^{-1} MDEA	m_2 / mol.kg^{-1} 2-MPZ	P_{CO2} / kPa	α_{CO2}
303.2	3.509	0.509	4.3	0.189
	3.509	0.509	9.8	0.331
	3.509	0.509	21.2	0.462
	3.509	0.509	41.2	0.569
	3.509	0.509	65.1	0.644
	3.509	0.509	98.5	0.683
	3.509	0.509	119.1	0.708
	3.509	0.509	143.1	0.722
	3.509	0.509	197.3	0.749
	3.509	0.509	203.2	0.753
313.2	3.509	0.509	5.7	0.1654
	3.509	0.509	15.2	0.335
	3.509	0.509	40.3	0.459
	3.509	0.509	72.7	0.546
	3.509	0.509	90.5	0.605
	3.509	0.509	114.3	0.642
	3.509	0.509	133.7	0.671
	3.509	0.509	157.8	0.761
	3.509	0.509	199.3	0.775
323.2	3.509	0.509	6.6	0.139
	3.509	0.509	18.1	0.270
	3.509	0.509	33.8	0.376
	3.509	0.509	56.1	0.454
	3.509	0.509	73.6	0.513
	3.509	0.509	99.4	0.548
	3.509	0.509	114.2	0.578

Table 5.5 Equilibrium CO_2 solubility data in aqueous (3.017 + 1.008) molal (m) (MDEA + 2-MPZ) solution

T / K	m_1 / mol.kg^{-1} MDEA	m_2 / mol.kg^{-1} 2-MPZ	P_{CO2} / kPa	α_{CO2}
303.2	3.017	1.008	2.3	0.183
	3.017	1.008	10.1	0.345
	3.017	1.008	20.0	0.506
	3.017	1.008	44.5	0.627
	3.017	1.008	86.5	0.706
	3.017	1.008	118.8	0.737
	3.017	1.008	146.2	0.759
	3.017	1.008	183.5	0.774
	3.017	1.008	235.7	0.786
	3.017	1.008	279.9	0.873
	3.017	1.008	335.4	1.013
313.2	3.017	1.008	5.0	0.155
	3.017	1.008	11.5	0.303
	3.017	1.008	27.0	0.435
	3.017	1.008	57.9	0.534
	3.017	1.008	77.6	0.596
	3.017	1.008	99.2	0.638
	3.017	1.008	116.9	0.670
	3.017	1.008	157.4	0.760
	3.017	1.008	200.0	0.767
323.2	3.017	1.008	5.0	0.141
	3.017	1.008	15.1	0.300
	3.017	1.008	34.5	0.422
	3.017	1.008	72.0	0.494
	3.017	1.008	82.9	0.554
	3.017	1.008	104.0	0.596
	3.017	1.008	129.6	0.624
	3.017	1.008	192.9	0.672

Table 5.6 Equilibrium CO_2 solubility data in aqueous (2.502 + 1.509) molal (*m*) (MDEA + 2-MPZ) solution

T / K	m_1 / mol.kg^{-1} MDEA	m_2 / mol.kg^{-1} 2-MPZ	P_{CO2} / kPa	α_{CO2}
303.2	2.502	1.509	3.0	0.171
	2.502	1.509	6.8	0.319
	2.502	1.509	24.3	0.443
	2.502	1.509	35.9	0.553
	2.502	1.509	77.6	0.617
	2.502	1.509	108.9	0.651
	2.502	1.509	127.6	0.669
	2.502	1.509	160.3	0.679
	2.502	1.509	241.1	0.706
	2.502	1.509	251.2	0.707
313.2	2.502	1.509	3.7	0.134
	2.502	1.509	7.9	0.284
	2.502	1.509	18.5	0.422
	2.502	1.509	44.2	0.524
	2.502	1.509	69.4	0.598
	2.502	1.509	97.1	0.646
	2.502	1.509	118.1	0.671
	2.502	1.509	136.4	0.723
	2.502	1.509	149.0	0.829
	2.502	1.509	180.8	0.856
323.2	2.502	1.509	5.5	0.119
	2.502	1.509	13.2	0.249
	2.502	1.509	26.5	0.377
	2.502	1.509	50.5	0.485
	2.502	1.509	75.4	0.550
	2.502	1.509	104.4	0.585
	2.502	1.509	126.9	0.609
	2.502	1.509	157.0	0.634

Table 5.7 Equilibrium CO_2 solubility data in aqueous (3.501 + 0.509) molal (m) ($TMSO_2$ + 2-MPZ) solution

T / K	m_1 / mol.kg^{-1} $TMSO_2$	m_2 / mol.kg^{-1} 2-MPZ	P_{CO2} / kPa	α_{CO2}
303.2	3.501	0.509	62.7	0.124
	3.501	0.509	128.5	0.133
	3.501	0.509	160.7	0.141
	3.501	0.509	195.1	0.150
	3.501	0.509	252.4	0.156
	3.501	0.509	343.9	0.167
	3.501	0.509	316.3	0.285
	3.501	0.509	317.6	0.289
313.2	3.501	0.509	45.6	0.089
	3.501	0.509	123.8	0.097
	3.501	0.509	161.8	0.105
	3.501	0.509	201.9	0.112
	3.501	0.509	257.7	0.117
	3.501	0.509	302.3	0.125
	3.501	0.509	356.1	0.139
323.2	3.501	0.509	49.2	0.079
	3.501	0.509	114.0	0.084
	3.501	0.509	142.4	0.090
	3.501	0.509	168.0	0.095
	3.501	0.509	178.0	0.128
	3.501	0.509	183.8	0.151

Table 5.8 Equilibrium CO_2 solubility data in aqueous (3.012 + 1.008) molal (m) ($TMSO_2$ + 2-MPZ) solution

T / K	m_1 / mol.kg^{-1} $TMSO_2$	m_2 / mol.kg^{-1} 2-MPZ	P_{CO2} / kPa	α_{CO2}
303.2	3.012	1.008	4.9	0.167
	3.012	1.008	87.5	0.214
	3.012	1.008	130.0	0.220
	3.012	1.008	165.8	0.222
	3.012	1.008	196.5	0.226
	3.012	1.008	293.7	0.245
	3.012	1.008	303.4	0.259
313.2	3.012	1.008	9.8	0.126
	3.012	1.008	84.3	0.176
	3.012	1.008	125.7	0.183
	3.012	1.008	159.8	0.191
	3.012	1.008	200.2	0.203
	3.012	1.008	235.7	0.211
	3.012	1.008	299.2	0.240
323.2	3.012	1.008	21.5	0.144
	3.012	1.008	78.7	0.205
	3.012	1.008	123.4	0.224
	3.012	1.008	171.9	0.232
	3.012	1.008	223.3	0.231
	3.012	1.008	246.6	0.235

Table 5.9 Equilibrium CO_2 solubility data in aqueous (2.500 + 1.509) molal (m) ($TMSO_2$ + 2-MPZ) solution

T / K	m_1 / mol.kg^{-1} $TMSO_2$	m_2 / mol.kg^{-1} 2-MPZ	P_{CO2} / kPa	α_{CO2}
303.2	2.500	1.509	2.0	0.161
	2.500	1.509	36.7	0.281
	2.500	1.509	113.8	0.302
	2.500	1.509	138.7	0.306
	2.500	1.509	167.0	0.312
	2.500	1.509	200.3	0.313
	2.500	1.509	238.6	0.315
	2.500	1.509	280.6	0.369
	2.500	1.509	316.3	0.399
313.2	2.500	1.509	3.8	0.149
	2.500	1.509	38.9	0.262
	2.500	1.509	105.8	0.293
	2.500	1.509	157.8	0.305
	2.500	1.509	187.6	0.313
	2.500	1.509	207.2	0.324
	2.500	1.509	249.9	0.334
323.2	2.500	1.509	3.9	0.131
	2.500	1.509	18.6	0.249
	2.500	1.509	89.4	0.287
	2.500	1.509	117.1	0.295
	2.500	1.509	147.7	0.296
	2.500	1.509	172.1	0.293

Table 5.10 Equilibrium CO_2 solubility data in aqueous (3.507 + 0.509) molal (*m*) ([bmim] [Ac] + 2-MPZ) solution

T / K	m_1 / mol.kg^{-1} [bmim][Ac]	m_2 / mol.kg^{-1} 2-MPZ	P_{CO2} / kPa	α_{CO2}
	3.507	0.509	64.4	0.085
	3.507	0.509	114.9	0.105
	3.507	0.509	149.9	0.113
303.2	3.507	0.509	197.3	0.118
	3.507	0.509	235.9	0.125
	3.507	0.509	300.2	0.148
	3.507	0.509	313.0	0.176
	3.507	0.509	87.6	0.056
	3.507	0.509	121.0	0.086
	3.507	0.509	178.5	0.093
313.2	3.507	0.509	221.7	0.104
	3.507	0.509	254.0	0.122
	3.507	0.509	293.3	0.142
	3.507	0.509	318.5	0.191
	3.507	0.509	62.7	0.047
	3.507	0.509	98.2	0.072
	3.507	0.509	121.1	0.073
323.2	3.507	0.509	153.0	0.077
	3.507	0.509	180.2	0.082
	3.507	0.509	205.5	0.086
	3.507	0.509	247.7	0.092

Table 5.11 Equilibrium CO_2 solubility data in aqueous (3.002 + 1.008) molal (*m*) ([bmim] [Ac] + 2-MPZ) solution

T / K	m_1 / mol.kg^{-1} [bmim][Ac]	m_2 / mol.kg^{-1} 2-MPZ	P_{CO2} / kPa	α_{CO2}
303.2	3.002	1.008	22.2	0.144
	3.002	1.008	104.8	0.178
	3.002	1.008	128.1	0.187
	3.002	1.008	163.9	0.191
	3.002	1.008	202.8	0.199
	3.002	1.008	247.5	0.205
	3.002	1.008	269.8	0.288
	3.002	1.008	317.4	0.254
313.2	3.002	1.008	35.7	0.113
	3.002	1.008	99.1	0.158
	3.002	1.008	144.9	0.180
	3.002	1.008	192.4	0.187
	3.002	1.008	248.7	0.191
	3.002	1.008	302.5	0.197
	3.002	1.008	326.1	0.268
	3.002	1.008	370.1	0.299
323.2	3.002	1.008	23.0	0.107
	3.002	1.008	87.6	0.150
	3.002	1.008	129.1	0.160
	3.002	1.008	176.2	0.169
	3.002	1.008	213.7	0.174
	3.002	1.008	255.7	0.183

Table 5.12 Equilibrium CO_2 solubility data in aqueous (2.510 + 1.509) molal (*m*) ([bmim] [Ac] + 2-MPZ) solution

T / K	m_1 / mol.kg^{-1} [bmim][Ac]	m_2 / mol.kg^{-1} 2-MPZ	P_{CO2} / kPa	α_{CO2}
303.2	2.510	1.509	3.5	0.183
	2.510	1.509	68.1	0.273
	2.510	1.509	126.2	0.283
	2.510	1.509	162.7	0.291
	2.510	1.509	208.2	0.297
	2.510	1.509	243.3	0.303
	2.510	1.509	262.2	0.372
	2.510	1.509	301.3	0.363
313.2	2.510	1.509	4.6	0.152
	2.510	1.509	83.7	0.219
	2.510	1.509	104.2	0.253
	2.510	1.509	125.4	0.270
	2.510	1.509	156.4	0.276
	2.510	1.509	193.9	0.284
	2.510	1.509	222.8	0.356
323.2	2.510	1.509	5.0	0.122
	2.510	1.509	59.71	0.194
	2.510	1.509	98.1	0.225
	2.510	1.5	132.7	0.244
	2.510	1.5	148.9	0.275
	2.510	1.5	157.4	0.328

5.4.1 Co-relation using modified KE model

The experimental VLE data has been correlated using modified KE model. In this work, equilibrium constants K_4, K_5, K_6, and K_7 which correspond to the deprotonation and carbamate hydrolysis reactions of 2-MPZ and [bmim] [Ac], respectively, are estimated. The equilibrium constants which are function of P_{CO2}, *T* and solvent concentration are evaluated using non-linear regression analysis in MATLAB17® as discussed in earlier **Chapters 3** & **4**. The evaluated

equilibrium constants (K_4, K_5, K_6, *and* K_7) in terms of concentration of solvents, T, and P_{CO2} can be expressed as follows:

$$K_4\left(or/K_6\right)=g+\left(h\times M\right)+\left(k\times T\right)+\left(l\times M\times T\right)+\left(n\times T^2\right)+\left(p\times P_{CO_2}\right)+\left(q\times P_{CO_2}^2\right) \quad (5.1)$$

$$K_5\left(or/K_7\right)=g+\left(h\times M\right)+\left(k\times T\right)+\left(l\times M^2\right)+\left(n\times M\times T\right)+\left(p\times T^2\right)+\left(q\times P_{CO2}\right)+\left(r\times P_{CO_2}^2\right) \quad (5.2)$$

Where, g, h, k, l, n, p, q, and r, are coefficients associated with equilibrium constants and are calculated using optimization. The calculated values of equilibrium constants are given in Table 5.13. The equilibrium constants obtained through the KE model were in turn used to predict α_{CO2}. The calculated % AAD for aq. (MDEA + 2-MPZ), aq. ([bmim] [Ac] + 2-MPZ), and aq. ($TMSO_2$ + 2-MPZ) systems are 7.56, 22.64, and 30.05, respectively. A good agreement between the experimental and predicted data is observed through the realization of residual amid the two (Figure 5.3).

Table 5.13 (a) Coefficients of the equilibrium constants estimated in the present work

System	aq. (MDEA + 2-MPZ)		aq. ([bmim][Ac] +2-MPZ)			
K_i / kmol.m^{-3}	K_4	K_5	K_4	K_5	K_6	K_7
g	-3.149×10^{-8}	3.596×10^{4}	-9.782×10^{-9}	-2.485×10^{3}	-4.318×10^{-6}	-1.591×10^{7}
h	-9.834×10^{-10}	-1.182×10^{2}	-4.436×10^{-9}	-4.826×10^{3}	-3.719×10^{-4}	-1.263×10^{5}
k	1.021×10^{-10}	2.571×10	6.745×10^{-11}	-5.974×10	1.707×10^{-7}	-2.282×10^{3}
l	6.076×10^{-12}	6.973×10^{-1}	-2.327×10^{-11}	-1.627×10^{3}	1.647×10^{-8}	-3.688×10^{6}
n	1.589×10^{-14}	3.297×10	2.612×10^{-13}	5.822	6.384×10^{-9}	-1.471×10^{4}
p	-2.657×10^{-12}	3.279×10^{-2}	1.131×10^{-10}	-5.177×10^{-2}	-8.921×10^{-9}	3.714×10^{2}
q	3.111×10^{-14}	2.562×10^{-2}	1.555×10^{-24}	9.442×10^{2}	1.369×10^{-13}	-4.276×10^{4}
r	-	-6.515×10^{-5}	-	-1.359×10^{-3}	-	-6.654×10^{-1}
% AAD	7.56		22.64			

Table 5.13 (b) Coefficients of the equilibrium constants estimated in the present work

System	aq. ($TMSO_2$ + 2-MPZ)	
K_i / kmol.m^{-3}	K_4	K_5
g	2.586×10^{-5}	-5.336×10^{4}
h	-2.399×10^{-5}	-5.784×10
k	2.492×10^{-8}	5.792×10^{3}
l	-7.333×10^{-9}	-4.464×10^{2}
n	-5.254×10^{-11}	-1.566×10
p	9.924×10^{-10}	-2.026×10
q	-3.342×10^{-13}	1.005×10^{3}
r	-	-7.646×10^{-2}
% AAD	33.05	

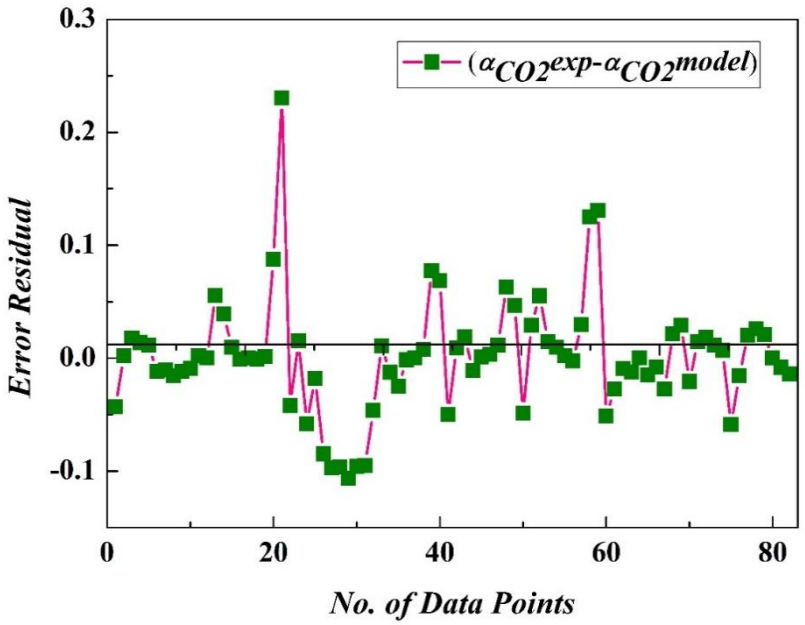

Figure 5.3 Residual plot of aq. (MDEA + 2-MPZ) system

5.4.2 Effect of reaction parameters on CO_2 solubility in studied solvents

The usual trend of reduction in solubility of CO_2 while increase in temperature is observed in the absorption using aq. (MDEA + 2-MPZ), aq. ([bmim] [Ac] + 2-MPZ), and aq. ($TMSO_2$ + 2-MPZ). This decrease in α_{CO2} is owing to the exothermic nature of reaction in proposed solvents and CO_2. With the rise in 2-MPZ activator concentration in the blend keeping the overall concentration of the solvents unchanged, an increase in CO_2 solubility is also perceived in the aqueous blends (Tables (5.4-5.12)). Also, with intensification in P_{CO2}, it is observed that α_{CO2} increases due to the fact that a rise in the system pressure results in growth in kinetic energy associated to the gas molecules. This further leads to the improvement of the rate of diffusion up to a positive maximum limit. The number of collisions amid gas molecules and liquid surface increases when P_{CO2} is increased thereby consequential in higher CO_2 loading, being the reason for the same. However, after this limiting value of P_{CO2} there is no remarkable rise in CO_2 loading. A decent covenant of the measured experimental data with modeled is offered for aq. (3.509 *m* MDEA + 0.509 *m* 2-MPZ) and aq. (3.002 *m* [bmim] [Ac] + 1.008 *m* 2-MPZ) (Figures (5.4-5.5)). Further, a contour design of aq. ($TMSO_2$ + 2-MPZ) system indicates that the system absorbed more CO_2 at low temperature and at high pressure (Figure 5.6).

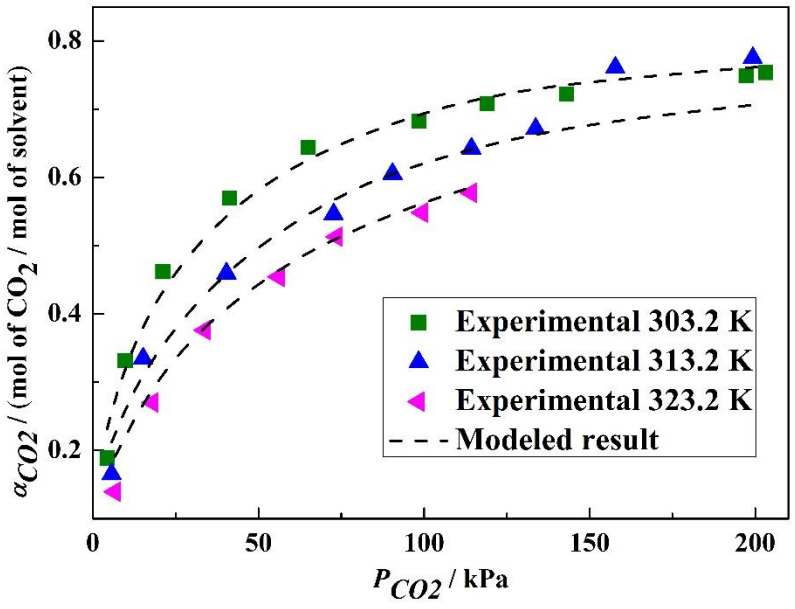

Figure 5.4 Effect of temperature on CO_2 solubility in aq. (3.509 *m* MDEA + 0.509 *m* 2-MPZ)

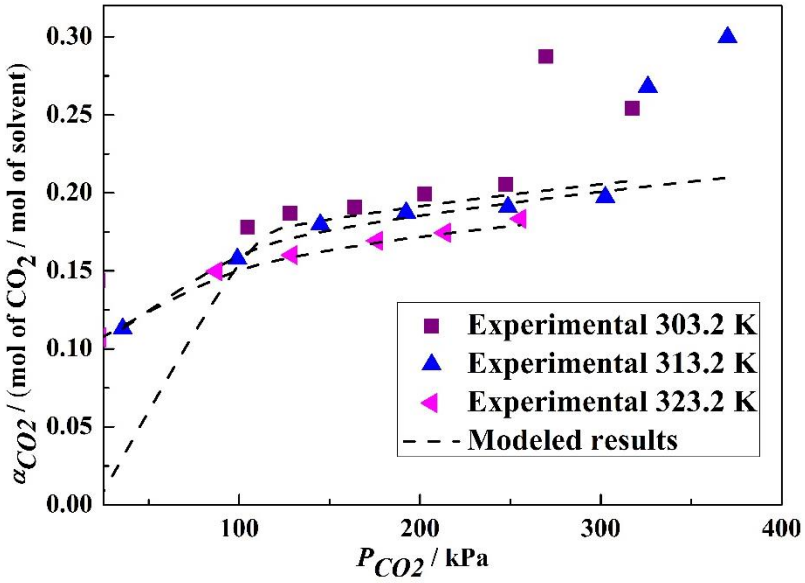

Figure 5.5 Effect of temperature on CO_2 solubility in aq. (3.002 *m* [bmim] [Ac] + 1.008 *m* 2-MPZ)

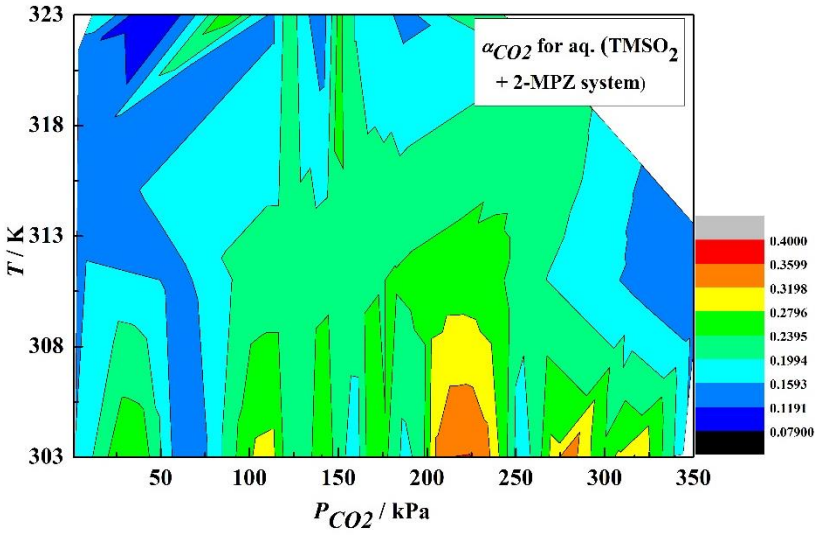

Figure 5.6 Contour plot of CO_2 solubility in aq. ($TMSO_2$ + 2-MPZ) as a function of *T* and P_{CO2}

The rise in concentration of 2-MPZ from 0.509 to 1.509 m in aq. solution of [bmim] [Ac] results in increase in α_{CO2} at all temperatures viz. (303.2, 313.2, 323.2) K (Figure 5.7). It can be concluded

from the figure that 1.509 *m* concentration of 2-MPZ is highly appreciable and provides far better CO_2 solubility in comparison to 0.509 *m* concentration of 2-MPZ blended system. The effect of base solvent with the activator, 2-MPZ, indicates that blends of MDEA with 2-MPZ provides superior α_{CO2} in comparison to [bmim] [Ac] or $TMSO_2$ at the same solvent concentration and temperature (Figure 5.8). This can be correlated with the fact that both ionic liquids and physical solvents react only physically majorly, which is quite low at low P_{CO2} whereas MDEA majorly contributes through chemical absorption. Along with this, ionic liquid blended with 2-MPZ has shown better performance than with $TMSO_2$. Hence it can be concluded that the CO_2 solubility is in the order of MDEA > [bmim] [Ac] > $TMSO_2$ with the same activator concentration (2-MPZ) in all blended solutions. Further, quantifying the CO_2 solubility data indicates that for aq. (MDEA + 2-MPZ) system at 313.2 K and 200 kPa, the rise in α_{CO2} observed is only 1.059 % with an increase in 2-MPZ concentration from 0.509 to 1.008 *m*. Whereas, the subsequent increase in the concentration of 2-MPZ from 0.509 to 1.509 *m* results in rise in α_{CO2} by 16.13 %.

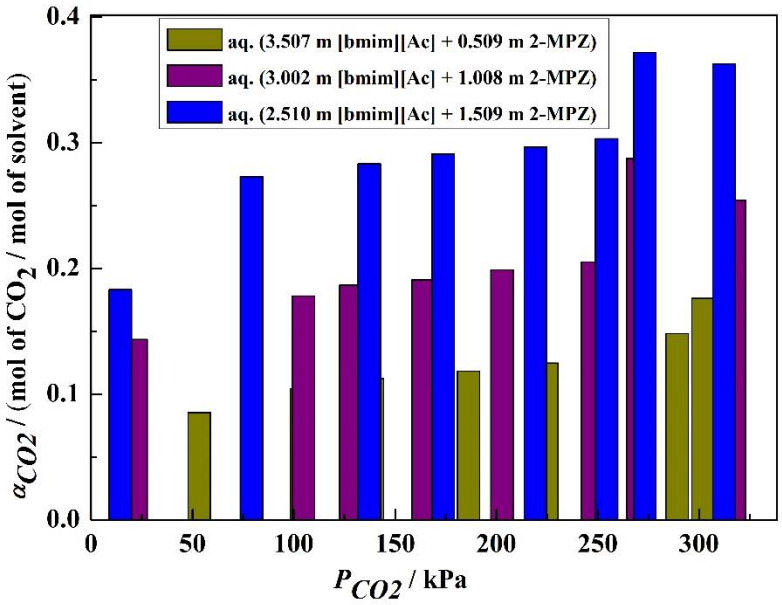

Figure 5.7 Effect on CO_2 solubility by addition of 2-MPZ in aq. [bmim] [Ac] at 303.2 K

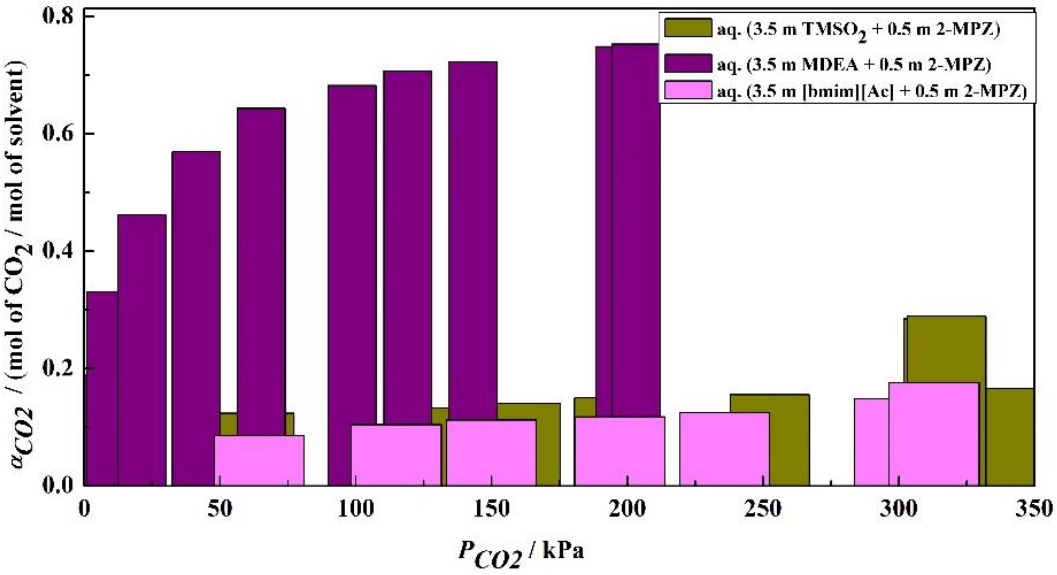

Figure 5.8 Comparison of CO_2 solubility in $TMSO_2$, MDEA and [bmim] [Ac] with 2-MPZ at 303.2 K

5.4.3 Liquid phase speciation profile, pH

The equilibrium concentrations of different species available in the solvent phase are further predicted as a function of α_{CO2} using the modified KE model. The concentration profiles of diverse species for CO_2 loaded, (3.509 *m* MDEA + 0.509 *m* 2-MPZ) at 303.2 K and (3.002 m [bmim] [Ac] + 1.008 m 2-MPZ) at 313.2 K have been represented in Figures 5.9 and 5.10, respectively. As indicated, there is a sharp decrease in the concentrations of 2-MPZ as a function of α_{CO2} indicating it to be a limiting reactant for CO_2 solubility reaction. Also, it is evident from the speciation HCO_3^- and carbamate corresponding to ionic liquid and amine associated to be the major reaction products. The estimation of pH of the reactants, products as well as intermediate species is one of the major important design parameters for absorption and stripping tower systems. The reaction products of the CO_2 solubility systems are usually in the pH range of (7-12) [33]. In the current work, modified KE model is further used to evaluate pH of blended solvent systems as a function of α_{CO2}. For aq. (2.500 *m* $TMSO_2$ + 1.509 *m* 2-MPZ) system, the maximum pH of 8.9 was observed at a low temperature of 303.2 K (Figure 5.11). With the rise in *T* and α_{CO2}, pH was observed to

decrease inevitably because of the fact that there are higher H^+ ions in the systems in comparison to OH^- ions at lower temperatures.

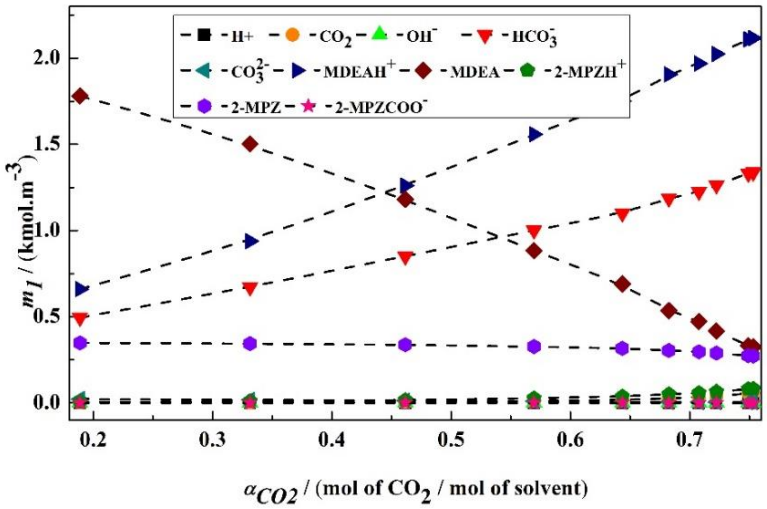

Figure 5.9 Modified KE model predicted equilibrium liquid phase concentration of various species in CO_2 loaded aq. (3.509 *m* MDEA + 0.509 *m* 2-MPZ) at T=303.2 K

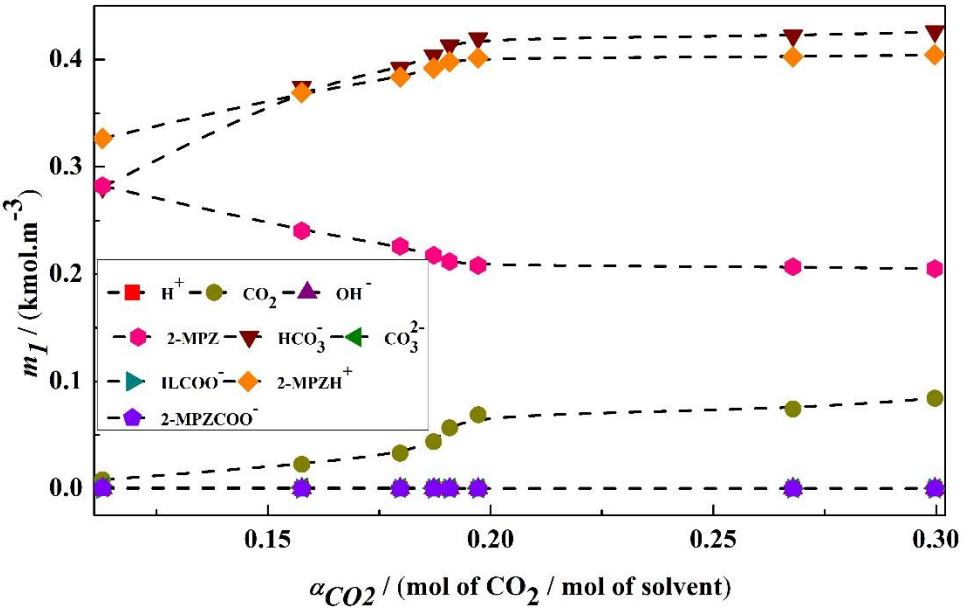

Figure 5.10 Modified KE model predicted equilibrium liquid phase concentration of various species in CO_2 loaded aq. (3.002 *m* [bmim][Ac] + 1.008 *m* 2-MPZ) at T=313.2 K

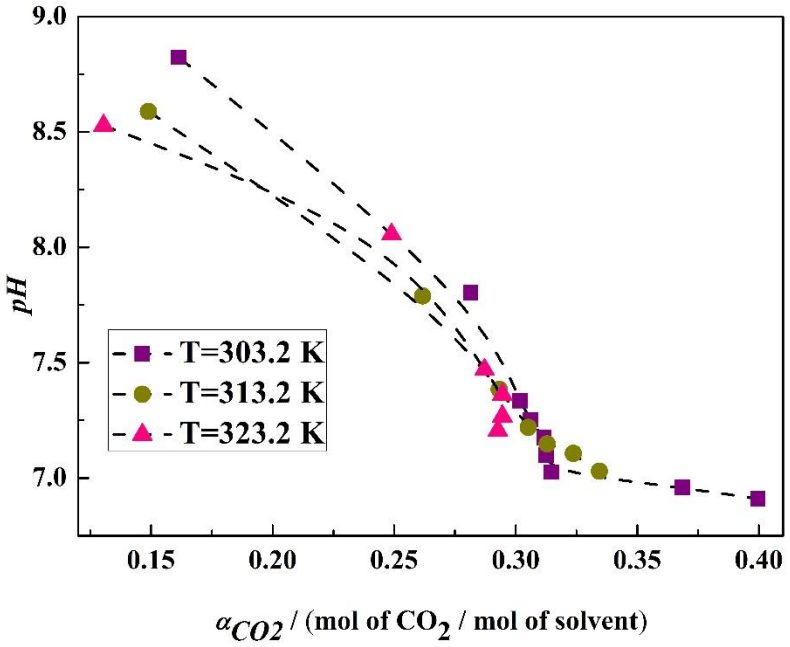

Figure 5.11 Modified KE model predicted pH as a function of CO_2 loading in aq. (2.500 *m* $TMSO_2$ + 1.509 *m* 2-MPZ)

5.4.4 CO_2 cyclic capacity and heat of absorption of aq. (MDEA + 2-MPZ) solution

The solvent transmission rate in the absorption-regeneration route is often taken as a performance indicator which is directly a function of CO_2 cyclic capacity [34]. In the present work, CO_2 cyclic capacity has been estimated for aq. (MDEA + 2-MPZ) system using Eq. (5.3):

$$capacity\left(\frac{molesCO_2}{kgsolvent}\right)=(\alpha_{PCO2,rich}-\alpha_{PCO2,lean})\times[MDEA/2-MPZ]\left(\frac{mole(MDEA/2-MPZ)}{kgsolvent}\right) \quad (5.3)$$

Where, $\alpha_{PCO2,\,rich}$ is evaluated at 20, 30, and 40 kPa and $\alpha_{PCO2,\,lean}$ is calculated at 5 kPa. The CO_2 cyclic capacity of the system has been evaluated at 303.2 K with respect to MDEA and 2-MPZ concentration and the same has been presented in Figures 12(a) and 12(b), respectively. The total CO_2 cyclic capacity of the ca. 4 *m* (MDEA + 2-MPZ) system is observed to be 1.0392. But, with respect to MDEA and 2-MPZ concentrations, the maximum of the parameter was observed at

0.9076 and 0.3068 at 40 kPa as the rich partial pressure of the system. It indicates that owing to the much larger concentration of MDEA in comparison to 2-MPZ, the CO_2 cyclic capacity depends on MDEA rather than 2-MPZ. The analysis of dependency of CO_2 cyclic capacity on temperature concludes that while rise in *T*, CO_2 cyclic capacity also tends to decrease similar to α_{CO2} (Figure 12(c)).

The energy requirements for any solvent desorption process is dictated by the heat of CO_2 absorption. The later can either be measured experimentally using instruments such as reaction calorimeter or can be evaluated from VLE data using Gibbs-Helmholtz equation [35]. The equation is presented as follows:

$$\frac{d(\ln P_{CO2})}{d\left(\frac{1}{T}\right)} = \frac{\Delta H_a}{R} \tag{5.4}$$

The heat of absorption in aq. (3.509 *m* MDEA + 0.509 *m* 2-MPZ) is obtained by eq. (14) using the slope of plot of $ln(P_{CO2})$ vs $(1/T)$. The described plots were made with α_{CO2} = 0.37, 0.47 and 0.57 corresponding to which the acquired slopes were -4783.69, -4675.13 and -4873.65, respectively (Figure 12(d)). The obtained heat of absorption is presented in Table 5.14. In comparison to activated or aqueous MEA or DEA systems i.e. primary or secondary amines, tertiary amines exhibit a lower heat of absorption. Comparable interpretations have also been reported in the literature [36-38].

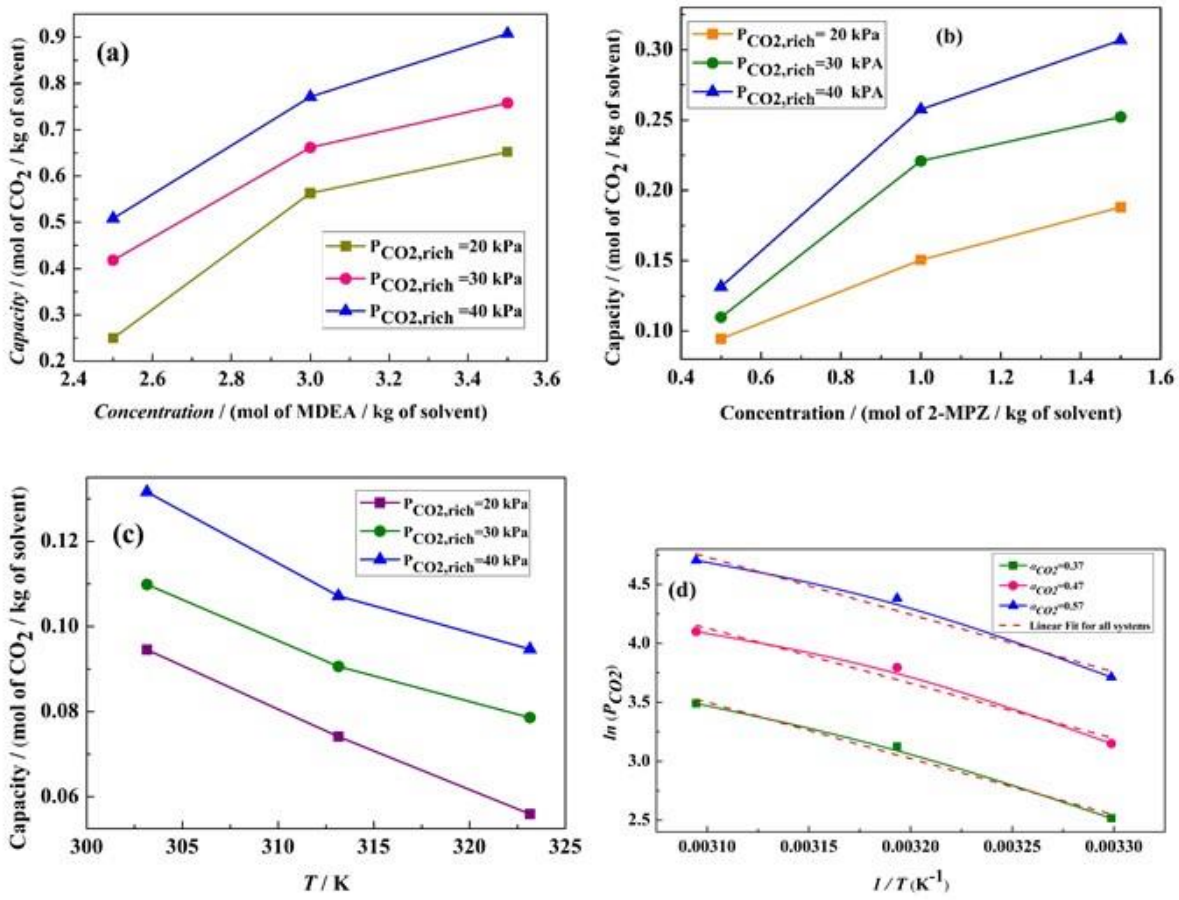

Figure 5.12 CO_2 cyclic capacity of aqueous (MDEA + 2-MPZ) system at 303.2 K with $P_{CO2,\ lean}$=5 kPa (a) as a function of MDEA concentration **(b)** as a function of 2-MPZ concentration (c) CO_2 cyclic capacity of aqueous (3.509 *m* MDEA + 0.509 *m* 2-MPZ) system with $P_{CO2,\ lean}$=5 kPa as a function of temperature (d) plot of *ln* (P_{CO2}) with *1/T* for calculation of heat of absorption for aq. (MDEA + 2-MPZ) system

Table 5.14 Heat of absorption in aq. (3.509 *m* MDEA + 0.509 *m* 2-MPZ) at various compositions within temperature range of (303.2-333.2) K

α_{CO2}	0.37	0.47	0.57
ΔHa (kJ/mol)	-39.77	-38.87	-40.52

5.4.5. Comparison of solvent performance with other conventional amines/blends

An assessment of the studied solvents is done with the available literature. However, due to the lack of literature in the studied range of composition, the nearest available literature was considered. CO_2 solubility in the blend of aq. (3.017 *m* MDEA + 1. 008 *m* 2-MPZ) solution is quite competitive to literature available data [2, 39, 40] (Figure 5.13). In addition, a comparison of aq. (3.501 *m* $TMSO_2$ + 0.509 *m* 2-MPZ) with near aq. composition of 0.0999 mole fractions of $TMSO_2$ [12] indicates that the former provides a maximum CO_2 solubility of 0.0191 mole fraction at 317.57 kPa. On the other hand, aq. $TMSO_2$ provides a CO_2 solubility of 0.0106 mole fraction at 1.108 MPa and at 303.2 K. Hence, it can be concluded that with the addition of 0.509 m 2-MPZ to nearly the same composition of $TMSO_2$, the newly developed blend outperforms the aqueous blend of $TMSO_2$.

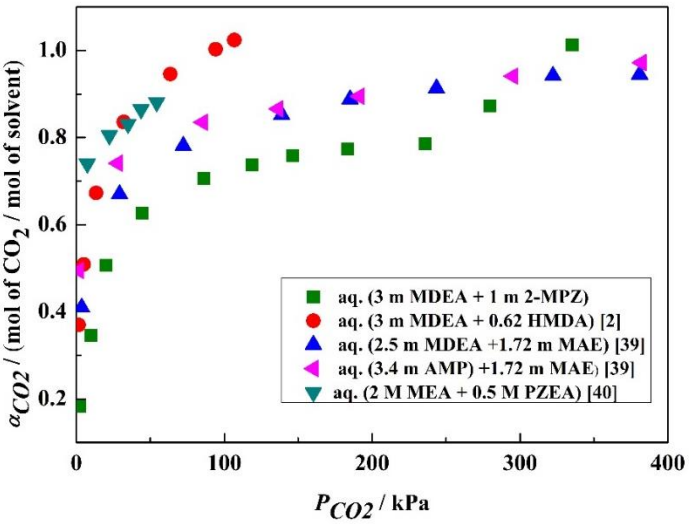

Figure 5.13 Comparison of CO_2 solubility in aq. (3.017 m MDEA + 1.008 m 2-MPZ) with literature at 303.2 K

5.5 Conclusions

CO_2 solubility in aqueous MDEA, $TMSO_2$ and [bmim] [Ac] enhanced by PZ based amine activator viz. 2-MPZ were studied over inclusive variations in experimental conditions. Qualitative analysis through FTIR and ^{13}C NMR of the unloaded and loaded solvents indicated carbamate formation by 2-MPZ reacting with CO_2. The results evidently specify that CO_2 solubility increases with respect to rise in both P_{CO2} and concentrations of activator in solvent blends. Modified KE model inclusive of gas phase non-ideality were developed to correlate the CO_2 solubility data. Results indicated a rise in 2-MPZ in blends of aq. MDEA, $TMSO_2$ or [bmim] [Ac], improved the CO_2 solubility tremendously. The optimized equilibrium constants associated with various reactions as a function of P_{CO2}, solvent concentration, and T of absorption have been estimated using regression analysis. The speciation and pH data as a function of α_{CO2} has been estimated by means of modified KE model. CO_2 cyclic capacity and low heat of absorption of aq. (MDEA + 2-MPZ) solvent indicated it be a prospective solvent for CO_2 capture. In addition, an assessment of CO_2 solubility data of solvents blends with literature reveals that the considered solvents have well imminent for post-combustion CO_2 capture applications.

References

[1]B. Das, B. Deogam, B. P. Mandal. Absorption of CO_2 into novel aqueous bis (3-aminopropyl) amine and enhancement of CO_2 absorption into its blends with *N*-methyldiethanolamine. International Journal of Greenhouse Gas Control 60 (2017) 172-185.

[2]B. K. Mondal, S. S. Bandyopadhyay, A. N. Samanta. Equilibrium solubility measurement and Kent-Eisenberg modeling of CO_2 absorption in aqueous mixture of *N*-methyldiethanolamine and hexamethylenediamine. Greenhouse Gases: Science and Technology (2016) 1-13.

[3]A. Hafizi, M.H. Mokari, R. Khalifeh, M. Farsi, M.R. Rahimpour. Improving the CO_2 solubility in aqueous mixture of MDEA and different polyamine promoters: The effects of primary and secondary functional groups. Journal of Molecular Liquids (2019) 111803.

[4]R. Ramezani, R. D. Felice. Experimental study of CO_2 absorption in different blend solutions as solvent for CO_2 capture. International Journal of Chemical and Molecular engineering. 11 (2017) 5-10.

[5]B. Sherman, P. T. Frailie, L. Li, N. Salta, G. T. Rochelle. Thermodynamic and kinetic modeling of piperazine/ 2-methylpiperazine. Energy Procedia 63 (2014) 1243-1255.

[6]Y. Yuan, B. Sherman, G. T. Rochelle. Effects of viscosity on CO_2 absorption in aqueous piperazine / 2-methylpiperazine. Energy Procedia 114 (2017) 2103-2120.

[7]X. Chen, G. T. Rochelle. Modeling of CO_2 absorption kinetics in aqueous 2-methylpiperazine. Industrial and Engineering Chemistry Research 52 (2013) 4239-4248.

[8]X. Chen, G. T. Rochelle. Thermodynamics of CO_2 / 2-methylpiperazine/ water. Industrial and Engineering Chemistry Research 52 (2013) 4229-4238.

[9]B. Sherman, X. Chen, T. Nguyen, Q. Xu, H. Rafique, S. A. Freeman, A. K. Voice, G. T. Rochelle. Carbon capture with 4 m piperazine / 4 m 2-methylpiperazine. Energy Procedia 37 (2013) 436-447.

[10]Y. E. Kim, J. H. Choi, S. C. Nam, Y. I. Yoon. CO_2 absorption capacity using aqueous potassium carbonate with 2-methylpiperazine and piperazine. Journal of Industrial and Engineering Chemistry 18 (2012) 105-110.

[11]F. M. Guevara, A. R. Martinez, A. Trejo. Solubilities of carbon dioxide and hydrogen sulphide in propylene carbonate, N- methylpyrrolidone and sulfolane. Fluid Phase Equilibria 44 (1988) 105-115.

[12]M. Shokouhi, A. H. Jalili, A. T. Zoghi, J. S. Ahari. Carbon dioxide solubility in aqueous sulfolane solution. Journal of Chemical Thermodynamics 132 (2019) 62-72.

[13]A. H. Jalili, M. Shokouhi, F. Samani, M. H. Jenab. Measuring the solubility of CO_2 and H_2S in sulfolane and the density and viscosity of saturated liquid binary mixtures of (sulfolane + CO_2) and (sulfolane + H_2S). Journal of Chemical Thermodynamics 85 (2015) 13-25.

[14]F. Y. Jou, A. E. Mather. Solubility of carbon dioxide in an aqueous mixture of methyldiethanolamine and N-methylpyrrolidone at elevated pressures. Fluid Phase Equilibria (2005) 465-469.

[15]L. Zong, C. C. Chen. Thermodynamic modeling of CO_2 and H_2S solubilities in aqueous DIPA solution, aqueous sulfolane-DIPA solution, and aqueous sulfolane-MDEA solution with electrolyte NRTL model. Fluid Phase Equilibria 306 (2011) 190-203.

[16]S. K. Dash, S. S. Bandyopadhyay. Studies on the effect of addition of piperazine and sulfolane into aqueous solution of *N*-methyldiethanolamine for CO_2 capture and VLE modelling using e-NRTL equation. International Journal of Greenhouse Gas control 44 (2016) 227-237.

[17]H. A. Shirazizadeh, A. Haghtalab. Simultaneous solubility measurement of (ethyl mercaptans + carbon dioxide) into the aqueous solutions of (*N*-methyl diethanolamine + sulfolane + water). Journal of Chemical Thermodynamics 133 (2019) 111-122.

[18]W. Luo, D. Guo, J. Zheng, S. Gao, J. Chen. CO_2 absorption using biphasic solvent: blends of diethylenetriamine, sulfolane, and water. International Journal of Greenhouse Gas Control 53 (2016) 141-148.

[19]L. Wang, S. Yu, Q. Li, Y. Zhang, S. An, S. Zhang. Performance of sulfolane / DETA hybrids for CO_2 absorption: phase splitting behaviour, kinetics and thermodynamics. Applied Energy 228 (2018) 568-576.

[20]R. Krupiczka, A. Rotkegel, Z. Ziobrowski. Comparative study of CO_2 absorption in packed column using imidazolium based ionic liquids and MEA solution. Separation and Purification Technology 149 (2015) 228-236.

[21]J. G. Lu, Z. Y. Lu, Y. Chen, J. T. Wang, L. Gao, X. Gao, Y. Q. Tang, D. G. Liu. CO_2 absorption into aqueous blends of ionic liquid and amine in a membrane contactor. Separation and Purification Technology 150 (2015) 278-285.

[22]K. G. Bogolitsyn, T. E. Skrebets, T. A. Makhova. Physiochemical properties of 1-butyl-3-methylimidazolium acetate. Russian Journal of General Chemistry 79 (2009) 125-128.

[23]A. Haghtalab, A. Shojaeian. Volumetric and viscometric behavior of the binary systems of N-methyldiethanolamine and diethanolamine with 1-butyl-3-methylimidazolium acetate at various temperatures. Journal of Chemical Thermodynamics 68 (2014) 128-137.

[24]J. Safarov, M. Geppert-Rybczynska, I. Kul, E. Hassel. Thermophysical properties of 1-butyl-3-methylimidazolium acetate over a wide range of temperatures and pressures. Fluid phase Equilibria 383 (2014) 144-155.

[25]S. N. Khan, S. M. Hailegiorgis, Z. Man, A. M. Shariff, S. Garg. Thermophysical properties of aqueous 1-butyl-3-methylimidazolium acetate [bmim] [Ac] + monoethanolamine (MEA) hybrid as a solvent for CO_2 capture. Procedia Engineering 148 (2016) 1326-1331.

[26]Y. Hiraga, A. Kato, Y. Sato, R. L. Smith. Densities at pressures up to 200 MPa and atmospheric pressure viscosities of ionic liquids 1-ethyl-3-methylimidazolium methylphosphate, 1-ethyl-3-methylimidazolium diethylphosphate, 1-butyl-3-methylimidazolium acetate, and 1-butyl-3-methylimidazolium Bis-(trifluoromethylsulfonyl) imide. Journal of Chemical and Engineering Data 60 (3) (2015) 876-885.

[27]S. Balchandani, B. P. Mandal, S. Dharaskar. Measurements and modeling of vapor liquid equilibrium of CO_2 in amine activated imidazolium ionic liquid solvents. Fluid Phase Equilibria 521 (2020) 112643.

[28]S. Balchandani, R. Singh. COSMO-RS analysis of CO_2 solubility in *N*-methyldiethanolamine, sulfolane, and 1-butyl-3-methyl-imidazolium acetate activated by 2-methyl piperazine for post combustion carbon capture. ACS Omega 6 (2021) 747-761.

[29]A. Dey, S. K. Dash, S. C. Balchandani, B. P. Mandal. Investigation on the inclusion of 1-(2-aminoethyl) piperazine as a promoter on the equilibrium CO_2 solubility of aqueous 2-amino-2-methyl-1-propanol. Journal of Molecular Liquids 289 (2019) 111036.

[30]B. Das, B. Deogam, B. P. Mandal. Experimental and theoretical studies on efficient carbon dioxide capture using novel bis (3-aminopropyl) amine (APA) –activated aqueous 2-amino-2-methyl-1-propanol (AMP) solutions. RSC Advances 7 (2017) 21518-21530.

[31]Y. Du, G. T. Rochelle. Thermodynamic modeling of aqueous piperazine / (N-(2-aminoethyl) piperazine for CO_2 capture. Energy Procedia 63 (2014) 997-1017.

[32]M. B. Shiflett, D. J. Kasprzak, C. P. Junk, A. Yokozeki. Phase behavior of {carbon dioxide + [bmim] [Ac]} mixtures. Journal of Chemical Thermodynamics 40 (2008) 25-31.

[33]S. K. Dash, A. N. Samanta, S. S. Bandyopadhyay. Solubility of carbon dioxide in aqueous solution of 2-amino-2-methyl-1-propanol and piperazine. Fluid Phase Equilibria 307 (2011) 166-174.

[34]P. M. Mathias, S. Reddy, A. Smith, K. Afshar. Thermodynamic analysis of CO_2 capture solvents. International Journal of Greenhouse Gas Control 19 (2013) 262-270.

[35]J. K. Carson, K. N. Marsh, A. E. Mather. Enthalpy of solution of carbon dioxide in (water + monoethanolamine, or diethanolamine, or *N*-methyldiethanolamine) and (water + monoethanolamine + *N*-methyldiethanolamine) at T=298.15 K. Journal of Chemical Thermodynamics 32 (2000) 1285-96.

[36]F. A. Chowdhury, H. Okabe, S. Shimizu, M. Onoda, Y. Fujioka. Development of novel tertiary amine absorbents for CO2 capture. Energy Procedia 1 (2009) 1241-8.

[37]Y. Liang, H. Liu, W. Rongwong, Z. Liang, R. Idem, P. Tontowachwuthikul. Solubility, absorption heat and mass transfer studies of CO_2 absorption into aqueous solution of 1-dimethylamino-2-propanol. Fuel 144 (2015) 121-129.

[38]H. Ling, S. Liu, H. Gao, H. Zhang, Z. Liang. Solubility of N_2O, equilibrium solubility, mass transfer study and modeling of CO_2 absorption into aqueous monoethanolamine (MEA)/1-dimethylamino-2-propanol (1DMA2P) solution for post-combustion CO_2 capture. Separation and Purification Technology 232 (2020) 115957.

[39]G. Kumar, M. Kundu. Solubility of CO_2 in aqueous blends of (N-methyl-2-ethanolamine + N-methyl-diethanolamine) and (N-methyl-2-ethanolamine + 2-amino-2-methyl-1-propanol). Journal of Chemical and Engineering Data 57 (2012) 3203-3209.

[40]R. Ramazani, S. Mazinani, A. Hafizi., A. Jahanmiri. Equilibrium solubility of carbon dioxide in aqueous blend of monoethanolamine (MEA) and 2-1-piperazinyl-ethlamine (PZEA) solutions: Experimental and optimization study. Process Safety and Environment Protection 98 (2015) 325-332.

Chapter 6

THERMOPHYSICAL PROPERTIES OF AQUEOUS / NON-AQUEOUS SELECTED IONIC LIQUIDS AND BLENDED AMINES

This chapter reports the important thermophysical properties such as density, viscosity, sound velocity, and refractive index data of (1) 2-hydroxy ethyl ammonium formate (HEF) + 1-(2-aminoethyl) piperazine (AEP), (2) 2-hydroxy ethyl ammonium formate (HEF) + 2-Amino-2-methyl-1-propanol (AMP), (3) aqueous 3-aminopropyl triethoxysilane (TESA) , (4) aqueous 3-aminopropyl triethoxysilane (TESA) + 1-(2-aminoethyl) piperazine (AEP), (5) aqueous 3-aminopropyl triethoxysilane (TESA) + bis (3-aminopropyl) amine (APA), (6) aqueous 1-butyl 3-methyl imidazolium acetate ([bmim][Ac]), (7) aqueous 1-butyl 3-methyl imidazolium acetate ([bmim][Ac]) + 1-(2-aminoethyl) piperazine (AEP), (8) aqueous 1-butyl 3-methyl imidazolium acetate ([bmim][Ac]) + bis (3-aminopropyl) amine (APA), (9) aqueous N-methyldiethanolamine (MDEA) + 2-methyl piperazine (2-MPZ), (10) aqueous N-sulfolane ($TMSO_2$) + 2-methyl piperazine (2-MPZ) and (11)) aqueous 1-butyl 3-methyl imidazolium acetate ([bmim][Ac]) + 2-methyl piperazine (2-MPZ). Surface tension has also been measured for the blends (3-11). All the measurements were conducted over the temperature range of (298.15 to 333.15) K at 0.1 MPa. The density and viscosity results were further correlated as a function of temperature and concentration of amine/ionic liquids with Redlich - Kister and Grunberg - Nissan models, respectively. Two new models (M_1 and M_2) have been proposed for sound velocity and refractive index and surface tension, respectively based on the dependence of properties on concentration and temperature. The experimental values have been further utilized to evaluate various useful thermodynamic and transport properties such as excess molar volumes, kinematic viscosity deviations, thermal expansion coefficients, diffusivity of CO_2/N_2O in proposed solvents, isentropic compressibility, enthalpy (ΔH^o), entropy (ΔS^o) and Gibbs energies (ΔG^o) of activation of viscous flow.

6.1 Introduction

A thorough knowledge of thermophysical properties over a wide range of experimental conditions is very useful for the industrial and lab-scale development of gas-liquid absorption system. The physiochemical properties can be further also utilized for vapor-liquid equilibrium relationships and kinetics of the reactions involved. The meticulous characterization of the industrial solvents is also required for the designing of the gas absorption systems [1-4]. The excess molar volumes which indicate the interactive nature of the molecules of solvent mixtures is dictated by the density measurements. Density and viscosity are also required for the calculation of mass transfer rates and kinetics of the reactions [5, 6]. The measurement of viscosity is also useful for estimating the diffusivity of various gases such as N_2O and CO_2 in the desired solvents [5]. Sound velocity and refractive index are the properties required for the knowledge of relationship between concentration and temperature with the properties. Also, the intermolecular interactions are attributed to these properties [6]. Along with the mass transfer characteristics, surface tension is required for the analysis of hydrodynamic characteristics of the system under study [7].

Hence, the present work emphasizes on the measurements of the density, viscosity, sound velocity, refractive index, and surface tension of (HEF + AEP), (HEF + AMP), aq. TESA, aq. (TESA + AEP), aq. (TESA + APA), aq. [bmim] [Ac], aq. ([bmim] [Ac] + AEP), aq. ([bmim] [Ac] + APA), aq. (MDEA + 2-MPZ), aq. ($TMSO_2$ + 2-MPZ) and aq. ([bmim] [Ac] +2-MPZ) in the temperature range of (298.15 to 333.15) K at atmospheric pressure. The measured density and viscosity data are correlated as a function of temperature and composition using Redlich–Kister equation [8] and Grunberg - Nissan model [9], respectively. Two novel models for sound velocity, refractive index (M_1), and surface tension (M_2) have been proposed and validated. The study is further extended by estimation of various useful physiochemical, rheological, and thermodynamic properties such as excess molar volume, kinematic viscosity deviation, thermal expansion coefficient, isentropic compressibility, diffusivities in N_2O and CO_2, Gibb's free energy, enthalpy and entropy of viscous flow.

6.2 Experimental section

6.2.1 Materials

The specifications of the reagents used in the present work are presented in Table 6.1. Double distilled deionized water was used for preparing all the blended solutions.

Table 6.1 Specifications of the reagents used in the present study

Chemical name	Chemical formula	Source	Purity in mass (%)	Purification method
2-Hydroxy Ethyl ammonium Formate (HEF)	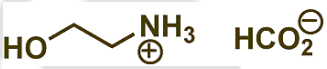	Iolitec	>97	Vacuum Drying
1-(2-Aminoethyl) Piperazine (AEP)	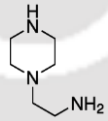	Sigma Aldrich Co.	99	None
2-Amino-2-Methyl-1-Propanol (AMP)	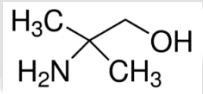	Sigma Aldrich Co.	99	None
3-aminopropyl triethoxysilane (TESA)	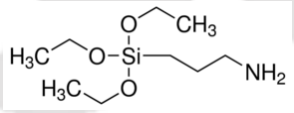	Sigma Aldrich Co.	0.99	None
Bis(3-aminopropyl)amine (APA)	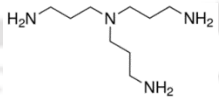	Sigma Aldrich Co.	0.98	None
1-butyl-3-methyl-imidazolium acetate ([bmim][Ac])	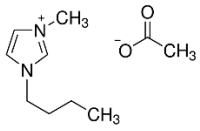	Sigma Aldrich Co.	≥0.95	Vacuum Drying
N- Methyldiethanolamine (MDEA)	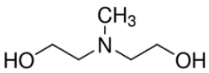	Sigma Aldrich Co.	≥99	None

2-Methyl Piperazine (2-MPZ)	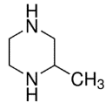	Sigma Aldrich Co.	95	None
Sulfolane ($TMSO_2$)	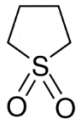	Sigma Aldrich Co.	99	None

6.2.2 Measurement of density and sound velocity

Density and sound velocity measurements of the systems were carried out with density and sound velocity meter (DSA 5000 M, Anton Paar, Austria) in the temperature range of (298.15 to 333.15) K at 0.1 MPa pressure. The precision of the apparatus is within 0.000005 $g.cm^{-3}$. The density and sound velocity meter was calibrated using double distilled deionized water and dehumidified air at NTP conditions. The measurements at each temperature were repeated thrice and the average value is reported in the present work. The capillary was first cleaned with double distilled deionized water (2-3 times) and then two times with methanol. Finally, it was dried in a hot air oven before each measurement. The standard uncertainties, *u*, for temperature, pressure, density, and sound velocity are $u(T) = 0.01$ K, $u(P) = 0.01$ MPa, $u(\rho) = 0.5$ $kg \cdot m^{-3}$, and $u(c) = 0.5$ $m.s^{-1}$, respectively.

6.2.3 Measurement of viscosity

The dynamic viscosities of the studied systems were measured using Anton Paar AMVn rolling ball viscometer, as a function of temperature from (298.15 to 333.15) K and at 0.1 MPa pressure. A 3-mm diameter capillary tube was used for the measurement at an angle of 70°. The capillary was cleaned before each measurement following the procedure described in section 6.2.2. The measurements were repeated thrice, and the average value is reported for each experimental temperature. The standard uncertainties, *u*, for temperature, pressure and dynamic viscosities are $u(T) = 0.01$ K, $u(P) = 0.01$ MPa, $u(\eta) = 0.07$ mPa.s, respectively.

6.2.4 Measurement of refractive index

The refractive indexes of the systems were measured using a METTLER TOLEDO RE40 refractometer within the temperature range of (298.15 to 333.15) K at 0.1 MPa pressure. For each measurement, the sapphire prism of the refractometer was cleaned with first double distilled water and then methanol to ensure accurate measurements. The prism temperature was maintained by a thermostat within thermal stability of ± 2×10^{-3} K. The measurements were repeated thrice at a particular temperature, and the average value is reported. The standard uncertainties, *u*, for temperature, pressure and refractive index are *u* (*T*) = 0.01 K, *u* (*P*) = 0.01 MPa, *u* (*nD*) = 0.001, respectively.

6.2.5 Measurement of surface tension

Surface tension of all blends was measured using Attention Sigma 700 instrument. The instrument consists of a platinum ring oriented perpendicular to the interface, and the force exerted on the ring due to wetting is measured by microbalance and was used to calculate surface tension. 50 ml of the solution was used for the measurement of surface tension. The instrument was connected to (F 32, JULABO, FRG) which provided the control of temperature within ± 0.10 K of the desired temperature by a circulating bath connected to circulator temperature controller. The tensiometer has a surface tension range of (1–2000) $mN\cdot m^{-1}$ with 0.001 resolutions.

6.3 Results and discussions

6.3.1 Modeling of density

The method used for the measurement of density is being validated by measuring pure AMP densities at various temperatures [10]. The results indicates a good agreement between the measured and literature values (Table 6.2). The experimental values of densities of all the systems under study have been presented in Tables 6.3-6.13. As indicated, the densities of all the systems are found to decrease with rise in temperature due to fewer intermolecular forces of attraction at higher temperatures.

Table 6.2 Comparison of the density (ρ) of pure AMP measured in the present work with literature values at pressure P= 0.1 MPa

T / K	ρ / kg.m^{-3}		
	Ref. 10	Ref. 14	This work
298.15	930.156	929.9	929.9
303.15	926.403	927	926.6
308.15	922.59	923.5	922.5
313.15	918.079	919.4	919.6
318.15	913.866	-	912.9
323.15	909.622	-	910.5
328.15	-	-	909.1
333.15	-	-	907.3
% AAD	0.424	0.169	

Table 6.3 (a) Experimental density (ρ), dynamic viscosity (η), sound velocity (c) and refractive index (nD) for (HEF + AEP) from 298.15 K to 333.15 K at 0.1 MPa

T/ K	Mole fraction (HEF)	Mole fraction (AEP)	ρ / kg.m^{-3}	η / mPa.s	c / m.s^{-1}	nD
298.15	0.232	0.768	1027.2	130.06	1641.1	1.499
303.15	0.232	0.768	1023.5	80.27	1624.3	1.499
308.15	0.232	0.768	1019.8	28.39	1607.5	1.495
313.15	0.232	0.768	1016.0	21.91	1590.7	1.493
318.15	0.232	0.768	1012.2	17.15	1574.0	1.491
323.15	0.232	0.768	1008.5	13.75	1557.4	1.489
328.15	0.232	0.768	1004.7	11.21	1541.1	1.488
333.15	0.232	0.768	1000.9	9.22	1524.5	1.485
298.15	0.341	0.659	1049.2	250.07	1669.0	1.499
303.15	0.341	0.659	1045.5	188.74	1652.8	1.497
308.15	0.341	0.659	1041.8	136.25	1636.6	1.495
313.15	0.341	0.659	1038.1	102.45	1620.5	1.493
318.15	0.341	0.659	1034.3	78.62	1604.4	1.491
323.15	0.341	0.659	1030.6	61.55	1588.7	1.489
328.15	0.341	0.659	1026.9	48.98	1572.9	1.487
333.15	0.341	0.659	1023.1	39.71	1556.9	1.484
298.15	0.446	0.554	1073.6	379.08	1697.2	1.498
303.15	0.446	0.554	1069.6	266.57	1681.5	1.496
308.15	0.446	0.554	1065.9	191.35	1665.9	1.494
313.15	0.446	0.554	1062.3	141.69	1650.4	1.492
318.15	0.446	0.554	1058.7	106.77	1635.1	1.491
323.15	0.446	0.554	1055.0	83.63	1620.2	1.488
328.15	0.446	0.554	1051.3	65.75	1604.9	1.485
333.15	0.446	0.554	1047.7	53.16	1589.8	1.484

Table 6.3 (b) Experimental density (ρ), dynamic viscosity (η), sound velocity (c) and refractive index (nD) for (HEF + AEP) from 298.15 K to 333.15 K at 0.1 MPa

T/ K	Mole fraction (HEF)	Mole fraction (AEP)	ρ / kg.m^{-3}	η / mPa.s	c / m.s^{-1}	nD
298.15	0.547	0.453	1093.5	466.87	1715.9	1.496
303.15	0.547	0.453	1089.9	322.46	1700.9	1.494
308.15	0.547	0.453	1086.3	230.52	1685.9	1.492
313.15	0.547	0.453	1082.8	169.99	1671.2	1.491
318.15	0.547	0.453	1079.2	127.93	1656.9	1.489
323.15	0.547	0.453	1075.6	98.95	1642.4	1.487
328.15	0.547	0.453	1071.9	77.51	1627.8	1.485
333.15	0.547	0.453	1068.3	62.39	1613.3	1.484
298.15	0.644	0.356	1113.4	462.42	1731.3	1.493
303.15	0.644	0.356	1109.9	323.28	1715.9	1.489
308.15	0.644	0.356	1106.3	234.88	1701.6	1.489
313.15	0.644	0.356	1102.8	173.64	1687.5	1.488
318.15	0.644	0.356	1099.2	131.77	1673.5	1.486
323.15	0.644	0.356	1095.7	102.14	1659.6	1.484
328.15	0.644	0.356	1092.1	81.99	1645.8	1.483
333.15	0.644	0.356	1088.5	64.97	1631.9	1.481
298.15	0.738	0.262	1132.2	357.84	1737.4	1.489
303.15	0.738	0.262	1128.7	259.01	1724.2	1.487
308.15	0.738	0.262	1125.2	191.96	1710.7	1.486
313.15	0.738	0.262	1121.7	146.63	1697.4	1.484
318.15	0.738	0.262	1118.2	113.71	1684.2	1.483
323.15	0.738	0.262	1114.7	89.85	1671.0	1.481
328.15	0.738	0.262	1111.2	71.94	1657.8	1.479
333.15	0.738	0.262	1107.7	58.96	1644.7	1.478
298.15	0.828	0.172	1150.5	264.86	1740.1	1.484
303.15	0.828	0.172	1147.1	196.55	1727.5	1.483
308.15	0.828	0.172	1143.7	149.13	1715.2	1.481
313.15	0.828	0.172	1140.3	115.78	1702.8	1.479
318.15	0.828	0.172	1136.9	91.74	1690.4	1.478
323.15	0.828	0.172	1133.4	74.36	1678.1	1.477
328.15	0.828	0.172	1130.0	60.82	1665.7	1.476
333.15	0.828	0.172	1126.6	50.81	1653.4	1.474

Table 6.4 (a) Experimental density (ρ), dynamic viscosity (η), sound velocity (c) and refractive index (nD) for (HEF + AMP) from 298.15 K to 333.15 K at 0.1 MPa

T/ K	Mole fraction (HEF)	Mole fraction (AMP)	ρ / kg.m^{-3}	η / mPa.s	c / m.s^{-1}	nD
298.15	0.147	0.853	986.2	170.561	1575.51	1.452
303.15	0.147	0.853	982.3	118.751	1557.97	1.449
308.15	0.147	0.853	978.4	82.334	1540.79	1.448
313.15	0.147	0.853	974.4	58.681	1523.71	1.45
318.15	0.147	0.853	970.5	42.885	1507.15	1.444
323.15	0.147	0.853	966.6	31.844	1490.45	1.443
328.15	0.147	0.853	962.6	24.217	1473.74	1.441
333.15	0.147	0.853	958.7	18.761	1457.04	1.439
298.15	0.229	0.771	1008.4	165.09	1600.0	1.455
303.15	0.229	0.771	1004.6	112.97	1583.6	1.453
308.15	0.229	0.771	1000.8	79.18	1567.7	1.451
313.15	0.229	0.771	996.9	57.28	1551.6	1.449
318.15	0.229	0.771	993.1	42.10	1535.5	1.448
323.15	0.229	0.771	989.3	31.65	1519.4	1.446
328.15	0.229	0.771	985.5	24.27	1503.4	1.445
333.15	0.229	0.771	981.6	18.99	1487.4	1.442
298.15	0.316	0.684	1032.9	148.28	1626.5	1.458
303.15	0.316	0.684	1029.3	103.17	1610.7	1.456
308.15	0.316	0.684	1025.6	74.33	1595.4	1.454
313.15	0.316	0.684	1021.9	54.44	1580.2	1.453
318.15	0.316	0.684	1018.2	40.82	1564.9	1.451
323.15	0.316	0.684	1014.5	31.24	1549.8	1.449
328.15	0.316	0.684	1010.8	24.25	1534.7	1.448
333.15	0.316	0.684	1007.2	19.15	1519.5	1.446
298.15	0.409	0.591	1058.5	126.51	1651.0	1.461
303.15	0.409	0.591	1054.9	90.68	1636.3	1.459
308.15	0.409	0.591	1051.3	66.23	1621.6	1.457
313.15	0.409	0.591	1047.7	49.47	1606.8	1.455
318.15	0.409	0.591	1044.1	37.69	1592.5	1.454
323.15	0.409	0.591	1040.4	29.32	1577.9	1.453
328.15	0.409	0.591	1036.8	23.17	1563.4	1.452
333.15	0.409	0.591	1033.2	18.58	1548.9	1.449

Table 6.4 (b) Experimental density (ρ), dynamic viscosity (η), sound velocity (c) and refractive index (nD) for (HEF + AMP) from 298.15 K to 333.15 K at 0.1 MPa

T/ K	Mole fraction (HEF)	Mole fraction (AMP)	ρ / kg.m^{-3}	η / mPa.s	c / m.s^{-1}	nD
298.15	0.509	0.491	1078.9	107.42	1668.5	1.463
303.15	0.509	0.491	1075.4	78.55	1654.6	1.462
308.15	0.509	0.491	1071.8	58.35	1640.8	1.459
313.15	0.509	0.491	1068.2	44.41	1627.4	1.458
318.15	0.509	0.491	1064.7	34.31	1613.7	1.457
323.15	0.509	0.491	1061.1	27.04	1599.9	1.455
328.15	0.509	0.491	1057.6	21.63	1585.9	1.453
333.15	0.509	0.491	1054.1	17.60	1572.2	1.452
298.15	0.617	0.383	1103.2	84.75	1691.7	1.466
303.15	0.617	0.383	1099.3	62.99	1675.7	1.464
308.15	0.617	0.383	1095.7	47.99	1663.1	1.462
313.15	0.617	0.383	1092.1	37.11	1650.4	1.461
318.15	0.617	0.383	1088.5	29.35	1637.7	1.460
323.15	0.617	0.383	1084.9	23.55	1624.9	1.459
328.15	0.617	0.383	1081.4	19.20	1612.1	1.457
333.15	0.617	0.383	1078.1	15.80	1599.2	1.455
298.15	0.735	0.265	1131.4	64.21	1705.8	1.467
303.15	0.735	0.265	1127.9	49.24	1694.2	1.466
308.15	0.735	0.265	1124.4	38.25	1682.5	1.464
313.15	0.735	0.265	1120.8	30.16	1670.7	1.463
318.15	0.735	0.265	1117.2	24.25	1659.0	1.461
323.15	0.735	0.265	1113.7	19.78	1647.3	1.459
328.15	0.735	0.265	1110.1	16.36	1635.6	1.458
333.15	0.735	0.265	1106.8	13.75	1623.7	1.456

Table 6.5 Experimental density (ρ), dynamic viscosity (η), surface tension (γ), sound velocity (c) and refractive index (nD) for aq. TESA from 298.15 K to 333.15 K at 0.1 MPa

T / K	TESA mol.kg^{-1}	ρ / kg.m^{-3}	η / mPa.s	γ / mN.m^{-1}	c / m.s^{-1}	nD
298.15	2.432	1018.6	5.32	34.471	1616.9	1.375
303.15	2.432	1015.1	4.37	34.003	1609.1	1.373
308.15	2.432	1011.5	3.78	33.994	1600.7	1.371
313.15	2.432	1007.7	3.42	33.857	1593.9	1.371
318.15	2.432	1003.8	3.00	33.800	1589.5	1.369
323.15	2.432	999.9	2.62	33.588	1584.4	1.368
328.15	2.432	995.9	2.54	33.456	1578.8	1.367
333.15	2.432	991.9	2.22	33.375	1572.4	1.366
298.15	1.506	1016.9	2.56	39.529	1603.3	1.363
303.15	1.506	1013.9	2.55	38.682	1600.8	1.362
308.15	1.506	1010.9	2.50	38.634	1597.6	1.361
313.15	1.506	1007.7	2.28	38.604	1592.0	1.359
318.15	1.506	1004.4	2.15	38.581	1582.9	1.359
323.15	1.506	1000.9	1.99	38.349	1573.5	1.358
328.15	1.506	997.5	1.73	37.998	1563.7	1.357
333.15	1.506	993.9	1.62	37.818	1553.6	1.355
298.15	0.797	1009.7	2.03	46.438	1581.2	1.351
303.15	0.797	1007.6	1.84	45.476	1575.3	1.351
308.15	0.797	1005.2	1.81	44.965	1571.9	1.349
313.15	0.797	1002.6	1.67	43.239	1569.8	1.348
318.15	0.797	999.9	1.60	42.981	1567.5	1.348
323.15	0.797	997.0	1.44	42.018	1565.1	1.347
328.15	0.797	994.0	1.26	41.987	1561.9	1.346
333.15	0.797	990.8	1.03	41.636	1552.0	1.344

Table 6.6 Experimental density (ρ), dynamic viscosity (η), surface tension (γ), sound velocity (c) and refractive index (nD) for aq. (TESA + AEP) from 298.15 K to 333.15 K at 0.1 MPa

T/ K	TESA mol.kg^{-1}	AEP mol.kg^{-1}	ρ / kg.m^{-3}	η / mPa.s	γ / mN.m^{-1}	c / m.s^{-1}	nD
298.15	2.528	0.498	1023.7	7.56	34.607	1640.0	1.383
303.15	2.528	0.498	1020.2	6.27	34.284	1630.8	1.382
308.15	2.528	0.498	1016.4	5.37	33.799	1621.2	1.379
313.15	2.528	0.498	1012.5	4.81	33.503	1611.2	1.379
318.15	2.528	0.498	1008.6	3.67	33.359	1600.7	1.377
323.15	2.528	0.498	1004.6	3.15	33.331	1590.2	1.376
328.15	2.528	0.498	1000.6	2.79	33.284	1579.1	1.375
333.15	2.528	0.498	996.5	2.75	33.221	1567.8	1.372
298.15	2.259	0.756	1026.3	6.67	36.247	1654.6	1.384
303.15	2.259	0.756	1022.7	5.57	35.553	1645.9	1.383
308.15	2.259	0.756	1019.0	4.70	35.229	1636.6	1.381
313.15	2.259	0.756	1015.3	4.01	34.693	1626.9	1.380
318.15	2.259	0.756	1011.4	3.11	34.796	1617.1	1.379
323.15	2.259	0.756	1007.6	2.55	34.714	1606.8	1.377
328.15	2.259	0.756	1003.6	2.28	34.685	1596.2	1.376
333.15	2.259	0.756	999.6	2.26	34.652	1585.2	1.375
298.15	2.044	1.004	1028.4	5.10	37.909	1667.3	1.385
303.15	2.044	1.004	1025.1	3.88	36.634	1659.1	1.384
308.15	2.044	1.004	1021.5	3.01	36.310	1650.3	1.382
313.15	2.044	1.004	1017.9	1.93	36.129	1641.2	1.381
318.15	2.044	1.004	1014.1	1.76	36.065	1631.6	1.379
323.15	2.044	1.004	1010.3	1.54	35.907	1621.8	1.379
328.15	2.044	1.004	1006.5	1.29	35.894	1611.5	1.377
333.15	2.044	1.004	1002.6	0.72	35.801	1600.9	1.377

Table 6.7 Experimental density (ρ), dynamic viscosity (η), surface tension (γ), sound velocity (c) and refractive index (nD) for aq. (TESA + APA) from 298.15 K to 333.15 K at 0.1 MPa

T / K	TESA mol.kg^{-1}	APA mol.kg^{-1}	ρ / kg.m^{-3}	η / mPa.s	γ / mN.m^{-1}	c / m.s^{-1}	nD
298.15	2.528	0.499	1020.9	7.12	34.734	1641.8	1.382
303.15	2.528	0.499	1017.3	6.37	34.568	1632.4	1.381
308.15	2.528	0.499	1013.5	5.46	34.035	1622.6	1.379
313.15	2.528	0.499	1009.6	4.84	33.926	1612.5	1.378
318.15	2.528	0.499	1005.7	4.34	33.754	1602.1	1.377
323.15	2.528	0.499	1001.7	4.01	33.248	1591.4	1.376
328.15	2.528	0.499	997.6	3.68	33.047	1580.4	1.374
333.15	2.528	0.499	993.5	3.50	32.928	1569.0	1.373
298.15	2.259	0.753	1021.6	6.74	36.130	1656.5	1.383
303.15	2.259	0.753	1018.1	5.56	35.621	1647.4	1.382
308.15	2.259	0.753	1014.5	4.72	35.356	1638.2	1.381
313.15	2.259	0.753	1010.8	4.13	35.247	1628.5	1.379
318.15	2.259	0.753	1006.9	3.74	35.101	1618.5	1.378
323.15	2.259	0.753	1003.1	3.31	34.996	1608.2	1.376
328.15	2.259	0.753	999.1	3.01	34.569	1597.5	1.375
333.15	2.259	0.753	995.2	2.87	34.003	1586.6	1.374
298.15	2.044	0.991	1022.3	5.05	37.544	1669.2	1.384
303.15	2.044	0.991	1018.7	3.59	36.589	1660.0	1.383
308.15	2.044	0.991	1015.0	2.75	36.415	1650.8	1.382
313.15	2.044	0.991	1011.2	2.08	36.243	1641.2	1.380
318.15	2.044	0.991	1007.4	1.64	36.113	1631.1	1.379
323.15	2.044	0.991	1003.4	1.1	36.096	1620.8	1.378
328.15	2.044	0.991	999.5	0.61	35.975	1610.2	1.376
333.15	2.044	0.991	995.5	0.55	35.472	1599.2	1.375

Table 6.8 Experimental density (ρ), dynamic viscosity (η), surface tension (γ), sound velocity (c) and refractive index (nD) for aq. [bmim] [Ac] from 298.15 K to 333.15 K at 0.1 MPa

T / K	[bmim][Ac] mol.kg^{-1}	ρ/ kg.m^{-3}	η / mPa.s	γ / mN.m^{-1}	c / m.s^{-1}	nD
298.15	2.500	1029.9	2.66	43.539	1765.3	1.387
303.15	2.500	1027.2	2.63	40.265	1758.3	1.386
308.15	2.500	1024.4	2.56	38.948	1751.1	1.385
313.15	2.500	1021.5	2.49	38.165	1743.3	1.384
318.15	2.500	1018.5	2.29	37.979	1735.3	1.383
323.15	2.500	1015.4	2.26	37.237	1726.8	1.382
328.15	2.500	1012.3	2.02	36.933	1717.9	1.380
333.15	2.500	1009.1	1.97	36.409	1708.7	1.380
298.15	2.251	1024.5	2.35	40.074	1748.9	1.384
303.15	2.251	1022.1	2.29	39.875	1743.2	1.383
308.15	2.251	1022.2	2.25	38.540	1737.0	1.381
313.15	2.251	1019.4	2.23	37.569	1730.4	1.380
318.15	2.251	1016.5	2.11	36.804	1723.3	1.379
323.15	2.251	1013.6	2.07	36.755	1715.7	1.378
328.15	2.251	1010.5	1.91	36.721	1707.7	1.377
333.15	2.251	1007.3	1.86	36.164	1699.3	1.376
298.15	2.006	1023.7	2.23	39.097	1730.9	1.379
303.15	2.006	1020.9	2.18	38.678	1726.4	1.378
308.15	2.006	1019.5	2.16	37.839	1721.4	1.378
313.15	2.006	1016.8	2.13	37.007	1715.9	1.376
318.15	2.006	1013.9	1.74	36.779	1709.9	1.375
323.15	2.006	1011.1	1.58	36.458	1703.4	1.374
328.15	2.006	1008.1	1.51	36.135	1696.5	1.373
333.15	2.006	1004.9	1.24	35.920	1689.0	1.370

Table 6.9 Experimental density (ρ), dynamic viscosity (η), surface tension (γ), sound velocity (c) and refractive index (nD) for aq. ([bmim] [Ac] + AEP) from 298.15 K to 333.15 K at 0.1 MPa

T / K	[bmim][Ac] mol.kg^{-1}	AEP mol.kg^{-1}	ρ / kg.m^{-3}	η / mPa.s	γ / mN.m^{-1}	c / m.s^{-1}	nD
298.15	2.500	0.503	1033.0	3.76	41.931	1786.7	1.394
303.15	2.500	0.503	1030.2	3.66	40.239	1778.5	1.392
308.15	2.500	0.503	1027.3	3.32	37.621	1769.9	1.391
313.15	2.500	0.503	1024.3	3.02	37.456	1761.0	1.390
318.15	2.500	0.503	1021.3	2.64	36.901	1751.8	1.389
323.15	2.500	0.503	1018.1	2.48	36.766	1742.2	1.388
328.15	2.500	0.503	1014.9	2.34	36.391	1732.3	1.387
333.15	2.500	0.503	1011.6	2.21	36.003	1721.9	1.385
298.15	2.251	0.756	1032.9	3.73	42.074	1785.4	1.394
303.15	2.251	0.756	1030.2	3.62	41.565	1777.1	1.393
308.15	2.251	0.756	1027.3	3.32	37.804	1768.5	1.391
313.15	2.251	0.756	1024.3	2.99	37.629	1759.6	1.390
318.15	2.251	0.756	1021.2	2.61	36.981	1750.3	1.389
323.15	2.251	0.756	1018.1	2.41	36.975	1740.8	1.388
328.15	2.251	0.756	1014.9	2.31	36.749	1730.9	1.387
333.15	2.251	0.756	1011.6	2.11	36.288	1720.6	1.386
298.15	2.006	1.004	1032.1	3.70	42.432	1783.9	1.394
303.15	2.006	1.004	1029.4	3.32	41.923	1776.2	1.393
308.15	2.006	1.004	1026.5	3.05	37.976	1767.8	1.392
313.15	2.006	1.004	1023.6	2.97	37.923	1759.1	1.391
318.15	2.006	1.004	1020.5	2.60	37.372	1750.1	1.390
323.15	2.006	1.004	1017.4	2.31	36.953	1740.7	1.389
328.15	2.006	1.004	1014.2	2.16	36.881	1730.9	1.387
333.15	2.006	1.004	1010.9	1.97	36.676	1720.8	1.386

Table 6.10 Experimental density (ρ), dynamic viscosity (η), surface tension (γ), sound velocity (c) and refractive index (nD) for aq. ([bmim] [Ac] + APA) from 298.15 K to 333.15 K at 0.1 MPa

T / K	[bmim][Ac] mol.kg^{-1}	APA mol.kg^{-1}	ρ / kg.m^{-3}	η / mPa.s	γ / mN.m^{-1}	c / m.s^{-1}	nD
298.15	2.500	0.504	1030.1	3.88	39.586	1789.1	1.394
303.15	2.500	0.504	1027.2	3.76	38.237	1780.4	1.393
308.15	2.500	0.504	1024.3	3.32	37.444	1771.4	1.392
313.15	2.500	0.504	1021.2	2.96	37.301	1762.1	1.390
318.15	2.500	0.504	1018.1	2.74	37.218	1752.5	1.389
323.15	2.500	0.504	1014.9	2.62	36.999	1742.6	1.388
328.15	2.500	0.504	1011.7	2.37	36.762	1732.4	1.387
333.15	2.500	0.504	1008.4	2.24	36.609	1721.9	1.386
298.15	2.251	0.753	1028.3	3.54	40.810	1788.4	1.393
303.15	2.251	0.753	1025.5	3.51	39.565	1779.9	1.392
308.15	2.251	0.753	1022.5	3.28	37.935	1770.9	1.391
313.15	2.251	0.753	1019.5	2.95	37.796	1761.7	1.389
318.15	2.251	0.753	1016.4	2.66	37.312	1752.2	1.389
323.15	2.251	0.753	1013.2	2.52	37.658	1742.4	1.388
328.15	2.251	0.753	1009.9	2.34	37.569	1732.3	1.386
333.15	2.251	0.753	1006.7	2.15	37.127	1721.9	1.385
298.15	2.006	0.996	1025.8	3.36	41.895	1786.2	1.393
303.15	2.006	0.996	1023.0	3.32	40.236	1777.9	1.391
308.15	2.006	0.996	1020.1	3.14	38.035	1769.1	1.390
313.15	2.006	0.996	1017.1	2.86	37.960	1760.1	1.389
318.15	2.006	0.996	1014.0	2.61	37.732	1750.7	1.388
323.15	2.006	0.996	1010.9	2.28	37.698	1741.1	1.387
328.15	2.006	0.996	1007.6	1.96	37.695	1731.1	1.386
333.15	2.006	0.996	1004.3	1.77	37.346	1720.8	1.384

Table 6.11 Experimental density (ρ), dynamic viscosity (η), surface tension (γ), sound velocity (c) and refractive index (nD) for aq. (MDEA + 2-MPZ) from 298.15 K to 333.15 K at 0.1 MPa

T/K	MDEA mol.kg^{-1}	2-MPZ mol.kg^{-1}	ρ / kg.m^{-3}	η / mPa.s	γ / mN.m^{-1}	c / m.s^{-1}	nD
298.15	3.509	0.509	1024.3	7.80	53.904	1683.3	1.379
303.15	3.509	0.509	1021.8	6.75	53.777	1680.9	1.379
308.15	3.509	0.509	1019.3	5.84	53.175	1677.7	1.378
313.15	3.509	0.509	1016.6	5.08	52.391	1673.8	1.377
318.15	3.509	0.509	1013.8	4.52	51.459	1669.1	1.376
323.15	3.509	0.509	1010.9	3.84	50.928	1663.6	1.375
328.15	3.509	0.509	1007.8	3.42	50.653	1657.6	1.374
333.15	3.509	0.509	1004.7	3.07	50.019	1650.8	1.373
298.15	3.017	1.008	1022.6	5/31	54.139	1692.9	1.379
303.15	3.017	1.008	1020.1	4.17	54.043	1689.8	1.379
308.15	3.017	1.008	1017.6	3.65	53.544	1685.9	1.378
313.15	3.017	1.008	1014.9	3.64	52.578	1681.4	1.377
318.15	3.017	1.008	1012.0	3.08	51.874	1676.1	1.376
323.15	3.017	1.008	1009.1	2.99	51.441	1670.1	1.375
328.15	3.017	1.008	1005.9	2.73	51.017	1663.5	1.374
333.15	3.017	1.008	1002.8	2.56	50.322	1656.3	1.373
298.15	2.502	1.509	1019.8	3.87	54.705	1696.5	1.381
303.15	2.502	1.509	1017.4	3.21	54.534	1693.3	1.379
308.15	2.502	1.509	1014.9	2.47	53.651	1689.4	1.379
313.15	2.502	1.509	1012.2	2.44	52.954	1684.7	1.378
318.15	2.502	1.509	1009.3	2.36	51.953	1679.4	1.377
323.15	2.502	1.509	1006.4	2.28	51.615	1673.3	1.375
328.15	2.502	1.509	1003.3	2.15	51.138	1666.7	1.375
333.15	2.502	1.509	1000.2	2.08	50.788	1659.5	1.374

Table 6.12 Experimental density (ρ), dynamic viscosity (η), surface tension (γ), sound velocity (c) and refractive index (nD) for aq. ($TMSO_2$ + 2-MPZ) from 298.15 K to 333.15 K at 0.1 MPa

T / K	$TMSO_2$ mol.kg^{-1}	2-MPZ mol.kg^{-1}	ρ/ kg.m^{-3}	η / mPa.s	γ / mN.m^{-1}	c / m.s^{-1}	nD
298.15	3.501	0.509	1067.7	2.67	44.870	1591.8	1.376
303.15	3.501	0.509	1064.9	2.53	44.757	1591.5	1.375
308.15	3.501	0.509	1062.0	2.49	44.316	1590.3	1.374
313.15	3.501	0.509	1059.0	2.38	44.294	1588.2	1.373
318.15	3.501	0.509	1055.9	2.25	44.225	1585.4	1.372
323.15	3.501	0.509	1052.6	2.08	44.214	1581.8	1.371
328.15	3.501	0.509	1049.3	2.03	44.054	1577.61	1.369
333.15	3.501	0.509	1045.8	1.99	43.973	1572.6	1.368
298.15	3.012	1.008	1060.1	2.35	47.492	1610.6	1.377
303.15	3.012	1.008	1057.4	2.14	47.363	1609.6	1.377
308.15	3.012	1.008	1054.5	1.84	47.275	1607.7	1.375
313.15	3.012	1.008	1051.5	1.65	47.169	1605.1	1.374
318.15	3.012	1.008	1048.4	1.48	47.093	1601.7	1.373
323.15	3.012	1.008	1045.2	1.27	46.948	1597.5	1.372
328.15	3.012	1.008	1041.9	1.23	46.543	1592.7	1.371
333.15	3.012	1.008	1038.5	1.11	46.290	1587.3	1.370
298.15	2.500	1.509	1051.6	1.82	48.402	1632.2	1.379
303.15	2.500	1.509	1048.9	1.51	48.258	1630.3	1.378
308.15	2.500	1.509	1046.1	1.38	48.078	1627.6	1.377
313.15	2.500	1.509	1043.1	1.28	47.674	1624.2	1.376
318.15	2.500	1.509	1040.0	1.17	47.416	1620.1	1.375
323.15	2.500	1.509	1036.8	1.05	47.232	1615.3	1.373
328.15	2.500	1.509	1033.5	0.89	46.977	1609.8	1.373
333.15	2.500	1.509	1030.2	0.70	46.801	1603.7	1.371

Table 6.13 Experimental density (ρ), dynamic viscosity (η), surface tension (γ), sound velocity (c) and refractive index (nD) for aq. ([bmim][Ac] + 2-MPZ) from 298.15 K to 333.15 K at 0.1 MPa

T / K	[bmim][Ac] mol.kg^{-1}	2-MPZ mol.kg^{-1}	ρ / kg.m^{-3}	η / mPa.s	γ / mN.m^{-1}	c / m.s^{-1}	nD
298.15	3.507	0.509	1038.8	4.03	39.456	1824.6	1.406
303.15	3.507	0.509	1035.7	3.78	39.181	1813.5	1.404
308.15	3.507	0.509	1032.5	3.72	39.003	1802.1	1.403
313.15	3.507	0.509	1029.2	3.24	38.845	1790.5	1.402
318.15	3.507	0.509	1025.9	3.11	38.745	1778.8	1.400
323.15	3.507	0.509	1022.5	2.89	38.347	1766.8	1.399
328.15	3.507	0.509	1019.1	2.54	37.854	1754.6	1.398
333.15	3.507	0.509	1015.6	2.03	37.448	1742.2	1.397
298.15	3.002	1.008	1035.5	3.58	39.789	1818.4	1.403
303.15	3.002	1.008	1032.3	3.38	39.571	1807.4	1.402
308.15	3.002	1.008	1029.1	3.16	39.184	1796.1	1.401
313.15	3.002	1.008	1025.9	3.02	38.769	1784.9	1.399
318.15	3.002	1.008	1022.6	2.84	38.199	1773.4	1.398
323.15	3.002	1.008	1019.2	2.52	38.055	1761.7	1.397
328.15	3.002	1.008	1015.8	2.47	37.765	1749.6	1.396
333.15	3.002	1.008	1012.4	1.83	37.227	1737.4	1.394
298.15	2.510	1.509	1031.7	3.46	41.203	1810.4	1.401
303.15	2.510	1.509	1028.6	3.23	40.436	1799.7	1.399
308.15	2.510	1.509	1025.5	2.82	39.954	1788.8	1.398
313.15	2.510	1.509	1022.3	2.64	39.236	1777.7	1.397
318.15	2.510	1.509	1018.9	2.39	38.778	1766.3	1.396
323.15	2.510	1.509	1015.6	1.91	38.751	1754.8	1.395
328.15	2.510	1.509	1012.2	1.31	38.594	1743.3	1.394
333.15	2.510	1.509	1008.8	1.16	38.401	1731.3	1.392

The modified Redlich- Kister equation is a semi-empirical model used for correlating density for the aqueous blends of amines [11, 12]. The Redlich-Kister equation also determines the excess molar volume which in turn depends on the molar composition [13]. A similar concept for IL-amine mixtures is utilized here. The equation can be expressed as:

$$V^{E}{}_{jk} = x_j x_k \sum_{p=0}^{N} A_p (x_j - x_k)^p \tag{6.1}$$

Where, V^E_{jk} is in $m^3.kmol^{-1}$, A_p indicates optimized pair parameter which is dependent on temperature and N represents interaction parameters prevailing in the system understudy. The interaction parameters are further expressed in terms of temperature as follows:

$$A_p = r + s(T/K) + t(T/K)^2 \tag{6.2}$$

Eq (6.3) represents the excess volume for the system:

$$V_E = V^{E}{}_{12} \tag{6.3}$$

The experimental density data are used to calculate the excess volume of the IL-amine mixtures using Eq (6.4).

$$V_E = V_m - \sum x_i V_i^o \tag{6.4}$$

Where, V_i^o is the pure component molar volume calculated using the values of experimentally measured density for the systems and V_m represents the molar volume of the IL-amine mixture at the system temperature. The molar volume of the IL-amine mixtures is in turn calculated from the measured density by the following equation:

$$V_m = \frac{\sum x_i M_i}{\rho_m} \tag{6.5}$$

Where, M_i is the pure component molar mass of component i, ρ_m is the experimentally measured liquid density, and x_i is mole fraction of the pure component i.

The temperature dependent parameters of Eq (6.1) for the systems has been calculated by regression of experimental data within the temperature range of (298.15 to 333.15) K (Tables 6.14-

6.18). The % (AAD) between the correlated and experimental results is determined by using Eq (6.6).

$$\%AAD = \frac{1}{n}\left[\sum_{i=1}^{n}\frac{\left|X_{calculated,i} - X_{experimental,i}\right|}{X_{experimental,i}} \times 100\right] \tag{6.6}$$

The standard deviation (SD) between the correlated and experimental results is calculated using Eq (6.7).

$$SD = \left[\sum_{i=1}^{n}\frac{\left(X_{calculated,i} - X_{experimental,i}\right)^2}{(n-1)}\right]^{\frac{1}{2}} \tag{6.7}$$

The AAD's between the experimental and correlated results for all the systems under study are found to be <1 % indicating a good agreement between the experimental and correlated values (Figures 6.1-6.4). The modeled excess molar volume calculated using Eq (6.1) is in turn applied to evaluate the modeled density of the solvent mixtures.

Table 6.14 Binary Redlich-Kister interaction parameters (A_0, A_1, and A_2) for the excess volume of density (ρ) of the (i) (HEF + AEP) & (ii) (HEF + AMP) systems

Parameters		(i) HEF + AEP	(ii) HEF + AMP
A_0	$r\times10^3$	2.709	-23.476
	$s\times10^5$	-4.362	14.943
	$t\times10^9$	8.822	-286.019
A_1	$r\times10^2$	-1.921	-1.461
	$s\times10^5$	10.131	8.771
	$t\times10^7$	-1.483	-1.255
A_2	$r\times10^2$	2.727	-3.084
	$s\times10^4$	-1.472	1.702
	$t\times10^7$	1.801	-2.499
100AAD		0.055	0.120
SD		0.714	1.529

Table 6.15 Binary Redlich-Kister interaction parameters (A_0, A_1, and A_2) for the excess volume of density (ρ) of the (i) aq. TESA, (ii) aq. (TESA + AEP) & (ii) aq. (TESA + APA) systems

Parameters		aq. TESA	aq. (TESA + AEP)			aq. (TESA + APA)		
		TESA + H_2O	TESA + AEP	AEP + H_2O	TESA + H_2O	TESA + APA	APA + H_2O	TESA + H_2O
A_0	*r*	-2.442×10^{2}	-1.184×10^{-1}	2.062×10^{-1}	2.913×10^{-1}	5.227×10^{-1}	-8.865×10^{-1}	-1.349
	s	1.641	5.604×10^{-4}	-1.018×10^{-3}	-1.411×10^{-3}	-1.793×10^{-3}	3.061×10^{-3}	4.641×10^{-3}
	t	-2.742×10^{-3}	-6.199×10^{-7}	1.104×10^{-6}	1.530×10^{-6}	8.788×10^{-8}	-3.332×10^{-7}	-4.078×10^{-7}
A_1	*r*	-5.141×10^{2}	-1.106×10^{-2}	2.385×10^{-2}	8.271×10^{-2}	4.703×10^{-2}	-2.086×10^{-2}	-1.564×10^{-1}
	s	3.456	5.247×10^{-5}	-7.715×10^{-5}	-3.657×10^{-4}	-1.614×10^{-4}	5.326×10^{-5}	5.235×10^{-4}
	t	-5.777×10^{-3}	-5.798×10^{-8}	1.042×10^{-7}	4.306×10^{-7}	8.378×10^{-9}	1.580×10^{-7}	1.262×10^{-7}
A_2	*r*	-2.705×10^{2}	-1.875×10^{-4}	-2.228×10^{-1}	-3.863×10^{-1}	8.016×10^{-4}	8.063×10^{-1}	1.376
	s	1.819	8.901×10^{-7}	1.024×10^{-3}	1.808×10^{-3}	-2.750×10^{-6}	-2.749×10^{-3}	-4.710×10^{-3}
	t	-3.041×10^{-3}	-9.836×10^{-10}	-1.149×10^{-6}	-2.022×10^{-6}	1.444×10^{-10}	-5.488×10^{-9}	1.035×10^{-7}
100AAD		5.811×10^{-3}	1.713×10^{-3}			1.457×10^{-3}		
SD		8.267×10^{-2}	2.057×10^{-2}			1.843×10^{-2}		

Table 6.16 Binary Redlich-Kister interaction parameters (A_0, A_1, and A_2) for the excess volume of density (ρ) of the (i) aq. [bmim] [Ac], (ii) aq. ([bmim] [Ac] + AEP) & (ii) aq. ([bmim] [Ac] + APA) systems

System		aq. [bmim][Ac]	aq. ([bmim] [Ac]+AEP)			aq.([bmim] [Ac]+APA)		
Parameters		[bmim] [Ac]+H_2O	[bmim] [Ac]+AEP	AEP+H_2O	[bmim] [Ac]+H_2O	[bmim] [Ac]+APA	APA+H_2O	[bmim] [Ac]+H_2O
A_0	*r*	-3.9428×10^{3}	-4.0175×10^{-1}	3.9713×10^{-1}	3.4342×10^{-1}	-7.2478×10^{-1}	6.8130×10^{-1}	6.2001×10^{-1}
	s	2.4453×10	1.4067×10^{-3}	-1.3998×10^{-3}	-1.1733×10^{-3}	3.9528×10^{-3}	-3.7429×10^{-3}	-3.4070×10^{-3}
	t	-3.7870×10^{-2}	-1.4076×10^{-6}	1.3858×10^{-6}	1.1475×10^{-6}	-6.2994×10^{-6}	5.9735×10^{-6}	5.4801×10^{-6}
A_1	*r*	-8.5444×10^{3}	-3.2055×10^{-2}	4.0196×10^{-2}	7.9695×10^{-2}	-5.6956×10^{-2}	6.2030×10^{-2}	1.2247×10^{-1}
	s	5.2992×10	1.1227×10^{-4}	-1.3241×10^{-4}	-3.0525×10^{-4}	3.1069×10^{-4}	-3.1381×10^{-4}	-6.4492×10^{-4}
	t	-8.2070×10^{-2}	-1.1230×10^{-7}	1.4583×10^{-7}	3.2922×10^{-7}	-4.9515×10^{-7}	4.9247×10^{-7}	9.8251×10^{-7}
A_2	*r*	-4.6288×10^{3}	-5.7973×10^{-4}	-4.1769×10^{-1}	-4.1492×10^{-1}	-1.0253×10^{-3}	-7.0393×10^{-1}	-7.0901×10^{-1}
	s	2.8707×10	2.0308×10^{-6}	1.4551×10^{-3}	1.4764×10^{-3}	5.5932×10^{-6}	3.8171×10^{-3}	3.8461×10^{-3}
	t	-4.4460×10^{-2}	-2.0313×10^{-9}	-1.4679×10^{-6}	-1.4986×10^{-6}	-8.9138×10^{-9}	-6.0764×10^{-6}	-6.0888×10^{-6}
100AAD		1.9536×10^{-2}		9.9260×10^{-4}			9.2511×10^{-4}	
SD		3.3875×10^{-1}		1.2589×10^{-2}			1.2153×10^{-2}	

Table 6.17 Binary Redlich-Kister interaction parameters (A_0, A_1, and A_2) for the excess volume of density (ρ) of the (i) aq. (MDEA + 2-MPZ) and (ii) aq. ($TMSO_2$ + 2-MPZ)

		aq. (MDEA + 2-MPZ)			aq. ($TMSO_2$ + 2-MPZ)		
Parameters		MDEA + 2-MPZ	2-MPZ + H_2O	MDEA + H_2O	$TMSO_2$ + 2-MPZ	2-MPZ + H_2O	$TMSO_2$ + H_2O
A_0	*r*	6.433×10^{-2}	-7.434×10^{-2}	-5.409×10^{-2}	3.306×10^{-2}	-4.939×10^{-2}	-3.057×10^{-2}
	s	-9.828×10^{-4}	9.198×10^{-4}	7.068×10^{-4}	-1.971×10^{-4}	2.417×10^{-4}	1.081×10^{-4}
	t	2.138×10^{-6}	-1.956×10^{-6}	-1.502×10^{-6}	9.277×10^{-8}	-1.701×10^{-7}	-1.608×10^{-8}
A_1	*r*	6.662×10^{-3}	1.009×10^{-2}	8.873×10^{-4}	3.477×10^{-3}	1.428×10^{-2}	2.610×10^{-3}
	s	-1.010×10^{-4}	3.362×10^{-5}	9.189×10^{-5}	-2.053×10^{-5}	-3.934×10^{-5}	4.906×10^{-5}
	t	2.194×10^{-7}	-1.124×10^{-7}	-2.312×10^{-7}	9.890×10^{-9}	6.741×10^{-8}	-5.281×10^{-8}
A_2	*r*	1.692×10^{-4}	4.285×10^{-2}	3.740×10^{-2}	8.848×10^{-5}	1.473×10^{-2}	1.759×10^{-2}
	s	-2.559×10^{-6}	-8.174×10^{-4}	-6.648×10^{-4}	-5.219×10^{-7}	-1.275×10^{-4}	-1.613×10^{-4}
	t	5.561×10^{-9}	1.812×10^{-6}	1.474×10^{-6}	2.538×10^{-10}	1.767×10^{-8}	1.012×10^{-7}
100AAD			3.788×10^{-3}			6.075×10^{-3}	
SD			5.446×10^{-2}			7.536×10^{-2}	

Table 6.18 Binary Redlich-Kister interaction parameters (A_0, A_1, and A_2) for the excess volume of density (ρ) of aq. ([bmim] [Ac] + 2-MPZ) system

		aq. ([bmim] [Ac] + 2-MPZ)		
Parameters		[bmim] [Ac] + 2-MPZ	2-MPZ + H_2O	[bmim] [Ac] + H_2O
A_0	*r*	-1.851×10^{-1}	1.667×10^{-1}	1.583×10^{-1}
	s	1.119×10^{-3}	-1.066×10^{-3}	-1.003×10^{-3}
	t	-1.733×10^{-6}	1.674×10^{-6}	1.601×10^{-6}
A_1	*r*	-1.948×10^{-2}	4.001×10^{-2}	6.426×10^{-2}
	s	1.180×10^{-4}	-1.915×10^{-4}	-3.487×10^{-4}
	t	-1.828×10^{-7}	2.770×10^{-7}	4.996×10^{-7}
A_2	*r*	-4.798×10^{-4}	-2.099×10^{-1}	-2.274×10^{-1}
	s	2.907×10^{-6}	1.225×10^{-3}	1.340×10^{-3}
	t	-4.505×10^{-9}	-1.881×10^{-6}	-2.041×10^{-6}
100AAD			9.301×10^{-4}	
SD			1.250×10^{-2}	

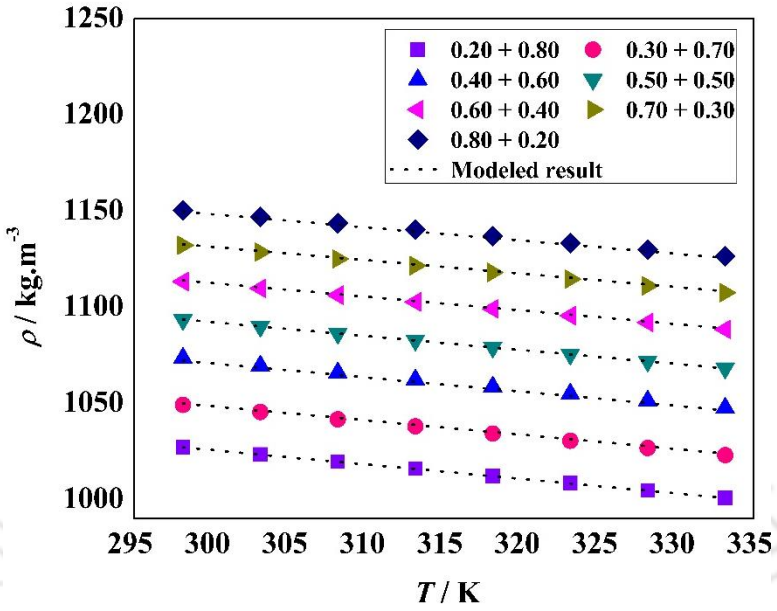

Figure 6.1 Density of (**HEF + AEP**) system at various temperatures and composition (mass fraction)

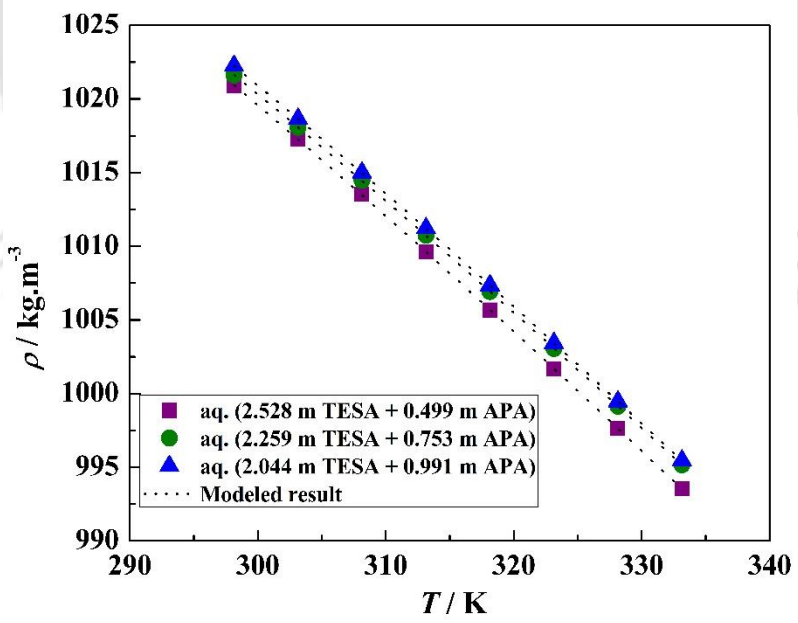

Figure 6.2 Density of aqueous **(TESA + APA**) system at various temperatures and composition (molal)

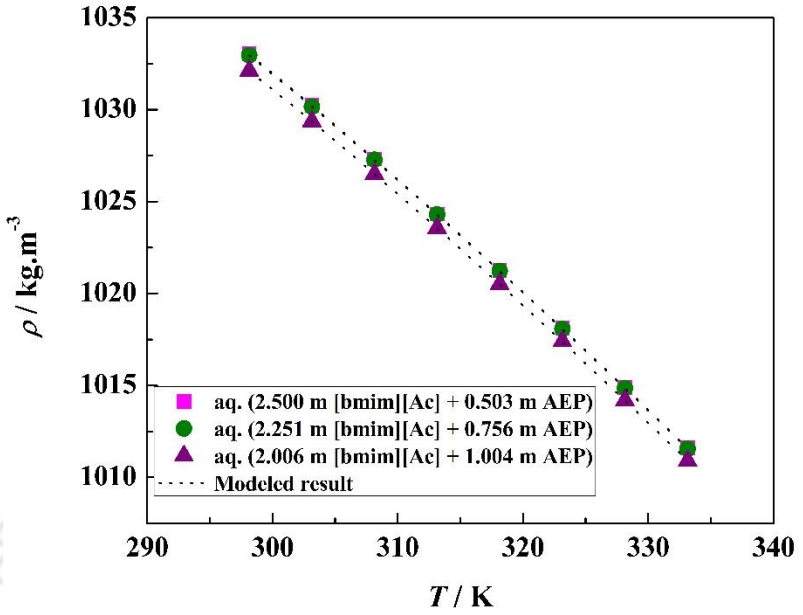

Figure 6.3 Density of aqueous (**[bmim][Ac] + AEP**) system at various temperatures and composition (molal)

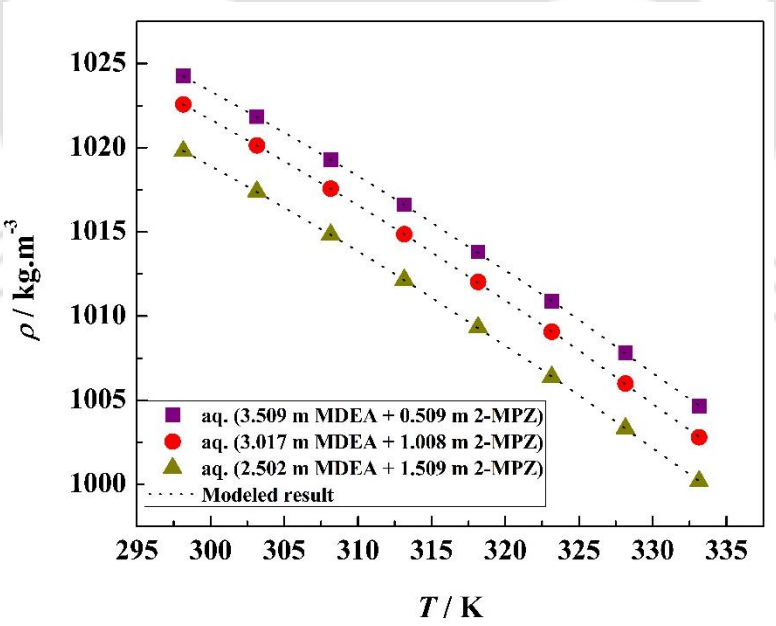

Figure 6.4 Density of aqueous (**MDEA + 2-MPZ**) system at various temperatures and composition (molal)

The behavior of excess molar volumes for all the systems at studied range of temperatures are found to be either positive or negative depending on each systems individual interaction amid the constituent molecules (Table 6.19-6.29). Since the deviations in the two consecutive values of excess molar are very less, the values are presented till fourth significant digit after the decimal place. Excess molar volume may be discussed in terms of several effects such as physical, chemical, and geometrical contributions. The physical interactions involve mainly dispersion forces giving a positive contribution. The chemical interactions result in the overall volume contraction and this includes mainly charge transfer type forces, hydrogen bond formation / breakage, and other complex interactions like donor-acceptor, dipole-dipole, and dipole induced dipole. And finally, the structural contributions which arises from the geometrical fitting of one component into the other, due to deviations in molar volume and free volume between the constituents result in a negative contribution to the excess molar volume. The interactions among the unlike molecules is indicated by the negative values of excess molar volume.

Table 6.19 (a) Estimated excess molar volumes (V_E), kinematic viscosities deviations ($\delta\upsilon$), thermal expansion coefficients (α), diffusivity (D_{N2O}, D_{CO2}), isentropic compressibility (Ks) and Gibbs energies of activation of viscous flow (ΔG^0) for (HEF + AEP) from 298.15 K to 333.15 K at 0.1 MPa

T / K	Mole fraction (HEF)	Mole fraction (AEP)	V_E / $m^3.kgmol^{-1}$	$\delta\upsilon \times 10^6$ / m^2s^{-1}	$\alpha \times 10^3$/ K^{-1}	$D_{N2O} \times 10^{11}$ / m^2s^{-1}	$D_{CO2} \times 10^{11}$ / m^2s^{-1}	$Ks \times 10^9$/ $m.s^{-2}.kg^{-1}$	ΔG^0/kJmol^{-1}
298.15	0.232	0.768	-1.524×10^{-3}	99.682	0.732	3.308	3.570	0.362	60.474
303.15	0.232	0.768	-1.570×10^{-3}	54.826	0.735	5.080	5.407	0.370	60.281
308.15	0.232	0.768	-1.616×10^{-3}	8.611	0.737	12.200	12.811	0.379	58.622
313.15	0.232	0.768	-1.661×10^{-3}	6.129	0.740	15.706	16.279	0.389	58.908
318.15	0.232	0.768	-1.706×10^{-3}	4.035	0.743	20.007	20.476	0.399	59.210
323.15	0.232	0.768	-1.751×10^{-3}	2.976	0.746	25.006	25.279	0.409	59.557
328.15	0.232	0.768	-1.796×10^{-3}	1.774	0.748	30.843	30.812	0.419	59.931
333.15	0.232	0.768	-1.840×10^{-3}	0.970	0.751	37.757	37.288	0.429	60.315
298.15	0.341	0.659	-2.006×10^{-3}	205.673	0.711	1.961	2.116	0.342	61.994
303.15	0.341	0.659	-2.053×10^{-3}	152.637	0.713	2.564	2.729	0.350	62.333
308.15	0.341	0.659	-2.100×10^{-3}	107.996	0.716	3.479	3.653	0.358	62.535
313.15	0.341	0.659	-2.147×10^{-3}	80.209	0.718	4.572	4.739	0.367	62.817
318.15	0.341	0.659	-2.195×10^{-3}	60.498	0.721	5.917	6.056	0.376	63.129
323.15	0.341	0.659	-2.243×10^{-3}	46.813	0.723	7.537	7.619	0.384	63.474
328.15	0.341	0.659	-2.292×10^{-3}	36.379	0.726	9.479	9.469	0.394	63.842
333.15	0.341	0.659	-2.342×10^{-3}	28.904	0.729	11.743	11.597	0.403	64.244
298.15	0.446	0.554	-2.306×10^{-3}	314.909	0.686	1.406	1.517	0.323	62.920
303.15	0.446	0.554	-2.350×10^{-3}	217.217	0.689	1.945	2.070	0.331	63.097
308.15	0.446	0.554	-2.394×10^{-3}	153.296	0.691	2.651	2.784	0.338	63.297
313.15	0.446	0.554	-2.440×10^{-3}	111.959	0.694	3.528	3.656	0.346	63.551
318.15	0.446	0.554	-2.487×10^{-3}	82.829	0.696	4.632	4.741	0.353	63.826
323.15	0.446	0.554	-2.535×10^{-3}	64.191	0.698	5.898	5.962	0.361	64.183
328.15	0.446	0.554	-2.585×10^{-3}	49.362	0.701	7.489	7.482	0.369	64.529
333.15	0.446	0.554	-2.635×10^{-3}	39.225	0.703	9.299	9.184	0.378	64.933

Table 6.19 (b) Estimated excess molar volumes (V_E), kinematic viscosities deviations ($\delta\upsilon$), thermal expansion coefficients (α), diffusivity (D_{N2O}, D_{CO2}), isentropic compressibility (Ks) and Gibbs energies of activation of viscous flow (ΔG^0) for (HEF + AEP) from 298.15 K to 333.15 K at 0.1 MPa

T / K	Mole fraction (HEF)	Mole fraction (AEP)	V_E / $m^3.kgmol^{-1}$	$\delta\upsilon \times 10^6$ / m^2s^{-1}	$\alpha \times 10^3$/ K^{-1}	$D_{N2O} \times 10^{11}$ / m^2s^{-1}	$D_{CO2} \times 10^{11}$ / m^2s^{-1}	$K_s \times 10^9$/ $m.s^{-2}.kg^{-1}$	ΔG^0/ $kJmol^{-1}$
298.15	0.547	0.453	-2.420×10^{-3}	383.454	0.658	1.189	1.284	0.311	63.344
303.15	0.547	0.453	-2.461×10^{-3}	259.884	0.660	1.670	1.778	0.317	63.482
308.15	0.547	0.453	-2.504×10^{-3}	182.688	0.662	2.284	2.398	0.324	63.677
313.15	0.547	0.453	-2.548×10^{-3}	132.759	0.664	3.049	3.160	0.331	63.926
318.15	0.547	0.453	-2.593×10^{-3}	98.107	0.667	4.008	4.102	0.338	64.204
323.15	0.547	0.453	-2.640×10^{-3}	74.819	0.669	5.156	5.212	0.345	64.532
328.15	0.547	0.453	-2.688×10^{-3}	57.337	0.671	6.565	6.559	0.352	64.873
333.15	0.547	0.453	-2.737×10^{-3}	45.349	0.673	8.180	8.079	0.359	65.270
298.15	0.644	0.356	-2.342×10^{-3}	366.732	0.639	1.199	1.294	0.299	63.229
303.15	0.644	0.356	-2.383×10^{-3}	251.494	0.641	1.667	1.774	0.306	63.396
308.15	0.644	0.356	-2.425×10^{-3}	179.624	0.643	2.250	2.363	0.312	63.631
313.15	0.644	0.356	-2.467×10^{-3}	130.494	0.645	2.998	3.107	0.318	63.886
318.15	0.644	0.356	-2.511×10^{-3}	97.110	0.647	3.915	4.006	0.325	64.184
323.15	0.644	0.356	-2.555×10^{-3}	74.028	0.649	5.026	5.082	0.331	64.517
328.15	0.644	0.356	-2.601×10^{-3}	58.378	0.651	6.277	6.271	0.338	64.925
333.15	0.644	0.356	-2.647×10^{-3}	45.144	0.653	7.920	7.822	0.345	65.279
298.15	0.738	0.262	-2.068×10^{-3}	262.544	0.618	1.472	1.589	0.293	62.508
303.15	0.738	0.262	-2.107×10^{-3}	186.024	0.620	1.990	2.118	0.298	62.749
308.15	0.738	0.262	-2.147×10^{-3}	134.867	0.622	2.644	2.776	0.304	63.025
313.15	0.738	0.262	-2.187×10^{-3}	101.136	0.624	3.432	3.557	0.309	63.354
318.15	0.738	0.262	-2.227×10^{-3}	76.688	0.626	4.405	4.508	0.315	63.701
323.15	0.738	0.262	-2.268×10^{-3}	59.473	0.628	5.569	5.630	0.321	64.078
328.15	0.738	0.262	-2.309×10^{-3}	46.377	0.630	6.969	6.962	0.327	64.471
333.15	0.738	0.262	-2.351×10^{-3}	37.258	0.632	8.559	8.453	0.334	64.912
298.15	0.828	0.172	-1.590×10^{-3}	171.937	0.594	1.873	2.021	0.287	61.678
303.15	0.828	0.172	-1.625×10^{-3}	124.342	0.596	2.482	2.642	0.292	61.968
308.15	0.828	0.172	-1.659×10^{-3}	91.701	0.598	3.236	3.398	0.297	62.290
313.15	0.828	0.172	-1.694×10^{-3}	69.417	0.599	4.146	4.297	0.303	62.649
318.15	0.828	0.172	-1.728×10^{-3}	53.527	0.601	5.229	5.352	0.308	63.042
323.15	0.828	0.172	-1.761×10^{-3}	42.603	0.603	6.479	6.550	0.313	63.477
328.15	0.828	0.172	-1.795×10^{-3}	33.849	0.605	7.971	7.963	0.319	63.919
333.15	0.828	0.172	-1.828×10^{-3}	27.747	0.607	9.641	9.522	0.325	64.403

Table 6.20 (a) Estimated excess molar volumes (V_E), kinematic viscosities deviations ($\delta\upsilon$), thermal expansion coefficients (α), diffusivity (D_{N2O}, D_{CO2}), isentropic compressibility (Ks) and Gibbs energies of activation of viscous flow (ΔG^0) for (HEF + AMP) from 298.15 K to 333.15 K at 0.1 MPa

T / K	Mole fraction (HEF)	Mole fraction (AMP)	V_E / $m^3.kgmol^{-1}$	$\delta\upsilon \times 10^6$ / m^2s^{-1}	$\alpha \times 10^3$/ K^{-1}	$D_{N2O}\times 10^{11}$ / m^2s^{-1}	$D_{CO2}\times 10^{11}$/ m^2s^{-1}	$Ks \times 10^9$/ $m.s^{-2}.kg^{-1}$	ΔG^0/ $kJmol^{-1}$
298.15	0.232	0.768	-1.379×10^{-3}	42.819	0.797	2.663	2.874	0.409	60.499
303.15	0.232	0.768	-1.453×10^{-3}	22.194	0.801	3.714	3.953	0.419	60.612
308.15	0.232	0.768	-1.492×10^{-3}	13.484	0.804	5.205	5.465	0.431	60.684
313.15	0.232	0.768	-1.496×10^{-3}	10.762	0.807	7.141	7.401	0.442	60.797
318.15	0.232	0.768	-1.466×10^{-3}	9.829	0.810	9.609	9.834	0.454	60.949
323.15	0.232	0.768	-1.401×10^{-3}	6.539	0.814	12.769	12.909	0.466	61.118
328.15	0.232	0.768	-1.300×10^{-3}	4.492	0.817	16.652	16.635	0.478	61.328
333.15	0.232	0.768	-1.166×10^{-3}	3.409	0.820	21.393	21.127	0.491	61.567
298.15	0.341	0.659	-1.580×10^{-3}	39.566	0.759	2.733	2.949	0.387	60.403
303.15	0.341	0.659	-1.664×10^{-3}	18.035	0.762	3.865	4.114	0.397	60.469
308.15	0.341	0.659	-1.712×10^{-3}	10.954	0.765	5.369	5.639	0.407	60.566
313.15	0.341	0.659	-1.724×10^{-3}	9.189	0.768	7.280	7.545	0.417	60.716
318.15	0.341	0.659	-1.701×10^{-3}	8.325	0.771	9.752	9.981	0.427	60.881
323.15	0.341	0.659	-1.642×10^{-3}	5.576	0.774	12.831	12.971	0.438	61.082
328.15	0.341	0.659	-1.547×10^{-3}	3.739	0.777	16.622	16.605	0.449	61.313
333.15	0.341	0.659	-1.417×10^{-3}	2.822	0.779	21.186	20.922	0.461	61.578
298.15	0.446	0.554	-1.592×10^{-3}	25.819	0.715	2.978	3.215	0.366	60.118
303.15	0.446	0.554	-1.674×10^{-3}	10.410	0.717	4.156	4.424	0.375	60.221
308.15	0.446	0.554	-1.726×10^{-3}	7.004	0.719	5.649	5.931	0.383	60.384
313.15	0.446	0.554	-1.746×10^{-3}	6.289	0.723	7.583	7.859	0.392	60.562
318.15	0.446	0.554	-1.735×10^{-3}	6.336	0.725	9.997	10.231	0.401	60.777
323.15	0.446	0.554	-1.694×10^{-3}	4.356	0.728	12.968	13.109	0.410	61.023
328.15	0.446	0.554	-1.622×10^{-3}	2.857	0.730	16.635	16.619	0.420	61.286
333.15	0.446	0.554	-1.519×10^{-3}	2.099	0.733	21.045	20.784	0.430	61.576

Table 6.20 (b) Estimated excess molar volumes (V_E), kinematic viscosities deviations ($\delta\upsilon$), thermal expansion coefficients (α), diffusivity (D_{N2O}, D_{CO2}), isentropic compressibility (Ks) and Gibbs energies of activation of viscous flow (ΔG^0) for (HEF + AMP) from 298.15 K to 333.15 K at 0.1 MPa

T / K	Mole fraction (HEF)	Mole fraction (AMP)	V_E / $m^3.kgmol^{-1}$	$\delta\upsilon \times 10^6$ / m^2s^{-1}	$\alpha \times 10^3$/ K^{-1}	$D_{N2O} \times 10^{11}$ / m^2s^{-1}	$D_{CO2} \times 10^{11}$/ m^2s^{-1}	$Ks \times 10^9$/ $m.s^{-2}.kg^{-1}$	ΔG^0/ $kJmol^{-1}$
298.15	0.547	0.453	-1.505×10^{-3}	8.672	0.684	3.382	3.649	0.347	59.708
303.15	0.547	0.453	-1.577×10^{-3}	1.052	0.686	4.608	4.905	0.354	59.878
308.15	0.547	0.453	-1.626×10^{-3}	0.421	0.688	6.194	6.504	0.362	60.069
313.15	0.547	0.453	-1.651×10^{-3}	1.608	0.691	8.186	8.484	0.369	60.294
318.15	0.547	0.453	-1.652×10^{-3}	2.687	0.693	10.655	10.905	0.378	60.546
323.15	0.547	0.453	-1.631×10^{-3}	1.729	0.696	13.642	13.791	0.386	60.832
328.15	0.547	0.453	-1.586×10^{-3}	0.959	0.698	17.252	17.235	0.395	61.141
333.15	0.547	0.453	-1.517×10^{-3}	0.648	0.700	21.564	21.296	0.403	61.470
298.15	0.644	0.356	-1.380×10^{-3}	-3.899	0.658	3.855	4.160	0.333	59.301
303.15	0.644	0.356	-1.438×10^{-3}	-6.573	0.660	5.169	5.502	0.339	59.515
308.15	0.644	0.356	-1.480×10^{-3}	-5.031	0.662	6.855	7.198	0.347	59.743
313.15	0.644	0.356	-1.505×10^{-3}	-2.567	0.665	8.925	9.249	0.354	60.010
318.15	0.644	0.356	-1.514×10^{-3}	-0.818	0.667	11.485	11.754	0.361	60.295
323.15	0.644	0.356	-1.506×10^{-3}	-0.989	0.669	14.556	14.715	0.368	60.611
328.15	0.644	0.356	-1.482×10^{-3}	-1.209	0.671	18.225	18.207	0.376	60.949
333.15	0.644	0.356	-1.442×10^{-3}	-1.081	0.674	22.514	22.234	0.384	61.317
298.15	0.738	0.262	-1.243×10^{-3}	-18.651	0.650	4.659	5.029	0.317	58.707
303.15	0.738	0.262	-1.286×10^{-3}	-16.611	0.652	6.168	6.565	0.324	58.952
308.15	0.738	0.262	-1.318×10^{-3}	-12.336	0.655	8.016	8.417	0.330	59.236
313.15	0.738	0.262	-1.338×10^{-3}	-8.570	0.657	10.304	10.679	0.336	59.536
318.15	0.738	0.262	-1.346×10^{-3}	-5.694	0.659	13.016	13.321	0.343	59.875
323.15	0.738	0.262	-1.343×10^{-3}	-4.784	0.661	16.258	16.436	0.349	60.233
328.15	0.738	0.262	-1.328×10^{-3}	-4.205	0.663	20.048	20.029	0.356	60.617
333.15	0.738	0.262	-1.302×10^{-3}	-3.606	0.665	24.543	24.238	0.363	61.009
298.15	0.828	0.172	-1.061×10^{-3}	-30.094	0.625	5.818	6.279	0.304	58.007
303.15	0.828	0.172	-1.090×10^{-3}	-24.074	0.627	7.511	7.994	0.309	58.319
308.15	0.828	0.172	-1.111×10^{-3}	-18.485	0.629	9.609	10.091	0.314	58.642
313.15	0.828	0.172	-1.122×10^{-3}	-13.917	0.631	12.162	12.606	0.319	58.983
318.15	0.828	0.172	-1.123×10^{-3}	-10.531	0.633	15.165	15.519	0.325	59.356
323.15	0.828	0.172	-1.116×10^{-3}	-8.751	0.635	18.692	18.897	0.331	59.749
328.15	0.828	0.172	-1.099×10^{-3}	-7.550	0.637	22.792	22.769	0.337	60.165
333.15	0.828	0.172	-1.072×10^{-3}	-6.361	0.639	27.427	27.086	0.343	60.609

Table 6.21 Estimated excess molar volumes (V_E), kinematic viscosities deviations ($\delta\upsilon$), thermal expansion coefficients (α), diffusivity (D_{N2O}, D_{CO2}), isentropic compressibility (Ks) and Gibbs energies of activation of viscous flow (ΔG^0) for aq. TESA from 298.15 K to 333.15 K at 0.1 MPa

T / K	TESA mol.kg^{-1}	V_E / m^3.kgmol^{-1}	$\delta\upsilon$ ×10^6 / m^{2}s^{-1}	α ×10^3/ K^{-1}	D_{N2O}× 10^9 / m^{2}s^{-1}	D_{CO2}×10^9 / m^{2}s^{-1}	Ks ×10^9/ m.s^{-2}.kg^{-1}	ΔG^0/ kJmol^{-1}
298.15	2.432	-1.093×10^{-3}	4.257	0.750	0.426	0.460	0.376	48.749
303.15	2.432	-1.074×10^{-3}	3.383	0.753	0.522	0.555	0.380	49.075
308.15	2.432	-1.060×10^{-3}	2.948	0.755	0.612	0.642	0.386	49.527
313.15	2.432	-1.050×10^{-3}	2.652	0.758	0.696	0.722	0.391	50.067
318.15	2.432	-1.043×10^{-3}	2.336	0.761	0.806	0.825	0.394	50.544
323.15	2.432	-1.041×10^{-3}	2.005	0.764	0.945	0.956	0.398	50.969
328.15	2.432	-1.042×10^{-3}	1.992	0.767	1.011	1.010	0.403	51.698
333.15	2.432	-1.048×10^{-3}	1.701	0.770	1.185	1.169	0.408	52.109
298.15	1.506	-7.896×10^{-4}	1.573	0.647	0.766	0.827	0.383	46.625
303.15	1.506	-7.800×10^{-4}	1.622	0.649	0.803	0.854	0.385	47.402
308.15	1.506	-7.685×10^{-4}	1.708	0.651	0.852	0.895	0.388	48.143
313.15	1.506	-7.552×10^{-4}	1.562	0.653	0.959	0.995	0.392	48.693
318.15	1.506	-7.400×10^{-4}	1.502	0.655	1.055	1.079	0.397	49.319
323.15	1.506	-7.229×10^{-4}	1.403	0.658	1.174	1.187	0.403	49.897
328.15	1.506	-7.040×10^{-4}	1.188	0.659	1.378	1.377	0.410	50.292
333.15	1.506	-6.833×10^{-4}	1.125	0.662	1.517	1.498	0.417	50.895
298.15	0.797	-4.420×10^{-4}	1.083	0.537	0.923	0.996	0.396	45.784
303.15	0.797	-4.386×10^{-4}	0.957	0.539	1.041	1.108	0.400	46.315
308.15	0.797	-4.352×10^{-4}	1.050	0.539	1.105	1.161	0.401	47.035
313.15	0.797	-4.318×10^{-4}	0.979	0.541	1.234	1.279	0.405	47.593
318.15	0.797	-4.284×10^{-4}	0.984	0.543	1.332	1.363	0.407	48.261
323.15	0.797	-4.250×10^{-4}	0.877	0.544	1.518	1.534	0.409	48.743
328.15	0.797	-4.216×10^{-4}	0.740	0.546	1.772	1.770	0.412	49.136
333.15	0.797	-4.182×10^{-4}	0.551	0.548	2.176	2.149	0.419	49.343

Table 6.22 Estimated excess molar volumes (V_E), kinematic viscosities deviations (δv), thermal expansion coefficients (α), diffusivity (D_{N2O}, D_{CO2}), isentropic compressibility (Ks) and Gibbs energies of activation of viscous flow (ΔG^0) for aq. (TESA + AEP) from 298.15 K to 333.15 K at 0.1 MPa

T / K	TESA mol.kg^{-1}	AEP mol.kg^{-1}	V_E / m^3.kgmol^{-1}	δv ×10^6 / m^{2}s^{-1}	α ×10^3/ K^{-1}	D_{N2O}× 10^9 / m^{2}s^{-1}	D_{CO2}×10^9 / m^{2}s^{-1}	Ks ×10^9/ m.s^{-2}.kg^{-1}	ΔG^0/ kJmol^{-1}
298.15	2.528	0.498	-1.288×10^{-3}	6.296	0.762	0.322	0.348	0.363	49.715
303.15	2.528	0.498	-1.271×10^{-3}	5.110	0.765	0.391	0.416	0.369	50.085
308.15	2.528	0.498	-1.255×10^{-3}	4.394	0.767	0.462	0.486	0.374	50.523
313.15	2.528	0.498	-1.240×10^{-3}	3.946	0.770	0.529	0.548	0.381	51.064
318.15	2.528	0.498	-1.226×10^{-3}	2.919	0.773	0.688	0.704	0.387	51.174
323.15	2.528	0.498	-1.213×10^{-3}	2.481	0.776	0.814	0.823	0.394	51.578
328.15	2.528	0.498	-1.201×10^{-3}	2.188	0.779	0.938	0.937	0.401	52.061
333.15	2.528	0.498	-1.191×10^{-3}	2.192	0.783	0.995	0.983	0.408	52.820
298.15	2.259	0.756	-1.291×10^{-3}	5.355	0.741	0.356	0.384	0.356	49.358
303.15	2.259	0.756	-1.276×10^{-3}	4.357	0.744	0.429	0.457	0.361	49.739
308.15	2.259	0.756	-1.262×10^{-3}	3.688	0.746	0.514	0.539	0.366	50.137
313.15	2.259	0.756	-1.248×10^{-3}	3.117	0.749	0.612	0.634	0.372	50.542
318.15	2.259	0.756	-1.236×10^{-3}	2.335	0.752	0.784	0.803	0.378	50.689
323.15	2.259	0.756	-1.225×10^{-3}	1.861	0.755	0.963	0.974	0.384	50.961
328.15	2.259	0.756	-1.215×10^{-3}	1.659	0.758	1.101	1.099	0.391	51.462
333.15	2.259	0.756	-1.206×10^{-3}	1.689	0.761	1.161	1.147	0.398	52.233
298.15	2.044	1.004	-1.304×10^{-3}	3.766	0.721	0.441	0.476	0.349	48.664
303.15	2.044	1.004	-1.291×10^{-3}	2.648	0.723	0.573	0.610	0.354	48.799
308.15	2.044	1.004	-1.279×10^{-3}	1.981	0.726	0.734	0.771	0.359	48.962
313.15	2.044	1.004	-1.268×10^{-3}	1.035	0.728	1.098	1.138	0.365	48.603
318.15	2.044	1.004	-1.257×10^{-3}	0.975	0.731	1.235	1.264	0.370	49.152
323.15	2.044	1.004	-1.248×10^{-3}	0.839	0.734	1.440	1.456	0.376	49.575
328.15	2.044	1.004	-1.240×10^{-3}	0.646	0.736	1.742	1.740	0.383	49.861
333.15	2.044	1.004	-1.232×10^{-3}	0.129	0.739	2.901	2.865	0.389	49.026

Table 6.23 Estimated excess molar volumes (V_E), kinematic viscosities deviations ($\delta\upsilon$), thermal expansion coefficients (α), diffusivity (D_{N2O}, D_{CO2}), isentropic compressibility (Ks) and Gibbs energies of activation of viscous flow (ΔG^0) for aq. (TESA + APA) from 298.15 K to 333.15 K at 0.1 MPa

T / K	TESA mol.kg^{-1}	APA mol.kg^{-1}	V_E / m^3.kgmol^{-1}	$\delta\upsilon$ ×10^6 / m^{2}s^{-1}	α ×10^3/ K^{-1}	D_{N2O}× 10^9 / m^{2}s^{-1}	D_{CO2}×10^9 / m^{2}s^{-1}	Ks ×10^9/ m.s^{-2}.kg^{-1}	ΔG^0/ kJmol^{-1}
298.15	2.528	0.499	-1.277×10^{-3}	5.936	0.768	0.338	0.365	0.363	49.576
303.15	2.528	0.499	-1.259×10^{-3}	5.285	0.771	0.386	0.411	0.369	50.134
308.15	2.528	0.499	-1.243×10^{-3}	4.547	0.774	0.46	0.479	0.375	50.577
313.15	2.528	0.499	-1.227×10^{-3}	4.024	0.777	0.526	0.545	0.381	51.093
318.15	2.528	0.499	-1.213×10^{-3}	3.621	0.779	0.600	0.615	0.387	51.631
323.15	2.528	0.499	-1.199×10^{-3}	3.362	0.783	0.671	0.678	0.394	52.237
328.15	2.528	0.499	-1.187×10^{-3}	3.101	0.786	0.751	0.751	0.401	52.827
333.15	2.528	0.499	-1.176×10^{-3}	2.97	0.789	0.819	0.809	0.409	53.505
298.15	2.259	0.753	-1.269×10^{-3}	5.527	0.750	0.353	0.381	0.357	49.398
303.15	2.259	0.753	-1.254×10^{-3}	4.465	0.753	0.430	0.458	0.362	49.749
308.15	2.259	0.753	-1.240×10^{-3}	3.795	0.756	0.512	0.538	0.367	50.160
313.15	2.259	0.753	-1.227×10^{-3}	3.300	0.758	0.597	0.619	0.373	50.634
318.15	2.259	0.753	-1.216×10^{-3}	3.005	0.761	0.676	0.692	0.379	51.191
323.15	2.259	0.753	-1.205×10^{-3}	2.647	0.764	0.782	0.791	0.386	51.674
328.15	2.259	0.753	-1.196×10^{-3}	2.412	0.767	0.883	0.882	0.392	52.228
333.15	2.259	0.753	-1.187×10^{-3}	2.319	0.770	0.962	0.949	0.399	52.900
298.15	2.044	0.991	-1.271×10^{-3}	3.837	0.741	0.445	0.481	0.351	48.651
303.15	2.044	0.991	-1.254×10^{-3}	2.501	0.744	0.611	0.650	0.356	48.616
308.15	2.044	0.991	-1.238×10^{-3}	1.831	0.747	0.790	0.829	0.362	48.745
313.15	2.044	0.991	-1.223×10^{-3}	1.262	0.749	1.032	1.069	0.367	48.824
318.15	2.044	0.991	-1.209×10^{-3}	0.909	0.752	1.306	1.337	0.373	48.986
323.15	2.044	0.991	-1.197×10^{-3}	0.437	0.755	1.886	1.906	0.379	48.688
328.15	2.044	0.991	-1.185×10^{-3}	-0.004	0.758	3.187	3.184	0.386	47.822
333.15	2.044	0.991	-1.175×10^{-3}	-0.018	0.761	3.618	3.573	0.393	48.282

Table 6.24 Estimated excess molar volumes (V_E), kinematic viscosities deviations ($\delta\upsilon$), thermal expansion coefficients (α), diffusivity (D_{N2O}, D_{CO2}), isentropic compressibility (Ks) and Gibbs energies of activation of viscous flow (ΔG^0) for aq. [bmim] [Ac] from 298.15 K to 333.15 K at 0.1 MPa

T /K	[bmim][Ac] mol.kg^{-1}	V_E / m^3.kgmol^{-1}	$\delta\upsilon$ ×10^6 / m^{2}s^{-1}	α ×10^3/ K^{-1}	D_{N2O}× 10^9 / m^{2}s^{-1}	D_{CO2}×10^9 / m^{2}s^{-1}	Ks ×10^9/ m.s^{-2}.kg^{-1}	ΔG^0/ kJmol^{-1}
298.15	2.500	-3.753×10^{-4}	-14.319	0.578	0.743	0.802	0.312	46.929
303.15	2.500	-3.578×10^{-4}	-9.993	0.580	0.783	0.833	0.315	47.693
308.15	2.500	-3.410×10^{-4}	-6.676	0.582	0.835	0.877	0.318	48.422
313.15	2.500	-3.249×10^{-4}	-4.506	0.583	0.894	0.926	0.322	49.143
318.15	2.500	-3.096×10^{-4}	-3.079	0.585	1.003	1.026	0.326	49.706
323.15	2.500	-2.951×10^{-4}	-1.984	0.587	1.059	1.071	0.330	50.467
328.15	2.500	-2.813×10^{-4}	-1.385	0.589	1.213	1.212	0.335	50.951
333.15	2.500	-2.683×10^{-4}	-0.844	0.590	1.300	1.284	0.339	51.657
298.15	2.251	-2.625×10^{-4}	-13.091	0.482	0.819	0.885	0.319	46.565
303.15	2.251	-2.774×10^{-4}	-9.205	0.483	0.875	0.931	0.322	47.283
308.15	2.251	-2.863×10^{-4}	-6.176	0.483	0.927	0.974	0.324	48.018
313.15	2.251	-2.890×10^{-4}	-4.169	0.485	0.979	1.014	0.328	48.775
318.15	2.251	-2.855×10^{-4}	-2.802	0.486	1.069	1.095	0.331	49.420
323.15	2.251	-2.760×10^{-4}	-1.826	0.488	1.139	1.151	0.335	50.151
328.15	2.251	-2.603×10^{-4}	-1.227	0.489	1.273	1.272	0.339	50.712
333.15	2.251	-2.384×10^{-4}	-0.726	0.491	1.359	1.342	0.344	51.429
298.15	2.006	-2.654×10^{-4}	-11.685	0.518	0.855	0.923	0.326	46.362
303.15	2.006	-2.617×10^{-4}	-8.196	0.519	0.909	0.968	0.329	47.087
308.15	2.006	-2.565×10^{-4}	-5.452	0.520	0.957	1.005	0.331	47.847
313.15	2.006	-2.497×10^{-4}	-3.662	0.522	1.015	1.052	0.334	48.586
318.15	2.006	-2.415×10^{-4}	-2.709	0.523	1.247	1.276	0.337	48.842
323.15	2.006	-2.317×10^{-4}	-1.951	0.525	1.409	1.424	0.341	49.362
328.15	2.006	-2.204×10^{-4}	-1.346	0.526	1.537	1.536	0.345	49.994
333.15	2.006	-2.076×10^{-4}	-1.115	0.528	1.875	1.852	0.349	50.237

Table 6.25 Estimated excess molar volumes (V_E), kinematic viscosities deviations ($\delta\upsilon$), thermal expansion coefficients (α), diffusivity (D_{N2O}, D_{CO2}), isentropic compressibility (Ks) and Gibbs energies of activation of viscous flow (ΔG^0) for aq. ([bmim] [Ac] + AEP) from 298.15 K to 333.15 K at 0.1 MPa

T / K	[bmim][Ac] mol.kg^{-1}	AEP mol.kg^{-1}	V_E / m^3.kgmol^{-1}	$\delta\upsilon$ ×10^6 / m^{2}s^{-1}	α ×10^3/ K^{-1}	D_{N2O}× 10^9 / m^{2}s^{-1}	D_{CO2}×10^9 / m^{2}s^{-1}	Ks ×10^9/ m.s^{-2}.kg^{-1}	ΔG^0/ kJmol^{-1}
298.15	2.500	0.503	-5.050×10^{-4}	-13.266	0.593	0.563	0.608	0.303	47.864
303.15	2.500	0.503	-4.873×10^{-4}	-9.032	0.595	0.601	0.639	0.307	48.606
308.15	2.500	0.503	-4.704×10^{-4}	-5.977	0.597	0.679	0.713	0.312	49.166
313.15	2.500	0.503	-4.544×10^{-4}	-4.022	0.598	0.766	0.794	0.315	49.725
318.15	2.500	0.503	-4.391×10^{-4}	-2.760	0.600	0.893	0.914	0.319	50.172
323.15	2.500	0.503	-4.247×10^{-4}	-1.794	0.602	0.984	0.995	0.324	50.799
328.15	2.500	0.503	-4.111×10^{-4}	-1.098	0.604	1.079	1.079	0.328	51.434
333.15	2.500	0.503	-3.982×10^{-4}	-0.624	0.606	1.182	1.168	0.333	52.073
298.15	2.251	0.756	-5.469×10^{-4}	-11.774	0.593	0.567	0.613	0.304	47.813
303.15	2.251	0.756	-5.304×10^{-4}	-7.969	0.594	0.606	0.645	0.307	48.551
308.15	2.251	0.756	-5.146×10^{-4}	-5.187	0.596	0.679	0.713	0.311	49.137
313.15	2.251	0.756	-4.997×10^{-4}	-3.466	0.598	0.773	0.801	0.315	49.669
318.15	2.251	0.756	-4.854×10^{-4}	-2.354	0.599	0.902	0.923	0.319	50.110
323.15	2.251	0.756	-4.720×10^{-4}	-1.529	0.601	1.009	1.019	0.324	50.686
328.15	2.251	0.756	-4.594×10^{-4}	-0.867	0.603	1.092	1.091	0.329	51.366
333.15	2.251	0.756	-4.475×10^{-4}	-0.519	0.605	1.231	1.215	0.334	51.905
298.15	2.006	1.004	-5.693×10^{-4}	-10.292	0.588	0.570	0.615	0.304	47.774
303.15	2.006	1.004	-5.544×10^{-4}	-7.175	0.589	0.649	0.691	0.308	48.308
308.15	2.006	1.004	-5.402×10^{-4}	-4.677	0.591	0.728	0.764	0.312	48.889
313.15	2.006	1.004	-5.268×10^{-4}	-2.904	0.593	0.776	0.805	0.316	49.627
318.15	2.006	1.004	-5.141×10^{-4}	-1.926	0.595	0.904	0.925	0.319	50.077
323.15	2.006	1.004	-5.020×10^{-4}	-1.284	0.597	1.041	1.052	0.324	50.554
328.15	2.006	1.004	-4.907×10^{-4}	-0.748	0.598	1.150	1.149	0.329	51.161
333.15	2.006	1.004	-4.802×10^{-4}	-0.447	0.600	1.299	1.284	0.334	51.688

Table 6.26 Estimated excess molar volumes (V_E), kinematic viscosities deviations (δv), thermal expansion coefficients (α), diffusivity (D_{N2O}, D_{CO2}), isentropic compressibility (Ks) and Gibbs energies of activation of viscous flow (ΔG^0) for aq. ([bmim] [Ac] + APA) from 298.15 K to 333.15 K at 0.1 MPa

T / K	[bmim][Ac] mol.kg^{-1}	APA mol. kg^{-1}	V_E / m^3.kgmol^{-1}	$\delta v \times 10^6$ / m^{2}s^{-1}	$\alpha \times 10^3$/ K^{-1}	$D_{N2O} \times 10^9$ / m^{2}s^{-1}	$D_{CO2} \times 10^9$ / m^{2}s^{-1}	$Ks \times 10^9$/ m.s^{-2}. kg^{-1}	ΔG^0/ kJmol^{-1}
298.15	2.500	0.504	-4.964×10^{-4}	-13.094	0.603	0.549	0.593	0.303	47.950
303.15	2.500	0.504	-4.776×10^{-4}	-8.867	0.604	0.588	0.626	0.307	48.682
308.15	2.500	0.504	-4.598×10^{-4}	-5.925	0.606	0.679	0.713	0.311	49.175
313.15	2.500	0.504	-4.428×10^{-4}	-4.043	0.608	0.779	0.807	0.315	49.682
318.15	2.500	0.504	-4.267×10^{-4}	-2.635	0.609	0.867	0.887	0.319	50.280
323.15	2.500	0.504	-4.115×10^{-4}	-1.633	0.612	0.941	0.951	0.325	50.959
328.15	2.500	0.504	-3.972×10^{-4}	-1.053	0.613	1.070	1.069	0.329	51.476
333.15	2.500	0.504	-3.838×10^{-4}	-0.579	0.616	1.171	1.156	0.335	52.118
298.15	2.251	0.753	-5.282×10^{-4}	-11.855	0.602	0.591	0.638	0.304	47.708
303.15	2.251	0.753	-5.107×10^{-4}	-7.964	0.603	0.621	0.661	0.308	48.492
308.15	2.251	0.753	-4.941×10^{-4}	-5.134	0.605	0.685	0.720	0.312	49.128
313.15	2.251	0.753	-4.784×10^{-4}	-3.439	0.607	0.781	0.809	0.316	49.654
318.15	2.251	0.753	-4.636×10^{-4}	-2.254	0.609	0.888	0.909	0.321	50.183
323.15	2.251	0.753	-4.496×10^{-4}	-1.378	0.610	0.971	0.982	0.325	50.834
328.15	2.251	0.753	-4.366×10^{-4}	-0.800	0.612	1.079	1.079	0.329	51.426
333.15	2.251	0.753	-4.244×10^{-4}	-0.444	0.614	1.210	1.195	0.335	51.984
298.15	2.006	0.996	-5.420×10^{-4}	-10.517	0.600	0.616	0.665	0.306	47.546
303.15	2.006	0.996	-5.259×10^{-4}	-7.046	0.602	0.649	0.691	0.309	48.319
308.15	2.006	0.996	-5.106×10^{-4}	-4.482	0.603	0.709	0.745	0.313	48.981
313.15	2.006	0.996	-4.962×10^{-4}	-2.942	0.605	0.800	0.830	0.317	49.540
318.15	2.006	0.996	-4.826×10^{-4}	-1.872	0.607	0.902	0.923	0.322	50.095
323.15	2.006	0.996	-4.698×10^{-4}	-1.281	0.609	1.052	1.064	0.326	50.529
328.15	2.006	0.996	-4.578×10^{-4}	-0.913	0.611	1.242	1.241	0.331	50.912
333.15	2.006	0.996	-4.467×10^{-4}	-0.615	0.613	1.415	1.398	0.336	51.406

Table 6.27 Estimated excess molar volumes (V_E), kinematic viscosities deviations ($\delta\upsilon$), thermal expansion coefficients (α), diffusivity (D_{N2O}, D_{CO2}), isentropic compressibility (Ks) and Gibbs energies of activation of viscous flow (ΔG^0) for aq. (MDEA + 2-MPZ) from 298.15 K to 333.15 K at 0.1 MPa

T /K	MDEA mol.kg^{-1}	2-MPZ mol.kg^{-1}	V_E / m^3.kgmol^{-1}	$\delta\upsilon \times 10^6$ / m^{2}s^{-1}	$\alpha \times 10^3$/ K^{-1}	$D_{N2O} \times 10^9$ / m^{2}s^{-1}	$D_{CO2} \times 10^9$ / m^{2}s^{-1}	$Ks \times 10^9$/ m.s^{-2}.kg^{-1}	ΔG^0/ kJmol^{-1}
298.15	3.509	0.509	-5.062×10^{-4}	2.183	0.547	0.314	0.339	0.345	32.379
303.15	3.509	0.509	-5.013×10^{-4}	2.597	0.549	0.368	0.392	0.346	32.561
308.15	3.509	0.509	-4.969×10^{-4}	2.392	0.549	0.432	0.454	0.349	32.735
313.15	3.509	0.509	-4.931×10^{-4}	2.393	0.551	0.505	0.524	0.351	32.912
318.15	3.509	0.509	-4.898×10^{-4}	2.240	0.553	0.581	0.595	0.354	33.134
323.15	3.509	0.509	-4.871×10^{-4}	1.933	0.555	0.693	0.701	0.357	33.226
328.15	3.509	0.509	-4.850×10^{-4}	1.900	0.556	0.797	0.796	0.361	33.430
333.15	3.509	0.509	-4.834×10^{-4}	1.750	0.558	0.911	0.899	0.365	33.646
298.15	3.017	1.008	-6.175×10^{-4}	0.398	0.553	0.427	0.461	0.341	31.414
303.15	3.017	1.008	-6.119×10^{-4}	0.530	0.554	0.541	0.576	0.343	31.338
308.15	3.017	1.008	-6.067×10^{-4}	0.617	0.556	0.629	0.661	0.346	31.519
313.15	3.017	1.008	-6.021×10^{-4}	1.256	0.557	0.659	0.684	0.349	32.033
318.15	3.017	1.008	-5.980×10^{-4}	1.055	0.559	0.790	0.808	0.352	32.111
323.15	3.017	1.008	-5.944×10^{-4}	1.275	0.560	0.849	0.858	0.355	32.536
328.15	3.017	1.008	-5.914×10^{-4}	1.355	0.562	0.956	0.955	0.359	32.800
333.15	3.017	1.008	-5.889×10^{-4}	1.371	0.564	1.051	1.038	0.364	33.139
298.15	2.502	1.509	-7.055×10^{-4}	-0.332	0.551	0.550	0.594	0.341	30.618
303.15	2.502	1.509	-6.998×10^{-4}	-0.063	0.552	0.667	0.710	0.343	30.666
308.15	2.502	1.509	-6.947×10^{-4}	-0.150	0.553	0.860	0.903	0.345	30.507
313.15	2.502	1.509	-6.902×10^{-4}	0.365	0.555	0.909	0.942	0.348	30.977
318.15	2.502	1.509	-6.862×10^{-4}	0.582	0.556	0.979	1.002	0.351	31.388
323.15	2.502	1.509	-6.828×10^{-4}	0.772	0.558	1.054	1.066	0.355	31.795
328.15	2.502	1.509	-6.799×10^{-4}	0.934	0.559	1.155	1.154	0.359	32.142
333.15	2.502	1.509	-6.776×10^{-4}	1.019	0.561	1.241	1.226	0.363	32.550

Table 6.28 Estimated excess molar volumes (V_E), kinematic viscosities deviations (δv), thermal expansion coefficients (α), diffusivity (D_{N2O}, D_{CO2}), isentropic compressibility (Ks) and Gibbs energies of activation of viscous flow (ΔG^0) for aq. ($TMSO_2$ + 2-MPZ) from 298.15 K to 333.15 K at 0.1 MPa

T / K	$TMSO_2$ mol.kg^{-1}	2-MPZ mol.kg^{-1}	V_E / m^3.kgmol^{-1}	$\delta v \times 10^6$ / m^{2}s^{-1}	$\alpha \times 10^3$/ K^{-1}	$D_{N2O} \times 10^9$ / m^{2}s^{-1}	$D_{CO2} \times 10^9$ / m^{2}s^{-1}	$Ks \times 10^9$/ m.s^{-2}.kg^{-1}	ΔG^0/ kJmol^{-1}
298.15	3.501	0.509	-1.648×10^{-3}	0.965	0.586	0.741	0.799	0.369	29.6230
303.15	3.501	0.509	-1.645×10^{-3}	0.886	0.588	0.809	0.861	0.371	29.985
308.15	3.501	0.509	-1.642×10^{-3}	1.057	0.589	0.854	0.897	0.372	30.455
313.15	3.501	0.509	-1.638×10^{-3}	1.098	0.591	0.927	0.961	0.374	30.834
318.15	3.501	0.509	-1.635×10^{-3}	1.116	0.593	1.017	1.040	0.377	31.184
323.15	3.501	0.509	-1.631×10^{-3}	1.037	0.595	1.132	1.144	0.379	31.477
328.15	3.501	0.509	-1.627×10^{-3}	1.094	0.597	1.212	1.211	0.383	31.897
333.15	3.501	0.509	-1.623×10^{-3}	1.123	0.599	1.287	1.271	0.387	32.346
298.15	3.012	1.008	-1.605×10^{-3}	0.772	0.584	0.820	0.885	0.364	29.308
303.15	3.012	1.008	-1.602×10^{-3}	0.631	0.586	0.923	0.982	0.365	29.570
308.15	3.012	1.008	-1.598×10^{-3}	0.535	0.587	1.089	1.143	0.367	29.678
313.15	3.012	1.008	-1.594×10^{-3}	0.490	0.589	1.243	1.289	0.369	29.883
318.15	3.012	1.008	-1.590×10^{-3}	0.457	0.591	1.420	1.453	0.372	30.080
323.15	3.012	1.008	-1.586×10^{-3}	0.330	0.592	1.679	1.697	0.375	30.155
328.15	3.012	1.008	-1.582×10^{-3}	0.389	0.594	1.808	1.806	0.378	30.536
333.15	3.012	1.008	-1.577×10^{-3}	0.330	0.596	2.054	2.029	0.382	30.728
298.15	2.500	1.509	-1.542×10^{-3}	0.382	0.584	1.006	1.086	0.357	28.676
303.15	2.500	1.509	-1.537×10^{-3}	0.146	0.585	1.218	1.296	0.359	28.698
308.15	2.500	1.509	-1.532×10^{-3}	0.194	0.587	1.371	1.439	0.361	28.942
313.15	2.500	1.509	-1.527×10^{-3}	0.221	0.588	1.523	1.579	0.363	29.223
318.15	2.500	1.509	-1.523×10^{-3}	0.236	0.590	1.709	1.749	0.366	29.469
323.15	2.500	1.509	-1.518×10^{-3}	0.183	0.592	1.957	1.979	0.369	29.641
328.15	2.500	1.509	-1.513×10^{-3}	0.127	0.594	2.321	2.319	0.373	29.684
333.15	2.500	1.509	-1.508×10^{-3}	-0.014	0.596	2.970	2.933	0.377	29.453

Table 6.29 Estimated excess molar volumes (V_E), kinematic viscosities deviations ($\delta\upsilon$), thermal expansion coefficients (α), diffusivity (D_{N2O}, D_{CO2}), isentropic compressibility (Ks) and Gibbs energies of activation of viscous flow (ΔG^0) for aq. ([bmim] [Ac] + 2-MPZ) from 298.15 K to 333.15 K at 0.1 MPa

T / K	[bmim][Ac] mol.kg^{-1}	2-MPZ mol.kg^{-1}	V_E / m^3.kgmol^{-1}	$\delta\upsilon$ ×10^6 / m^{2}s^{-1}	α ×10^3/ K^{-1}	D_{N2O}×10^9 / m^{2}s^{-1}	D_{CO2}×10^9 / m^{2}s^{-1}	Ks ×10^9/ m.s^{-2}.kg^{-1}	ΔG^0/ kJmol^{-1}
298.15	3.507	0.509	-6.882×10^{-4}	-18.921	0.639	0.533	0.575	0.289	31.136
303.15	3.507	0.509	-6.621×10^{-4}	-13.223	0.641	0.586	0.624	0.294	31.499
308.15	3.507	0.509	-6.372×10^{-4}	-8.693	0.643	0.620	0.651	0.298	31.989
313.15	3.507	0.509	-6.136×10^{-4}	-6.121	0.645	0.725	0.752	0.303	32.154
318.15	3.507	0.509	-5.911×10^{-4}	-4.037	0.647	0.785	0.803	0.308	32.568
323.15	3.507	0.509	-5.699×10^{-4}	-2.731	0.649	0.870	0.879	0.313	32.897
328.15	3.507	0.509	-5.498×10^{-4}	-1.956	0.651	1.013	1.012	0.319	33.055
333.15	3.507	0.509	-5.309×10^{-4}	-1.653	0.654	1.269	1.254	0.324	32.947
298.15	3.002	1.008	-7.698×10^{-4}	-16.192	0.637	0.586	0.632	0.292	30.778
303.15	3.002	1.008	-7.450×10^{-4}	-11.291	0.639	0.641	0.682	0.297	31.153
308.15	3.002	1.008	-7.214×10^{-4}	-7.555	0.641	0.706	0.741	0.301	31.509
313.15	3.002	1.008	-6.990×10^{-4}	-5.079	0.643	0.766	0.794	0.306	31.909
318.15	3.002	1.008	-6.778×10^{-4}	-3.357	0.645	0.843	0.863	0.311	32.263
323.15	3.002	1.008	-6.578×10^{-4}	-2.371	0.647	0.973	0.983	0.316	32.454
328.15	3.002	1.008	-6.390×10^{-4}	-1.442	0.649	1.033	1.032	0.322	32.918
333.15	3.002	1.008	-6.215×10^{-4}	-1.388	0.652	1.379	1.362	0.327	32.588
298.15	2.510	1.509	-8.459×10^{-4}	-13.213	0.635	0.602	0.649	0.296	30.633
303.15	2.510	1.509	-8.227×10^{-4}	-9.165	0.637	0.664	0.706	0.300	30.981
308.15	2.510	1.509	-8.005×10^{-4}	-6.253	0.638	0.774	0.813	0.305	31.148
313.15	2.510	1.509	-7.796×10^{-4}	-4.229	0.641	0.853	0.884	0.309	31.496
318.15	2.510	1.509	-7.597×10^{-4}	-2.874	0.643	0.966	0.989	0.315	31.747
323.15	2.510	1.509	-7.410×10^{-4}	-2.252	0.645	1.211	1.225	0.319	31.649
328.15	2.510	1.509	-7.235×10^{-4}	-2.034	0.647	1.722	1.720	0.325	31.107
333.15	2.510	1.509	-7.071×10^{-4}	-1.593	0.649	1.979	1.954	0.331	31.269

6.3.2 Modeling of viscosity

The methodology applied for measurement of viscosity is validated by comparison of the viscosity of pure AMP at various temperatures [14] (Table 6.30). A good agreement is observed between the literature values of viscosity and the measured in the present work.

Table 6.30 Comparison of the viscosity (η) of pure AMP measured in the present work with literature values at pressure P= 0.1 MPa

T / K	η / mPa.s		
	Ref. 10	Ref. 14	This work
298.15	132.3	-	132.32
303.15	99.48	99.5	98.48
308.15	69.98	69	69.98
313.15	47.8	46.9	46.99
318.15	32.17	-	32.24
323.15	24.21	-	24.45
333.15	-	-	14.09
% AAD	3.798	2.638	

The viscosity data of the present work are correlated using the Grunberg and Nissan model. Usually, the Grunberg and Nissan model is used to model the experimental viscosity for the ternary liquid systems. Here, along with the ternary systems, binary systems are also modeled using the same model to check its accuracy for the two-liquid systems. The Grunberg and Nissan model is represented by the following equation [12]:

$$\ln \eta_m = \sum x_i \times \ln \eta_i + \sum\sum x_i \times x_j \times G_{ij} \tag{6.8}$$

Where, η_i *is in mPa.s* and x_i are the dynamic viscosity of the pure constituent and the mole fraction of the i^{th} constituent in the solution, respectively. For a two liquid system, the above mentioned equation can be represented as:

$$\ln \eta_m = x_1 \times \ln \eta_1 + x_2 \times \ln \eta_2 + x_1 \times x_2 \times G_{12} \tag{6.9}$$

Where, G_{ij} are temperature dependent parameters. G_{ij} are calculated using the Eq (6.10).

$$G_{ij} = r + s \times T + t \times T^2 \tag{6.10}$$

Where, T is in Kelvins. The experimental values of viscosities of all the blends under study were found to decrease with rise in temperature which can be explained by the decrease in intermolecular forces of attraction due to a rise in kinetic energy at higher temperatures (Table 6.3-6.13). Regression analysis is applied to the measured experimental data of the present work for calculation of the temperature dependent parameters of Eq (6.10) and are reported in Tables (6.31-6.34) along with the % AAD of each system into consideration. A comparison between the modeled and experimental dynamic viscosities for the (TESA + AEP), aq. ([bmim] [Ac] + APA) and aq. ($TMSO_2$ + 2-MPZ) systems indicates a good agreement between them (Figures 6.5-6.7).

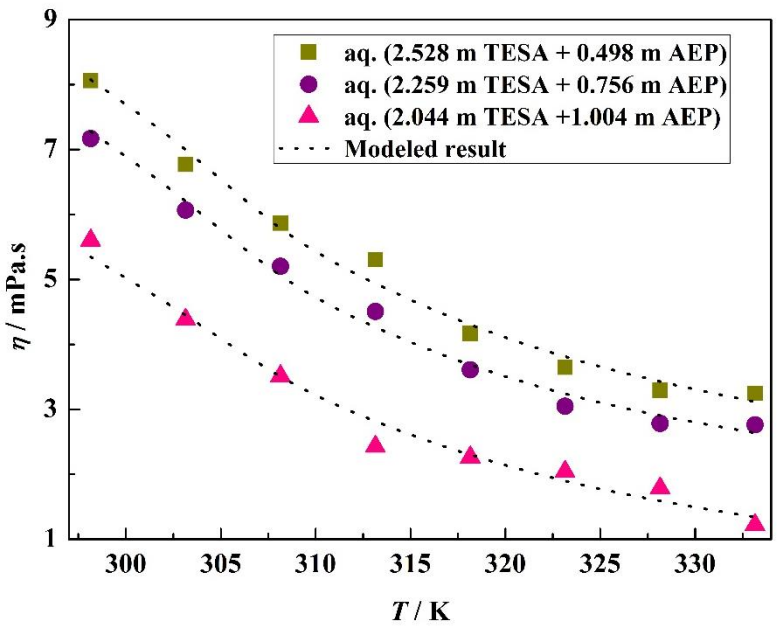

Figure 6.5 Viscosity of **(TESA + AEP)** system at various temperatures and composition (molal)

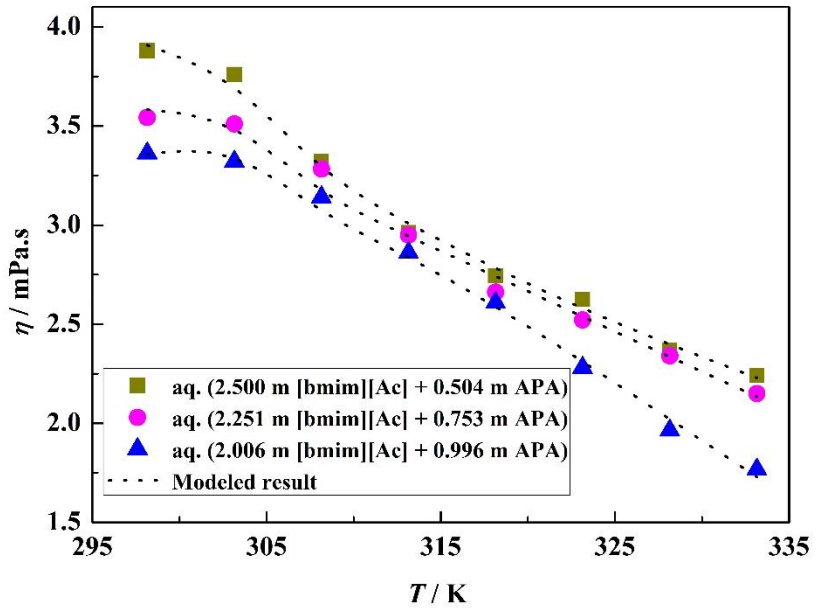

Figure 6.6 Viscosity of aqueous (**[bmim][Ac] + APA**) system at various temperatures and composition (molal)

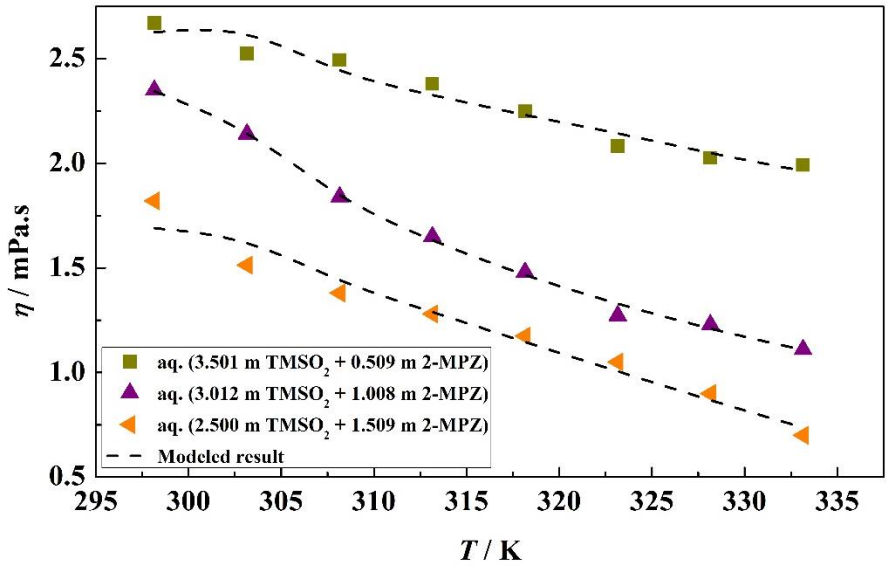

Figure 6.7 Viscosity of aqueous (**$TMSO_2$ + 2-MPZ**) system at various temperatures and composition (molal)

Table 6.31 Parameters of the Grunberg-Nissan model for (i) (HEF + AEP) & (ii) (HEF + AMP)

Parameters		(i)HEF + AEP	(ii) HEF + AMP
G_{12}	*r*	1.447×10^{2}	-1.439×10
	s	-7.836×10^{-1}	9.795×10^{-2}
	t	1.109×10^{-3}	-1.648×10^{-4}
100AAD		45.712	19.029
SD		25.183	9.644

Table 6.32 Parameters of the Grunberg-Nissan model for (i) aq. TESA, (ii) aq. (TESA + AEP) and (iii) aq. (TESA + APA) system

Parameters	Blend	aq. TESA	aq.(TESA + AEP)	aq.(TESA + APA)
G_{12}	*r*	-4.960×10^{4}	1.321×10^{6}	2.760×10^{6}
	s	3.438	-8.815×10^{3}	-1.873×10^{4}
	t	-5.472×10^{-3}	1.482×10	31.890
G_{23}	*r*	-	-4.297×10^{4}	-9.023×10^{4}
	s	-	2.881×10^{2}	6.145×10^{2}
	t	-	-4.864×10^{-1}	-1.049
G_{31}	*r*	-	-2.819×10^{3}	-6.547×10^{3}
	s	-	1.933×10	44.593
	t	-	-3.279×10^{-2}	-7.568×10^{-2}
	100AAD	16.151	5.878	3.083
	SD	0.370	0.193	0.113

Table 6.33 Parameters of the Grunberg-Nissan model for (i) aq. [bmim] [Ac], (ii) aq. ([bmim] [Ac] + AEP) and (iii) aq. ([bmim] [Ac] + APA) system

Parameters	Blend	aq. [bmim][Ac]	aq. ([bmim][Ac] + AEP)	aq. ([bmim][Ac] + APA)
	r	-1.088×10^{3}	2.144×10^{4}	3.657×10^{5}
G_{12}	*s*	6.804	-1.172×10^{2}	-2.465×10^{3}
	t	-1.036×10^{-2}	1.639×10^{-1}	4.148
	r		-1.927×10^{3}	-1.586×10^{4}
G_{23}	*s*	-	1.187×10	1.053×10^{2}
	t	-	-1.825×10^{-2}	-1.745×10^{-1}
	r	-	-2.225×10	-2.868×10^{2}
G_{31}	*s*	-	1.299×10^{-1}	2.280
	t	-	5.525×10^{-5}	-4.097×10^{-3}
	100AAD	2.075×10	2.056	1.396
	SD	4.955×10^{-1}	7.933×10^{-2}	5.129×10^{-2}

Table 6.34 Parameters of the Grunberg-Nissan model for (i) aq. (MDEA + 2-MPZ), (ii) aq. ($TMSO_2$ + 2-MPZ) and (iii) aq. ([bmim] [Ac] + 2-MPZ) system

Parameters	Blend	aq. (MDEA + 2-MPZ)	aq. ($TMSO_2$ + 2-MPZ)	aq. ([bmim][Ac] + 2-MPZ)
	r	-1.939×10^{4}	4.243×10^{5}	1.998×10^{5}
G_{12}	*s*	88.366	-2.621×10^{3}	-1.383×10^{3}
	t	-8.914×10^{-2}	4.032	2.383
	r	3.515×10^{3}	-1.819×10^{4}	-1.032×10^{4}
G_{23}	*s*	-21.439	1.132×10^{2}	7.085×10
	t	3.273×10^{-2}	-1.758×10^{-1}	-1.210×10^{-1}
	r	-3.728×10^{2}	-1.506×10^{3}	-1.341×10^{3}
G_{31}	*s*	2.876	9.161	8.873
	t	-5.017×10^{-3}	-1.364×10^{-2}	-1.444×10^{-2}
	100AAD	2.954	2.739	3.968
	SD	0.147	0.060	0.121

The viscosity deviations (δv) were calculated using the experimental viscosity values for the studied systems for various compositions and at different temperatures using the following equation [15]:

$$\delta v = v_{exp} - \sum x_i \times v_i \tag{6.11}$$

where, v_{exp} is the experimental values of kinematic viscosity calculated using the experimental density and dynamic viscosity values of the blended solutions under study tabulated in Tables (6.3-6.13) and x_i and v_i corresponds to the mole fractions and the kinematic viscosities of pure components of the system, respectively. The kinematic viscosity deviations for all the blends under study have been reported in Tables (6.19-6.29) and the same has been presented graphically in Figures (6.8-6.10). Following factors are responsible for viscosity deviations. (1) The variations in shape and sizes of the concerned species and the loss of dipolar associations results in a decrease in viscosity; (2) While the increase in viscosity can be the results of precise interactions between the unlike molecules. Positive values of Δv are indicative of strong interactions while weaker interactions lead to negative values.

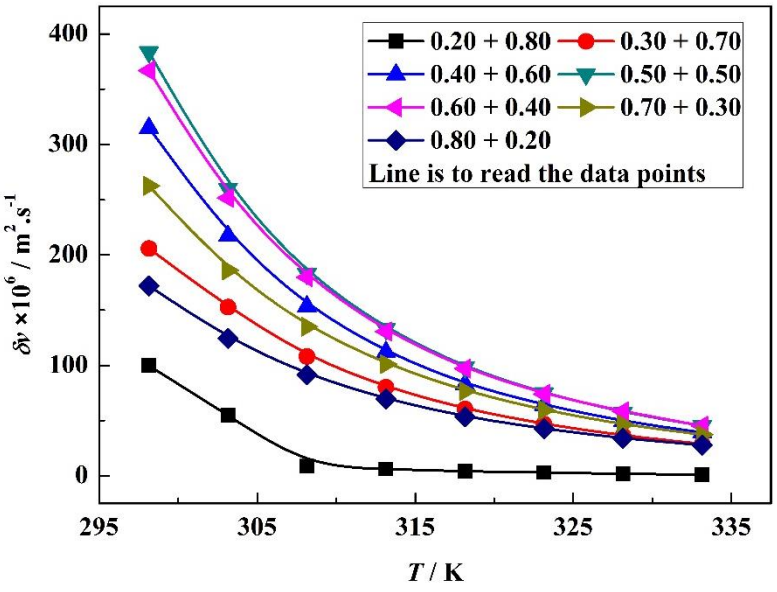

Figure 6.8 Kinematic viscosity deviations of (**HEF + AEP**) system at various temperatures and composition (mass fractions)

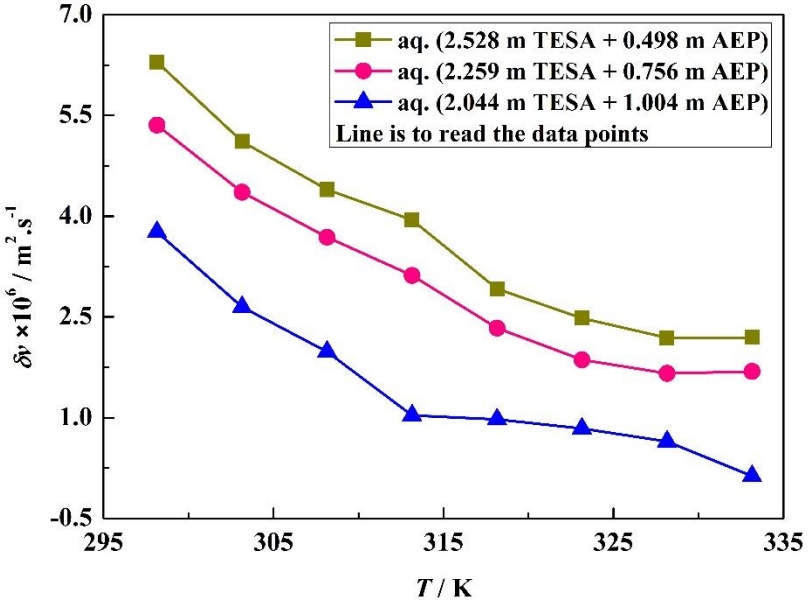

Figure 6.9 Kinematic viscosity deviations of aqueous (**TESA + AEP**) system at various temperatures and composition (molal)

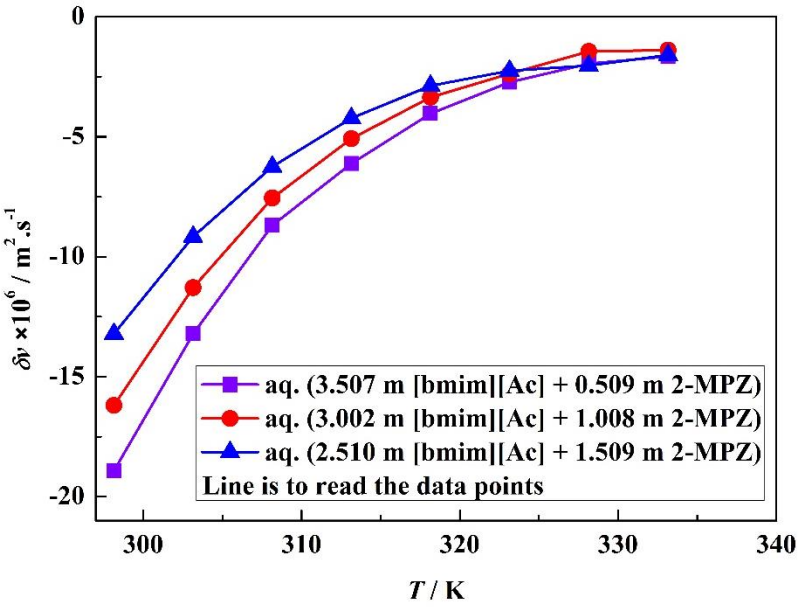

Figure 6.10 Kinematic viscosity deviations of aqueous (**[bmim][Ac] + 2-MPZ**) system at various temperatures and composition (molal)

6.3.3 Modeling of refractive index and sound velocity

Mach number directly relates the local flow velocity and sound velocity in the fluids which defines the compressible nature of fluids. The variations in sound velocity have a significant role in variations of pressure through a medium. Therefore, accurate measurements of the speed of sound or sound velocity for solvents are required as important data for the absorption of any gas in a solvent since the absorption operation depends on the pressure [16]. The method for measurement of sound velocity is validated using the literature values of pure AMP as given in Table 6.35 [10].

Refractive index *nD* of a material is a dimensionless number that indicates how light disseminates through that medium. It is represented by the following equation:

$$n = \frac{c}{v} \tag{6.12}$$

Where, *c* and *v*indicates the light velocity in vacuum and the phase velocity of light in the medium respectively. Refractive index has a relationship with many important properties such as density, concentration, etc. and hence, accurate measurements of refractive index are important. The experimental method used for measurement of refractive index is being validated using the comparison of refractive index values of pure [bmim] [Ac] with the literature [17] (Table 6.36). A good agreement between the measured values in this work and the literature values have thus been obtained.

Table 6.35 Comparison of the sound velocity (*c*) of pure AMP measured in the present work with literature values at pressure P= 0.1 MPa

	T / K	298.15	303.15	308.15	313.15	318.15	323.15	328.15	333.15	% AAD
c / m.s^{-1}	Ref. 10	1483.44	1461.22	1442.4	1423.8	1405.28	1386.93	-	-	0.041
	This work	1483.8	1460.9	1443.4	1423.2	1405.5	1387.9	1369.4	1345.8	

Table 6.36 Comparison of the refractive index (*nD*) of pure [bmim] [Ac] measured in the present work with literature values at pressure P= 0.1 MPa

	T / K	298.15	303.15	308.15	313.15	318.15	323.15	328.15	333.15	% AAD
nD	Ref. 17	1.489	1.488	1.487	1.486	1.485	1.484	1.483	-	0.16
	This work	1.492	1.491	1.489	1.488	1.487	1.486	1.485	1.48	

Many complex first principle models have been reported in the literature for correlating sound velocity and refractive index [18, 23]. However, the solution of these models would require a large amount of information about the systems under study. Hence, a new statistical non-rigorous model M_1 which requires very little information of the system and can be solved with less computation time and space has been proposed for the co-relation of sound velocity and refractive index. An empirical regressive model M_1 based on the trend of behavior of sound velocity and refractive index with respect to concentrations of major chemical constituents and temperature is proposed as follows and the efficiency of the model is also published by our research work [24]:

$$Y = A + (B \times x_1) + \left(\frac{C}{x_2}\right) + \left(\frac{D}{T}\right) + \left(E \times \frac{x_1}{x_2}\right) + \left(F \times \frac{x_1}{T}\right) + \left(\frac{G}{T \times x_2}\right) + \left(\frac{H \times x_1}{T \times x_2}\right) \quad (6.13)$$

Where, Y is sound velocity / $m.s^{-1}$ or refractive index, x_1= mass fraction of AEP or AMP or APA or 2-MPZ (amine activators) and x_2=mass fraction of HEF, TESA or [bmim] [Ac] or MDEA or $TMSO_2$ and A, B, C, D, E, F, G, H are constants of regression for the system in consideration. The mass fraction of water is constant in all the respective compositions and hence, it is not considered to be a variable in Eq. (6.13).

The effect of temperature rise on the solvents under study results in a decrease in the values of sound velocity as well as refractive index for all the blends. Sound velocity and refractive index both were found to rise with the increase in HEF, [bmim] [Ac], and 2-MPZ concentration in the respective studied blends whereas only for TESA studied blends the properties were observed to drop with rise in TESA concentration (Tables 6.3-6.13). The reason for decrease in sound velocity while there is increase in temperature of the system is due to enhancement of more intermolecular

movements which results in a decrease in the speed of sound. Similarly, as the temperature increases, the intermolecular collisions enhances, resulting the stray light to hit lesser molecules which further decreases the value of refractive index. In contrary, the rise in HEF or [bmim] [Ac] or 2-MPZ concentration, results in higher molecular density concluding the increment in refractive index. A similar observation has been also reported in the literature [25]. The % AAD and standard deviations for sound velocity and refractive index of blended mixtures using model M_1 have been calculated and presented in Tables 6.37-6.44. Both sound velocity and refractive index for all studied solvents indicated a good agreement with the proposed model since, the % AAD was found to be <1% in all cases (Figures 6.11-6.18).

Table 6.37 Constants, % AAD and standard deviation (SD) of M_1 model for sound velocity of (i) (HEF + AEP) & (ii) (HEF + AMP)

Blend	(i) HEF + AEP	(ii) HEF + AMP
Constants		
A	2.728×10^{2}	2.049×10^{2}
B	6.749×10^{2}	7.128×10^{2}
C	1.325×10^{2}	1.074×10^{2}
D	2.377×10^{5}	2.433×10^{5}
E	-1.403×10^{2}	-9.747×10
F	-1.182×10^{5}	-1.355×10^{5}
G	1.172×10^{5}	1.191×10^{5}
H	-1.207×10^{5}	-1.241×10^{5}
100AAD	0.179	0.099
SD	3.502	1.911

Table 6.38 Constants, % AAD and standard deviation (SD) of M_1 model for sound velocity of (i) aq. TESA (ii) aq. (TESA + AEP), and (iii) aq. (TESA + APA)

Blend	(i) aq. TESA	(ii) aq. (TESA + AEP)	(iii)aq. (TESA + APA)
Constants			
A	-7.032×10^{2}	3.500×10^{2}	-1.823×10^{3}
B	-1.180×10^{4}	-3.220×10	1.696×10^{3}
C	2.732×10^{3}	2.200×10^{2}	1.089×10^{3}
D	5.543×10^{5}	2.665×10^{5}	9.029×10^{5}
E	3.413×10^{3}	-2.761×10^{2}	-3.888×10^{3}
F	3.822×10^{6}	-7.343×10^{4}	-5.746×10^{5}
G	-7.084×10^{5}	-1.998×10^{4}	-2.741×10^{5}
H	-1.263×10^{6}	-7.591×10^{3}	1.048×10^{6}
100AAD	1.288	0.082	0.079
SD	2.760	1.565	1.502

Table 6.39 Constants, % AAD and standard deviation (SD) of M_1 model for sound velocity of (i) aq. [bmim] [Ac] (ii) aq. ([bmim] [Ac] + AEP), and (iii) aq. ([bmim] [Ac] + APA)

Blend	aq. [bmim] [Ac]	aq. ([bmim] [Ac] + AEP)	aq.([bmim] [Ac] + APA)
Constants			
A	1.599×10^{-1}	7.124×10^{-2}	7.548×10^{-2}
B	6.655×10^{-2}	-2.619×10^{-2}	3.417×10^{-2}
C	1.013×10^{-2}	1.693×10^{-2}	1.433×10^{-2}
D	-1.644×10^{-3}	1.308×10^{-3}	1.367×10^{-3}
E	-1.498×10^{-1}	-4.814×10^{-2}	-5.142×10^{-2}
F	1.127×10^{-3}	-1.879×10^{-4}	-1.950×10^{-4}
G	1.036×10^{-3}	2.106×10^{-4}	2.146×10^{-4}
H	2.680×10^{-3}	-9.293×10^{-4}	-9.705×10^{-4}
100AAD	0.077	0.072	0.068
SD	1.552	1.495	1.404

Table 6.40 Constants, % AAD and standard deviation (SD) of M_1 model for sound velocity of (i) aq. (MDEA + 2-MPZ), (ii) aq. ($TMSO_2$ + 2-MPZ) and (iii) aq. ([bmim] [Ac] + 2-MPZ)

Blend	aq. (MDEA + 2-MPZ)	aq. ($TMSO_2$ + 2-MPZ)	aq. ([bmim][Ac] + 2-MPZ)
Constants			
A	2.369×10^{2}	9.058×10^{2}	7.071×10^{2}
B	-2.511×10^{3}	-1.151×10	2.463×10^{2}
C	3.828×10^{2}	1.697×10^{2}	1.450×10^{2}
D	2.924×10^{5}	3.594×10^{4}	1.834×10^{5}
E	-9.639×10^{2}	-7.153×10^{2}	-4.939×10^{2}
F	1.021×10^{6}	1.779×10^{5}	-1.455×10^{5}
G	-7.038×10^{4}	2.551×10^{3}	2.429×10^{4}
H	9.521×10^{4}	2.743×10^{4}	-8.666×10^{4}
100AAD	0.103	0.105	0.063
SD	2.014	1.969	1.329

Table 6.41 Constants, % AAD and standard deviation (SD) of M_1 model for refractive index of (i) (HEF + AEP) and (ii) (HEF + AMP)

Blend	(i) HEF + AEP	(ii) HEF + AMP
Constants		
A	8.981×10^{-1}	8.759×10^{-1}
B	7.327×10^{-2}	9.639×10^{-2}
C	4.468×10^{-1}	4.349×10^{-1}
D	3.129×10	2.632×10
E	-4.514×10^{-1}	-4.410×10^{-1}
F	-2.488×10	-1.935×10
G	1.592×10	1.394×10
H	-1.537×10	-1.238×10
100AAD	0.034	0.014
SD	0.006×10^{-1}	0.003×10^{-1}

Table 6.42 Constants, % AAD and standard deviation (SD) of M_1 model for refractive index of (i) aq. TESA (ii) aq. (TESA + AEP), and (iii) aq. (TESA + APA)

Blend	aq. TESA	aq. (TESA + AEP)	aq.(TESA + APA)
Constants			
A	0.884	0.704	1.005
B	0.225	-0.071	-0.239
C	0.387	0.229	0.115
D	0.026×10^{2}	1.701×10^{2}	0.816×10^{2}
E	-0.496	-0.676	-0.306
F	-0.279×10^{2}	-0.786×10^{2}	-0.479×10^{2}
G	0.162×10^{2}	-0.549×10^{2}	-0.214×10^{2}
H	0.136×10^{2}	1.834×10^{2}	0.793×10^{2}
100AAD	0.009	0.014	0.011
SD	0.002×10^{-1}	0.003×10^{-1}	0.002×10^{-1}

Table 6.43 Constants, % AAD and standard deviation (SD) of M_1 model for refractive index of (i) aq. [bmim] [Ac] (ii) aq. ([bmim] [Ac] + AEP), and (iii) aq. ([bmim] [Ac] + APA)

Blend	aq. [bmim] [Ac]	aq. ([bmim] [Ac] + AEP)	aq.([bmim] [Ac] + APA)
Constants			
A	0.830	0.856	0.878
B	0.315	-0.055	0.081
C	0.397	0.173	0.164
D	21.523	13.484	14.471
E	-0.434	-0.602	-0.609
F	-5.140	-1.868	-2.003
G	6.519	3.285	3.261
H	-15.004	-9.268	-9.994
100AAD	0.017	0.007	0.0133
SD	0.004×10^{-1}	0.001×10^{-1}	0.002×10^{-1}

Table 6.44 Constants, % AAD and standard deviation (SD) of M_1 model for refractive index of (i) aq. (MDEA + 2-MPZ), (ii) aq. ($TMSO_2$ + 2-MPZ) and (iii) aq. ([bmim] [Ac] + 2-MPZ)

Blend	aq. (MDEA + 2-MPZ)	aq. ($TMSO_2$ + 2-MPZ)	aq. ([bmim][Ac] + 2-MPZ)
Constants			
A	0.691	1.056	0.946
B	-0.342	1.224	-0.304
C	0.203	0.074	0.169
D	53.542	-57.641	17.271
E	-0.638	-0.468	-0.530
F	161.862	-305.039	25.904
G	-11.492	27.379	3.188
H	9.027	-41.783	-16.486
100AAD	0.008	0.012	0.008
SD	0.001×10^{-1}	0.002×10^{-1}	0.001×10^{-1}

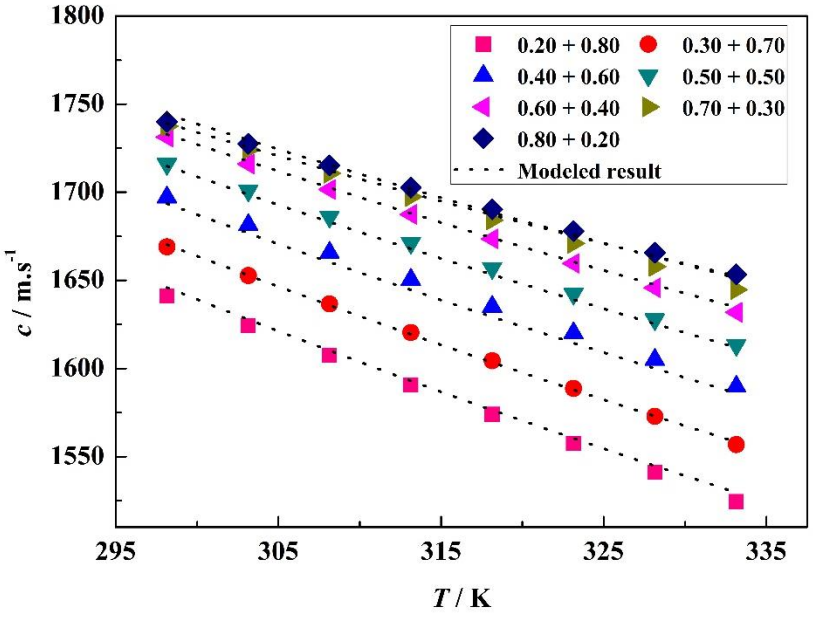

Figure 6.11 Sound velocity of (**HEF + AEP**) system at various temperatures and composition (mass fractions)

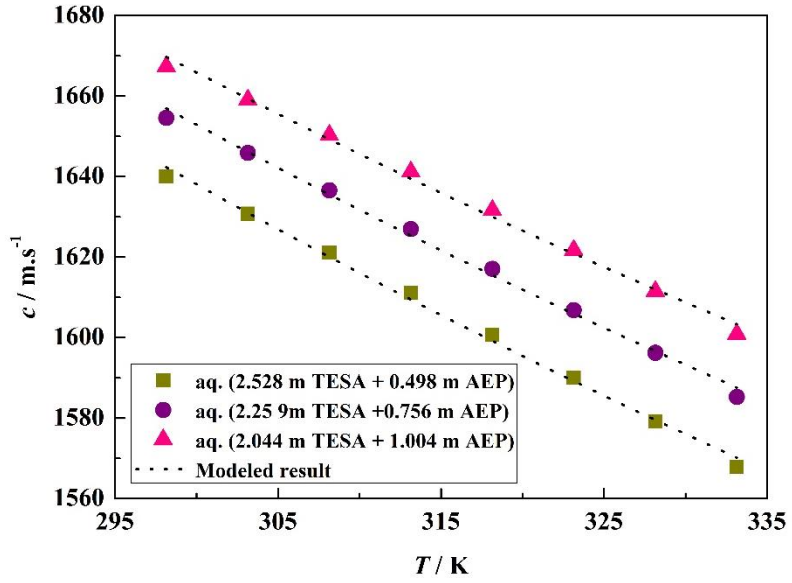

Figure 6.12 Sound velocity of aqueous (**TESA + AEP**) system at various temperatures and composition (molal)

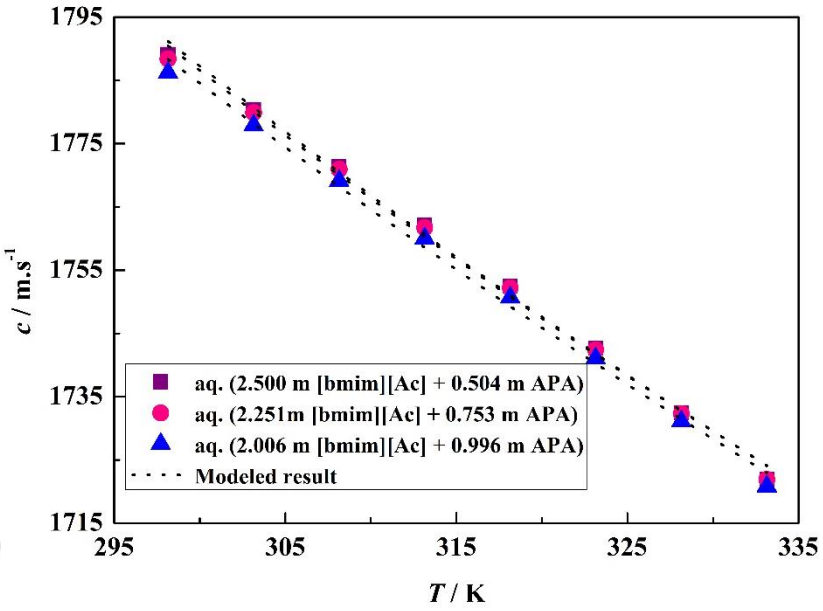

Figure 6.13 Sound velocity of aqueous **([bmim][Ac] + APA**) system at various temperatures and composition (molal)

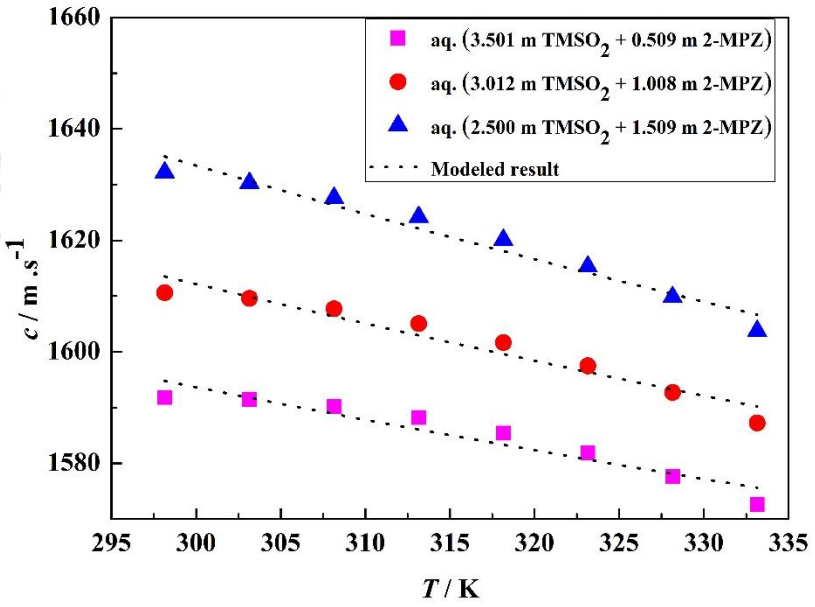

Figure 6.14 Sound velocity of aqueous (**$TMSO_2$ + 2-MPZ**) system at various temperatures and composition (molal)

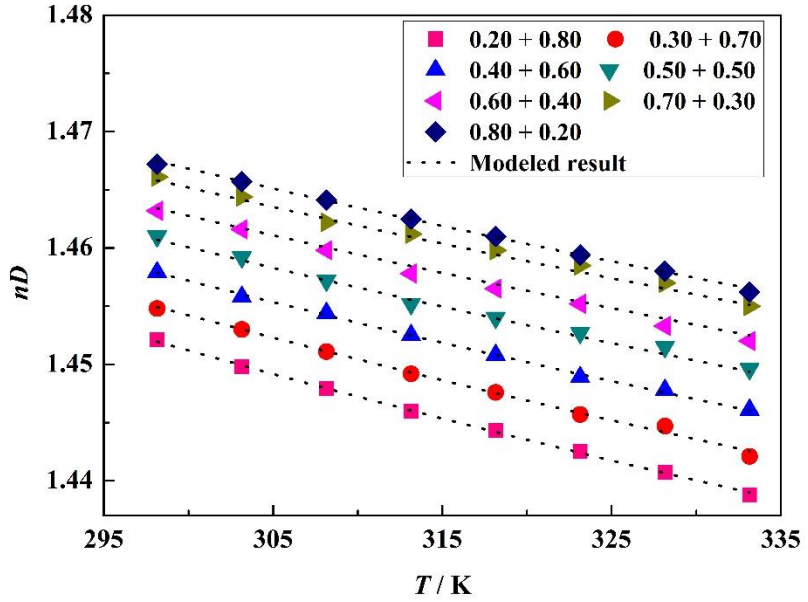

Figure 6.15 Refractive index of (**HEF + AMP**) system at various temperatures and composition (mass fraction)

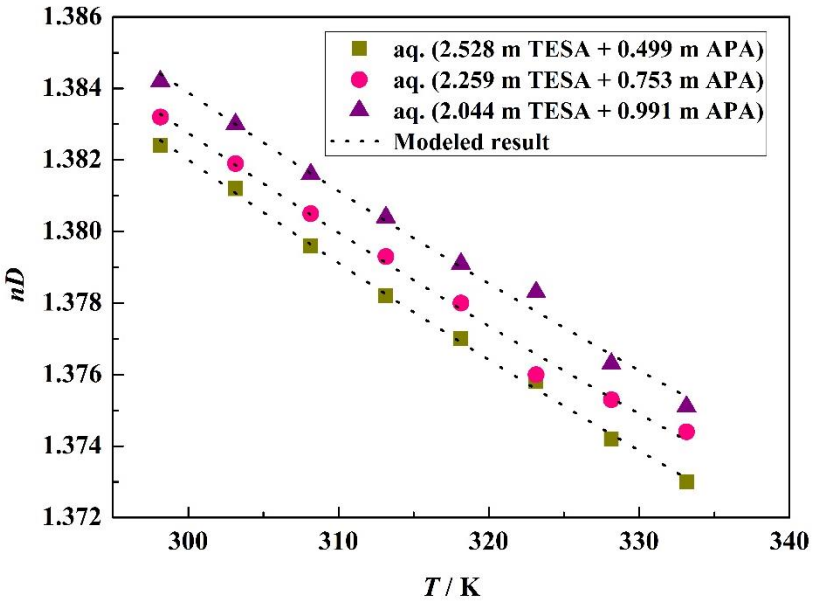

Figure 6.16 Refractive index of aqueous (**TESA + APA**) system at various temperatures and composition (molal)

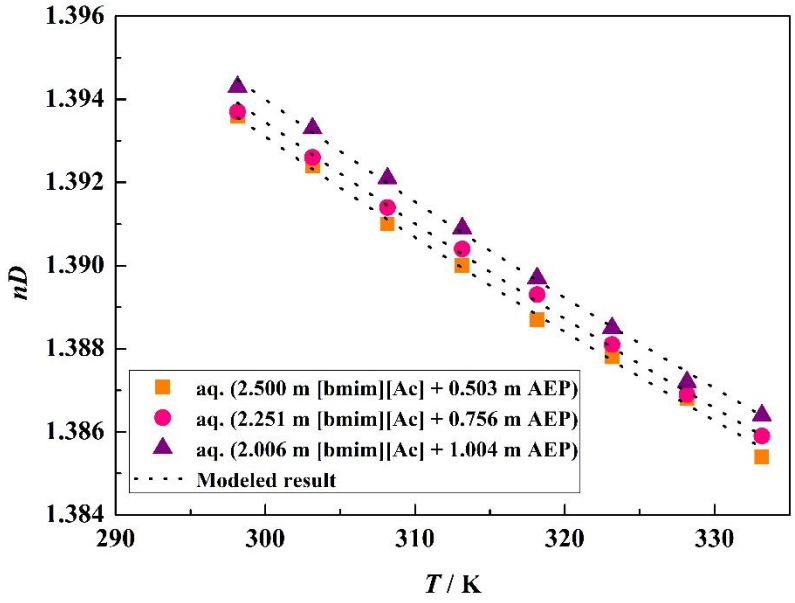

Figure 6.17 Refractive index of aqueous **([bmim][Ac] + AEP**) system at various temperatures and composition (molal)

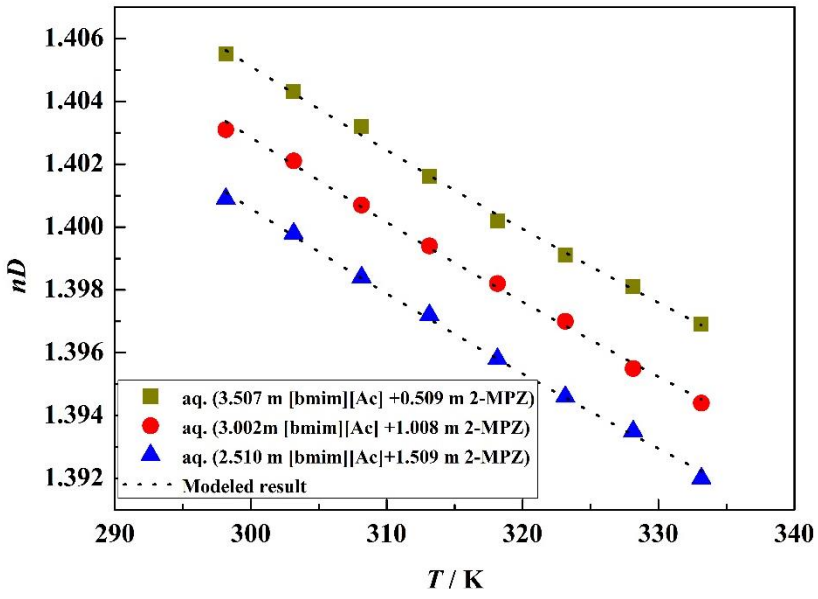

Figure 6.18 Refractive index of aqueous (**[bmim][Ac] + 2-MPZ**) system at various temperatures and composition (molal)

6.3.4 Modeling of surface tension

Hydrodynamic interaction in any gas-liquid depends greatly on the surface tension of the system. Surface tension has been incorporated in various mass transfer correlations suggesting a strong relationship amongst the properties [26]. The variation of surface tension with respect to temperature can be explained through the intermolecular forces of attraction. Liquid molecules with large attractive intermolecular forces usually have an immense surface tension e.g., water, since intermolecular forces between water molecules are due to hydrogen bonds that have high energy, and hence, surface tension for water is larger than many other liquids. All the blends studied in this work exhibit a lower surface tension than water molecules. While increase in temperature of any solvent, also results in an increase of inter-molecular interactions and thereby results in decrease of surface tension due to drop of cohesive forces amongst the molecules.

Several co-relations of surface tension as a function of viscosity for saturated normal fluids were proposed [27]. One of the correlations which were used to find viscosity using surface tension is given by Eq. (6.14).

$$\left(\frac{1}{\eta^{\phi}}\right) = A + B\ln(\gamma) \tag{6.14}$$

However, it is a known actuality that surface tension is also strongly dependent on temperature as well [28, 29]. Henceforth, here, a new non-linear model M_2 indicating a relationship between surface tension, viscosity, and temperature is being proposed as Eq. (6.15) and efficiency of the model is also published by our research work [30].

$$\ln(\gamma) = \ln(T) + \frac{1}{A} \times \left(\frac{1}{\eta^{\phi}}\right) \tag{6.15}$$

Where, A and ϕ are substance-dependent coefficients, η is the dynamic viscosity of the system (mPa.s) and γ (m N.m^{-1}) is the surface tension at temperature, T (K). The experimental methodology for measurement of surface tension has been validated by comparison of experimental available values of surface tension with measured for pure [bmim] [Ac] [31]. The results indicate a good agreement between the literature and measured values with a low AAD of 1.0985 % (Table 6.45). For all the aqueous systems under study, surface tension is found to decrease with enhancement in temperature (Tables 6.3 -6.13). However, surface tension is also a

function of composition of the constituents' elements. With the rise in TESA, [bmim] [Ac], and 2-MPZ, surface tension was found to increase for the corresponding blended solvents studied. The % AAD is calculated and presented in Table 6.46-6.48 along with the values of A and ϕ for the blends under study. The competency of the proposed model for aq. (TESA + APA), aq. ([bmim] [Ac] + AEP), and aq. (MDEA + 2-MPZ) systems is quite competitive with the experimental values (Figures 6.19 -6.21). The Matlab codes for the modeling of physiochemical properties have been provided in APPENDIX IV.

Table 6.45 Comparison of the surface tension (γ) of pure [bmim] [Ac] measured in the present work with literature values at pressure P= 0.1 MPa

T / K	γ / mN.m^{-1}	
	Ref. 31	This work
298.15	37.61	38.006
303.15	37.36	37.866
308.15	37.11	37.483
313.15	36.88	37.208
318.15	36.63	37.057
323.15	36.42	36.904
328.15	36.2	36.555
333.15	-	36.206
% AAD	1.099	

Table 6.46 Substance dependent coefficients and % AAD of M_2 model for surface tension of (i) aq. TESA, (ii) aq. (TESA + AEP) and (iii) aq. (TESA + APA)

Blend	aq. TESA	aq. (TESA + AEP)	aq.(TESA + APA)
Constants			
A	0.317	0.319	0.316
ϕ	0.018	0.007	0.005
100AAD	0.404	0.404	0.458

Table 6.47 Substance dependent coefficients and % AAD of M_2 model for surface tension of (i) aq. [bmim] [Ac], (ii) aq. ([bmim] [Ac] + AEP) and (iii) aq. ([bmim] [Ac] + APA)

Blend	aq. [bmim][Ac]	aq. ([bmim][Ac] + AEP)	aq. ([bmim][Ac] + APA)
Constants			
A	0.314	0.321	0.316
ϕ	-0.001	0.021	0.017
100AAD	0.571	0.214	0.263

Table 6.48 Substance dependent coefficients and %AAD of M_2 model for surface tension of (i) aq. (MDEA + 2-MPZ), (ii) aq. ($TMSO_2$ + 2-MPZ) and (iii) aq. ([bmim] [Ac] + 2-MPZ)

Blend	aq. (MDEA + 2-MPZ)	aq. ($TMSO_2$ + 2-MPZ)	aq.([bmim][Ac] + 2-MPZ)
Constants			
A	0.289	0.297	0.307
ϕ	0.002	0.012	0.006
100AAD	0.141	0.478	0.291

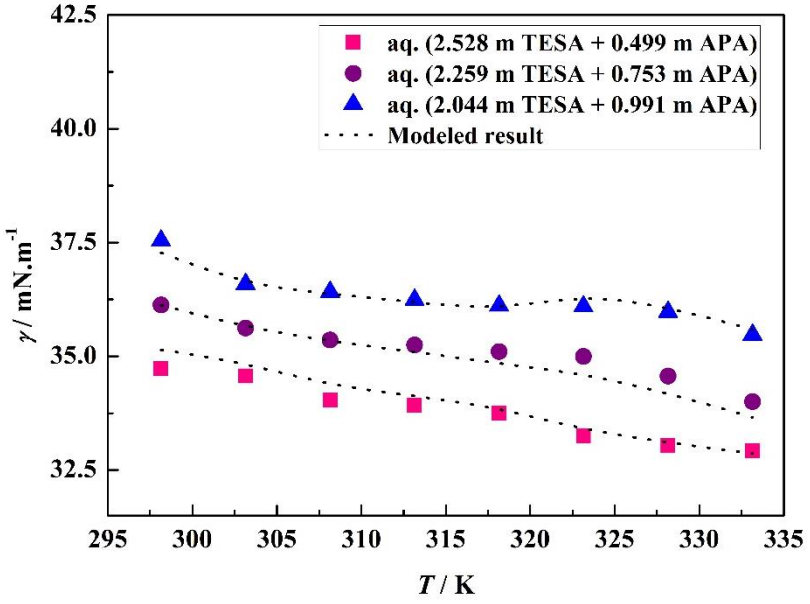

Figure 6.19 Surface tension of aqueous **(TESA + APA)** system at various temperatures and composition (molal)

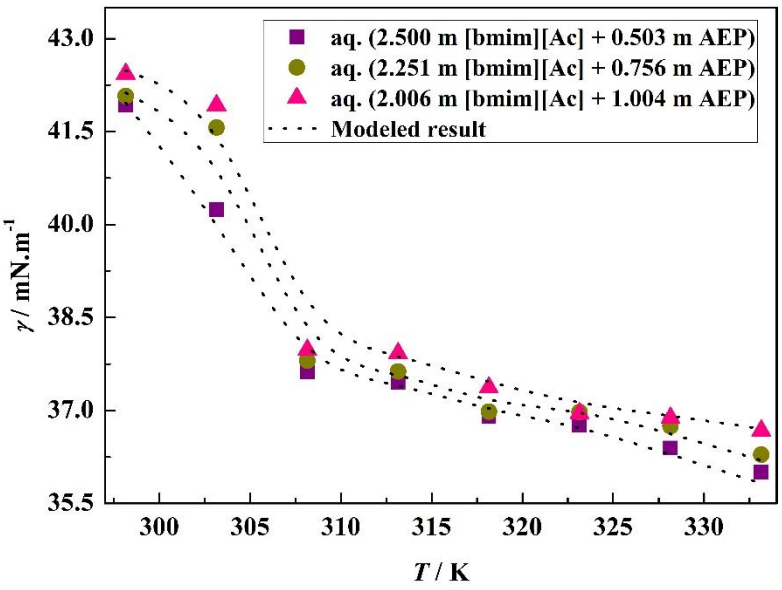

Figure 6.20 Surface tension of aqueous **([bmim][Ac] + AEP)** system at various temperatures and composition (molal)

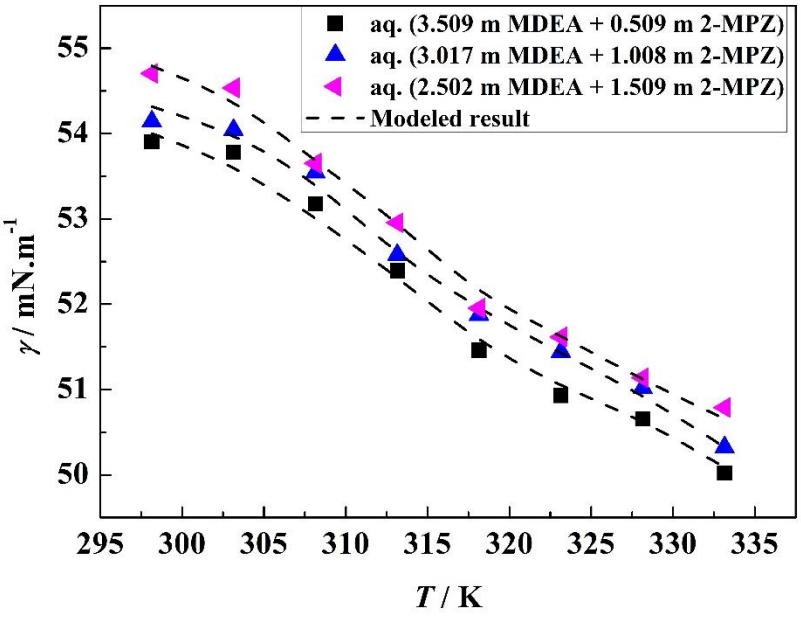

Figure 6.21 Surface tension of aqueous (**MDEA + 2-MPZ**) system at various temperatures and composition (molal)

6.3.5 Thermodynamic property estimation

6.3.5.1 Thermal expansion coefficient

The thermal expansion coefficients (α), of studied blended solvents were estimated using the respective experimentally measured density values in Tables 6.3-6.13, according to the Eq. (6.16) [32] and the same has been presented in Tables 6.19-6.29:

$$\alpha = -\frac{1}{\rho_m} \times \left(\frac{\delta \rho_m}{\delta T} \right)_P \tag{6.16}$$

Where, ρ_m, P and T are the measured solvent density, pressure, and temperature, respectively. It was observed that the values of α were all positive. The values of α for all the studied blends rise with a rise in temperature indicating elevated expansivities for the blended solvents.

6.3.5.2 Isentropic compressibility

The isentropic compressibility a thermo acoustic property has also been calculated using Eq. (6.17) and the same is represented in Tables 6.19-6.29 [24].

$$K_s / m.s^{-2}.kg^{-1} = \frac{1}{\rho \times c^2} \tag{6.17}$$

Where, K_s / m.s^{-2}.kg^{-1} is the isentropic compressibility, c / m.s^{-1} is the experimental sound velocity and ρ / kg.m^{-3} is the experimental density of the blends at various temperatures and compositions of amine/ionic liquid.

6.3.5.3 N_2O/CO_2 diffusivity

The N_2O diffusivity in the blended mixtures are estimated as a function of dynamic viscosity (η) using modified Stokes-Einstein correlation which is presented as follows [33]:

$$(D_{N2O} \times \eta^{0.8})_{TESA+AEP/APA} = Cons\tan t = (D_{N2O} \times \eta^{0.8})_{water} \tag{6.18}$$

The diffusivity of N_2O and CO_2 in water is estimated using the following correlations [34]:

$$D_{N2O} / m^2.s^{-1} = 5.07 \times 10^{-6} \times \exp\left(\frac{-2371}{T/K}\right) \tag{6.19}$$

$$D_{CO2} / m^2.s^{-1} = 2.35 \times 10^{-6} \times \exp\left(\frac{-2119}{T/K}\right) \tag{6.20}$$

The estimated values of diffusivities of N_2O and CO_2 in blended mixtures are given in Tables 6.19-6.29 which indicates that for all the systems, the diffusivity enhances with a rise in temperature and also, increase in the molality of activators AEP, AMP, APA, and 2-MPZ in the studied blends.

6.3.5.4 Estimation of thermodynamic properties

The thermodynamic properties of activation of viscous flow of the systems i.e. enthalpy of activation (ΔH^*), entropy of activation (ΔS^*) and Gibbs energies of activation (ΔG^*) are evaluated using Eyring's advance to Andrade's theory. In the Andrade's theory, kinematic viscosity is expressed in the following form [15]:

$$\eta = \frac{h \times N_A}{M} \times \exp\left(\frac{\Delta G^*}{R \times T}\right) \tag{6.21}$$

Where, $M=\Sigma\,(x_i M_i)$. h, N_A, R, and T are average molecular mass, Planck's constant (6.626×10^{-34} J.s), Avogadro number (6.023×10^{23} mol^{-1}), universal gas constant (8.314 $J.mol^{-1}$ K^{-1}), and absolute temperature, respectively. Using the experimental values of dynamic viscosities of the mixtures at different temperatures from Tables 6.3-6.13 for all the blends, ΔG^* values are evaluated using Eq. (6.21) and are represented in Tables 6.19-6.29. As indicated in Tables 6.19-6.29 that all ΔG^* values are positive for the present systems that indicates a strong and exact interaction amid the constituents in each individual blend under study.

Gibbs free energy can be articulated as by the subsequent thermodynamic equation:

$$\Delta G^* = \Delta H^* - T \times \Delta S^* \tag{6.22}$$

The equation (6.22) is analogous to the linear formula

$$y = mx + c \tag{6.23}$$

Using the calculated values of ΔG^* from equation (6.21), ΔH^* and ΔS^* are estimated using the linear regression method and presented in Tables 6.49-6.52 for the systems under study.

The ΔS^* values are found to be negative for all the systems over the entire composition range which infers that the flow prevails in a controlled manner and involves adjoining liquid layers which should hold on to their molecular arrangement even moving in a still steady state. ΔH^* values are found to be positive for all the systems again inferring a strong definite interaction among the components.

Table 6.49 Enthalpy of activation (ΔH^0 / kJmol^{-1}) and entropy of activation (ΔS^0/J K^{-1}mol^{-1}) for the viscous flow about HEF (1) + AEP (2) and HEF (1) + AMP (2)

Mole fraction (HEF)	Mole fraction (AEP/AMP)	ΔS^0/ J K^{-1} mol^{-1}	ΔH^0/ kJ mol^{-1}
		(HEF + AEP)	
0.232	0.768	2.562	60.470
0.341	0.659	-62.609	43.283
0.446	0.554	-57.073	45.777
0.547	0.453	-54.917	46.829
0.644	0.356	-58.930	45.529
0.738	0.262	-68.531	41.968
0.828	0.172	-77.649	38.418
		(HEF + AMP)	
0.148	0.853	-29.424	51.657
0.229	0.771	-33.303	50.364
0.316	0.684	-41.684	47.586
0.409	0.591	-50.089	44.682
0.509	0.491	-57.234	42.152
0.618	0.383	-65.817	38.995
0.735	0.265	-73.854	35.917

Table 6.50 Enthalpy of activation, ΔH^0/ kJ.mol^{-1}, and entropy of activation, ΔS^0 / J. K^{-1} mol^{-1}, for the viscous flow about (i) aq. TESA, (ii) aq. (TESA + AEP) and (iii) aq. (TESA + APA)

TESA mol.kg^{-1}	AEP/APA mol.kg^{-1}	ΔS^0/ J K^{-1} mol^{-1}	ΔH^0/ kJ mol^{-1}
		aq. TESA	
2.432	0.000	-98.315	19.309
1.506	0.000	-120.163	10.979
0.797	0.000	-107.462	13.856
		aq. (TESA + AEP)	
2.528	0.498	-82.722	25.016
2.259	0.756	-74.237	27.207
2.044	1.004	-24.615	41.311
		aq. (TESA + APA)	
2.528	0.499	-110.311	16.628
2.259	0.753	-99.499	19.585
2.044	0.991	-14.649	53.201

Table 6.51 Enthalpy of activation, ΔH^0/ kJ.mol^{-1}, and entropy of activation, ΔS^0 / J. K^{-1} mol^{-1}, for the viscous flow about (i) aq. [bmim] [Ac], (ii) aq. ([bmim] [Ac] + AEP) and (iii) aq. ([bmim] [Ac] + APA)

[bmim][Ac] mol.kg^{-1}	AEP/APA mol.kg^{-1}	ΔS^0/ J K^{-1} mol^{-1}	ΔH^0/ kJ mol^{-1}
		aq. [bmim] [Ac]	
2.500	0.000	-133.869	7.115
2.251	0.000	-138.883	5.206
2.006	0.000	-111.439	13.364
		aq. ([bmim] [Ac] + AEP)	
2.500	0.503	-116.546	13.192
2.251	0.756	-113.890	13.955
2.006	1.004	-112.324	14.305
		aq. ([bmim] [Ac] + APA)	
2.500	0.504	-116.835	13.161
2.251	0.753	-119.848	12.096
2.006	0.996	-108.330	15.472

Table 6.52 Enthalpy of activation, ΔH^0/ kJ.mol^{-1}, and entropy of activation, ΔS^0 / J. K^{-1} mol^{-1}, for the viscous flow about (i) aq. (MDEA + 2-MPZ), (ii) aq. ($TMSO_2$ + 2-MPZ) and (iii) aq. ([bmim] [Ac] + 2-MPZ)

(MDEA/$TMSO_2$/ [bmim][Ac]) mol.kg^{-1}	2-MPZ mol.kg^{-1}	ΔS^0/ J K^{-1} mol^{-1}	ΔH^0/ kJ mol^{-1}
		aq. (MDEA + 2-MPZ)	
3.509	0.509	-35.513	21.793
3.017	1.008	-53.127	15.342
2.502	1.509	--58.985	12.712
		aq. ($TMSO_2$ + 2-MPZ)	
3.501	0.509	-76.318	6.885
3.012	1.008	-38.889	17.717
2.500	1.509	-30.832	19.491
		aq.([bmim][Ac] + 2-MPZ)	
3.507	0.509	-56.943	14.307
3.002	1.008	-59.524	13.158
2.510	1.509	-17.684	25.672

6.4 Conclusions

Densities, viscosities, sound velocities, refractive indices, and surface tension of various systems were measured and modeled using various correlations over the temperature range (298.15 to 333.15) K at 0.1 MPa pressure over a wide concentration of ionic liquids. All the properties show temperature and concentration dependencies. The experimental densities, viscosities, sound velocities, and refractive indices decrease with rise in temperature. The first principle and fairly adopted literature models were used for correlation of experimental densities, and viscosities where as new models were proposed for sound velocities, refractive indices, and surface tension of systems. Both the literature and new models provided good conformity with the experimental data over the range of temperature and composition studied. Various other properties such as diffusivity of CO_2 in the studied systems, thermal expansion coefficients, isentropic compressibility, enthalpy of activation and entropy of activation, and Gibb's free energy of activation for the viscous flow are estimated using the viscosity of the systems over the entire temperature range. The results of all the studied properties indicate a strong interaction between the ionic liquid and amine systems.

References

[1]N. D. Khupse, A. Kumar. Ionic liquids: new materials with wide applications. Indian Journal of Chemistry 49 (2010) 635-648.

[2]S. Kumar, J. H. Cho, I. Moon. Ionic liquid-amine blends and CO_2 BOLs: prospective solvents for natural gas sweetening and CO_2 capture technology-a review. International Journal of Greenhouse Gas Control 20 (2014) 87–116.

[3]D. Wappel, G. Gronald, R. Kalb, J. Draxler. Ionic liquids for post-combustion CO_2 absorption. International Journal of Greenhouse Gas Control 4 (2010) 486-494.

[4]M. Ramdin, T. W. Loos, T. J. H. Vlugt. State-of-the-art of CO_2 capture with ionic liquids. Industrial and Engineering Chemistry Research 51(2012) 8149-8177.

[5]A. Ahmady, M. A. Hashim, M. K. Aroua. Density, viscosity, physical solubility and diffusivity of CO_2 in aqueous MDEA + [bmim] [BF_4] solutions from 303 to 333 K. Chemical Engineering Journal 172 (2011)763-770.

[6]A. García-Abuín, D. Gomez-Díaz, M. D. Rubia, J. M. Navaza. Density, speed of Sound, viscosity, refractive index, and excess volume of N-methyl-2-pyrrolidone + ethanol (or water or ethanolamine) from T = (293.15 to 323.15) K. Journal of Chemical and Engineering Data 56: (2011) 646–651.

[7]N. A. Ghani, N. A. Sairi, M. K. Aroua, Y. Alias. Density, surface tension, and viscosity of ionic liquids (1-ethyl-3-methylimidazolium diethylphosphate and 1, 3-dimethylimidazolium dimethyl phosphate) aqueous ternary mixtures with MDEA. Journal of Chemical and Engineering Data 59 (2014) 1737−1746.

[8]O. Redlich, A. T. Kister. Algebraic representation of thermodynamic properties and the classification of solutions. Industrial and Engineering Chemistry Research 40 (1948) 345-348.

[9]L. Grunberg, A. H. Nissan, Mixture law for viscosity. Nature 164 (1949) 799-800.

[10]K. E. A. Alvarez, D. Go´mez-Dı´az, M. D. L. Rubia, J M. Navaza. Densities and viscosities of aqueous ternary mixtures of 2-(methylamino) ethanol and 2-(ethylamino) ethanol with

diethanolamine, triethanolamine, *N*- methyldiethanolamine, or 2-amino-1-methyl-1-propanol from 298.15 to 323.15. Journal of Chemical and Engineering Data 51 (2006) 955-962.

[11]B. P. Mandal, M. Kundu, S. S. Bandhyopadhyay. Density and viscosity of aqueous solutions of (N-methyldiethanolamine+ monoethanolamine), (*N*-methyldiethanolamine+ diethanolamine), (2-amino-2-methyl-1-propanol + monoethanolamine) and (2-amino-2-methyl-1-propanol + diethanolamine). Journal of Chemical and Engineering Data 48 (2003) 703-707.

[12]S. Paul, B. P. Mandal. Density and viscosity of aqueous solutions of 2- piperidineethanol, (2-piperidinethanol + monoethanolamine), and (2-piperidinethanol + diethanolamine) from (288 to 333) K. Journal of Chemical and Engineering Data 51 (2006) 1406-1410.

[13]D. D. Pinto, J. G. M. Monteiro, B. Johnsen, H. F. Svendsen, H. Knuutila. Density measurements and modeling of loaded and unloaded aqueous solutions of MDEA (*N*-methyldiethanolamine), DMEA (*N*, *N*-dimethylethanolmine), DEEA (diethylethanolamine) and MAPA (*N*-methyl-1, 3-diaminopropane). International Journal of Greenhouse Gas Control 25 (2014) 173-185.

[14]O. N. Braun, U. A. Persson, H. T. Karlsson. Densities and viscosities of mono (ethylene glycol) + 2-amino-2-methyl-1-propanol + water. Journal of Chemical and Engineering Data 46 (2001) 805-808.

[15]L. Li, J. Zhang, Q. Li, B. Guo, T. Zhao, F. Sha. Density, viscosity, surface tension, and spectroscopic properties for binary system of 1, 2-ethanediamine + diethylene glycol. Thermochimica Acta 590 (2014) 91–99.

[16]E. Alvarez, C. Fernando, G. Diego, M. N. Jose. Density, speed of sound, isentropic compressibility, and excess volume of binary mixtures of 1-amino-2-propanol or 3-amino-1-propanol with 2-amino-2-methyl-1-propanol, diethanolamine, or triethanolamine from (293.15 to 323.15) K. Journal of Chemical and Engineering Data 55 (2010) 2567–2575.

[17]K. G. Bogolitsyn, T. E. Skrebets, T. A. Makhova. Physiochemical properties of 1-butyl-3-methylimidazolium acetate. Russian Journal of General Chemistry 79 (2009) 125-128.

[18]C. A. McCoy, M. C. Gregor, D. N. Polsin, D. E. Fratanduono, P. M. Celliers, T. R. Boehly , D. D. Meyerhofer. Measurements of the sound velocity of shock-compressed liquid silica to 1100 GPa. Journal of Applied Physics 120 (2016) 235901.

[19]S. Nithiyanantham. Ultrasonic velocity models in liquids (micro- and nanofluids): theoretical validations. International Nano Letters 9 (2) (2019) 89-97.

[20]O. S. H. Kristian, V. M. Kurt, M. N. Thomas, A. S. Per-Olof. Refractive index of liquid water in different solvent models .Journal of Physical Chemistry A 109 (2005) 905-914.

[21]B. Remi, M. Didier. Improved model for the refractive index: application to potential components of ambient aerosol. Physical Chemistry Chemical Physics 20 (2018) 22017-22026.

[22]L. Sergey, P. Anna, K. O. Magdalena. Sound velocity and acoustic nonlinearity parameter for fluids. Thermodynamic premises. arXiv:physics/0303117 (2003).

[23]Wu, Shin-Tson. A semi empirical model for liquid-crystal refractive index dispersions. Journal of Applied Physics 69(4) (1991) 2080–2087.

[24]S. Balchandani, B. P. Mandal, S. Dharaskar, A. Kumar, S. S. Bandyopadhyay.Thermally induced characterization and modeling of physicochemical, acoustic, rheological, and thermodynamic properties of novel blends of (HEF + AEP) and (HEF + AMP) for CO_2/H_2S absorption. Environmental Science and Pollution Research. (2019) https://doi.org/10.1007/s11356-019-06305-5.

[25]M. S. Shaikh, A. M. Shariff, M. A. Bustam, G. Murshid. Physical properties of aqueous blends of sodium glycinate (SG) and piperazine (PZ) as a solvent for CO_2 capture. Journal of chemical and engineering data 58 (2013) 634–638.

[26]N. Asprion. Surface tension models for aqueous amine blends. Industrial and Engineering Chemistry Research 44 (18) (2005) 7270–7278.

[27]T. Jianxiang, M. Angel. Improved correlation for viscosity from surface tension data for saturated normal fluids. Industrial and Engineering Chemistry Research 53 (2014) 9499 −9505.

[28]T. Z. Klaas, H. J. M. C. Mart, C. S. Jaap, T. T. Johan. Density, viscosity, and surface tension of liquid phase beckmann rearrangement mixtures. Journal of Chemical and Engineering Data 60 (4) (2015) 1056–1062.

[29]D. Diego, C. M. Juan, M. N. Jose, R. A. Antonio. Effect of composition and temperature upon density, viscosity, surface tension, and refractive index of 2, 2, 4-trimethylpentane + cyclohexane + decane ternary liquid systems. Journal of Chemical and Engineering Data 48 (2) (2003) 231–235.

[30]S. Balchandani, B.P. Mandal, S. Dharaskar. Measurements and modeling of vapor liquid equilibrium of CO_2 in amine activated imidazolium ionic liquid solvents. Fluid Phase Equilibria 521 (2020) 112643.

[31]J. Safarov, M. Geppert-Rybczynska, I. Kul, E. Hassel. Thermophysical properties of 1-butyl-3-methylimidazolium acetate over a wide range of temperatures and pressures. Fluid phase Equilibria 383 (2014) 144-155.

[32]B. Das, B. Deogam, B. P. Mandal. Experimental and theoretical studies on efficient carbon dioxide capture using novel bis (3-aminopropyl) amine (APA)-activated aqueous 2-amino-2-methyl-1-propanol (AMP) solutions. RSC Advances 7 (2017) 21518–21530.

[33]G. N. Patil, P. D. Vaidya, E. Y. Kenig. Reaction kinetics of CO_2 in aqueous methyl- and dimethyl monoethanolamine solutions. Industrial and Engineering Chemistry Research 51 (2012) 1592-1600.

[34]G. F. Versteeg, W. V. Swaalj. Solubility and diffusivity of acid gases (carbon dioxide, nitrous oxide) in aqueous alkanolamine solutions Journal of Chemical Engineering Data 33 (1988) 29-34.

Chapter 7

CONCLUSIONS AND FUTURE SCOPE

This chapter presents the main conclusions drawn from the work examined and reported in this dissertation. Various futuristic approach for the research are also proposed.

7.1 Overall conclusions

A detailed experimental and modeling analysis on the vapor-liquid equilibrium relationship of CO_2 in 27 different related blended solvents relating to 3-aminopropyl triethoxysilane (TESA), 1-(2-aminoethyl) piperazine (AEP), bis (3-aminopropyl) amine (APA), 1-butyl-3-methyl-imidazolium acetate ([bmim] [Ac]), 2-methyl piperazine (2-MPZ), *N*-methyldiethanolamine (MDEA), and sulfolane ($TMSO_2$) were carried out over a wide range of parametric settings. Additionally, various thermophysical properties of the blends are also studied. The imperative outcomes in the studied field are presented further.

- Vapour liquid equilibrium measurements of CO_2 in blended solvents of (TESA + H_2O), (TESA + H_2O + AEP), (TESA + H_2O + APA), ([bmim] [Ac] + H_2O), ([bmim] [Ac] + H_2O + AEP), ([bmim] [Ac] + H_2O + APA), (MDEA + H_2O + 2-MPZ), ($TMSO_2$ + H_2O + 2-MPZ) and ([bmim] [Ac] + H_2O + 2-MPZ) in the temperature range of (303.2-323.2) K and the CO_2 partial pressure range of (0-500) kPa were carried out. It is anticipated that the obtained data shall be useful in screening of effective CO_2 solvents for various applications viz. post or pre-combustion CO_2 capture processes.
- The reactions of CO_2 in the solvent blends have been proposed by analyzing the results of ^{13}C NMR and FTIR analysis of various loaded and unloaded solutions. The modified KE model is subsequently utilized for the prediction of reaction species profiles and pH of the systems. The results confirmed that all the amines and ionic liquids involved in the reaction undergo formation of protonated species and bicarbonate through carbamate hydrolysis.
- Modified Kent-Eisenberg model was used to correlate the experimental vapor liquid equilibrium data. The model is also explored for estimation of the equilibrium constants of the proposed chemical reactions amid various associated molecules. The % AAD between the

experimental and modeled data are obtained as follows: aq. (TESA) : 12.94, aq. (TESA + AEP) : 13.21, aq. (TESA + APA) : 16.21, aq. ([bmim] [Ac]) : 15.70, aq. ([bmim] [Ac] + AEP) : 3.31, aq. ([bmim] [Ac] + APA) : 5.05, aq. (MDEA + 2-MPZ) : 7.56, aq. ($TMSO_2$ + 2-MPZ) : 30.05 and aq. ([bmim] [Ac] + 2-MPZ) : 22.64.

- The major results infer that (i) inclusion of ≈ 0.5 m AEP/APA to 2.432 m aq. TESA intensified the CO_2 solubility by 17 and 50 %, respectively at 303.2 K (ii) α_{CO2} loading in 2.500 m aq. [bmim][Ac] along with the addition of 0.503 m AEP and 0.504 m APA yields an increase of CO_2 loading of 92.37 % and 135.90 %, respectively at 303.2 K, and (iii) for aq. (MDEA + 2-MPZ) system at 313.2 K and 200 kPa, with an increase in 2-MPZ concentration from 0.509 to 1.509 m results in a rise in α_{CO2} by 16.13 %.
- A two-layer feed forward artificial neural network model was applied for aq. ([bmim] [Ac]), aq. ([bmim] [Ac] + AEP) and aq. ([bmim] [Ac] + APA) solvent blends. The optimum number of neurons which is one of the factors dictating the accuracy of prediction was obtained through trial and error method. A comparison of the modified KE model and ANN model revealed that the latter model provides better prediction accuracy with the least deviation of 3.31 % AAD for aq. ([bmim] [Ac] + AEP) system.
- Highest CO_2 loading associated with each blend is evaluated as below:

Blend	Concentration ($mol.kg^{-1}$)	Temperature (K)	CO_2 partial pressure (P_{CO2} / *kPa*)	CO_2 loading (α_{CO2})
aq. ([bmim] [Ac])	2.500	313.2	334.7	0.275
aq. ([bmim] [Ac] + AEP)	(2.006 + 1.004)	303.2	294.8	0.612
aq. ([bmim] [Ac] + APA)	(2.006 + 0.996)	303.2	265.7	0.821
aq. (TESA)	2.432	303.2	237.4	0.894
aq. (TESA + AEP)	(2.044 + 1.004)	303.2	297.4	0.828
aq. (TESA + APA)	(2.044 + 0.991)	313.2	197.5	1.146
aq. (MDEA + 2-MPZ)	(3.017 + 1.008)	303.2	335.4	1.013
aq. ($TMSO_2$ + 2-MPZ)	(2.500 + 1.509)	303.2	316.3	0.399
aq. ([bmim][Ac] + 2-MPZ)	(2.510 + 1.509)	303.2	262.2	0.372

- Out of AEP, APA, and 2-MPZ activators, the blends associated with APA activators outperformed proving its better capabilities for enhancing CO_2 absorption.
- CO_2 cyclic capacity and heat of absorption were calculated for aq. (MDEA + 2-MPZ) system which indicates its competence for application.
- Furthermore, various essential thermophysical, acoustic, and flow properties associated with designing of CO_2 absorption processes such as density, viscosity, surface tension, refractive index, and sound velocity were measured. The interactive parameters of the constituent molecules have been extensively calculated using first principal models such as Redlich-Kister and Grunberg-Nissan model for density and viscosity, respectively. New models for correlating the experimental data of sound velocity, refractive index, and surface tension were proposed in the present work and the competence of the proposed model is determined with marginal deviation from experimental data.
- Additionally, different derived properties such as kinematic viscosity deviations, excess molar volumes, isentropic compressibility, thermal expansion coefficients, CO_2 and N_2O diffusivity, enthalpy, entropy and Gibbs' energy activation of viscous flow were estimated from the measured properties. A brief conclusion from either the measurement or calculated values of properties indicate the highly non-linear behavior of the systems under consideration. All the properties are also found to be a strong function of temperature and concentration over the studied range.
- Lastly, a detailed comparison of the CO_2 solubility in the proposed blends with the literature of conventional blends demonstrate their dominance in the application for CO_2 capture processes.

7.2 Future scope

- The current experimental conditions i.e. temperature range of (303.2-323.2) K and pressure range of (0-500) kPa are more applied to the absorption process. Extending the temperature and pressure range of the studied solvents may lead to regenerative conditions where more extensive analysis can be performed. This will also add the application of pre-combustion process rather than only with post-combustion process.

- The scrutiny of the solvents on a broad level can be carried out using various molecular simulation approaches such as sigma potential, sigma surface change density, polar and non-polar behavioral analysis, HOMO (Highest Occupied Molecular Orbital), and LUMO (Lowest Unoccupied Molecular Orbital), etc. The inferences deducted from the various basic studies can help to understand the CO_2 absorption mechanism and the possible energy losses in the system in a deep fashion. Along with this, a molecular dynamics simulation can also lead us to the confirmation of various species formed during the CO_2 reaction with ionic liquid and amines. The same can subsequently compared with the experimental studies.
- Various important experimental studies of the proposed solvents such as experimental heat of absorption through reaction calorimeter, thermophysical properties, corrosion and thermal or bio-degradation of the loaded and unloaded solvents can be taken as a future scope of the study.
- The mechanical design of absorption or regenerator tower and economic feasibility of application of selected solvents for CO_2 capture can be studied through commercially available softwares such as Aspen Plus® and Hysys. Further, the efficiency of selected solvents for simultaneous absorption of SO_x, NO_x, CO, H_2O, N_2, etc. can be carried out in specified softwares.

Appendix-I

Sample calculation

AI.1 Determination of solvent phase CO_2 loading (Chapters-3, 4 and 5)

Liquid phase CO_2 loading (α_{CO2}) can be defined as:

α_{CO2}= mol of CO_2 / mol of amine

The concentration of CO_2 in the solvent or aqueous phase have been evaluated by the procedure described in Chapter-3, section 3.2.2. The total moles of CO_2 transferred to the equilibrium cell from the buffer cell can be evaluated as:

$$n_{CO2} = \frac{V_b}{RT} \times \left(\frac{P_{b1}}{Z_1} - \frac{P_{b2}}{Z_2} \right) \quad (1)$$

Where,

P_{b1} : Initial buffer cell pressure

P_{b2} : Final buffer cell pressure

V_b : Volume of buffer cell

R : Universal Gas constant

T : Experimental temperature

Z_1 : Compressibility factor of CO_2 at T and P_{b1}

Z_2 : Compressibility factor of CO_2 at T and P_{b2}

Example: **Table 3.4** (solubility data of 2.500 *m* aqueous [bmim] [Ac] system)

P_{b1} = 808.8 kPa

P_{b2} = 754.9 kPa

V_b = 1200 ml

R = 8.314 m^3. kPa. $kmol^{-1}$. K^{-1}

T=303.2 K

Z_1=0.957

Z_2=0.9670

Using all the data given, n_{CO2} can be calculated using equation 1, n_{CO2}=0.086 mol.

The moles of CO_2 remaining in the gas phase (n^g_{CO2}) after the attainment of phase equilibrium can be further evaluated by:

$$n^g_{CO2} = \frac{V^g P_{CO2}}{Z_{CO2} RT} \tag{2}$$

V_g : Volume of gas phase in the equilibrium cell

P_{CO2} : Partial pressure of CO_2 = (P_T-P_v)

P_T : Total pressure of aqueous amine solution

Z_{CO2} : Compressibility factor of CO_2 at T and P_{CO2}

V_g = 550 ml P_T = 102.8 kPa P_v = 4.9 kPa

P_{CO2} = 97.9 kPa Z_{CO2} = 0.995

Using all these given data, we can calculate n^g_{CO2} from Eq. 2, n^g_{CO2} = 0.021 mol

The moles of CO_2 absorbed in the solvent is subsequently calculated from the following equation:

$$n^l_{CO2} = n_{CO2} - n^g_{CO2} \tag{3}$$

n^l_{CO2} = 0.0064

The CO_2 loading in the solvent phase is defined as:

$$\alpha_{CO2} = \frac{n^l_{CO2}}{n_{am}} \tag{4}$$

Where, n_{am} is the total mole of amine in the solvent phase.

n_{am} = 0.105

Therefore, α_{CO2} = 0.061 (mol of CO_2 / mol of amine)

Appendix-II

Error analysis

AII.1 Estimation of error in the determination of CO_2 loading in solvent phase

The following equations from (1-4) are required to be solved for estimating the error associated with estimating of CO_2 loading in the liquid solvent phase.

$$\alpha_{CO_2} = \frac{n^{l}_{CO_2}}{n_{am}} = \frac{n_{CO_2} - n^{g}_{CO_2}}{n_{am}} = \frac{n_{CO_2} - \left(V_g P_{CO_2} \Big/ Z_{CO_2}.RT \right)}{n_{am}} \tag{1}$$

Introducing the initial and final pressures associated with the buffer cell, Eq. (1) can be represented as:

$$\alpha_{CO_2} = \frac{\frac{V_b}{RT}\left[\frac{P_1}{Z_1} - \frac{P_2}{Z_2}\right] - \frac{V_g P_3}{Z_3 RT}}{m_1 \times V_l} \tag{2}$$

Where, P_3 = Cell Pressure

$$\alpha = \frac{V_b P_1}{RTZ_1 m_1 V_l} - \frac{V_b P_2}{RTZ_2 m_1 V_l} - \frac{V_g P_3}{RTZ_3 m_1 V_l} \tag{3}$$

Hence, we can state that the liquid phase CO_2 loading is a function of various other parameters and variables of the system under study and is represented in Eq. (4):

$$\alpha = f(P_1, P_2, P_3, T, V_g, V_b, V_l, m_1) \tag{4}$$

Partial Differentiation is applied to Eq. (3) with respect to various variables associated to the system and contributing to the error to calculation of α_{CO2}. The same is been presented in following equations (5-13):

$$\frac{\partial \alpha}{\partial P_1} = \frac{V_b}{RTZ_1 m_1 V_l} \tag{5}$$

$$\frac{\partial \alpha}{\partial V_b} = \frac{P_1}{RTZ_1 m_1 V_l} - \frac{P_2}{RTZ_2 m_1 V_l} = \frac{1}{RTm_1 V_l}\left[\frac{P_1}{Z_1} - \frac{P_2}{Z_2}\right] \tag{6}$$

$$\frac{\partial \alpha}{\partial P_1} = \frac{V_b}{RTZ_1 m_1 V_l} \tag{7}$$

$$\frac{\partial \alpha}{\partial m_1} = \frac{\frac{V_b}{RT}\left[\frac{P_1}{Z_1} - \frac{P_2}{Z_2}\right] - \frac{V_g P_3}{Z_3 RT}}{V_l} \cdot \left(\frac{-1}{m_1^2}\right) \tag{8}$$

$$\frac{\partial \alpha}{\partial V_l} = \frac{\frac{V_b}{RT}\left[\frac{P_1}{Z_1} - \frac{P_2}{Z_2}\right] - \frac{V_g P_3}{Z_3 RT}}{m_1} \cdot \left(\frac{-1}{V_l^2}\right) \tag{9}$$

$$\frac{\partial \alpha}{\partial P_2} = -\frac{V_b}{RTZ_2 m_1 V_l} \tag{10}$$

$$\frac{\partial \alpha}{\partial P_3} = -\frac{V_g}{RTZ_3 m_1 V_l} \tag{11}$$

$$\frac{\partial \alpha}{\partial V_g} = -\frac{P_3}{RTZ_3 m_1 V_l} \tag{12}$$

$$\frac{\partial \alpha}{\partial T} = \frac{\frac{V_b}{RT}\left[\frac{P_1}{Z_1} - \frac{P_2}{Z_2}\right] - \frac{V_g P_3}{Z_3 R}}{m_1 \times V_l}\left(-\frac{1}{T^2}\right) \tag{13}$$

The absolute error associated with the calculation of CO_2 loading can be calculated as following using equations (5-13):

$$E_a = \left|\Delta P_1 \frac{\partial \alpha}{\partial P_1}\right| + \left|\Delta P_2 \frac{\partial \alpha}{\partial P_2}\right| + \left|\Delta P_3 \frac{\partial \alpha}{\partial P_3}\right| + \left|\Delta T \frac{\partial \alpha}{\partial T}\right| + \left|\Delta V_g \frac{\partial \alpha}{\partial V_g}\right| + \left|\Delta V_b \frac{\partial \alpha}{\partial V_b}\right| + \left|\Delta V_l \frac{\partial \alpha}{\partial V_l}\right| + \left|\Delta m_1 \frac{\partial \alpha}{\partial m_1}\right|$$

AII.2 Sample calculation of estimated error in liquid phase CO_2 loading (Solubility data of 2.500 *m* aq. [bmim] [Ac])

Temperature, T = 303.2 K

Initial buffer cell pressure, P_1 = 808.7 kPa

Final buffer cell pressure, P_2 = 754.9 kPa

Compressibility factor, Z_1 = 0.957

Compressibility factor, Z_2 = 0.960

Volume of buffer cell, V_b = 0.0012 m^3

R (Universal gas constant) = 8.314 $kPa.m^3.kmol^{-1}.K^{-1}$

Volume of equilibrium cell = 0.0006 m^3

Volume of solvent in the equilibrium cell = 0.000050 m^3

Volume of gas phase in cell = 0.00055 m^3

Concentration of solution = 1.717 $kmol.m^{-3}$

ΔP_1 = 0.05 ΔP_2 = 0.05 ΔP_3 = 0.05 ΔT = 0.1 K ΔV_g = 0.000005 m^3

ΔV_b = 0.000005 m^3 $\Delta V_l = 1\times10^{-6}$ m_1=1.717 Δm_1= 0.00025 Z_1=0.957

Z_2 = 0.960 Z_3 = 0.995

$\frac{\partial \alpha}{\partial P_1} = 0.0058$ $\frac{\partial \alpha}{\partial V_b} = 270.6837$ $\frac{\partial \alpha}{\partial P_2} = -0.00578$ $\frac{\partial \alpha}{\partial m_1} = 0.0435$

$\frac{\partial \alpha}{\partial V_1} = -1493.89$ $\frac{\partial \alpha}{\partial P_3} = -0.0026$ $\frac{\partial \alpha}{\partial T} = 0.0008$ $\frac{\partial \alpha}{\partial V^g} = -454.774$

Calculated error in α_{CO2} =0.0044

Appendix-III

AIII.1 Derivation of modified Kent-Eisenberg Model for aq. (TESA+ AEP) system (Chapters-3)

The equilibrium reactions for (TESA+AEP+H_2O+CO_2) are expressed using reactions (RIII.1 to RIII.10) as given below:

Physical Solubility

$$CO_2(g) \xleftrightarrow{H_{CO2}} CO_2(aq) \quad \text{(RIII.1)}$$

Dissociation of bicarbonate ion

$$HCO^{3-} \xleftrightarrow{K_1} CO_3^{2-} + H^+ \quad \text{(RIII.2)}$$

Formation of bicarbonate ion

$$CO_2 + H_2O \xleftrightarrow{K_2} HCO_3^- + H^+ \quad \text{(RIII.3)}$$

Dissociation of water

$$H_2O \xleftrightarrow{K_3} OH^- + H^+ \quad \text{(RIII.4)}$$

Deprotonation of TESA

$$TESAH^+ \xleftrightarrow{K_4} TESA + H^+ \quad \text{(RIII.5)}$$

Carbamate hydrolysis of TESA

$$TESACOO^- + H_2O \xleftrightarrow{K_5} TESA + HCO_3^- \quad \text{(RIII.6)}$$

Deprotonation of AEP

$$AEPH^+ \xleftrightarrow{K_6} AEP + H^+ \quad \text{(RIII.7)}$$

Carbamate hydrolysis of AEP

$$AEPCOO^- + H_2O \xleftrightarrow{K_7} AEP + HCO_3^- \quad \text{(RIII.8)}$$

Deprotonation of APA

$$APAH^{+} \xleftrightarrow{K'_6} APA + H^{+} \quad \text{(RIII.9)}$$

Carbamate hydrolysis of APA

$$APACOO^{-} + H_2O \xleftrightarrow{K'_7} APA + HCO_3^{-} \quad \text{(RIII.10)}$$

In modified KE model, activity coefficients (γ_i) of all component species in liquid phase are considered unit. The concentration of component species based observable equilibrium constants of R_2- R_{10} are presented as:

$$K_1 = \frac{[CO_3^{2-}][H^+]}{[HCO_3^-]} \quad (1)$$

$$K_2 = \frac{[HCO^{3-}][H^+]}{[CO_2]} \quad (2)$$

$$K_3 = [H^+][OH^-] \quad (3)$$

$$K_4 = \frac{[TESA][H^+]}{[TESAH^+]} \quad (4)$$

$$K_5 = \frac{[TESA][HCO_3^-]}{[TESACOO^-]} \quad (5)$$

$$K_6 = \frac{[AEP][H^+]}{[AEPH^+]} \quad (6)$$

$$K_7 = \frac{[AEP][HCO_3^-]}{[AEPCOO^-]} \quad (7)$$

$$K'_6 = \frac{[APA][H^+]}{[APAH^+]} \quad (8)$$

$$K'_7 = \frac{[APA][HCO_3^-]}{[APACOO^-]} \quad (9)$$

Vapor phase equilibrium, which dictates the relationship between CO_2 partial pressure P_{CO_2} at equilibrium and physically dissolved CO_2 concentration [CO_2], is expressed here by Henry's law as presented in Eq. (10).

$$P_{CO_2} = H_{CO_2} \times [CO_2] \quad (10)$$

The general mass and charge balance of various molecular and ionic species present in the liquid phase can be presented as:

TESA Balance:

$$[TESA]_t = M_1 = [TESA] + [TESAH^+] + [TESACOO^-] \quad (11)$$

AEP Balance:

$$[AEP]_t = M_2 = [AEP] + [AEPH^+] + [AEPCOO^-] \quad (12)$$

CO_2 Balance for aqueous TESA+AEP system:

$$\alpha_{CO_2} \times (M_1 + M_2) = [CO_2] + [HCO^{3-}] + [CO_3^{2-}] + [TESACOO^-] + [AEPCOO^-] \quad (13)$$

Electro neutrality balance / Charge Balance for aqueous TESA +AEP system:

$$[H^+] + [AEPH^+] + [TESAH^+] = [HCO_3^-] + 2 \times [CO_3^{2-}] + [OH^-] + [AEPCOO^-] + [TESACOO^-] \quad (14)$$

Let us denote all the species with following notations:

a=[R_1]=[TESA]$_t$

b=[R_1H^+]=[$TESAH^+$]

c=[$R1COO^-$]=[$TESACOO^-$]

d=[HCO_3^-]

e=[CO_3^{2-}]

f=[OH^-]

g=[R_2]=[AEP]$_t$

h=[R_2H^+]=[$AEPH^+$]

q=[R_2COO^-]=[$AEPCOO^-$]

Using equation (3),

$$OH^- = f = \frac{K_3}{[H^+]} \tag{15}$$

Writing $[HCO_3^-]$ as a function of $[CO_2]$ and $[H^+]$ from equation (2),

$$d = [HCO_3^-] = \frac{K_2 \times [CO_2]}{[H^+]} \tag{16}$$

From equations (1) and (16),

$$e = [CO_3^{2-}] = \frac{K_1 \times [HCO_3^-]}{[H^+]} = \frac{K_1 \times K_2 \times [CO_2]}{[H^+]^2} \tag{17}$$

From equation (4),

$$K_4 = \frac{[R_1] \times [H^+]}{[R_1H^+]} = \frac{a \times [H^+]}{b} \tag{18}$$

Using equation (5),

$$[R_1COO^-] = \frac{[R_1] \times [HCO_3^-]}{K_5} \tag{19}$$

Using expressions (18) in (19),

$$c = \frac{a \times [HCO_3^-]}{K_5} = \frac{b \times K_2 \times K_4 \times [CO_2]}{[H^+]^2 \times K_5} \tag{20}$$

Using equation (11),

$$M_1 = a + b + c \tag{21}$$

Substituting the values of *a* and *c* from equations (18) and (20) in equation (21) and expressing the equation of *b* functional to M_1, $[H^+]$ and $[CO_2]$,

$$b = \frac{M_1 \times K_5 \times [H^+]^2}{\{K_4 \times K_5 \times [H^+] + K_5 \times [H^+]^2 \times K_2 \times K_4 \times [CO_2]\}} \quad (22)$$

Re-writing equation (14),

$$[H^+] + b + h = d + 2 \times e + f + c + q \quad (23)$$

The system of equations (15-23) can be utilized to develop polynomial equations which are formed in terms of $[H^+]$. The equation hence formed for systems considered associated with the coefficients can be given as follows:

$$A_2 \times [H^+]^7 + B_2 \times [H^+]^6 + C_2 \times [H^+]^5 + D_2 \times [H^+]^4 + E_2 \times [H^+]^3 + F_2 \times [H^+]^2 + G_2 \times [H^+] + I_2 = 0 \quad (24)$$

Where,

$$A_2 = K_5 \times K_7 \quad (24.1)$$

$$B_2 = K_5 \times K_7 \times (K_6 + K_4 + M_1 + M_2) \quad (24.2)$$

$$C_2 = K_4 \times K_7 \times \{K_5 \times K_6 + K_2 \times [CO_2] + M_2 \times K_5\} + K_5 \times K_7 \times \{M_1 \times K_6 + M_2 \times K_4 - K_2 \times [CO_2] - K_3\} + K_2 \times K_5 \times K_6 \times [CO_2] \quad (24.3)$$

$$D_2 = K_2 \times K_6 \times [CO_2] \times \{K_4 \times K_7 + K_4 \times K_5 + M_1 \times K_5 - K_5 \times K_7 - M_2 \times K_5\} + K_2 \times K_4 \times K_7 \times [CO_2] \times \{M_2 - K_5 - M_1\} - K_5 \times K_7 \times \{2 \times K_1 \times K_2 \times [CO_2] + K_3 \times K_4 + K_3 \times K_6\} \quad (24.4)$$

$$E_2 = K_2^2 \times [CO_2]^2 \times \{K_4 \times K_6 - K_5 \times K_6 - K_4 \times K_7\} - K_2 \times K_5 \times K_7 \times [CO_2] \times \{K_4 \times K_6 + 2 \times K_1 \times K_4 + 2 \times K_1 \times K_6\} - K_2 \times K_3 \times [CO_2] \times \{K_5 \times K_6 + K_4 \times K_7\} - K_2 \times K_4 \times K_6 \times [CO_2] \times \{K_7 \times M_1 + K_5 \times M_2\} - K_3 \times K_4 \times K_5 \times K_6 \times K_7 \quad (24.5)$$

$$F_2 = -K_2^2 \times [CO_2]^2 \times \{K_4 \times K_6 \times (K_5 + K_7) + 2 \times K_1 \times (K_5 \times K_6 + K_4 \times K_7) + K_4 \times K_6 \times (M_1 + M_2)\}$$
$$-K_2 \times K_4 \times K_6 \times [CO_2] \times \{2 \times K_1 \times K_5 \times K_7 + K_3 \times (K_5 + K_7)\}$$

(24.6)

$$G_2 = -K_2^2 \times K_4 \times K_6 \times [CO_2]^2 \times \{K_2 \times [CO_2] + 2 \times K_1 \times K_7 + K_3\} - 2 \times K_1 \times K_2^2 \times K_4 \times K_5 \times K_6$$

(24.7)

$$I_2 = -2 \times K_2^3 \times K_1 \times K_4 \times K_6 \times [CO_2]^3 \quad (24.8)$$

The modified form of loading equation for the aq. (TESA+AEP) system is represented as follows:

$$\alpha_{CO_2} = \frac{\varphi_{CO2} \times P_{CO_2}}{(H_{CO_2} \times (M_1 + M_2))} \left[1 + \frac{K_2}{[H^+]} + \frac{K_1 \times K_2}{[H^+]^2} + \frac{M_1 \times K_2 \times K_4}{K_4 \times K_5 \times [H^+] + K_5 \times [H^+]^2 + K_2 \times K_4 \times \left[\frac{P_{CO_2}}{H_{CO_2}} \right]} + \frac{M_2 \times K_2 \times K_6}{K_6 \times K_7 \times [H^+] + K_7 \times [H^+]^2 + K_2 \times K_6 \times \left[\frac{P_{CO_2}}{H_{CO_2}} \right]} \right]$$

(25)

Appendix-IV

Typical M-File and Program output

AIV.1 Modeling of vapor liquid equilibrium data using Modified Kent-Eisenberg Model for aq. (TESA + AEP) system including gas phase non-ideality

Main file

```
clc
clear
format long e
xo=[-2.49386074321245e-09,2.27778545507644e-12,-2.56611303407048e-
12,2.22418842711348e-13,1.01970217354535e-13,-5.60429202308921e-11,-
5.74143642480112e-24,29.4762084601375,-0.462551867426009,-1.12601753379377,-
0.363687399354544,1.09415878425581,-0.0284331449590179,2.20081401476630,-
0.0240774019404149]
options=optimset('MaxFunEvals',100,'TolX',1e-500,'TolFun',1e-
40,'MaxIter',40000,'PlotFcns',{@optimplotx,@optimplotfunccount,@optimplotfval,@optimp
lotstepsize});
[AAD,fval]=fminsearch(@adjKENAS_tesa_aep,xo,options)
%parameters [-2.49386074321245e-09,2.27778545507644e-12,-2.56611303407048e-
12,2.22418842711348e-13,1.01970217354535e-13,-5.60429202308921e-11,-
5.88497233542115e-24,29.4762084601375,-0.462551867426009,-1.12601753379377,-
0.363687399354544,1.12151275386221,-0.0284331449590179,2.20081401476630,-
0.0240774019404149;]
%fval = 1.321366022660457e+001
```

Function file

```
function [AAD] = adjKENAS_tesa_aep(xo)
%UNTITLED Summary of this function goes here
%   Detailed explanation goes here
```

```
g=xo(1);
h=xo(2);
q=xo(3);
r=xo(4);
s=xo(5);
y=xo(6);
z=xo(7);
g1=xo(8);
h1=xo(9);
q1=xo(10);
r1=xo(11);
s1=xo(12);
y1=xo(13);
z1=xo(14);
d1=xo(15);
P_exp=[67.22388075 109.2818985 139.6188293 184.9863303 219.4601153
257.519174 305.4377351 4.61948719 69.29230785 130.1730122 179.6084199
206.2911294 265.5170921 315.6419755 333.4304485 348.6678615 7.03265214
22.7526981 98.87081538 153.8220287 195.2595182 254.140743 297.3708694
9.23897438 41.16169929 123.8987833 168.0941757 211.3243021 227.5959286
255.9333798 9.79055494 32.33641033 92.94132436 118.3140301 180.3668431
232.1464682 301.3008809 9.37686952 20.61532343 91.63132053 156.648879
198.500054 244.2122929 12.61740531 20.54637586 129.9661695 180.9873713
213.9443097 257.7260167 11.51424419 23.99375436 97.97449697 132.0345966
158.579411 201.9474325 9.92845008 17.16794493 72.94652906 139.9635671
178.298416 179.263682 187.606338 216.8401077];
alfa_exp=[0.444398336 0.532762167 0.58077516 0.618111013 0.647062827
0.693309353 0.718838715 0.318635094 0.53600126 0.619614582 0.661474526
0.698991289 0.724889274 0.779276183 0.827177751 0.874022452 0.297825518
0.545531672 0.665894905 0.723932585 0.777568845 0.810641093 0.827679043
0.306323432 0.498447477 0.608722566 0.643811292 0.703263464 0.761619563
0.772471363 0.26674329 0.507267863 0.613032199 0.729127732 0.761204562
0.778366669 0.796273731 0.234615626 0.477400721 0.595879541 0.637138883
0.651907054 0.667416215 0.332104444 0.463599488 0.611467567 0.642928253
```

0.660032057 0.674281931 0.241085417 0.470965622 0.576241498 0.612622462
0.635465657 0.668509665 0.234680578 0.446810405 0.574302231 0.623914992
0.650415263 0.682262981 0.76935112 0.740643039];

T_exp=[303.15 303.15 303.15 303.15 303.15 303.15 303.15 303.15 303.15 303.15
303.15 303.15 303.15 303.15 303.15 303.15 303.15 303.15 303.15 303.15 303.15
303.15 313.15 313.15 313.15 313.15 313.15 313.15 313.15 313.15 313.15 313.15
313.15 313.15 313.15 313.15 313.15 313.15 313.15 313.15 313.15 323.15 323.15
323.15 323.15 323.15 323.15 323.15 323.15 323.15 323.15 323.15 323.15 323.15
323.15 323.15 323.15 323.15 323.15];

m1_exp=[1.587923617 1.587923617 1.587923617 1.587923617 1.587923617
1.587923617 1.587923617 1.445837454 1.445837454 1.445837454 1.445837454
1.445837454 1.445837454 1.445837454 1.445837454 1.445837454 1.324008679
1.324008679 1.324008679 1.324008679 1.324008679 1.324008679 1.324008679
1.576072 1.576072 1.576072 1.576072 1.576072 1.576072
1.576072 1.435369919 1.435369919 1.435369919 1.435369919 1.435369919
1.435369919 1.435369919 1.314717948 1.314717948 1.314717948 1.314717948
1.314717948 1.314717948 1.563748747 1.563748747 1.563748747 1.563748747
1.563748747 1.563748747 1.42444291 1.42444291 1.42444291 1.42444291
1.42444291 1.42444291 1.304982894 1.304982894 1.304982894 1.304982894
1.304982894 1.304982894 1.304982894 1.304982894];

m2_exp=[0.312570616 0.312570616 0.312570616 0.312570616 0.312570616
0.312570616 0.312570616 0.483622693 0.483622693 0.483622693 0.483622693
0.483622693 0.483622693 0.483622693 0.483622693 0.483622693 0.650663391
0.650663391 0.650663391 0.650663391 0.650663391 0.650663391 0.650663391
0.310237716 0.310237716 0.310237716 0.310237716 0.310237716 0.310237716
0.310237716 0.480121375 0.480121375 0.480121375 0.480121375 0.480121375
0.480121375 0.480121375 0.646097606 0.646097606 0.646097606 0.646097606
0.646097606 0.646097606 0.307811978 0.307811978 0.307811978 0.307811978
0.307811978 0.307811978 0.476466365 0.476466365 0.476466365 0.476466365
0.476466365 0.476466365 0.641313465 0.641313465 0.641313465 0.641313465
0.641313465 0.641313465 0.641313465 0.641313465];

phi=[0.99681052 0.994820225 0.993387071 0.991247704 0.989625127
0.987836887 0.985589983 0.999780499 0.996712543 0.993833081 0.991501066
0.990244638 0.987461508 0.985112166 0.984279769 0.983567306 0.999665854

```
0.998919343  0.995312534  0.992716803  0.990763898  0.987995495  0.985967881
0.999607594  0.998252926  0.994750448  0.99288458   0.991062849  0.990378024
0.989186513  0.999584171  0.998627251  0.996059518  0.994986478  0.992367065
0.99018659   0.98728192   0.999601738  0.999124618  0.996114951  0.993367448
0.991602918  0.989679178  0.99951971   0.999218006  0.995063785  0.993132628
0.991887197  0.990235118  0.999561693  0.999086859  0.996276588  0.994985422
0.993980309  0.992340374  0.999622048  0.999346547  0.997226428  0.994685087
0.993234312  0.993197809  0.992882374  0.991777841];
data=[P_exp' m1_exp' m2_exp' T_exp' alfa_exp' phi'];
for i=1:length(data)
PCO2=data(i,1)*data(i,6)   % Pco2=P_exp*fugacity coeff;
m1=data(i,2);
m2=data(i,3);
T=data(i,4);
alpha=data(i,5);
%constants
% find the values of K1, K2, K3, K6  from the literature data
% using eq. ln Ki= ai+(bi/T) + ci lnT----------------------------------
%--------HCO3- <---> Co3(2-) +H+  K1 is the equilibrium constant
a1=220.067;
b1=-12431.7;
c1=-35.4819;
lnk1=a1+(b1/T) + (c1*log(T));
k1=exp(lnk1);
%----CO2+H2O <---> HCO3- +H+    K2 is the equilibrium constant
a2=235.485;
b2=-12092.1;
c2= -36.7816;
lnk2=a2+(b2/T) + (c2*log(T));
k2=exp(lnk2);
%------ H2O <---> OH- + H+  K3 is the equilibrium constant
a3=140.932;
b3=-13445.9;
c3=-22.4773;
```

```
lnk3=a3+(b3/T) + (c3*log(T));
k3=exp(lnk3);
% ah=-6789.04; %for henry's law
% bh=-11.4519;
% ch=-0.010454;
% dh=94.4914;
%
% Hco2=exp((ah/T)+(bh*log(T))+(ch*T)+dh);
Hco2=exp((20.2669)-(1.3806*(10^4)/T)+(0.06913*(10^8)/(T^2))-
(0.015589*(10^11)/(T^3))+(0.012*(10^13)/(T^4)));% Henry's constant is in k Pa.m3/kmol
k4=     (-1.0157E-10)+          (1.1560E-08*(m1))+(-2.1104E-11*(T))+(1.9059E-
12*(T*m1))+(1.2301E-13*(T^2))+(-7.0939E-12*(PCO2))+(-3.6388E-18*(PCO2^2));
k5=     22.16128717+(-0.004034554*(m1))+(-
0.007910704*(T))+(0.001534304*(m1^2))+(0.008261233*(T*m1))+(-
0.000219904*(T^2))+(0.070282165*PCO2)+(-0.00021608*(PCO2^2));
% k4=g+h*m1+q*T+r*T*m1+s*T^2+y*PCO2+z*PCO2^2
% k5=g1+h1*m1+q1*T+r*m1^2+s1*T*m1+y1*T^2+z1*PCO2+d1*PCO2^2
m=m1+m2;
k6=g+h*m+q*T+r*T*m+s*T^2+y*PCO2+z*PCO2^2
k7=g1+h1*m+q1*T+r*m^2+s1*T*m+y1*T^2+z1*PCO2+d1*PCO2^2
Cx=PCO2/Hco2;
A=k5*k7;
B=k5*(k5*k6*k7)+(k4*k5*k7)+(m1*k5*k7)+(m2*k5*k7);
C=(k4*k5*k6*k7)+(k2*k4*k7*Cx)+(k2*k5*k6*Cx)+(m1*k5*k6*k7)+(m2*k4*k5*k7)-
(k2*k5*k7*Cx)-(k3*k5*k7);
D=(k2*k4*k6*k7*Cx)+(k2*k4*k5*k6*Cx)+(m1*k2*k5*k6*Cx)+(m2*k2*k4*k7*Cx)-
(k2*k4*k5*k7*Cx)-(k2*k5*k6*k7*Cx)-(2*k1*k2*k5*k7*Cx)-(k3*k4*k5*k7)-
(k3*k5*k6*k7)-(k2*k4*k7*m1*Cx)-(k2*k5*k6*Cx*m2);
E=(k2*k2*k4*k6*Cx*Cx)-(k2*k4*k5*k6*k7*Cx)-(k2*k2*k5*k6*Cx*Cx)-
(k2*k2*k4*k7*Cx*Cx)-(2*k1*k2*k4*k5*k7*Cx)-(2*k1*k2*k5*k6*k7*Cx)-
(k3*k4*k5*k6*k7)-(k2*k3*k5*k6*Cx)-(k2*k3*k4*k7*Cx)-(k2*k4*k6*k7*m1*Cx)-
(k2*k4*k5*k6*m2*Cx);
```

```
F=-(k2*k2*k4*k5*k6*Cx*Cx)-(k2*k2*k4*k6*k7*Cx*Cx)-(2*k1*k2*k4*k5*k6*k7*Cx)-
(2*k1*k2*k2*k5*k6*Cx*Cx)-(2*k1*k2*k2*k4*k7*Cx*Cx)-(k2*k3*k4*k5*k6*Cx)-
(k2*k3*k4*k6*k7*Cx)-(k2*k2*k4*k6*m1*Cx*Cx)-(k2*k2*k4*k6*m2*Cx*Cx);
G=-(k2*k2*k2*k4*k6*Cx*Cx*Cx)-(2*k1*k2*k2*k4*k5*k6)-
(2*k1*k2*k2*k4*k6*k7*Cx*Cx)-(k2*k2*k3*k4*k6*Cx*Cx)
I=-(2*k1*k2*k2*k2*k4*k6*Cx*Cx*Cx)
eq=[A B C D E F G I];
HR=roots(eq);
HA=HR(HR>=1e-12&HR<=1e-5); %select the valid value of [H+]
H=real(HA(1)); %in case there are 2 values of [H+]
alpha= (Cx + (k2*Cx/H) + (k1*k2*Cx/H^2) + ((m1*k2*k4*Cx)/(k4*k5*H + k5*H*H +
k2*k4*Cx))+((m2*k2*k6*Cx)/(k7*k6*H + k7*H*H + k2*k6*Cx)))/(m)
%Cx/AM*(1+(AM*k2/(kc*H+kc*H^2/k1+k2*Cx))+k2*k3/H^2+k2/H);
error=((alpha-data(i,5)));
cal1(i,1)=alpha;
cal2(i,1)=abs(alpha-data(i,5))/data(i,5)*100;
end
results=[cal1,cal2]
AAD=sum(cal2)/numel(cal2)
end
```

Program output:

```
results =4.192729700329720e-01    5.653793889774606e+00
    5.055169356822654e-01    5.113957597843955e+00
    5.556857267374387e-01    4.319990762442613e+00
    6.194723195500689e-01    2.202365790995590e-01
    6.613994580726523e-01    2.215647457159886e+00
    7.020702717252741e-01    1.263637752377788e+00
    7.428913736066878e-01    3.346043848888664e+00
    1.727275601062467e-01    4.579141991614814e+01
    4.588697343248438e-01    1.439017618636871e+01
    5.897198678979987e-01    4.824727333805918e+00
    6.735364250643934e-01    1.823486557726241e+00
```

7.140900129909509e-01	2.160073269661436e+00
7.941915237281534e-01	9.560391112664380e+00
8.417262842747283e-01	8.013859865999303e+00
8.449879283045837e-01	2.153125768077347e+00
8.317405926985438e-01	4.837617066324071e+00
2.461748923560117e-01	1.734257896732284e+01
3.200384088551571e-01	4.133458692107668e+01
5.657523158821782e-01	1.503879791929356e+01
6.855016105972842e-01	5.308639947836554e+00
7.672387485401297e-01	1.328512134494054e+00
8.798842538221972e-01	8.541777787990471e+00
9.549829509887345e-01	1.538083017389321e+01
2.289402580615695e-01	2.526191791244703e+01
3.328708980504939e-01	3.321846063823213e+01
5.075246478597697e-01	1.662463719806147e+01
5.721911216409183e-01	1.112440419250702e+01
6.261029728971768e-01	1.097177587812570e+01
6.444174604036298e-01	1.538853625748715e+01
6.736458154962965e-01	1.279342539248325e+01
2.655933983472852e-01	4.310855027374224e-01
3.282270652057668e-01	3.529511937448189e+01
4.910979488359071e-01	1.989035002777937e+01
5.416001432098786e-01	2.571944263808655e+01
6.468693766730131e-01	1.502029691290616e+01
7.224126508800551e-01	7.188645191068020e+00
7.978625118132665e-01	1.995269655914998e-01
2.910860584831466e-01	2.406933990114817e+01
2.989136324164771e-01	3.738726833291124e+01
5.211769647870940e-01	1.253652308443763e+01
6.602752795980587e-01	3.631295658667039e+00
7.416971598668929e-01	1.377345210731419e+01
8.289866725773841e-01	2.420835064329147e+01
2.233457827727315e-01	3.274833059062242e+01
2.540441990828528e-01	4.520179472612946e+01

4.929589003161670e-01	1.938102249073712e+01
5.630609940863330e-01	1.242242171517495e+01
6.023392126835918e-01	8.740915491080186e+00
6.473313807690292e-01	3.996926061922133e+00
2.408563879710406e-01	9.499912180894694e-02
2.878612615801491e-01	3.887849810401890e+01
4.767165404621555e-01	1.727139712833465e+01
5.394570185019176e-01	1.194299067311743e+01
5.837409111100891e-01	8.139660313682528e+00
6.501973714449341e-01	2.739271324531399e+00
2.537328124455304e-01	8.118368638724915e+00
2.796979676286142e-01	3.740119645857080e+01
4.499217341064885e-01	2.165767259460838e+01
5.955322161414559e-01	4.549141505249179e+00
6.699789291437142e-01	3.007873162981753e+00
6.718243910468064e-01	1.529995066989233e+00
6.877442816569183e-01	1.060722941991451e+01
7.432357151490563e-01	3.500574517728424e-01

AAD =1.354726229628581e+01

AIV.2 Determining excess molar volume and binary interaction parameters using Redlich-Kister equation for aq. (TESA + AEP) system.

```
clc
clear
format long e
%1 is for TESA, 2 for AEP and 3 for H20
% %calculation of densities of pure components
rho=[943.51    938.77 934.02 929.28 924.54 919.80 915.06 910.32;980.60 976.60 972.50
968.40 964.20 960.20 956.10 952.00;997.05 995.65 994.03 992.22 990.21 988.04 985.69
983.20] ;
```

```
%rhom is experimental densities of mixtures in kg/m3
%row indicates composition and column indicates temperature
%-------------------------------------------------------------------
T=[ 298.15      303.15 308.15 313.15 318.15 323.15 328.15 333.15];
M=[221.37 129.21 18]'; %M is molecular weights
%rhom is experimental densities of mixtures in kg/m3
%row indicates coposition and column indicates temperature
rhom=[1023.741      1020.152      1016.398      1012.538      1008.605      1004.621
1000.595      996.527
1026.163      1022.684      1019.036      1015.28      1011.443      1007.551
1003.608      999.62
1028.433      1025.064      1021.523      1017.871      1014.134      1010.334
1006.478      1002.569]
%2.5 M 2.25 M and third row is 2.0 M of TESA
%-----------------------------------------------------------
%calculation of pure component volume at set of experimental temperatures from density
above
for j=1:8
V01(j)=M(1)/rho(1,j);
V02(j)=M(2)/rho(2,j);
V03(j)=M(3)/rho(3,j);
V0=[ V01; V02; V03];% V0
end
%x1,x2,x3 are weight percentage 1 is for silane , 2 for AEP and 3 for H20
x1=[ 34.45747801 31.29657228 28.59292701];
x2=[ 3.958944282 6.110283159 8.20165538];
x3=[61.58357771 62.59314456 63.20541761];
%-------------------------------------------------------------------
% mole fractions are found using mass percentage
for ii=1:3 % 3 indicates the number of composition taken
xf1(ii)=(x1(ii)/M(1))/((x1(ii)/M(1))+(x2(ii)/M(2))+(x3(ii)/M(3))); %mole fraction of silane %
xf1=(wt%X1M1)/(wt%X1M1+wt%X2M2+wt%X2M2)
xf2(ii)=(x2(ii)/M(2))/((x1(ii)/M(1))+(x2(ii)/M(2))+(x3(ii)/M(3))); %mole fraction of AEP
xf3(ii)=(x3(ii)/M(3))/((x1(ii)/M(1))+(x2(ii)/M(2))+(x3(ii)/M(3))); %mole fraction of Water
```

```
xm(ii)=xf1(ii)*M(1)+xf2(ii)*M(2)+xf3(ii)*M(3); %xm is the average molecular weight of components summation(sigma)of (mole fraction *molecular mass)
xf1;
xf2;
xf3;
xm;
for j=1:8
s1(ii,j)=xf1(ii)*V0(1,j)+xf2(ii)*V0(2,j)+xf3(ii)*V0(3,j);% s1 is summation(sigma) of (mole fractions *pure component volume)
%excess volume of liquid mixtures VE=Vm- sigma(x*Vio) %s1 indicates this sigma(x*Vio)
%Vm is the molar volume of the liquid mixture and Vi0 is the molar volume of the pure fluids at the system temperature
end
end
s1;
xm;
%-------------------------------------------------------------
%------------ CALCULATION OF EXPERIMENTAL MOLAR VOLUMES
for jj=1:8 %Vm is molar volume calculate using mole fractions and density
VM1(jj)=xm(1)/rhom(1,jj); %jj is because of no of compositions taken
VM2(jj)=xm(2)/rhom(2,jj);
VM3(jj)=xm(3)/rhom(3,jj);
end
VM=[VM1;VM2;VM3];
VE=VM-s1;
 % VE IS EXPERIMENTAL EXCESS MOLAR VOLUMES----------------------
 %-------------------------------------------------------------------
 %-------------CALCULATION OF Ai ( pair temperature dependent parameter)---------
for ii=1:3
p1(ii)=xf1(ii)*xf2(ii);
p2(ii)=p1(ii)*(xf1(ii)-xf2(ii));
p3(ii)=p1(ii)*(xf1(ii)-xf2(ii))^2;
p11(ii)=xf2(ii)*xf3(ii);
p21(ii)=p11(ii)*(xf2(ii)-xf3(ii));
```

```
p31(ii)=p11(ii)*(xf2(ii)-xf3(ii))^2;
p12(ii)=xf1(ii)*xf3(ii);
p22(ii)=p12(ii)*(xf1(ii)-xf3(ii));
p32(ii)=p12(ii)*(xf1(ii)-xf3(ii))^2;
end
v12=[p1; p2; p3]';
v23=[p11; p21; p31]';
v31=[p12; p22; p32]';
V=[v12 v23 v31];
r=pinv(V);
A=r*VE;
A1=A';
for j=1:8
t(j)=T(j);
t2(j)=T(j)^2;
end
t1=t;
t12=t2;
T2=[ones(1,8); t1; t12];
T3=T2';
B=pinv(T3);
coef=B*A1
%-----------------------------------------------------------------------
a=coef(1,:)
b=coef(2,:)
c=coef(3,:)
for kk=1:8
for nn=1:9
bb(nn,kk)=b(nn)*T(kk);
cc(nn,kk)=c(nn)*(T(kk))^2;
end
end
for mm=1:8
Ai1(mm)=a(1)+bb(1,mm)+cc(1,mm);
```

```
Ai2(mm)=a(2)+bb(2,mm)+cc(2,mm);
Ai3(mm)=a(3)+bb(3,mm)+cc(3,mm);
Ai4(mm)=a(4)+bb(4,mm)+cc(4,mm);
Ai5(mm)=a(5)+bb(5,mm)+cc(5,mm);
Ai6(mm)=a(6)+bb(6,mm)+cc(6,mm);
Ai7(mm)=a(7)+bb(7,mm)+cc(7,mm);
Ai8(mm)=a(8)+bb(8,mm)+cc(8,mm);
Ai9(mm)=a(9)+bb(9,mm)+cc(9,mm);
AiSILAEP=[Ai1;Ai2;Ai3];
AiAEPH2O=[Ai4;Ai5;Ai6];
AiSILH2O=[Ai7;Ai8;Ai9];
end
for rr=1:8
VE121(rr)=p1(1,1)*AiSILAEP(1,rr)+p2(1,1)*AiSILAEP(2,rr)+p3(1,1)*AiSILAEP(3,rr);
VE122(rr)=p1(1,2)*AiSILAEP(1,rr)+p2(1,2)*AiSILAEP(2,rr)+p3(1,2)*AiSILAEP(3,rr);
VE123(rr)=p1(1,3)*AiSILAEP(1,rr)+p2(1,3)*AiSILAEP(2,rr)+p3(1,3)*AiSILAEP(3,rr);
VE12=[VE121;VE122;VE123];
VE231(rr)=p11(1,1)*AiAEPH2O(1,rr)+p21(1,1)*AiAEPH2O(2,rr)+p31(1,1)*AiAEPH2O(3,
rr);
VE232(rr)=p11(1,2)*AiAEPH2O(1,rr)+p21(1,2)*AiAEPH2O(2,rr)+p31(1,2)*AiAEPH2O(3,
rr);
VE233(rr)=p11(1,3)*AiAEPH2O(1,rr)+p21(1,3)*AiAEPH2O(2,rr)+p31(1,3)*AiAEPH2O(3,
rr);
VE23=[VE231;VE232;VE233];
VE131(rr)=p12(1,1)*AiSILH2O(1,rr)+p22(1,1)*AiSILH2O(2,rr)+p32(1,1)*AiSILH2O(3,rr);
VE132(rr)=p12(1,2)*AiSILH2O(1,rr)+p22(1,2)*AiSILH2O(2,rr)+p32(1,2)*AiSILH2O(3,rr);
VE133(rr)=p12(1,3)*AiSILH2O(1,rr)+p22(1,3)*AiSILH2O(2,rr)+p32(1,3)*AiSILH2O(3,rr);
VE13=[VE131;VE132;VE133];
ve=VE12+VE23+VE13;
end
Vm=ve+s1;
for zz=1:8
Rhom1(zz)=xm(1,1)/Vm(1,zz);
Rhom2(zz)=xm(1,2)/Vm(2,zz);
```

```
Rhom3(zz)=xm(1,3)/Vm(3,zz);
Rhom=[Rhom1;Rhom2;Rhom3];
end
%rhom is experimental densities of mixtures
rhom;
%Rhom is calculated densities of mixtures
Rhom;
%standard deviation calculation
x=Rhom-rhom;
x1=x.^2;
x2=sum(x1);
x3=sum(x2');
sd=sqrt(x3/(24-1))
%average absolute absolute deviation calculation
b_tr=abs(x);
P=b_tr./rhom;
P1=sum(P);
P2=sum(P1');
aad=(P2*100)/24
```

Program output:

```
coef =
  Columns 1 through 5
   -1.183700644305393e-01   -1.105887844489999e-02   -1.875250401364329e-04
2.062416907500227e-01   2.385036375595077e-02
    5.604233812710142e-04   5.246831797651241e-05   8.901375219554871e-07   -
1.017553084113732e-03   -7.715293019869327e-05
   -6.199269988126743e-07   -5.798167723092930e-08   -9.835695310026115e-10
1.103846677074999e-06   1.042414149560008e-07
  Columns 6 through 9
   -2.228274620129711e-01   2.913280404639027e-01   8.270886381935133e-02   -
3.862639106249180e-01
```

1.024002177991518e-03 -1.411099608311610e-03 -3.656633930625299e-04 1.807869261513970e-03

-1.149065346677366e-06 1.530160368304744e-06 4.306334114025248e-07 -2.021963747113982e-06

sd =2.056989247380804e-02

aad =1.713373584526378e-03

AIV.3 Determining binary interaction parameters for viscosity using Grunberg-Nissan Model for aq. (TESA + AEP) system.

```
clc
clear
% viscosity regression using Grunberg-Nissan correlation
format long e
%1 is for tesa, 2 for aep and 3 for H20
M=[221.37 129.21 18];
%x1, x2, x3 are weight percentage 1 is for tesa, 2 for aep and 3 for H20
x1=[34.45747801 31.29657228 28.59292701];
x2=[3.958944282 6.110283159 8.20165538 ];
x3=[61.58357771 62.59314456 63.20541761];
T=[298.15 303.15 308.15 313.15 318.15 323.15 328.15 333.15];
%-------------------------------------------------------------------------
% mole fractions are found using mass percentages
for i=1:3
xf1(i)=(x1(i)/M(1))/((x1(i)/M(1))+(x2(i)/M(2))+(x3(i)/M(3)));
xf2(i)=(x2(i)/M(2))/((x1(i)/M(1))+(x2(i)/M(2))+(x3(i)/M(3)));
xf3(i)=(x3(i)/M(3))/((x1(i)/M(1))+(x2(i)/M(2))+(x3(i)/M(3))) ;
end
%-------------------------------------------------------------------------
% eta1, eta2 and eta3 are the viscosities of the pure components
eta1=[2.370 2.320 2.20522122 2.15500032 1.75847508 1.6078104 1.5235749
        1.55391624]
```

```
eta2=[14.481   14.181 11.34231826   8.669032962   7.101917546   5.626076423
        5.036316278   4.480937966]
eta3=[0.9 0.845 0.7190596    0.65276838    0.59580334    0.5464628     0.50359413
        0.4660368];
% etam is the experimental viscosities
etam=[7.561   6.269   5.368   4.805   3.665   3.145   2.791   2.746
6.669   5.568   4.703   4.006   3.109   2.548   2.284   2.264
5.103   3.882   3.012   1.927   1.762   1.541   1.287   0.721];
% Viscosities of pure component
for j=1:8
lneta1(j)=log(eta1(j));
lneta2(j)=log(eta2(j));
lneta3(j)=log(eta3(j));
end
%----------Viscosities of measured viscosities-------
for ii=1:3 %ii indicates composition
for n=1:8 %n indicates temperature
lnetam(ii,n)=log(etam(ii,n));
end
end
%-------------------------------------------------------------------
%ln etam=sigma(xlnetai)  + doublesigma (xixjiGij)
%A=sigma(xlnetai)
%B=doublesigma (xixjiGij)
lnetam1=lnetam;
for m=1:3
for k=1:8
A(m,k)=(xf1(m))*(lneta1(k))+(xf2(m))*(lneta2(k))+(xf3(m))*(lneta3(k));
end
end
%-------------------------------------------------------------------
B=lnetam1-A;
for kk=1:3
x12(kk)=xf1(kk)*xf2(kk); % calculation of coefficient attached to G
```

```
x13(kk)=xf1(kk)*xf3(kk);
x23(kk)=xf2(kk)*xf3(kk);
end
x123=[x12;x23;x13];
C=x123;
B1=B';
D=pinv(C);
G123=B1*D;
%-------------------------------------------------------------------
%------------Gij=a+bT+cT2-------------------------------------------
for j=1:8
t(j)=T(j);
t2(j)=T(j)^2;
end
t1=t;
t12=t2;
T2=[ones(1,8); t1; t12];
T3=T2';
B=pinv(T3);
coef=B*G123
%------------------------calculation of viscosity using the coefficients
a=coef(1,:);
b=coef(2,:);
c=coef(3,:);
for ii=1:8
for jj=1:3
bb(ii,jj)=b(jj)*T(ii);
cc(ii,jj)=c(jj)*T(ii)^2;
end
end
G12=coef(1,1)*ones(8,1)+bb(:,1)+cc(:,1);
G23=coef(1,2)*ones(8,1)+bb(:,2)+cc(:,2);
G13=coef(1,3)*ones(8,1)+bb(:,3)+cc(:,3);
for mm=1:3
```

```
for                                                                    nn=1:8
Lnetam(mm,nn)=xf1(mm)*lneta1(nn)+xf2(mm)*lneta2(nn)+xf3(mm)*lneta3(nn)+x12(mm)*
G12(nn)+x23(mm)*G23(nn)+x13(mm)*G13(nn);
end
end
 % Etam is the calculated viscosity
Etam=exp(Lnetam);
% etam is the experimental viscosity
Etam;
%calculation of standard deviation
error=Etam-etam;
m=error.^2;
m1=sum(m);
m2=sum(m1)';
sd=sqrt(m2/23)
%calculation of average absolute deviation
b=abs(error);
P=b./etam;
P1=sum(P);
P2=sum(P1');
aad=(P2*100)/24
```

Program output:

```
coef =1.320558368355392e+06   -4.296781083925447e+04   -2.819410931348333e+03
   -8.814950460051812e+03    2.881164645556320e+02    1.931661778075687e+01
    1.481797494443090e+01   -4.864050232727746e-01   -3.279773488013758e-02
sd =1.931970777787389e-01
aad =5.877874891058145e+00
```

AIV.4 Correlation of sound velocity using model M_1 for aq. (TESA + AEP) system.

```
clc
clear
format long e
%x1= mass fraction of aep amine % x2 is mass fraction of tesa
T=[298.15 303.15 308.15 313.15 318.15 323.15 328.15 333.15 298.15 303.15 308.15
313.15 318.15 323.15 328.15 333.15 298.15 303.15 308.15 313.15 318.15 323.15 328.15
333.15 ];
x2_tesa=[34.45747801 34.45747801 34.45747801 34.45747801 34.45747801
34.45747801 34.45747801 34.45747801 31.29657228 31.29657228 31.29657228
31.29657228 31.29657228 31.29657228 31.29657228 31.29657228 28.59292701
28.59292701 28.59292701 28.59292701 28.59292701 28.59292701 28.59292701
28.59292701];
x1_aep=[3.958944282 3.958944282 3.958944282 3.958944282 3.958944282
3.958944282 3.958944282 3.958944282 6.110283159 6.110283159 6.110283159
6.110283159 6.110283159 6.110283159 6.110283159 6.110283159 8.20165538
8.20165538 8.20165538 8.20165538 8.20165538 8.20165538 8.20165538
8.20165538];
var=[1639.97 1630.78 1621.06 1611.05 1600.7 1590.05 1579.1
1567.82 1654.58 1645.85 1636.58 1626.98 1617.06
1606.81 1596.2 1585.24 1667.32 1659.07 1650.29 1641.15
1631.63 1621.75 1611.52 1600.88];
x1=x1_aep/100;
x2=x2_tesa/100;
number=length(var);
for i=1:number
x1_square(i)=x1(i)*x1(i);
aa(i)=1./x2(i);
bb(i)=1./T(i);
cc(i)=x1(i)./x2(i);
dd(i)=x1(i)./T(i);
```

```
ee(i)=1./(x2(i)*T(i));
ff(i)=x1(i)./(x2(i)*T(i));
m(i)=aa(i)*aa(i);
n(i)=bb(i)*bb(i);
o(i)=cc(i)*cc(i);
p(i)=dd(i)*dd(i);
q(i)=ee(i)*ee(i);
r(i)=ff(i)*ff(i);
m2(i)=bb(i)*cc(i);
n2(i)=bb(i)*dd(i);
o2(i)=bb(i)*ee(i);
q2(i)=bb(i)*ff(i);
m1(i)=aa(i)*bb(i);
n1(i)=aa(i)*cc(i);
o1(i)=aa(i)*dd(i);
p1(i)=aa(i)*ee(i);
q1(i)=aa(i)*ff(i);
m6(i)=aa(i)*x1(i);
n7(i)=bb(i)*x1(i);
o7(i)=cc(i)*x1(i);
p7(i)=dd(i)*x1(i);
q7(i)=ee(i)*x1(i);
r7(i)=ff(i)*x1(i);
m3(i)=cc(i)*dd(i);
n3(i)=cc(i)*ee(i);
o3(i)=cc(i)*ff(i);
m4(i)=dd(i)*ee(i);
n4(i)=dd(i)*ff(i);
m5(i)=ff(i)*ee(i);
m8(i)=var(i)*x1(i);
n8(i)=var(i)*aa(i);
o8(i)=var(i)*bb(i);
p8(i)=var(i)*cc(i);
q8(i)=var(i)*dd(i);
```

```
r8(i)=var(i)*ee(i);
s8(i)=var(i)*ff(i);
end
% calculations of summations
AA=sum(aa);
BB=sum(bb);
CC=sum(cc);
DD=sum(dd);
EE=sum(ee);
FF=sum(ff);
M=sum(m);
N=sum(n);
O=sum(o);
P=sum(p);
Q=sum(q);
R=sum(r);
M2=sum(m2);
N2=sum(n2);
O2=sum(o2);
Q2=sum(q2);
M1=sum(m1);
N1=sum(n1);
O1=sum(o1);
P1=sum(p1);
Q1=sum(q1);
M6=sum(m6);
N7=sum(n7);
O7=sum(o7);
P7=sum(p7);
Q7=sum(q7);
R7=sum(r7);
M3=sum(m3);
N3=sum(n3);
O3=sum(o3);
```

```
M4=sum(m4);
N4=sum(n4);
M5=sum(m5);
M8=sum(m8);
N8=sum(n8);
O8=sum(o8);
P8=sum(p8);
Q8=sum(q8);
R8=sum(r8);
S8=sum(s8);
X1=sum(x1);
VAR=sum(var);
X1_S=sum(x1_square);
main_matrix=[number X1 AA BB CC DD EE FF;X1 X1_S M6 N7 O7 P7 Q7 R7;AA M6 M M1 N1 O1 P1 Q1;BB N7 M1 N M2 N2 O2 Q2;CC O7 N1 M2 O M3 N3 O3;DD P7 O1 N2 M3 P M4 N4;EE Q7 P1 O2 N3 M4 Q M5;FF R7 Q1 Q2 O3 N4 M5 R];
sub_matrix=[VAR M8 N8 O8 P8 Q8 R8 S8];
Answer=pinv(main_matrix)*sub_matrix'
A=Answer(1);
B=Answer(2);
C=Answer(3);
D=Answer(4);
E=Answer(5);
F=Answer(6);
G=Answer(7);
H=Answer(8);
for i=1:number
var_new(i)=A+(B*x1(i))+(C*1/x2(i))+(D*1/(T(i)))+(E*x1(i)/x2(i))+(F*x1(i)/T(i))+(G*1/(x2(i)*T(i)))+(H*x1(i)/(x2(i)*T(i)));
end
var_new;
% %standard deviation calculation
nu=var_new-var;
nu1=nu.^2;
```

```
nu2=sum(nu1);
nu3=sum(nu2');
sd=sqrt(nu3/(number-1))
% %average absolute absolute deviation calculation
mu=abs(nu);
Pu=mu./var;
Pu1=sum(Pu);
Pu2=sum(Pu1');
a1ad=(Pu2*100)/number
[x1;x2;T;var;var_new]';
```

Program output:

```
3.510198669433594e+02
-2.846784973144531e+01
2.196089591979981e+02
2.665093066406250e+05
-2.755265274047852e+02
-7.342539550781250e+04
-1.998095312500000e+04
-7.589328125000000e+03

sd =1.565181679953265e+00
a1ad =8.187528364901475e-02
```

AIV.5 Correlation of refractive index using model M_1 for aq. (TESA + AEP) system.

```
clc
clear
format long e
%x1= mass fraction of aep amine % x2 is mass fraction of tesa
T=[298.15 303.15 308.15      313.15 318.15 323.15 328.15 333.15 298.15 303.15 308.15
313.15 318.15 323.15 328.15 333.15 298.15 303.15 308.15 313.15 318.15 323.15 328.15
```

```
333.15 ];
x2_tesa=[34.45747801 34.45747801 34.45747801 34.45747801 34.45747801
34.45747801 34.45747801 34.45747801 31.29657228 31.29657228 31.29657228
31.29657228 31.29657228 31.29657228 31.29657228 31.29657228 28.59292701
28.59292701 28.59292701 28.59292701 28.59292701 28.59292701 28.59292701
28.59292701];
x1_aep=[3.958944282 3.958944282 3.958944282 3.958944282 3.958944282
3.958944282 3.958944282 3.958944282 6.110283159 6.110283159 6.110283159
6.110283159 6.110283159 6.110283159 6.110283159 6.110283159 8.20165538
8.20165538 8.20165538 8.20165538 8.20165538 8.20165538 8.20165538
8.20165538];
x1=x1_aep/100;
x2=x2_tesa/100;
var=[1.3828 1.3815 1.3796 1.3787 1.3774 1.3759 1.3746 1.3722 1.3838 1.3825 1.3812
1.3802 1.3786 1.3774 1.3761 1.3748 1.3848 1.3835 1.3822 1.3812 1.3795 1.3785 1.3772
1.3766];
number=length(var);
for i=1:number
x1_square(i)=x1(i)*x1(i);
aa(i)=1./x2(i);
bb(i)=1./T(i);
cc(i)=x1(i)./x2(i);
dd(i)=x1(i)./T(i);
ee(i)=1./(x2(i)*T(i));
ff(i)=x1(i)./(x2(i)*T(i));
m(i)=aa(i)*aa(i);
n(i)=bb(i)*bb(i);
o(i)=cc(i)*cc(i);
p(i)=dd(i)*dd(i);
q(i)=ee(i)*ee(i);
r(i)=ff(i)*ff(i);
m2(i)=bb(i)*cc(i);
n2(i)=bb(i)*dd(i);
o2(i)=bb(i)*ee(i);
```

```
q2(i)=bb(i)*ff(i);
m1(i)=aa(i)*bb(i);
n1(i)=aa(i)*cc(i);
o1(i)=aa(i)*dd(i);
p1(i)=aa(i)*ee(i);
q1(i)=aa(i)*ff(i);
m6(i)=aa(i)*x1(i);
n7(i)=bb(i)*x1(i);
o7(i)=cc(i)*x1(i);
p7(i)=dd(i)*x1(i);
q7(i)=ee(i)*x1(i);
r7(i)=ff(i)*x1(i);
m3(i)=cc(i)*dd(i);
n3(i)=cc(i)*ee(i);
o3(i)=cc(i)*ff(i);
m4(i)=dd(i)*ee(i);
n4(i)=dd(i)*ff(i);
m5(i)=ff(i)*ee(i);
m8(i)=var(i)*x1(i);
n8(i)=var(i)*aa(i);
o8(i)=var(i)*bb(i);
p8(i)=var(i)*cc(i);
q8(i)=var(i)*dd(i);
r8(i)=var(i)*ee(i);
s8(i)=var(i)*ff(i);
end
% calculations of summations
AA=sum(aa);
BB=sum(bb);
CC=sum(cc);
DD=sum(dd);
EE=sum(ee);
FF=sum(ff);
M=sum(m);
```

```
N=sum(n);
O=sum(o);
P=sum(p);
Q=sum(q);
R=sum(r);
M2=sum(m2);
N2=sum(n2);
O2=sum(o2);
Q2=sum(q2);
M1=sum(m1);
N1=sum(n1);
O1=sum(o1);
P1=sum(p1);
Q1=sum(q1);
M6=sum(m6);
N7=sum(n7);
O7=sum(o7);
P7=sum(p7);
Q7=sum(q7);
R7=sum(r7);
M3=sum(m3);
N3=sum(n3);
O3=sum(o3);
M4=sum(m4);
N4=sum(n4);
M5=sum(m5);
M8=sum(m8);
N8=sum(n8);
O8=sum(o8);
P8=sum(p8);
Q8=sum(q8);
R8=sum(r8);
S8=sum(s8);
X1=sum(x1);
```

```
VAR=sum(var);
X1_S=sum(x1_square);
main_matrix=[number X1 AA BB CC DD EE FF;X1 X1_S M6 N7 O7 P7 Q7 R7;AA M6 M
M1 N1 O1 P1 Q1;BB N7 M1 N M2 N2 O2 Q2;CC O7 N1 M2 O M3 N3 O3;DD P7 O1 N2
M3 P M4 N4;EE Q7 P1 O2 N3 M4 Q M5;FF R7 Q1 Q2 O3 N4 M5 R];
sub_matrix=[VAR M8 N8 O8 P8 Q8 R8 S8];
Answer=pinv(main_matrix)*sub_matrix'
A=Answer(1);
B=Answer(2);
C=Answer(3);
D=Answer(4);
E=Answer(5);
F=Answer(6);
G=Answer(7);
H=Answer(8);
for i=1:number
var_new(i)=A+(B*x1(i))+(C*1/x2(i))+(D*1/(T(i)))+(E*x1(i)/x2(i))+(F*x1(i)/T(i))+(G*1/(x2
(i)*T(i)))+(H*x1(i)/(x2(i)*T(i)));
end
var_new;
% %standard deviation calculation
nu=var_new-var;
nu1=nu.^2;
nu2=sum(nu1);
nu3=sum(nu2');
sd=sqrt(nu3/(number-1))
% %average absolute deviation calculation
mu=abs(nu);
Pu=mu./var;
Pu1=sum(Pu);
Pu2=sum(Pu1');
a1ad=(Pu2*100)/number
[x1;x2;T;var;var_new]';
```

Answer =7.057902701199055e-01
-6.477949209511280e-02
2.279139235615730e-01
1.700760974884033e+02
-6.746962592005730e-01
-7.863866519927979e+01
-5.493921899795532e+01
1.833684005737305e+02
sd =2.622510646353239e-04
a1ad =1.386005254106350e-02

AIV.6 Correlation of surface tension using model M_2 for aq. (TESA + AEP) system.

```
clc
clear
format long e
%eta is dynamic viscosity in mPa s, st is surface tension in mN/m and T is
%in kelvin
T=[298.15 303.15 308.15 313.15 318.15 323.15 328.15 333.15 298.15 303.15 308.15
313.15 318.15 323.15 328.15 333.15 298.15 303.15 308.15 313.15 318.15 323.15 328.15
333.15];
eta=[7.561 6.269 5.368 4.805 3.665 3.145 2.791 2.746 6.669 5.568 4.703  4.006  3.109  2.548
2.284 2.264 5.103 3.882 3.012 1.927 1.762 1.541 1.287 0.721];
st=[34.6070 34.2843 33.7993 33.5028 33.3593 33.3313 33.2843 33.2213 36.2470 35.5530
35.2297  34.0097  34.7963  34.7140  34.6845  34.6520  37.9090  36.6340  36.3103  36.1290
36.0653 35.9067 35.8937 35.8007];
x1=log(1./eta);
y=log(log(st));
act_x2=log(1-(log(T)./log(st)));
%x2=log(1-(log(T)./log(st)));
x2=real(act_x2);
```

```
n=length(T);
for i=1:n
b(i)=y(i)*x1(i);
d(i)=y(i)*x2(i);
e(i)=x1(i)*x1(i);
f(i)=x2(i)*x2(i);
g(i)=x1(i)*x2(i);
end
sig_x1=sum(x1);
sig_x2=sum(x2);
sig_y=sum(y);
sig_yx1=sum(b);
sig_yx2=sum(d);
sig_x12=sum(e);
sig_x22=sum(f);
sig_x1x2=sum(g);
A=[n sig_x1 sig_x2;sig_x1 sig_x12 sig_x1x2; sig_x2 sig_x1x2 sig_x22];
B=[sig_y;sig_yx1; sig_yx2];
C=inv(A)*B;
a0=C(1)
a1=C(2)
a2=C(3)
for i=1:n
y_pred(i)=a0+(a1*x1(i))+(a2*x2(i));
end
y_pred;
st_pred=exp(exp(y_pred));
for i=1:n
err_1(i)=(abs(st_pred(i)-st(i))/st(i));
end
aad=sum(err_1)*100/n
Phi=a1
A=exp(-a0)
```

Program output:

a0 =1.142961635439377e+00

a1 =7.374623535147507e-03

a2 =-2.782983461964932e-01

aad =4.170571615922533e-01

Phi =7.374623535147507e-03

A =3.188732356952660e-01